**DOCTOR OF PHILOSOPHY**

# The physical oceanography of the Cape Saõ Vicente upwelling region observed from sea, land and space

Relvas de Almeida, Paulo José

*Award date:*
1999

*Awarding institution:*
University of Wales, Bangor

# The physical oceanography of the Cape São Vicente upwelling region observed from sea, land and space

by

**Paulo José Relvas de Almeida**

A thesis submitted in accordance with the requirements of the University of Wales for the degree of Doctor of Philosophy

School of Ocean Sciences
University of Wales
Menai Bridge
Gwynedd

January 1999

# Abstract

A description of the physical oceanography of the coastal ocean around Cape São Vicente is presented. This region of the Iberian Peninsula, where the west and south coasts meet at right angles, forms part of the eastern boundary of the North Atlantic. The description is based on four data sets: 1. The historical hydrographic data base recorded between 1900 and 1990; 2. Sea level, meteorology, and nearshore sea surface temperature time series, from 1981 to 1992, at coastal sites within 200 km of Cape São Vicente; 3. Over 1200 advanced very high resolution (AVHRR) satellite images of sea surface temperature (SST) from 1981 to 1995; 4. *in situ* data from June 1994, which include underway meteorology, acoustic doppler current profiler (ADCP) and conductivity-temperature-depth probe (CTD) surveys.

The large scale hydrography shows a marked seasonality of the surface fields. Though rather uniform in winter, they show strong gradients in summer when the isolines tend to parallel the coastline as a result of upwelling of cooler and fresher water inshore. A mean alongshore pressure gradient, stronger in summer and off the southern coast, tends to force the flow westward along the southern coast and northward around the Cape. During upwelling favourable winds the alongshore flow can be reversed, at least in the upper layers, more easily off the western coast. Upwelling and non-upwelling patterns of SST are investigated. Cold waters upwelled off the western coast are observed primarily to turn cyclonically around the Cape, but also to feed the equatorward development of the Cape São Vicente filament, which at times develops a westward branch by meandering of the upwelling jet. A coastal warm countercurrent is observed during upwelling unfavourable winds. The cruise principally observed the region during such a relaxation period. Remnants of the previous upwelling episode, advecting cold low spiciness water cyclonically around the Cape from regions further north, and an inshore warm counterflow, turning poleward around the Cape with speeds up to 0.4 m/s were identified in the data. No cold filament feature was present in the region at the time. The wind stress and the alongshore pressure gradient are the major forcings acting in the region. The relative strength of these mechanisms dictates the alongshore circulation of the upper coastal ocean.

# Acknowledgements

First, and foremost, I would like to thank my supervisor Dr. Des Barton, for all his support and encouragement over the past few years. His guidance on many of the interpretations developed in this thesis was fundamental.

Special thanks are due to Lúcilia Coelho and Uwe Piaktowskifor allowing me to join the research cruise which was important for this work. Also a big "thank you" to Alice Newton for introducing me to the School of Ocean Siences.

Many thanks are due to those colleagues and friends, both in the Algarve and at Menai Bridge, who helped me during this time. I would like to thank Tomaz Boski for giving me access to the ERDAS system.

Thank you to the Instituto de Meteorologia for the meteorological data and to the Instituto Hidrográfico for the sea level data.

Thanks are due to Steve Groom and Peter Miller, from the NERC Remote Sensing Data Analysis Service at CCMS-PLM, for their help with the satellite image processing.

This work was funded by the JNICT grants Ciência BD/1532/91-IG and PRAXIS XXI BD/4079/94.

# Contents

# List of Figures

# Chapter 1

# Introduction

## 1.1 General

The Cape São Vicente region represents the southwestern tip of the Iberian Peninsula. The Iberian Peninsula lies at the northern extremity of the eastern boundary of the North Atlantic sub-tropical gyre and is a transitional region of the North Atlantic Ocean lying between the equatorward flowing surface Canary Current and the north-eastward flowing North Atlantic Current. Due to its geographical location, the coastal ocean off the Iberian Peninsula is part of the Atlantic eastern boundary and falls within the general concept of oceanic eastern boundaries regions. Therefore, the typical general near surface patterns observed in the region largely result from the local atmospheric circulation and the presence of a continental margin.

The Cape São Vicente region is a particular and interesting case among the eastern boundaries regions, because it represents the southern limit of the Iberian boundary region. There, the western and southern coast of Iberia intersect in an almost right angle. Whether the coastal ocean off the southern coast of Iberia follows the general pattern of an eastern boundary region, allowing it to be considered as a prolongation of the western coast, or if it has a different regime, is a question addressed in this study. Cape São Vicente is the northern limit of the major discontinuity, represented by the entrance of the Mediterranean sea, which divides the North Atlantic eastern boundary into two sections, the Northwestern African coast and the Iberian coast.

Physical processes typical of eastern boundary regions include coastal upwelling driven by equatorward winds that prevail for at least part of the year. Upwelling, by replacing coastal surface waters with cold dense subsurface waters that flow towards the coast, surfacing in a coastal band alongshore, induces a rise of the isopycnals against the coast that drives an equatorward alongshore current jet in the upper layers. Such an equatorward surface flow is established along the western coast of Iberia during the summer upwelling season. Cape São Vicente is the southernmost point where the physical constraint imposed by the presence of a continental land mass disappears. Therefore, it is in this region that the continuation of the west coast equatorward flow is determined and where, presumably, dissipative mechanisms associated with the kinetic energy of the equatorward flow operate. Cape São Vicente is potentially a region of strong exchange of cool nutrient rich coastal water to the offshore ocean.

Accepting the validity of the Ekman transport mechanism, a rather uniform upwelling front, separating the cold upwelled water from the warmer waters offshore, might be expected to occur over long stretches of the eastern boundaries. Similarly to other eastern boundary regions, sea surface temperature satellite imagery has documented that in the Iberian eastern boundary upwelling is not a simple two-dimensional process, uniform along the coast, but a more complex three-dimensional phenomenon, with upwelling being intensified in specific locations. Such locations are often associated with cold filaments, which are contorted tongues of upwelled water that can extend offshore for hundreds of kilometres. The filaments off Iberia commonly occur during the summer upwelling season, when their transport capacity substantially exceeds the exchange that would result from the offshore wind-driven transport that drives the upwelling. Filament dynamics provides a potential mechanism for export of upwelled water and its properties out of the coastal region. Common locations for the filament formation along the western coast of Iberia are, in general, the major coastal topographic features. Cape São Vicente itself is the root of a large cold filament formation, which has been observed in satellite imagery to grow in different directions. It southward development terminates, at times, in a dipole pair populated with small scale protuberances in its outer border.

This thesis presents a description of the oceanography of the coastal ocean around Cape São Vicente. This description is based in the analysis of three groups of data:

— data collected on land comprise time series of sea level data from four tide gauges, of wind data from three meteorological stations, and of nearshore sea surface temperature from three different locations along the coast. Results from the analysis revealed that a mean alongshore pressure gradient act in the region with particular incidence during summer, forcing the flow westward along the southern coast and bending northward around the Cape. Under certain wind conditions the alongshore flow is reversed, at least in the upper layers.

— data collected from space comprise an archive with over 1200 advanced very high resolution (AVHRR) satellite images of the sea surface temperature spanning from 1981 to 1995. The upwelling and non-upwelling patterns of the sea surface temperature and associated features were elucidated. The evolution and preferred directions of development of the Cape São Vicente cold filament were described and the implications for the regional oceanography were analysed.

— data collected at sea comprise wind and other meteorological data, hydrographic data (CTD - Conductivity, Temperature and Depth) and current data (ADCP - Acoustic Doppler Current Profiler), undertaken during a cruise in June 1994 on board the R/V Poseidon. The results presented in this thesis indicate that the cruise occurred just after the cessation of an upwelling event and that no cold filament feature was present in the region at the time. However, a coastal warm counterflow, turning poleward around the Cape, was clearly identified in the data.

## 1.2 Objective

The overall aim of the present research was to improve the understanding of the oceanography of the Cape São Vicente region. During the summer, when upwelling is a persistent phenomenon in the region, the oceanography of the Cape São Vicente region is frequently dominated by the presence of a cold filament feature associated with the Cape itself. Filaments are separated from the offshore oceanic waters by significant thermal fronts. It is known from observation in other eastern boudary regions, especially off California, that their structure include strong offshore current jets. Filaments off Iberia have only been observed in satellite imagery and little is known about their structure and dynamics. The cold filament associated with the Cape São Vicente is one of the largest and most persistent filaments observed off Iberia. Satellite imagery has revealed its singular development and configuration.

The original purpose of the present research included the detailed *in situ* sampling of the Cape São Vicente filament to determine its three-dimensional structure and dynamics, and to investigate its relation with the surrounding flow field. However, when the *in situ* sampling component of the research took place, in June 1994, no sign of the filament feature was evident in the thermal satellite images and its absence was confirmed in the analysis of the measured data. The cruise took place well inside the upwelling season of the region, when in past years the filament had been observed. However, the fieldwork coincided with very light winds, in a post-upwelling situation. Just after the cruise finished a plume of cold water was observed in the remote sensing data to grow from the Cape, following the onset of stronger winds.

As a consequence, the initial objectives related to the filament structure and dynamics could only be addressed through the analysis of remote sensing data and coastal data. Additional objectives were defined, pertinent to the field results, so that the major objectives of the research then became:

- investigate to what extent the coastal region off southern Iberia has a regime similar to the eastern boundary region observed off the western coast.
- describe the mesoscale patterns in the Cape São Vicente region, in particular the cold filament feature, and determine the major processes involved in their formation and evolution.
- investigate the nature of the warm coastal counterflow observed during the summer months and to understand the physical processes involved in its formation, development and decay.
- identify the forcing factors that drive the flow in the region, in particular during the summer season, improving the understanding of the dynamics of the Cape São Vicente region.

## 1.3 Thesis outline

This thesis is organized in nine chapters. The first three chapters provide the essential background to the thesis. The first chapter is this general introduction. Chapter 2 describes the main patterns and features of eastern boundaries regions of the oceans and the associated dynamics and forcing factors. Special emphasis is given to the formation of cold filaments, mainly based on the knowledge acquired from experiments in the coastal transition zone off California. The last part of Chapter 2 is dedicated to the coastal transition zone off the Iberian Peninsula, with particular attention to the known oceanography of the region around the Cape São Vicente and off the southern coast of Portugal. Chapter 3 describes research based in historical data from the National Oceanographic Data Center (NODC) data base, which was used to define the mean hydrographic structure and its seasonal variability off the southwestern Iberia.

Chapters 4 to 7 describe the research undertaken that provides the title of this thesis. Chapter 4 comprises the land observations. Sea level, wind velocity, and coastal sea surface temperature time series from tide gauges and meteorological stations located along the coast of southwestern Iberia are analysed in terms of mean sea surface conditions and seasonal variations. The relation of the sea level behaviour to the wind pattern is discussed.

Chapter 5 comprises the space observations. The mesoscale patterns of the sea surface temperature in the Cape São Vicente region observed from advanced very high resolution radiometer (AVHRR) satellite imagery are described and analysed. Characteristic features are identified on the basis of an AVHRR imagery archive with over 1200 scenes and their formation processes are discussed.

Chapters 6 and 7 comprise observations made at sea. Chapter 6 presents the physical oceanography experiment carried out in the Cape São Vicente region during June 1994 and describes the data acquisition and basic processing of the various data sets. In Chapter 7 the results from the *in situ* observations are presented and discussed, and the implications for the knowledge of the ocean dynamics of the region is considered.

Chapter 8 provides a summary of the results obtained during this research, summarizes the final conclusions and makes suggestions for future research in the coastal transition zone off southwestern Iberia.

All the locations referred to in the text of the present thesis are labeled in a large map of the western part of the Iberian Peninsula provided in the last page of the thesis.

# Chapter 2

# Eastern boundaries

## 2.1 The coastal ocean at the eastern boundaries

### 2.1.1 Introduction

The eastern boundary regions of the oceans have many common characteristics related to their source waters and surface patterns, the nature of the flow and the phenomena resulting from local atmospheric circulation, and the presence of boundaries imposed by the continental land masses. The ocean circulation in eastern boundaries differs from the circulation in western boundaries mainly due curvature of the earth. The variation of the Coriolis parameter with the latitude ($\beta$ effect) leads to the generation of planetary Rossby waves that propagate information westward. So, eastern boundaries are little influenced by what happens in the ocean interior, while the circulation in western boundaries is largely a response to what happens in the ocean interior. In many instances, the flow over the shelf may be considered independent of the motion farther offshore [*Allen*, 1980]. The dominant spatial scales of the eastern boundaries regime are dictated mainly by the geometry of the continental shelf, by the wind stress function and by scales intrinsic to the fluid motion. Typically the alongshore scale is thousands of kilometres and the cross-shelf scale about one or two hundreds of kilometres. The vertical scale is the water depth, which over the shelf and upper slope may be several hundreds of meters.

In the absence of influence from the ocean interior, effects caused by local external forcing have a large influence in the circulation near eastern boundaries. Some external forcing is a response to the relative position between the Sun and the Earth. Mechanisms of interaction between the atmosphere and the ocean transmit this annual cycle to the coastal ocean, resulting therefore in a strong and well defined seasonality of the major features in these regions.

### 2.1.2 Characteristic features

The seasonal variations observed in the eastern coastal ocean have little relation with the cycles observed farther offshore. *Reid and Mantyla* [1976] observed that the coastal elevations measured at tide gauges and the geopotential anomaly in midocean are out of phase, at the same latitude in the North Pacific. The typical mid-oceanic annual heating and cooling cycle is not very noticeable in the nearshore annual cycle of the sea elevation. Also the sea surface temperature pattern shows different behaviour inshore and offshore: *Huyer* [1977] observed that the water in the halocline in the continental shelf off Oregon is colder in summer than in winter, although the difference is not as great at 45 km offshore as it is at 25 km offshore and has disappeared by 150 km offshore. The amplitude of the seasonal cycle in the steric height and sea level analysis decreases rapidly with distance from shore, within a distance of about 200 km from the coast.

On the eastern sides of the oceans, surface isotherms run more or less meridionally along the coasts, in contrast to their zonal configuration farther west [*Wooster and Reid*, 1963]. This is more evident during summer, when the strongest negative gradient towards the coast is reached, due to the cold water upwelled along the coast. It is difficult to find a general rule for salinity. Its surface pattern depends on the balance between precipitation and evaporation at the high latitudes from which the currents flow and depends on the vertical structure of the salinity and the modification caused by the upwelling.

A typical temperature cycle of the coastal surface waters, as observed off Oregon, in the Pacific coast of North America, is a low value in winter, increasing in spring, lowest in summer, highest in early fall and decreasing in winter [*Huyer*, 1977]. The temperature cycle is only partially determined by the heating and cooling cycle, since the summer minimum is associated with the coastal upwelling forced by the wind pattern. The surface salinity is generally decreased by coastal upwelling seasonally, except in the upwelling region of the Californian Current, where the salinity increases with depth.

A major driving factor on eastern boundaries is the alongshore wind forcing, responsible for upwelling, a basic feature of the eastern currents. Apart from the small scale relaxation events of the wind, the regime is mostly seasonal, forcing two main oceanographic patterns in those regions. Generally during summer, the mean winds blow equatorward, leading to low coastal sea levels and relatively cool water temperature. During winter, the southward component weakens or the mean wind blows towards the pole, leading to high coastal sea levels and warmer water temperatures. The time scale of these two regimes varies from region to region, but is broadly associated with ”summer” and “winter”. Usually the seasonal differences are greater than the variability within the same season. However, exceptions exist, as for instance in the eastern boundary region of the North Atlantic south of 20ºN, where upwelling occurs only during winter [*Van Camp et al.*, 1991].

The time scale of the seasonal southward wind cycle varies with latitude, increasing in length towards the south in the middle latitudes. *Strub et al.* [1987] observed that, for the northeast Pacific continental shelf between 35ºN and 48ºS, the monthly mean winds during winter were northward for 3-6 months, longer in the north than in south, and for the summer were southward also 3-6 months, but longer in the south than in the north. Because of this, the upwelling cycle is not uniform, being longer, or even permanent, in the southern parts on the mid-latitudes regions. For example, along the eastern boundary of the North Atlantic, a permanent upwelling occurs between 20ºN and 25ºN while further north a seasonal upwelling develops only during summer months [*Wooster et al.*, 1976].

The magnitude of the seasonal cycles along the eastern boundary regions of the northern hemisphere, also varies. The maximum magnitudes of the seasonal cycles of temperature, winds and sea level occur in general in the mid-latitudes, decreasing more strongly equatorward than poleward [*Strub et al.*, 1987].

The primary causes of the seasonal variations, as observed by *Huyer* [1977] off Oregon, are the seasonal cycles of the surface heat balance, precipitation and runoff, local wind and the larger scale circulation. These processes can combine to produce secondary phenomena, such as coastal upwelling and concentration of surface runoff, which determine the seasonality of the temperature, salinity and sigma-$t$ distributions.

### 2.1.3 Coastal upwelling

The dynamic effect of the wind stress at the sea surface is described by the well known Ekman theory. The theory shows that the Coriolis force from the earth's rotation and frictional forces in the upper ocean result in a net vertically integrated transport of water 90° to the right of the wind in the northern hemisphere (90° to the left in the southern hemisphere). The water velocity decays exponentially and rotates clockwise in a spiral with the depth in the northern hemisphere (anticlockwise in the southern hemisphere). Direct observations have demonstrated that most of the total Ekman transport is concentrated in the surface mixed layer, typically 0-20 meters thick in the coastal upwelling regions, but a significant fraction occurs in the transition layer below the surface mixed layer [*Lentz*, 1992].

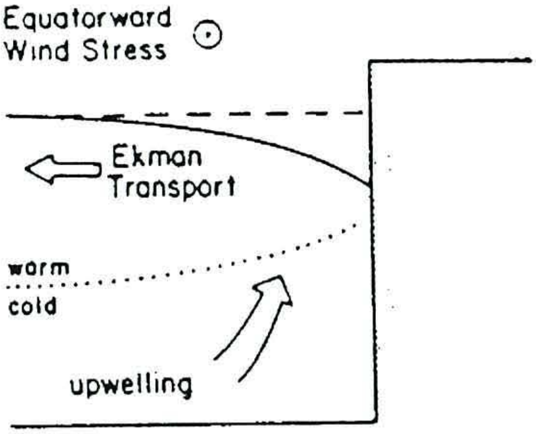

Figure 2.1: Schematic diagram of a coastal upwelling event in the northern hemisphere. Surface slope is significantly enlarged (typically 1000 times the interface slope) [from *Chelton and Enfield*, 1986].

In the northern hemisphere, winds blowing from the north along an eastern boundary result in an offshore transport in the surface waters. To conserve mass, this transport of relatively warm surface water must be compensated by a vertical transport of colder subsurface water at the coast. This classical picture of coastal upwelling is represented in Fig. 2.1. Since the recently upwelled water is colder and more dense, it replaces a smaller volume than the original warm water present before the upwelling. Consequently the sea level at the coast drops in response to the equatorward winds. The nearshore ocean responds to the sea surface slope induced by the coastal upwelling by forming a geostrophic alongshore current flowing equatorward (Fig. 2.2). The boundary response occurs within an offshore scale of the order of tens kilometres, dictated by the local Rossby radius of deformation, $R_i = (Hg^*)^{1/2}/f$, where $g^*$ is the reduced gravity (equal to the gravitation acceleration, $g$, times the fractional increase in density between layers), $H$ is the depth of the upper layer, and $f$ the Coriolis parameter.

The above picture is a simplistic view of the complex dynamics which take place during the coastal upwelling. The offshore transport is restricted to the near surface region during coastal upwelling, leading cold water to accumulate rather quickly in the surface region near the coast, overlying warmer subsurface water and producing an

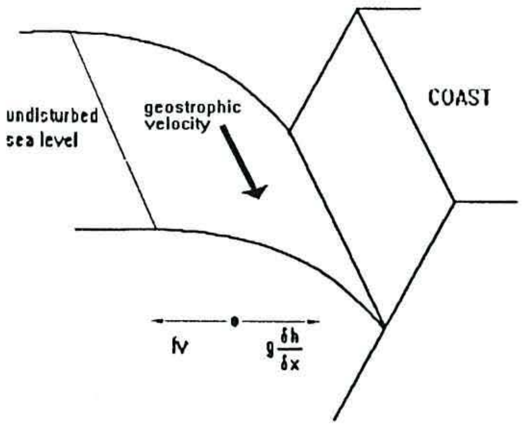

Figure 2.2: Schematic diagram of the forced flow along an eastern ocean boundary during a coastal upwelling event in the northern hemisphere.

unstable situation where mixing must occur. Irregularities in the shelf topography and coast line, as well as non-linear interactions, can play an important role transferring energy between different dynamic scales (particularly into smaller scales) during coastal upwelling.

### 2.1.4 Flow patterns

*Wooster and Reid* [1963] categorised eastern boundary flow as slow, broad and with small transport compared with western circulations. However, eastern boundary current regions are associated with intense mesoscale activity. The width of the eastern boundary currents is difficult to determine since there is no abrupt change of velocity as in the western boundary, but all the transport occurs within 1000 km from the coast, decaying away from the coast. The region where the continental waters and the open ocean waters interact is commonly referred as the coastal transition zone.

It has been observed that nearshore flow in many eastern boundary regions is poleward, for at least part of the year; this appears to be a common feature of the eastern boundaries even in the subtropical gyres. Over the continental shelf off Oregon, *Huyer et al.* [1975] observed that during the winter the alongshore flow is generally poleward and independent of depth, while during summer the surface flow is southward and the deep flow remains poleward. The analysis of the observed T-S characteristics suggests that the seasonal variation of the flow extends seaward to at least 80 km from the coast [*Huyer*, 1977]. The alongshore currents observed farther south, in the California Current system, show a poleward flow during all the year in the subsurface layers over the continental slope (the California Undercurrent). During the winter, a poleward surface current is also observed near the coast, over the continental shelf. This evidence suggests the extension to the surface of the California Undercurrent [*Lynn and Simpson*, 1987] when the surface southward flow weakens, probably related to seasonal variations in the wind stress [*Hickey*, 1979]. According to *Bray and Greengrove* [1993], "the poleward flow dominates the circulation in the easternmost part of the California Current System much more than the historical description would indicate".

A poleward current, flowing at subsurface levels, along the western coast of northwest Africa was reported by *Wooster and Reid* [1963]. Later, this alongshore undercurrent flowing poleward along the continental slope has been consistently observed [*Barton*, 1989]. The poleward undercurrent appears to be restricted within 30 km of the slope, with the core about 200-300 meters deep reaching velocities of 10 cm/s [*Barton et al.*, 1977]. During upwelling events the alongshore flow over the shelf and in the shallow layers is generally equatorward. During wind relaxation, the poleward flow extends to the surface over the slope.

Farther north, off the Iberian Peninsula, a surface poleward flow of about 25-40 km wide with velocities of 20-30 cm/s is also observed to be characteristic of the winter circulation [*Frouin et al.*, 1990]. This circulation is reversed in summer months, when cool upwelled water is advected equatorward at surface layers, in response to southward winds [*Wooster et al.*, 1976]. In deeper layers it is supposed that the northward flow persists as a slope undercurrent. Observations conducted by *Haynes and Barton* [1990] suggest that the weaker the equatorward wind stress, the stronger the poleward flow observed. An apparent continuity seems to exist in the poleward flow along the eastern boundary of the subtropical north Atlantic, despite the physical discontinuity represented by the entrance to the Mediterranean Sea.

In the southern hemisphere, off the west coast of Australia, a permanent poleward coastal flow (the Leeuwin Current) is observed, though the wind regime is equatorward during all the year. The poleward flow intensifies when the equatorward alongshore winds are weaker [*Thompson*, 1984].

## 2.2 Cold filament features

### 2.2.1 Introduction

In many eastern boundary current regions, cold surface features are often found growing out from the shelf and extending offshore as narrow tongues. This offshore development varies from tens to hundreds of kilometres and typically they are less than 100 km wide. Frequently, they are accompanied by rather high concentrations of chlorophyll [*Brink and Cowles,* 1991]. Such structures have been documented, for example, off the coasts of California, the Iberian Peninsula and southwestern Africa, during the upwelling seasons. These features began to be observed in satellite infrared imagery in the late seventies [*Bernstein et al.*, 1977] and they are known as "filaments". In the earlier eighties the first surveys were carried out specifically to study such structures. *Traganza et al.* [1980] showed that the filaments were not only simple superficial features and that they had biological and chemical implications. *Breaker and Gilliland* [1981] concluded that the filaments appeared to respond to wind forcing and therefore were strongly related with coastal upwelling. The basic process of coastal upwelling is described by the Ekman theory, which suggests that, under a favourable wind field, a uniform coastal upwelling would be generated along the ocean boundary. However, satellite imagery and *in situ* observations of the coastal upwelling regions of the world show that a contorted front develops between the upwelled and oceanic waters, with regions of variable upwelling intensity and the appearance of cold filaments stretching offshore. So, other processes in the coastal transition zone interact with the upwelling regime.

The most ambitious and complete program to understand the dynamics and implications of the coastal filaments was put forward in the mid-1980s [*Brink and Cowles,* 1991]. This program took place along the coastal transition zone off California and brought a step forward in the understanding of the coastal filament dynamics and structure. The program also showed the enormous complexity of the phenomena and the wide range of factors that can force and govern the development and evolution of the filaments.

### 2.2.2 Structure of a filament: an overview

Many topics related to the structure of the filaments are still under discussion. However, some aspects are well understood on the basis of repeated and consistent observations. Then, there are other features observed in some surveys, but not in all, which cannot be taken as a general characteristic of filament structure. Nevertheless, a general overview of the spatial structure of a filament can be attempted, at least for the California region.

A robust result is that the filament separates oceanic warm water of low salinity on its offshore (northern) side from high salinity cold recently upwelled water on its inshore (southern) side [e.g. *Kosro and Huyer*, 1986; *Ramp et al.*, 1991]. The core of the filament is a narrow jet of cold water that stretches seaward. The offshore flow associated with the filament is $O(50-150\,\mathrm{km})$ wide, while the jet, where the highest speeds are reached, is $O(10\,\mathrm{km})$ wide. The offshore velocity inside the jet is $O(0.5-1.0\,\mathrm{ms}^{-1})$ [*Flament et al.*, 1985; *Strub et al.*, 1991; *Dewey et al.*, 1991; *Brink et al.*, 1991; *Huyer et al.*, 1991].

In the filament structure it is possible to separate the offshore waters to the north of the jet, jet waters and inshore waters to the south of the jet [*Huyer et al.*, 1991]. The offshore northern waters are warm and relatively fresh and the flow field is offshore. A continuity of this flow with waters farther north can be established, suggesting its origin in the continental shelf, north of the filament [*Strub et al.*, 1991; *Huyer et al.*,1991; *Kadko et al.*, 1991]. The offshore transport in the filament is clearly larger than the wind-driven Ekman transport during an upwelling event, also suggesting that the filament is fed by northern coastal waters [*Flament et al.*, 1985]. To the south of the jet, an onshore return flow considerably weaker than the jet, transports warmer waters onshore *Flament et al.* [1985] reported it to be about 30 km wide with a velocity of 0.35 $\mathrm{ms}^{-1}$. The return flow seems to be a consistent characteristic of filament features [e.g. *Strub et al.*, 1991; *Ramp et al.*, 1991].

The current jet of the filament penetrates to depths of 100 meters or more, far below the surface mixed layer [*Brink and Cowles*, 1991]. Its intensity decreases by about a factor of three between the surface and 100 meters [*Kosro et al.*, 1991], though a weak signature of the jet is still detected by *Huyer et al.* [1991] at 200 meter depth in the coastal transition zone off northern California. Some large filaments appear to have smaller intense filaments embedded within them [*Rienecker and Mooers*, 1989; *Ramp et al.*, 1991].

Southern boundaries of filaments typically have a sharp transition in sea surface temperature from cold to warm water, while the northern boundaries usually exhibit a smoother, more diffuse transition in sea surface temperature [e.g. *Flament et al.*, 1985; *Kosro and Huyer*, 1986; *Ramp et al.*, 1991]. The sharp southern boundary of filaments have been observed to be density compensated [*Flament et al.*, 1985; *Kosro and Huyer*, 1986; *Rienecker and Mooers*, 1989] and non-density compensated [*Rienecker et al.*, 1985; *Kosro and Huyer*, 1986; *Ramp et al.*, 1991].

In the southern front of the filament, between the offshore jet and the onshore flow the development of cyclonic eddies with scales $O$(10-50 km) is often observed [*Flament et al.*, 1985; *Rienecker and Mooers*, 1989]. However, the existence of eddies on both sides, inshore and offshore, of a filament is supported by drifter data in the coastal transition zone off California [*Strub et al.*, 1991]. These eddies are an important mechanism for dissipating the kinetic energy of the jet. They are barotropic instabilities, so it is the kinetic rather than the potential energy of the flow that feeds the growing perturbations. It is also often observed that the outer part of the filament bends cyclonically. The relative vorticity field around the filament is negative to the north and more strongly positive to the south [*Dewey et al.*,1991].

The offshore jet is much colder than the onshore flow and observations show a strong gradient of temperature in the outer edge of the filaments. This can be explained by downwelling of the cold filament-core waters that would allow the initially cold water to sink below warmer ambient water by the time the surface velocity core has turned back onshore. This dynamics is suggested by *Brink et al.* [1991], who detected convergence zones offshore in the jet and computed an associated downwelling rate of 12 $\mathrm{md}^{-1}$, much of it occurring more than 100 km offshore. *Kadko et al.* [1991], based on biological and chemical tracers, estimated the rate of sinking about 25 $\mathrm{md}^{-1}$. By analysis of phytoplankton layers in the water column, *Washburn et al.* [1991] arrived to the conclusion that there is evidence that some water masses sink over 100 meters as they are advected offshore along the filament jet (though they also found sinking outside the filament). The same authors estimate a vertical volume flux of water being subducted of 5 to 8 $\mathrm{km}^3\mathrm{d}^{-1}$ in the filament studied off the Californian coast.

The physical processes governing the subduction are not established and it remains to be seen whether the subduction is exclusive to the filaments or happens in all the coastal transition zone. A primitive equation model used by *Wang* [1993a] to study frontogenesis, suggests an intense surface subduction ($50 - 100\,\mathrm{md}^{-1}$) in all the frontal

| | subduction rate | study based on |
|---|---|---|
| *Flament et al.* [1985] | $9\,md^{-1}$ | observations |
| *Swenson et al.* [1992] | $> 20\,md^{-1}$ | drifters observations |
| *Brink et al.* [1991] | $12\,md^{-1}$ | drifters observations |
| *Kadko et al.* [1991] | $27\,md^{-1}$ | biological and chemical tracers |
| *Dewey et al.* [1991] | $10 - 40\,md^{-1}$ | microstructure observations |
| *Washburn et al.* [1991] | $6 - 10\,md^{-1}$ | geostrophic calculations on $\sigma_t$ surfaces |
| *Haidvogel et al.* [1991] | $30 - 40\,md^{-1}$ | primitive equations dynamic model |
| *Hofmann et al.* [1991] | $< 6\,md^{-1}$ | numerical model: simulated drifters |

Table 2.1: Some subduction rates of cold filament waters presented in the literature and reference to the type of study of origin.

zone and a similar model used by *Spall* [1995] points towards vertical velocities of $O(30\,\text{md}^{-1})$ associated with frontogenesis.

*Flament et al.* [1985], *Kosro and Huyer* [1986], *Rienecker and Mooers* [1989], *Ramp et al.* [1991], all found strong thermal gradients and convergence of water masses at the southern boundary of the filaments. In a numerical model study, *Onken et al.* [1990] also suggests downwelling in the cyclonic side of the jet, caused by the ageostrophic mass flux across the jet axis. A summary of some subduction rates found in cold filament studies is presented in Table 2.1.

*Strub et al.* [1991] found that the coldest water in a filament is much fresher than coastally upwelled water inshore (southward) of the jet, but is similar to the deeper water slightly farther offshore (northward) in the jet. So they suggest that upwelling occurs locally within the jet, with a source in the fresher water located deeper in the offshore (northern) half of the jet. From momentum analysis of filaments based in a microstructure survey, *Dewey et al.* [1991] found three dominant regions of vertical motion within the filament: a central region coinciding with the horizontal velocity maximum is a region of upwelling with speeds $O\,(10 - 40\,\text{md}^{-1})$ and about 70 meters thick, bounded on either side and below by regions of downwelling. The regions of vertical motion are typically tens of meters thick and tens of kilometres wide.

Some models has been attempted to explain the internal dynamics and structure of the filament features [e.g. *Allen et al.*, 1991; *Haidvogel et al.*, 1991; *Walstad et al.*, 1991]. Although they reproduce appropriate space and time variability, current patterns and speeds, and topographic forcing, they do not match in the scale of the *in situ* upwelling-downwelling features. A mechanism for *in situ* upwelling due to wind blowing along the jet is proposed by *Paduan and Niiler* [1990]. However the observations show upwelling within the jet with the wind blowing in a cross-jet direction [*Strub et al.*, 1991]. The existence of upwelling within the jet is a constant feature of observations, but the mechanism for it is not yet established, and no definite relation between this upwelling and the subduction described earlier has been determined.

### 2.2.3 Large scale variability of the filaments

The occurrence of filaments suggests a close relation with the larger scale circulation and, therefore, a strong seasonal variability. The eastern boundaries of the oceans, in the northern hemisphere, are characterized during the winter by little eddy activity with poleward currents flowing along the coast. Surveys carried out during the winter showed the absence of obvious filament structures. *Kosro et al.* [1991] surveyed the zone off northern California during February, March, May and June. From the two winter cruises the picture that emerges is a coastal transition zone characterized by deep mixed layers, weak horizontal gradients and flat sea level across the transition zone. However, by late spring the upwelling regime yielded low sea level near the coast. The activity increased and the upwelling front meandered widely, with along-front current jets directed toward and away from the coast. Also a survey, carried out during fall, in the coastal transition zone off the Iberian Peninsula showed the absence of temperature fronts and eddy activity [*Haynes and Barton*, 1990]. *Strub et al.*

[1991] demonstrated that eddy variability is seasonally dependent, being substantially stronger in the summer than in the winter with the minimum in late winter and early spring. For the Californian Coast between 37°N and 42°N they noticed a seasonal increase in the range of dynamic height fields from winter–spring to summer–fall.

Satellite estimates of surface temperatures are often used to observe the seasonal distribution and evolution of filaments. *Haynes et al.* [1993] reported that off the western coast of the Iberian Peninsula, where the regime is broadly similar to that observed in the California Current system, the onset of filaments occurs in summer consistent with the upwelling cycle. There, the peak of the development of the filaments is observed to be in late summer, although they become common in early July, but in the initial degree of development. By late October, filaments are already relatively rare. Further, they suggest that on time scales shorter than seasonal, fluctuations in the wind stress have influence on the growth rate of the filaments.

### 2.2.4 Small scale variability of the filaments

The rate of growth and decay of a filament is very variable. However the process takes place between certain temporal limits related to the spatial scale of the feature. In general, the variations in the sea surface temperature structure are not related with the variations in the flow field. It is observed that development and decay of frontal meanders occurs on time scales of a few weeks [*Kosro et al.*, 1991]. *Strub et al.* [1991] suggest that, off California, individual features can grow from 100-150 km to 200-250 km in offshore extent in two weeks or less, and diminish equally quickly, leaving cut-off eddies offshore. *Ramp et al.* [1991] observed small intense filaments come and go on time scales of about 6-10 days, while the surrounding larger filaments persist for a month or so. Strong features, such as offshore jets related to prominent capes, may persist for a month in one position and then reorient in a period of a week or two. *Rienecker and Mooers* [1989] reported that off Point Arena, California, the core of a cold filament migrated about 5 km northward in 14 hours and then 15 km southward in 2 days, although the velocity field was less variable. Even more rapid changes in position, with little variation in the flow structure, were noted in a cold filament off Cape Blanco, Oregon, by *Moum et al.* [1988].

### 2.2.5 Filament formation: conceptual models

During the summer upwelling season an unstable alongshore jet flowing southward is established along the front that separates the warm surface waters of the open ocean from the freshly upwelled waters inshore. It is along this meandering flow and probably as part of it, that the seaward filament structures grow (see Figure 12 of *Strub et al.*, [1991]). Ideas of what causes these filaments have been advanced by several authors, based either on satellite imagery, shipboard studies or numerical and physical models. What cames out of the literature is that it is not only one exclusive process that is involved in the filament's formation and growth, but two or more forcing mechanisms interacting. In general, the flow pattern at the upwelling front is so complicated, that the individual effects of each mechanism may be hard to extract. Coastline perturbations, bottom topography, offshore curl in the surface wind-stress and interaction with the offshore eddy field are among the important factors thought to influence these wind driven coastal currents and fronts.

According to *Haidvogel et al.* [1991], a minimum of four physical factors are necessary to produce phenomenologically realistic filaments as observed in the coastal transition zones: **(1)** a forced equatorward flow at the surface, which in general arises from the wind forcing, but can be a consequence of the larger-scale ocean circulation too, **(2)** a source of cold water along the coast, in general a result of active upwelling, **(3)** finite amplitude bottom topography and **(4)** irregular coastline geometry. The wind forcing, as a forcing mechanism for the coastal jet flow, may be able to precondition the filament formation and development, due to its spatial variability.

A possible physical cause for the formation of the cold filaments is the interaction of the coastal upwelled water with a pre-existing offshore eddy field [*Mooers and Robinson*, 1984; *Rienecker and Mooers*, 1989]. The coupled effect of cyclonic and anticyclonic mesoscale eddies could draw the recently upwelled water seaward, producing surface temperature signatures comparable to the observed filaments. Indeed, data show a good agreement between increasing eddy activity and filament generation [*Strub et al.*, 1991], and the interaction of these eddy fields with the equatorward meandering jet associated with the upwelling season, must play a significant role in determining the structure of the offshore transport [*Ramp et al.*, 1991]. The inspection of satellite infrared images from northern California realized by *Huyer et al.* [1991], reveals a strong eddy-jet interaction, in which the eddy was entraining cold water from the coastal region. However, off Iberia, the observed spatial distribution of the filaments, mostly associated with topographic protuberances, does not match with a purely random interaction expected of the oceanic eddy field [*Haynes et al.*, 1993]. Apart from the offshore eddy field, observations also show the existence of smaller nearshore eddies that could advect the small filaments offshore [see *Ramp et al.*, 1991, fig. 18; *Flament et al.*, 1985; *Huyer and Kosro*, 1987]. Although the origin of these small eddies is not clear, there is some evidence that they move into the shelf from offshore regions [*Huyer et al.*, 1991].

Among other causes, the eddy field could be generated by the interaction of the mean current with the bottom topography or by both the surface wind stress and the variations in the surface wind stress [*Batteen et al.*, 1989]. It is observed that the surface equatorward flow associated with the upwelling is unstable and begins to meander. Disturbances start to grow along the temperature front, and may culminate in detached eddies that are advected offshore. *Ikeda et al.* [1984] argue that the vertical shear between the equatorward surface current and the poleward undercurrent is the energy source that maintains, through baroclinic instability, the growth of the

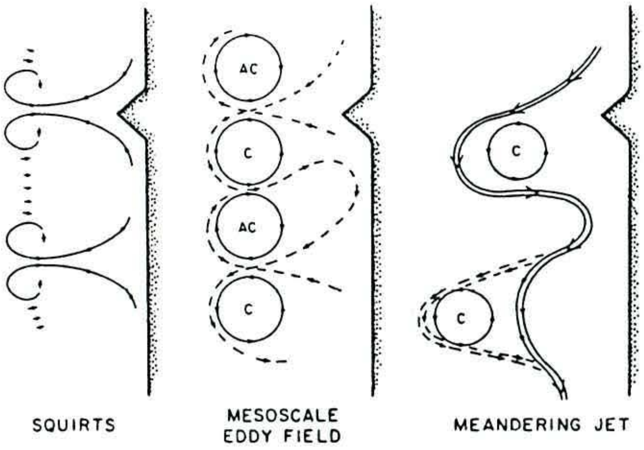

Figure 2.3: Conceptual models for the formation of filament structures [from *Strub et al.*, 1991].

meanders and formation of detached eddies. Off Oregon and northern California, *Ikeda and Emery* [1984] also observed the separation of cold cyclonic eddies from the longer-scale meanders, accompanied by anticyclonic rotations on their northern sides. According to the authors, it is possible that this same baroclinic instability is the main source of energy that feeds the growth of filaments initially excited by the interaction between the mean flow and coastline. In this proposed mechanism for the filament generation, the role attributed to the wind is minimum.

Three conceptual models for the formation of the cold filaments were summarized by *Strub et al.* [1991] (Fig. 2.3):

**(a)** "Squirts" are one-way jets, transporting coastally upwelled water to the open ocean, perhaps terminating in a counterrotating vortex pair, with a "mushroom" or "T" shape in the field of the sea surface temperature. Onshore return flow may occur in both sides of the jet. Possibly "squirts" are induced by topographic irregularities (coastline or shelf) or wind variations in space or time. **(b)** Another conceptual model consists in the pre-existence of a mesoscale eddy field that draws the recently upwelled water offshore in a jet-like flow. The resulting surface temperature pattern is similar to the "squirts" model, but now the energy source is the offshore eddy field, while in the "squirts" model the energy source was the convergence in the nearshore region. **(c)** The last conceptual model consists on the meandering of the equatorward jet associated with the upwelling regime. During its onshore excursion, the jet may entrain coastally upwelled water and create a filament of cold water, which extends offshore on the next meander. On both sides of the jet the formation of eddies is, possible due to instabilities of the flow, but the main source of energy in this model is the jet itself. By continuity considerations, this model requires the presence in the jet of water from father upstream, which is not the case in the other two hypotheses.

The authors argue that the data strongly support the meandering jet model in the coastal transition zone off California, between 39°N and 42°N. Studies conducted by *Ramp et al.* [1991] near Point Arena, off California, show a baroclinic equatorward jet that develops along the upwelling front which at some point begins to meander, but the cause for the meandering is not well established. *Walstad et al.* [1991] identified a jet meander dynamics off northern California, which supports the characterization of the flow field as a meandering jet which gradually propagates offshore. The numerical simulations realized by *Haidvogel et al.* [1991] also address the viability of the meandering jet model, with the topographic forcing playing an important role in the initial excitement of the meanders. The meandering jet concept is now the received view of filament formation off California [*Smith*, 1995]. Analysis of satellite imagery from the coastal transition zone off the Iberian Peninsula, demonstrate that both the "squirts" and meandering jet model are possible models to describe the dynamic processes involved in the filament generation in the region, but do not support the pre-existent eddy field model [*Haynes et al.*, 1993].

### 2.2.6 Topographic forcing

Irregular coastline geometry, in particular the existence of well defined capes, has an important effect on upwelling patterns [*Crépon et al.*, 1984] and, therefore, seems to play an important role in the filament generation mechanism. Dynamical simulations realized by *Haidvogel et al.* [1991] using a primitive equation model showed that the removal of an irregular coastal geometry inhibits the filament formation.

As part of a set of laboratory experiments with a rotating cylindrical tank, *Narimousa and Maxworthy* [1987b] found that the presence of a cape creates a diverging rotary flow just downstream, between the cape and a large amplitude downstream standing wave, which is able to produce thin offshore extending filaments of upwelled water. In this experiment, the upwelling maxima does not occur at the cape as it is suggested by field observations and satellite imagery [*Brink et al.*, 1980; *Kelly*, 1985], but a reasonable agreement between these laboratory results and features seen on the satellite infrared images from the Pacific coast of Baja California is pointed out in a later paper by the same authors [*Narimousa and Maxworthy*, 1989]. The systematic observations of satellite imagery of the Atlantic coast of the Iberian Peninsula over more than 9 years also showed that most of the observed filaments are associated with major topographic features, in particular the large capes [*Haynes et al.*, 1993]. The topographic anchoring of the filament features is also observed in the dynamic simulations performed by *Haidvogel et al.* [1991] with a primitive equation model. Results from observations realized by *Kosro and Huyer* [1986] support the idea that cold tongues and cross-shore current jets occur preferentially at coastal capes and promontories.

The variations in bottom topography are found to play an important role in explaining the observed mesoscale features of the upwelling circulation. *Peffley and O'Brien* [1976] using a wind-driven nonlinear numerical model with nearshore bathymetry characteristic of the Oregon region, concluded that the topographic variations dominate over coastline irregularities in determining the alongshore structure of upwelling. In particular, the upwelling maxima at capes are a result of the interaction between the ridge usually associated with the major capes and the upwelling circulation. This is confirmed by the set of laboratory experiments summarized by *Narimousa and Maxworthy* [1989], where they observed permanent standing plumes or upwelling maxima at ridges, but not at capes.

In general, coastal perturbations produce standing features which tend to dominate the upwelling system. In experiments without any coastline or bottom protuberances a uniform, migrating, upwelled front and associated small scale frontal baroclinic eddies develop at the surface [*Narimousa and Maxworthy*, 1987a]. An empirical criterion to determine the occurrence of instability is the value of a control parameter defined as [*Narimousa and Maxworthy*, 1985]

$$\theta^* = \frac{g' h_o}{u^* f \lambda_s} \tag{2.1}$$

where $g' = g \frac{\Delta\rho}{\rho}$ is the reduced gravity between the upper and lower layer with $\Delta\rho$ the density difference between the layers, $h_o$ is the upper layer depth, $f$ is the Coriolis parameter, $u^*$ is the surface friction velocity at the upwelled front and $\lambda_s$ is the mean with of the upwelled band at surface. At values of $\theta^* < 6$ the upwelled front should became unstable. Higher values of $\theta^*$ corresponds to a larger wavelength of the standing waves, while lower values of $\theta^*$ corresponds to smaller wavelength.

The laboratory model also allowed the prediction of the wavelength of the baroclinic instabilities at the upwelled front, the size of the offshore eddies, the distance downstream from the ridge or cape and the amplitude of the first and the most significant downstream standing wave, and the amplitude of the meander over the ridge. The determination of these parameters is very useful in order to establish the effectiveness of the topographic forcing. Quantitative applications of the relations found in the laboratory to upwelling events off the west coast of North America, Baja California (Mexico) and Peru, are in agreement with those measured from satellite infrared images and with previous field measurements in the case of the coast of Peru [*Narimousa and*

*Maxworthy*, 1989]. The parameters were also in agreement with observed data off the Iberian Peninsula, where some upwelling filaments are produced without an evident direct relation with the capes or ridges [*Haynes et al.*, 1993].

The topographic forcing is a likely mechanism to explain the appearance of upwelling filaments, but hardly can be the only process involved in the growth of such features, with offshore developments of about 200 km.

### 2.2.7 Wind forcing

The upwelling of cold subsurface water at the eastern ocean boundaries is itself a wind-driven process. However, it seems that the influence of the wind forcing is not limited to upwelling generation and the wind stress plays an important role in the development and evolution of coastal mesoscale features such as cold filaments and jets. Based in observations, numerical models and laboratory models, different hypotheses have been presented for the role of the wind, either as the fundamental physical cause of the filament generation, or as a significant modifier of filaments initially excited by other mechanisms.

Numerical model simulations realized by *Batteen et al.* [1989], with steady uniform alongshore winds, a flat bottom and a straight coastline, shows the development of a equatorward coastal jet and a poleward undercurrent that became unstable, resulting in the generation of eddies and jets. If an alongshore variation in the wind stress is introduced, the location of the eddy generation region is restricted. The growth of these features can be fed by the shear between the southward and northward flow, as is suggested by *Ikeda et al.*, [1984]. The alongshore variability of the coastal wind stress could cause locally convergent currents nearshore, which being constrained by the coastline on the inshore side, must necessarily cause offshore flowing currents [*Ramp et al.*, 1991]. This mechanism would generate "squirts" during upwelling events with localized areas of weak wind caused by the presence of large capes [*Huyer and Kosro*, 1987].

Simulations of the effect of the wind stress curl were carried out by *Narimousa and Maxworthy* [1986] in the cylindrical rotating tank, with the introduction of an offshore curl in the surface stress. The experiment showed the formation of eddies that moved offshore, playing an important role in the offshore transport of the upwelled water. In particular, when bottom topography is introduced and the upwelling maximum generated at a ridge interacts with the offshore curl in the wind stress, a variety of offshore extending features develops. However, when *McCreary et al.* [1991] force their $2\frac{1}{2}$ layer numerical model with a seasonal upwelling favourable wind field without curl, the solution is the development of a seasonal upwelling front and jet, that eventually becomes unstable, producing meanders and eddies. Thus, spatially uniform wind forcing alone, without coastal or topographic features, can cause the development of an unstable jet, which moves offshore and develops into a jet and eddy field. It is interesting to notice that the initial stages of the frontal disturbances are small scale features with a finger-like appearance, that grow offshore rapidly, and which compares favourably with observed features off the Iberian Peninsula [*Haynes et al.*, 1993].

It is widely observed that coastal currents respond rapidly to variations of the local wind stress on time scales of days. *Kosro et al.* [1991] report dramatic variations in the sea level due to wind reversals off the northern California coast. Although the wind forcing may not be the mechanism responsible for the initial excitement of the filaments, it is suggested by several authors that it is an important factor in the subsequent evolution of the filaments and the most probable forcing mechanism governing their variability. Observed dramatic reorientation of filament features are in general well related to variations in forcing by the nearshore wind stress and wind stress curl [*Rienecker et al.*, 1987; *Rienecker and Mooers*, 1989; *Washburn et al.*, 1991]. *Flament et al.* [1985] reports that after 4 days of slack wind, the shape of the cold filament under observation changed dramatically: it broke into distinct patches of cold water, frontal instabilities grew and eddies were shed along the southern boundary. The authors suggest that the observed break in the filament may be the result of the interruption in the source of cold water, that fed the filament, during the wind relaxation.

## 2.3 The Coastal transition zone off the Iberian Peninsula

### 2.3.1 Meteorological overview

The location of Portugal on the northern fringe of the subtropical anticyclone belt and on the eastern coast of a large ocean determines most of the climatology and oceanography of its coastal ocean. The seasonal migration of the atmospheric systems at these latitudes seems to be closely related to the evolution of the subtropical front, which separates the mid-latitudes from the tropical air masses.

The wind conditions off the Iberian coast are regulated by the meridional migration of the subtropical front and the seasonal regime of the oceanic semi-permanent high pressure cell of the Açores. During the summer months, the Açores high pressure cell is located in the central Atlantic and the Iceland low diminishes in intensity (Figure 2.4(**right**)). The resulting pressure gradient forces a southward, upwelling favourable, wind pattern along the western coast of Iberia.

During the winter months, the Açores high pressure cell weakens, and frequently migrates southward. The Iceland low pressure cell increase in intensity and is located off the southeastern coast of Greenland (Figure 2.4(**left**)). The resulting pressure gradient forces a mean westerly wind field off Iberia, although this mean winter pattern is modified by energetic transient fronts that cross the Iberia during the winter months.

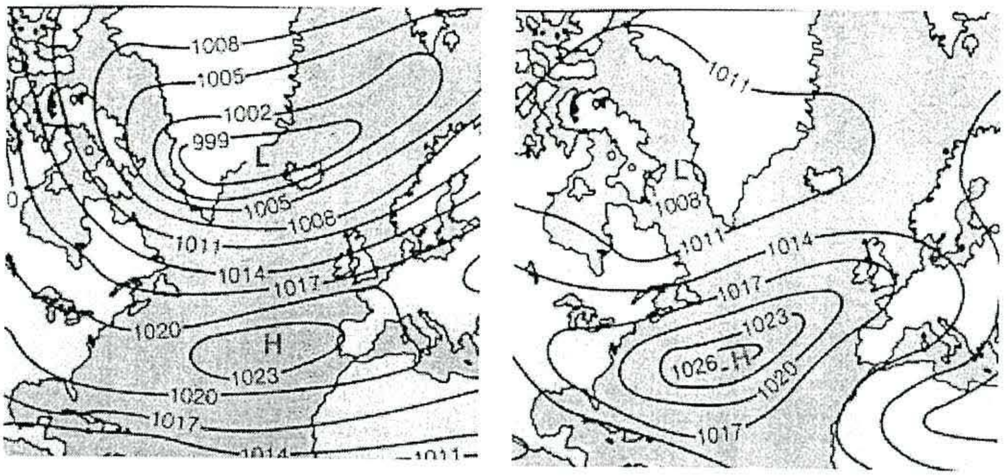

Figure 2.4: Barometric charts showing the typical meteorological pattern of the North Atlantic in (**left**) winter and in (**right**) summer (adapted from *Moran and Morgan* [1994]).

However, the strength of the mean northerly wind field observed during the summer is considerably higher than the westerly mean circulation observed during the winter.

### 2.3.2 Oceanographic structure

The general bathymetry and coastal morphology of the Iberian region is represented in Fig. 2.5. It includes the typical physiographic aspects of the continental shelf, the slope and the rise. The margin is cut in some places by submarine canyons which generally define boundaries between regions with relatively similar bathymetric conditions. North of the Nazaré canyon (39.5°N) the shelf is wide and very flat till the east-west ridge that develops at the latitude of the Cape Finisterra. The shoreline extends almost meridionally up to about 42°N where the coast presents strong indentations (the Galician "rias") until Cape Finisterra. South of Nazaré as far as the Lisbon region, the shelf is more irregular and is dominated by a well pronounced zonal ridge. South of the Setúbal canyon, the shelf is fairly flat up to Cape Sines, but then becomes very steep up to Cape São Vicente, practically without a shelf break. The coastline is again oriented very nearly in the meridional direction. At the latitude of Cape São Vicente a large ridge of minimum depth extends offshore, separated from the continental slope by a deep valley.

The observations from California and the Iberian Peninsula reveal that the basic circulation regime is similar [*Fiúza*, 1982; *Haynes et al.*, 1993]. As an eastern ocean boundary, the coastal transition zone off the Iberian is characterized by a marked seasonality, probably related to the large scale wind climatology. Both satellite imagery and *in situ* observations of the coastal ocean reveal a surface poleward current as a persistent feature of the winter circulation in this region. This structure appears as a warm and saline intrusion (temperature $1-3°C$ and salinity 0.2-0.3 psu higher than surrounding values), within about 50 km of the shelf break, about 200 m to 600 m deep, and flowing poleward along the slope with characteristics velocities of $0.2-0.3\,ms^{-1}$, with transport increasing in the flow direction [*Frouin et al.*, 1990; *Haynes and Barton*, 1990]. The deployment of satellite tracked drifters in the Iberian coastal transition zone during the autumn and winter seasons, reported by *Haynes and Barton* [1991], revealed an inhomogeneous velocity field with eddies of different scales, superimposed on the poleward mean flow.

Possible mechanisms responsible for the generation of this mean flow include density and wind forcing. The geostrophic flow of the northeast Atlantic is directed eastwards in a broad band north of 33°N, where a meridional density gradient, associated with the poleward cooling of the sea surface, is observed in the upper 200-300 meters [*Pollard and Pu*, 1985]. Such a density gradient can force a poleward current which becomes intensified over the slope and which increases northward [*Huthnance*, 1984]. A strong intensification of the Iceland low pressure cell associated with a southward displacement of the Açores high pressure cell results in a wind pattern with a southerly component, particularly in the northern part of the Iberian Peninsula. Such wind pattern can contribute for the generation of the observed winter poleward current off Iberian [*Frouin et al.*, 1990].

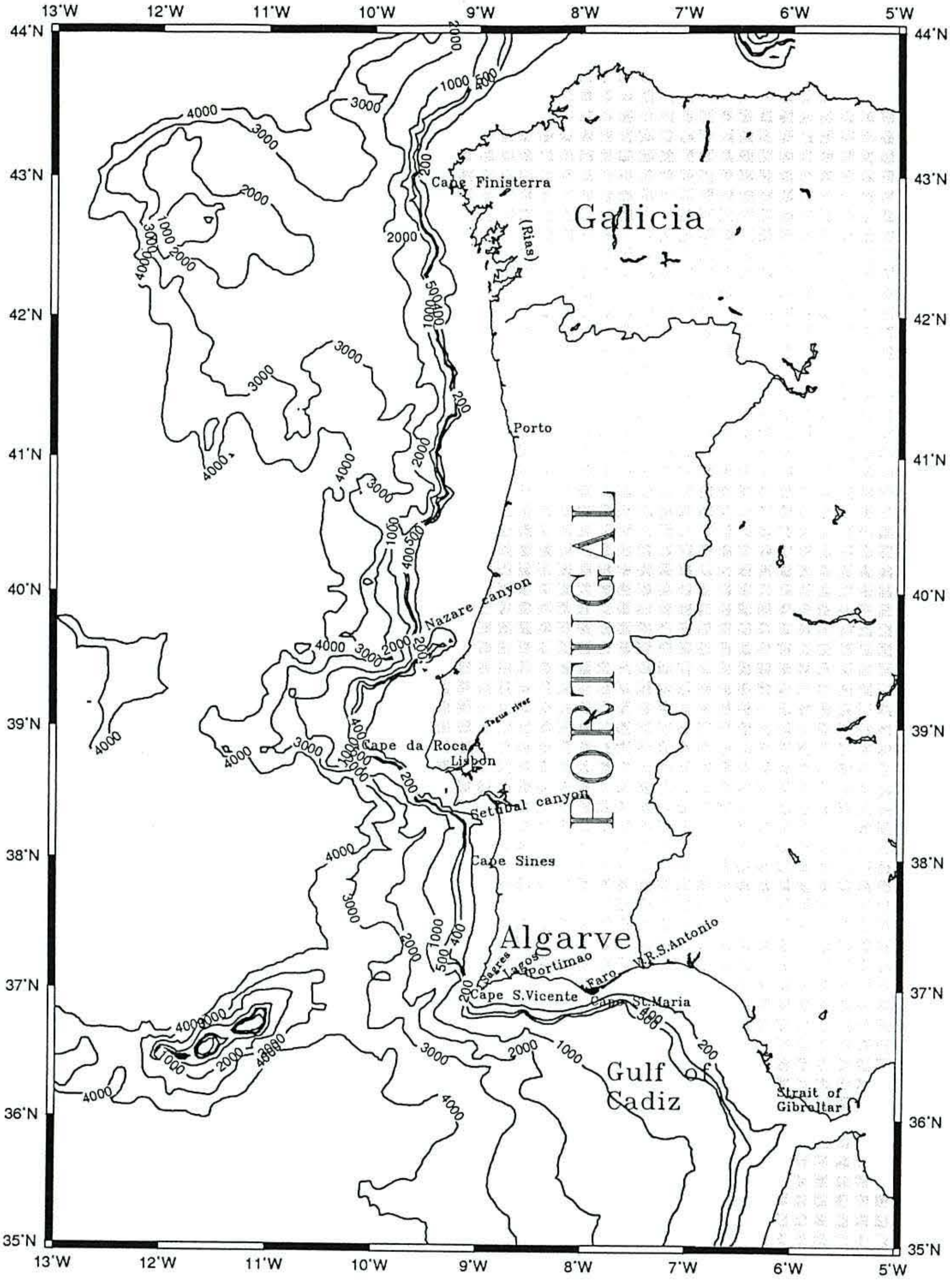

Figure 2.5: General bathymetry and coastal morphology of Iberian region. Bathymetric contours are in meters.

During the summer months a somewhat different picture is observed. The northward progression of the Açores high pressure cell and the weakening of the Iceland low pressure cell both help establish an equatorward wind regime off the western Iberian coast. These northerly winds drive an offshore Ekman transport and force upwelling along the coast. A well defined upwelling season occurs between March and September, with strongest upwelling favourable winds in July and August [*Wooster et al.*, 1976; *Fiúza et al.*, 1982]. Exceptional and brief episodes of nearshore upwelling are occasionally visible in satellite imagery during winter, in response to short-lived episodes of upwelling favourable winds. The Iberian upwelling system appears to respond very fast to northerly winds, particularly south of the capes, appearing first along the coastline and then spreading offshore as the upwelling event progresses [*Fiúza et al.*, 1982]. During the upwelling period, the wind forcing is then opposite to the density forcing. Upwelling causes the surface dynamic height to decrease towards the coast and the resulting equatorward geostrophic current is enough to counter the poleward slope current at and near the surface, establishing a southward flow. However, the deeper waters, below 100-200 meters, still flow poleward as an undercurrent, as indicated by all the observational evidence [*Haynes and Barton*, 1990].

The undercurrent advects northward predominantly waters of subtropical and Mediterranean origin. Below the surface layer, where the seasonal influence is well defined, the waters are typically North Atlantic Central Water or a subdivision termed Eastern North Atlantic Central Water with subtropical origin [*Fiúza*, 1982]. This water reaches the surface in winter and extends down to 500-600 meters. From this level to approximately 1500 meters lies the Mediterranean Water with warm and saline characteristics. A shallow core of Mediterranean Water was detected by *Ambar* [1983] at depths as shallow as 400 meters, or even less, off the southern part of Iberian. This layer represents a continuous northward flow of Mediterranean Water along the Iberian shelf break and slope [*Meincke et al.*, 1975; *Zenk*, 1975; *Ambar and Howe*, 1979]. Observations show that the Mediterranean Water does not flow northward as a simple jet along the continental slope, but it exhibits several isolated eddy structures at middepth within the flow [*Haynes and Barton*, 1990; *Hinrichsen et al.*, 1993].

### 2.3.3 Frontal structure and variability

During the upwelling season a strong temperature front develops along the western coast of Iberian Peninsula, separating the cold water recently upwelled from the offshore oceanic water. The sea surface temperature patterns of the upwelled water seems to be closely related to the bathymetry of the continental shelf and slope and to the coastal morphology [*Fiúza*, 1983]. The front is not uniform along the coast and has a very time varying shape. During periods of weak northerly winds, the upwelled waters reach up to only 30-50 km from the west coast, roughly reaching the 1000 meters depth contour (Fig. 2.5). These cold waters extend further seaward, up to 100 to 200 km from the shore in response to stronger pulses of the upwelling favourable north wind.

Observations have shown that, superimposed on the broader scale, the Iberian coastal transition zone is rich in highly energetic mesoscale features [*Haynes and Barton*, 1991]. In particular, satellite images of the sea surface temperature distribution off Iberian, taken during periods of wind favourable for upwelling, have shown evidence of cold water filaments extending offshore and mesoscale eddies with horizontal dimensions of $O(100 \text{ km})$ [*Fiúza*, 1983; *Haynes et al.*, 1993]. It is observed that these filament structures are features with high phytoplankton pigment concentration [*Sousa and Bricaud*, 1992].

These filaments correspond to the deformation of the upwelling front. Early in the upwelling season, a narrow band of cold water of quite uniform width develops along the western coast of Iberian. The associated temperature front has the shape of a succession of regular finger-like perturbations that extend 20 to 30 km offshore. This pattern is a feature of the early stages of upwelling and filament formation [*Haynes* *et al.*, 1993]. This finger-like perturbations are more frequent north of Cape Espichel (Fig. 2.5). Similar disturbances resembling those reported off Iberia are observed by *McCreary et al.*, [1991] when they force a $2\frac{1}{2}$ layer numerical model with a seasonal upwelling favourable wind field without curl. The larger scale disturbances grow rapidly resulting in filaments.

Based in a long set of satellite infrared imagery taken between 1982 and 1990, *Haynes et al.* [1993] investigated the variability of the Iberian filaments. Five or six well developed filaments were detected along the western Iberian coast. Although the upwelling regime usually starts in late May or early June, the major filaments generally do not start to grow until late July or August. Their full development is observed in September and in late October they became relatively rare. Despite this general cycle, large variations of the spatial and temporal patterns of the filaments are observed in different years. Filaments may persist for up to three months in some years, in others only one month or so and in others they may appear only episodically. The authors argue that the most probable dominant dynamic processes associated with the formation of these filament are related with the topographic forcing. In fact, most of the observed filaments are associated with the major topographic features of the western Iberian coast, in particular the large capes. *Sousa and Bricaud* [1992] also observed that the location of the filaments coincided with topographic features such as submarine ridges. The exceptions are two filaments commonly observed off the northern coast of Portugal. The meandering of the southward flowing current, resulting from the flow instability instigated by the large capes of the northern Spanish coast, is the most probable dominant dynamic process leading to the formation of these filaments.

The results from numerical experiments realized with a primitive equation ocean model by *Batteen et al.* [1992] support the hypothesis that, off the northwest coast of the Iberian Peninsula, the wind forcing is also an important mechanism in the filament generation. A band of steady equatorward winds, which are uniform alongshore but with zonal variability generating an anticyclonic wind stress curl, was used as forcing in the model, simulating the typical wind climatology off Iberia. The result was the setup of a northward surface current offshore and a southward coastal surface current nearshore, leading to the formation of anticyclonic warm core eddies due to a barotropic instability process. Cold water filaments appeared where the circulation of the eddies advected the upwelled water offshore, in a fashion similar to that hypothesized by *Rienecker and Mooers* [1989] for the Californian coast.

It should be noted that to isolate the effects of wind forcing *Batteen et al.* [1992] employed the constraints of a regular, straight coastline and a flat bottom, so the combined effect with other possible forcing mechanisms was not carried out. The forcing mechanisms are not mutually exclusive and the most likely scenario to describe the observations off Iberian are those in which two or more forcing mechanisms interact.

### 2.3.4 The region off the south coast and Cape São Vicente

As it can be seen in Fig. 2.5, the southern coast of Algarve is zonal, except for the protrusion of the Cape Santa Maria area. The whole southern shelf extends with a small inclination down to an extremely sharp edge at about 100-130 meters depth, defined by a sudden step down to the 700 meters contour. This pronounced feature, which is well shown in very detailed charts, extends around the southwest tip of Portugal, reaching about 10 km north of Cape São Vicente. As seen before, the shelf off the western coast of Algarve is very steep and the offshore region is dominated by a pronounced east-west ridge.

During the summer months, the prevailing wind along the western coast of Portugal blows from the north. However, along the southern coast, the summer wind pattern is predominantly from the west. The establishment of a low pressure centre of thermal origin over the Iberian Peninsula during the summer months is largely responsible by the deformation of the near surface wind field, who is compelled to turn eastward over southern Portugal to follow the isobars. The local orography, characterized by a zonal ridge along the Algarve whose maximum altitude ($\approx$900 m) is reached in it western part, may contribute to the observed deformation of the wind field.

The circulation regime off the southern coast of Algarve seems to be predominantly westwards [*Fiúza*, 1983]. At the deeper layers off the continental shelf, the westward circulations transports warm and saline Mediterranean water as an undercurrent or contour current flowing along miscellaneous topographic features such as submarine canyons [*Madelain*, 1970]. After entering the Gulf of Cadiz at depths about 300 meters [*Ochoa and Bray*, 1991], the Mediterranean water splits into several cores flowing westward at different depths [*Zenk*, 1975; *Ambar and Howe*, 1979]. South and southwest of Cape São Vicente the Mediterranean water is observed to be present at depths such as 1200 meters, turning clockwise around Cape São Vicente and being advected northward along the western Portuguese coast [*Meincke et al.*, 1975; *Zenk and Armi*, 1990; *Rhein and Hinrichsen*, 1993]. The presence of eddy features in this region at depths between 1000 and 1500 meters is reported by *Swallow* [1969]. However, a shallow core of the Mediterranean outflow propagates close to the Iberian Peninsula, and follows westward along the southern shelf break off Algarve [see *Zenk*, 1975, fig. 1]. This core, which is distinct and has a warmer signature than the deeper flow, flows at depths as shallow as 400-600 meters and turns northward around Cape São Vicente following along the western continental slope [*Ambar*, 1983; *Ochoa and Bray*, 1991]. The spreading pattern of the Mediterranean water reveals the frequent existence of highly energetic eddies (called meddies) at that level [*Richardson et al*, 1991]. Several areas have been suggested for the meddy generation, among them the Gulf of Cadiz [*Ochoa and Bray*, 1991; *Rhein and Hinrichsen*, 1993]. Possibly the meddies are originated from instability of the Mediterranean undercurrent at the continental slope, triggered and enhanced by the irregularities at middepth of the bottom topography as *e.g.* the canyon near Cape São Vicente [*Käse et al.*, 1989] or the sharp bend of the coastline at Cape São Vicente [*Prater and Sanford*, 1990].

The coastal upper layers off Algarve show a strong variability through the year. During the upwelling events off the western coast of Iberian, forced by cycles of moderate to strong northerly winds, the associated equatorward surface flow of cold waters turns anticlockwise around Cape São Vicente, itself a strong upwelling centre under local northerly winds, and propagates eastward along the continental shelf edge [*Fiúza*, 1983]. The south coast of Algarve, in particular the half west of Cape Santa Maria (Faro), is also directly affected by upwelling events under westerly favourable winds. These winds are usually weaker than the upwelling favourable winds off the western coast and blow only occasionally, more frequently during the late spring/summer season. The intensity and frequency of the upwelling decreases from west to east along the Portuguese south coast, as can be seen by the position of the outer limit of the upwelled waters [see *Fiúza*, 1983, fig. 3]. Under these conditions, the coastal flow along southern Algarve is towards the east, whether it results from an eastward extension around Cape São Vicente of the upwelling associated flow along the western coast or from locally induced upwelling. However, the warmer oceanic waters lying offshore of the Algarve continental shelf flow westward [*Barton*, 1991].

On the boundary between the cold inshore waters, locally upwelled or proceeding from the western coast by turning eastwards around Cape São Vicente, and the warmer offshore waters, there is evidence of wave-like features. *Barton* [1991] observed that these features propagate eastwards along the temperature front, with a phase speed and wavelength that is compatible with the baroclinic instability of the front. The position of the observed disturbances coincide with the edge of the continental shelf, that in this region is very well defined, with a strong bathymetric step of about 500 meters high. Similar disturbances, with the same wavelength ($O(25\text{ km})$), were also observed by *Fiúza* [1982] in a different occasion, developing further east in the same temperature front.

An intriguing feature observed in late summer in this region is also described by *Fiúza* [1982]. A coastal countercurrent seems to carry warm surface waters to the west, progressing close to the Algarve shore, reaching Cape São Vicente and even turning clockwise around it and then flowing northward along the west coast of Portugal. The development of this feature was coincident with a period of very weak winds along the southern coast of Algarve. This counterflow is similar to one observed in the Santa Barbara Channel, south of Point Conception, California [*Harms and Winant*, 1998]. When this counterflow is developing, or during the upwelling spin-down off Algarve, a zonal intrusion of cold upwelled waters extending eastwards remains for some time over the shelf break. This cold tongue is interleaving with warmer waters both inshore and offshore and is linked to the upwelled waters off the western coast. The outer boundary of the cold intrusion is contorted by small cold protrusions, whose scale coincides with those observed by *Barton* [1991] along the temperature front off Algarve. It should be noted that a similar pattern could be achieved by local upwelling generated in the pronounced shelf break, although there is no observational evidence of this mechanism.

At Cape São Vicente itself a large and well developed cold filament is often anchored during the upwelling season [*Haynes et al.*, 1993]. Another filament, with a much smaller scale, is occasionally observed developing from Cape Santa Maria (Faro) during upwelling events in the south coast of Algarve [*Fiúza*, 1982]. Cape São Vicente is even one of the major sites with an associated filament, along all the Iberian coast. Based in a nine years of infrared AVHRR imagery archive, *Haynes et al.* [1993] observed that its maximum offshore extent reaches 250 Km and its common orientation is more toward the south than the filaments observed off the west coast of Iberian. It is sometimes observed even to bend around eastward into the Gulf of Cadiz. The authors suggest that the Cape São Vicente filament, particularly when it has a north south orientation, can be formed as a consequence of the overshooting of the southward coastal flow associated with the upwelling along the western coast of the Iberian Peninsula.

A remarkable pattern of the Cape São Vicente filament was observed in the satellite imagery by *Barton* [1991] in July 1982, when the filament reached its maximum extent ever reported (almost 300 km). The filament presented a mushroom shape with the origin at Cape São Vicente and developing equatorward, probably fed with cold water originating in the coastal upwelling flow along the Atlantic coast. The dipole eddy that constituted the head of the mushroom was about 170 km diameter. On the front separating the dipole pair from the surrounding warmer water, small amplitude wave-like features grew into finger-like protuberances and then evolved into a regularly spaced series of small dipole eddies oriented outwards from the colder water. The scale of these mushroom-like features was about 20 km and they seemed to replicate, in a much smaller scale, the main filament structure. On a large dipole feature observed off Vancouver Island, *Ikeda and Emery* [1984] also report small scale dipole features on the temperature front, with similar shape of the main features.

There are frequent reports of mesoscale dipole eddies observations in literature [e.g. *Simpson and Lynn*, 1990] and some successful attempts to reproduce such features in laboratory models [*Stern and Whitehead*, 1990; *Voropayev et al.*, 1991]. However, the observation of the small scale features, referred above, suggests that these dipole features are not only components of the mesoscale, expressed by the large filaments, but are also part of the smaller scale phenomena.

The Cape São Vicente filament represents a particular case in the filament formation mechanisms, because there the coastline forms a pronounced angle, bending from a meridional coast to a zonal coast. The exact conjunction of forcing mechanisms leading to the observed filament are not known. Also, the small scale horizontal structure, the vertical structure and the internal dynamics of the feature are open questions.

# Chapter 3

# Historical data

## 3.1 Historical hydrographic data and processing

A large scale picture of the hydrographic and flow regimes of the coastal transition region off the southwest tip of the Iberian Peninsula was built based on historical data from the National Oceanographic Data Center (NODC). The data base contains a world-wide set of temperature and salinity profiles taken between 1900 and 1990. A subset of the NODC data base was extracted, corresponding to the region of interest for the present study. The selected area was defined between 35°N and 40°N in latitude and 6°W and 13°W in longitude. Around 3700 profiles of variable depth were found. Profiles falling in the area of influence of the outflow of the two major rivers in the region (Tagus and Sado rivers) were not considered.

A set of Fortran 77 programmes were built to read, process and analyse the original raw data. Data were extracted at depths of 0, 10, 20, 30, 50, 75, 100, 150, 200, 250, 300, 400 and 500 meters. An average of the data between zero and five meters depth was considered for the surface level. For all the other levels an average of the data inside a bin of depth $\pm 10\%$ was considered.

A monthly analysis of the temperature and salinity surface values was done, and the spatial and temporal distribution of the outlying values was analysed. It was decided to erase all profiles with surface values less than 12°C in temperature or less than 34.8 psu in salinity as erroneous.

There are a number of obvious limitations imposed by the coarse spatial and intermittent temporal sampling of the NODC data and the possible aliasing of higher frequency variability in the monthly observations. An analysis of the spatial distribution of the data in every month was performed. Most months showed a density of profiles, within 200 km of the coastline, considered adequate to define the mean monthly fields in the region. The most sparse distributions were found in January, March and December.

For all levels in each month, the values inside cells of 25 km × 25 km were averaged. In this way a regular grid was built for each level, with the nodes centred in the grid cells and the data points representing the average values within each cell. In some regions of the domain, there are some grid cells without data value. The cell averaged values of temperature and salinity were used to calculate the specific density anomaly ($\sigma_t$) from the equation of state of sea-water [*UNESCO*, 1981] using standard algorithms [*Fofonoff and Millard*, 1983]. This processing provided a three dimensional description of the mean monthly fields of temperature, salinity and density for the region off southwest Iberia.

An objective analysis scheme based in the inverse of the distance with a cubic spline smoothing function was applied to the surface data in order to represent the contour lines of the surface hydrographic fields.

## 3.2 Seasonal variations of the surface hydrographic fields

### 3.2.1 Temperature fields

The monthly mean fields of the surface temperature are displayed in Figure 3.1. The mean surface temperatures in the region are representative of the annual heating balance for these latitudes. The lowest temperatures of the year are reached during the winter (January - March) and the highest temperatures during summer and early autumn (August - October).

During the winter and early spring months the surface temperature field is very uniform, with a weak meridional gradient, positive towards the south. An exception appears in March, off southern Iberia, where an almost constant temperature field occurs. The lowest temperature in the study region occurs in the months of December, February and March, north of Cape da Roca. In May warm water appears off the south coast of Iberia.

In the summer months the zonal trend of the isotherms is lost and stronger temperature gradients are observed in the coastal transition zone off southwest Iberia. The isotherms tend to parallel to the coast, and continue around Cape São Vicente. Temperatures are lower close to shore, a direct implication of the seasonal upwelling regime in the region. However, this upwelling pattern of the isotherms does not spread very far eastwards along the south coast of Iberia, in particular in August and September, suggesting that intense upwelling does not extend very far beyond Cape Santa Maria ($\approx 7.9°$W). In July there is evidence of two troughs of colder water directed westward and southward of Cape São Vicente, possibly related to the preferential directions of development of the Cape São Vicente filament [*Haynes et al.*, 1993]. The pattern of the sea surface temperature field observed during the summer remains during autumn but is losing definition and the gradients are getting weaker.

The annual field of the sea surface temperature (Figure 3.2) shows a positive gradient equatorward but the effect of seasonal upwelling is evident, with the isotherms getting a meridional trend close to the continental shelf leaving the colder water inshore.

### 3.2.2 Salinity fields

The monthly mean fields of the surface salinity are displayed in Figure 3.3. Although the data profiles close to the river mouths have been removed from the data set, some influence from the river outflows is still observed in some months. Apart from this influence, surface salinity increases from north to south. The strongest salinity gradients are observed from March till October.

Close to shore around Cape São Vicente, a decrease in surface salinity is observed during spring and summer. For instance, the 36.1 psu isohaline is as far south as Cape São Vicente only from March till September and remains about 100 km north of the Cape during the rest of the year. In early spring the isohalines start to show a meridional trend along the western coast of south Iberia, bending eastwards around Cape São Vicente. As the summer season develops, a more zonal pattern of the salinity field is observed along the south of Portugal, with a region of stronger gradient close to Cape São Vicente. In winter the surface salinity field tend to be more uniform.

The annual mean field of the surface salinity (Figure 3.4) shows an almost zonal pattern increasing southward, with a range of values between 36.0 psu and 36.4 psu. Observed lower values are considered to be the influence of fresh water from the Tagus River.

### 3.2.3 Density fields

The monthly mean fields of the surface density anomaly ($\sigma_t$) show no sign of the zonal trend in the distribution of the surface temperature and salinity (Figure 3.5). Higher

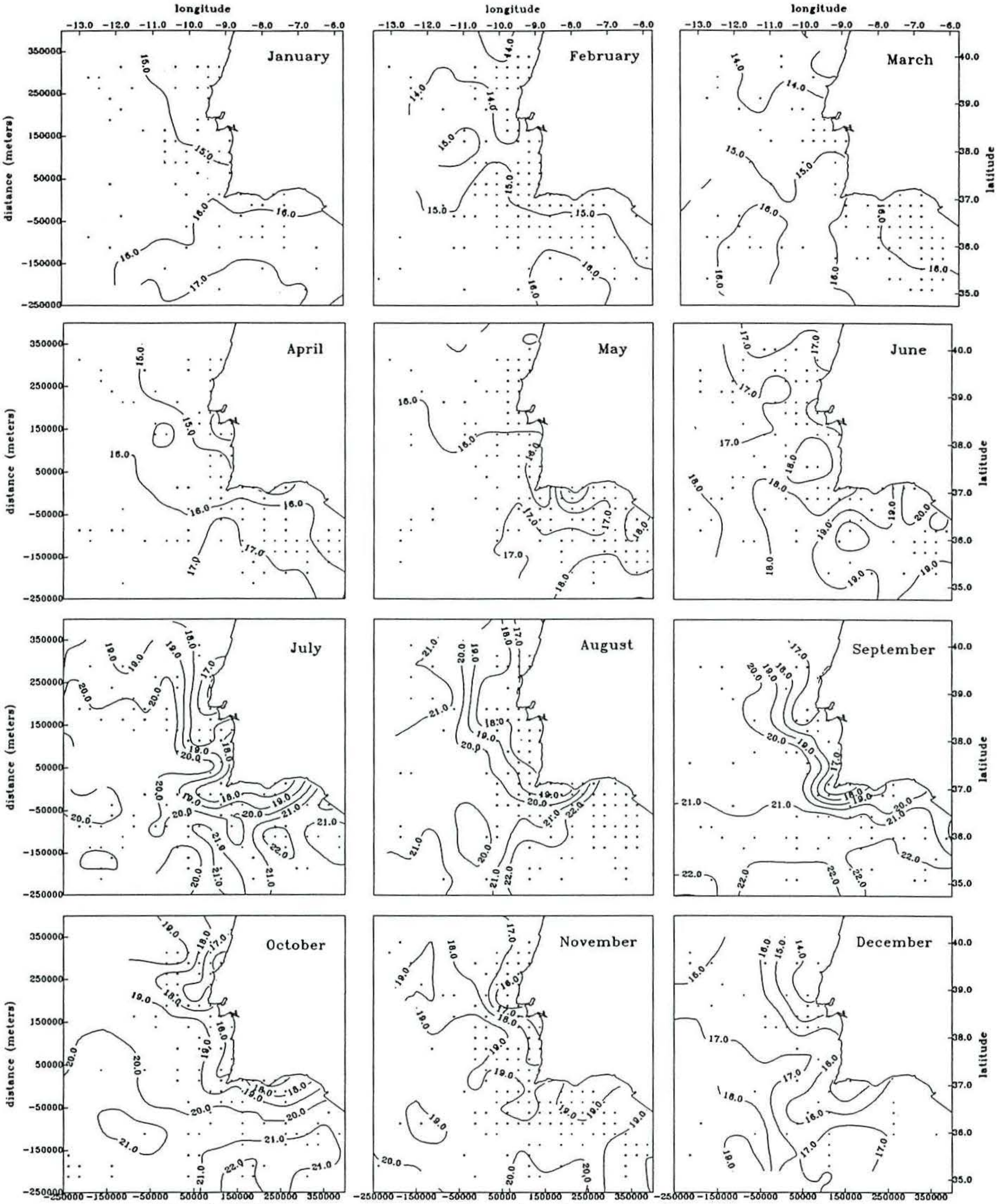

Figure 3.1: Monthly mean fields of sea surface temperature. Dots represent the central point of the grid cells with sea surface temperature value.

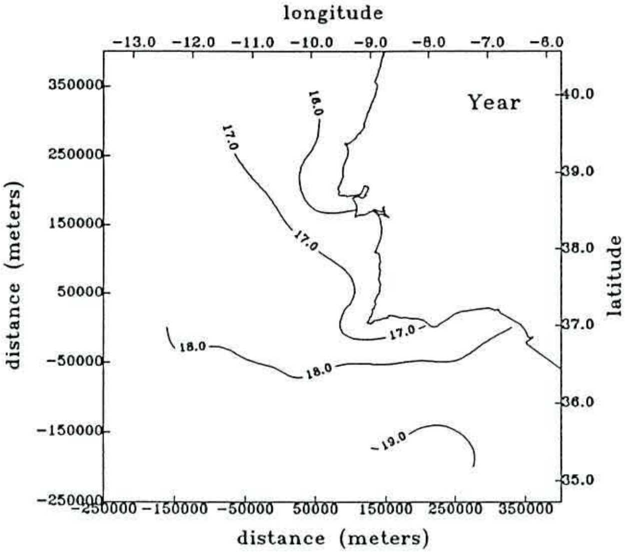

Figure 3.2: Annual mean field of sea surface temperature.

density values in the region are observed in winter and lower values in summer. A marked seasonality is observed in the patterns.

During winter the surface density field is very uniform. The summer season is characterized by stronger gradients and the pattern of the surface density fields follows the pattern of the surface temperature fields, showing that the temperature is the controlling factor. During the summer upwelling season, a positive density gradient is established towards the coast, although the surface temperature and salinity gradients act on the density field in opposite directions. The upwelling signal in the density field is strongest in the coastal region centred on Cape São Vicente.

A particular pattern occurs in May when an intrusion of less dense water is observed coming from east along the south coast of Portugal. A check on the distribution of the original NODC data profiles in May showed that this feature is well sustained by a good concentration of data points in the region.

The mean annual field of the surface density anomaly (Figure 3.6) shows a rather uniform field with a weak meridional gradient and a stronger increase of density towards the coastal regions.

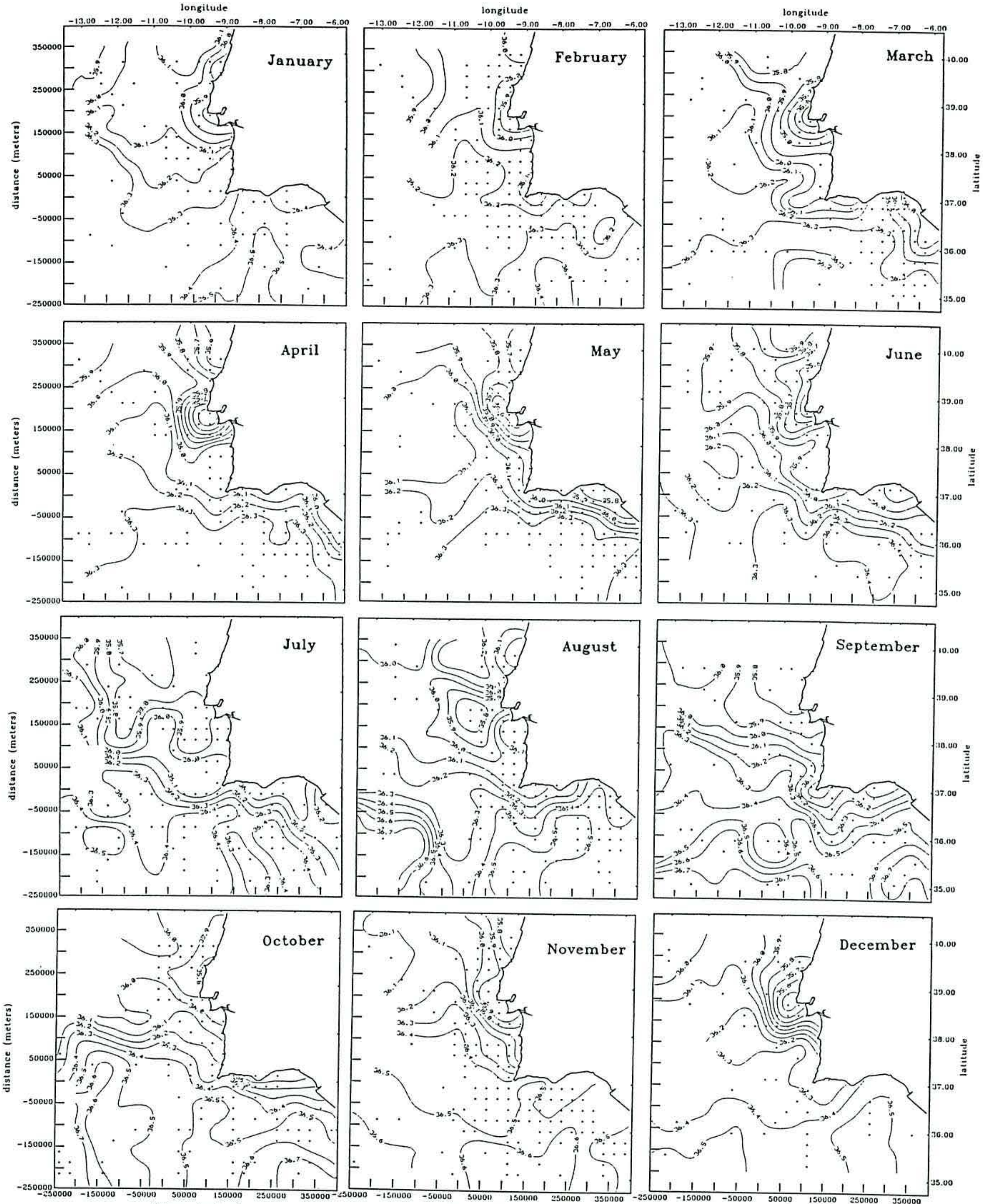

Figure 3.3: Monthly mean fields of surface salinity. Dots represent the central point of the grid cells with surface salinity value.

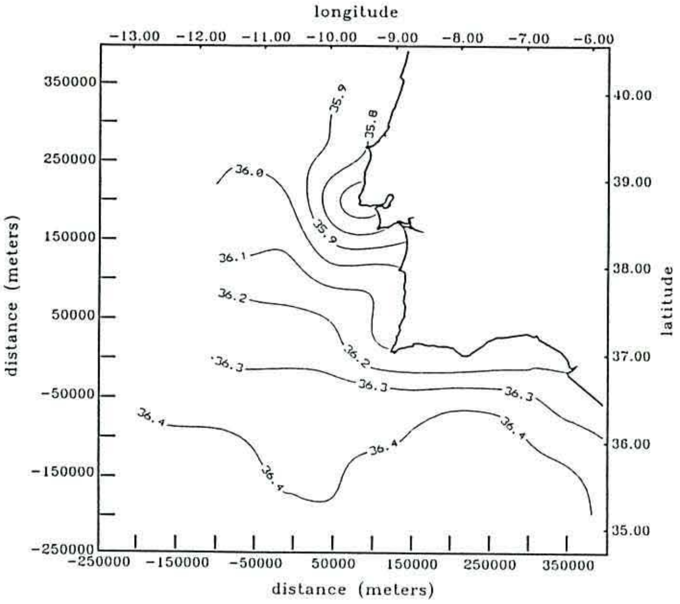

Figure 3.4: Annual mean field of surface salinity.

## 3.3 Seasonal changes in the vertical structure of the temperature

The seasonal changes in the vertical temperature structure were investigated at some nodes. The objective was to compare the seasonal variation of the structure nearshore and offshore, off the western and southern coasts. The selected locations are shown in Figure 3.7, along with the time-versus-depth plots of the temperature at those locations, built with an objective analysis scheme. In all locations the temporal evolution showed the influence of the annual heating cycle. The surface layers show a good stratification during summer, in contrast with the development of a 100 meters thick surface mixed layer during winter.

The offshore locations (P1, P2 and P3) follow clearly the heating cycle, but while in the northernmost location (P1) the maximum surface temperature is reached in July/August, in the southern locations this maximum is reached with a delay of more than one month. The summer build-up and winter destruction of the thermocline is evident in all locations. In the southernmost location (P3) the near-surface temperature has a smoother transition pattern between summer and winter time than in the two

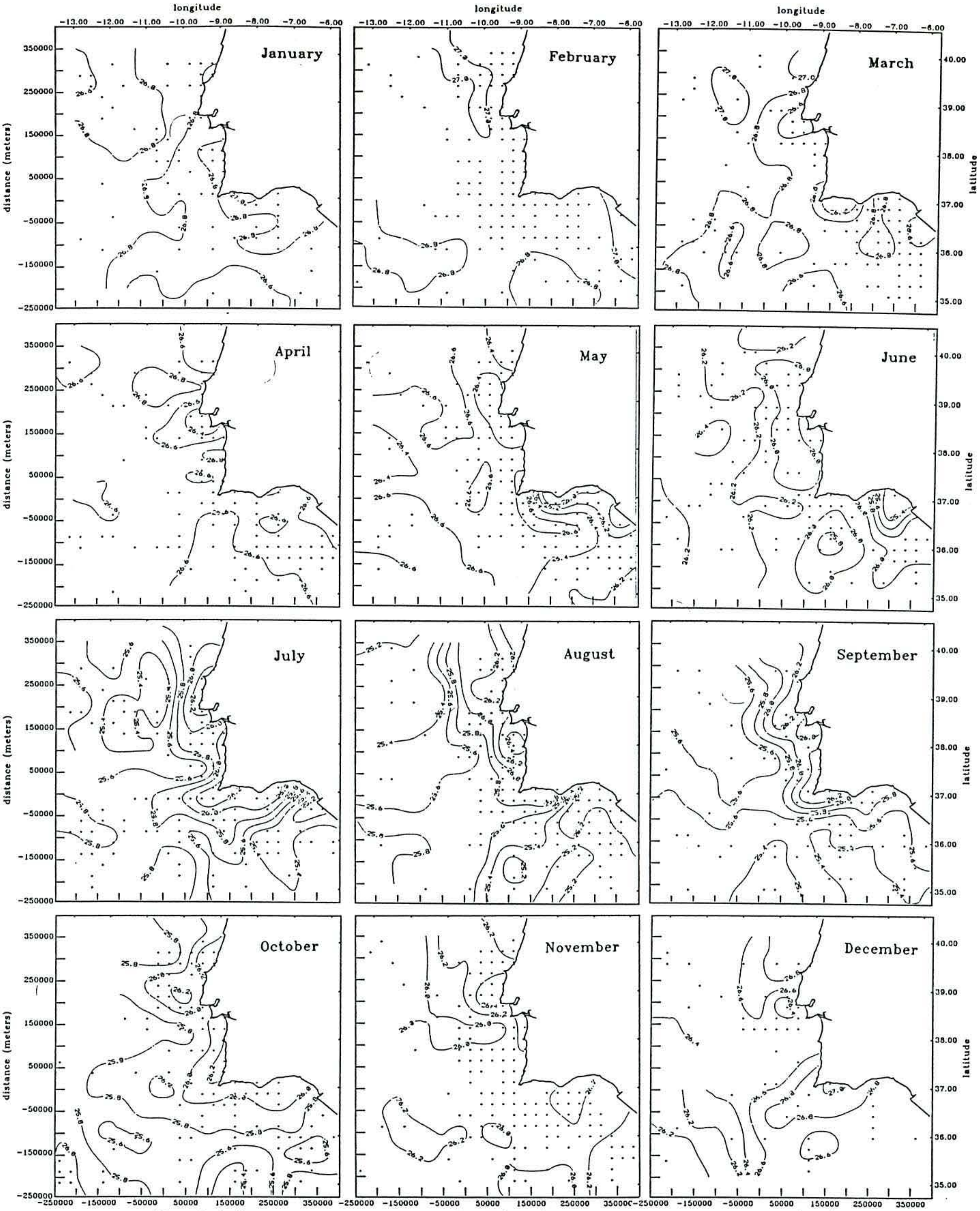

Figure 3.5: Monthly mean fields of surface density anomaly ($\sigma_t$). Dots represent the central point of the grid cells with surface density value.

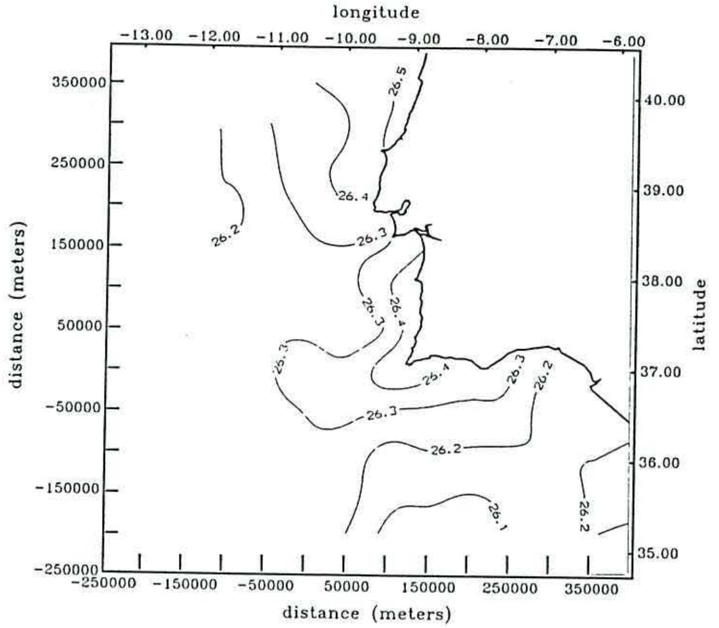

Figure 3.6: Annual mean field of surface density anomaly ($\sigma_t$).

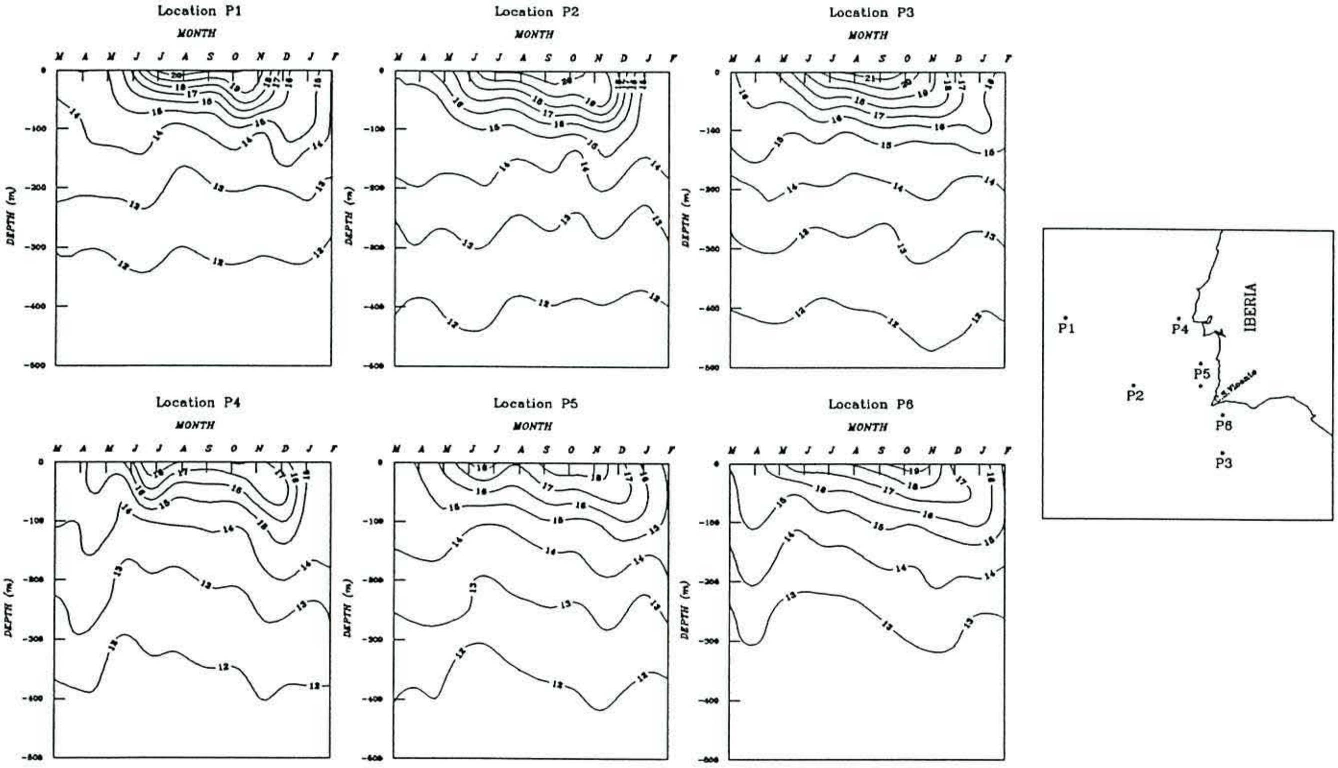

Figure 3.7: Temporal variation in the temperature structure at selected locations off southwest Iberia. Locations are also sketched. The months are indicated only by the first letter.

locations further north, off the western coast. Location P1 shows a stronger summer thermocline than the two southern locations. The sinking of the thermocline in autumn observed in locations P1 and P2, probably associated with the wind regime, is not evident further south in location P3. The subsurface waters are cooler in location P1 than in locations P2 and P3: the 12°C isotherm lies at about 300 meters depth in location P1 and about 400 meters depth at locations P2 and P3.

The nearshore location P4 shows a significantly different pattern from the offshore location at almost the same latitude (P1). During the summer season, the surface waters are colder than offshore and the effect of the coastal upwelling is evident, distorting the annual heating cycle pattern. At this location, upwelling is clearly observed to extend from August to November. This time period is somewhat delayed from the seasonal upwelling period referred in earlier studies for this region, which is from June to October with maximum intensity in August and September [e.g. *Fiuza*, 1982; *Haynes et al.*, 1993].

More equatorward along the coast (location P5), the upwelling signal in the temporal evolution of the thermocline becomes weaker and centred in August. East of Cape São Vicente, the upwelling signal does not appear in the representation (location P6). However the temperature of the surface layers are lower nearshore than at points located directly offshore (P2 off the southern part of the western coast and P3 off the south coast). These patterns suggest a decrease of the upwelling intensity in the southern part of Iberia, weakening even more to the east of Cape São Vicente. The occurrence of upwelling events, both off the western and southern coasts around Cape São Vicente, are reported in previous studies based in observations of AVHRR sea surface temperature satellite images [*Sousa and Bricaud*, 1992; *Haynes et al.*, 1993]. Possibly the short time scale and the intermittent occurrence of the upwelling events in the region, does not allow a typical upwelling pattern to be clearly seen in representations based in mean historical data. Also the 25 km cell is comparable in width to the nearshore upwelling zone.

Nearshore Algarve, at location P6, the warmest sea surface temperature is obtained in October/November, later in the year than was expected if the heating balance were the only forcing mechanism. This feature could be associated possibly with the southeasterly wind events that occur often during this time of the year, mainly off the eastern part of Algarve, leading to a coastal convergence in the region[1].

## 3.4 Dynamic height and circulation patterns

### 3.4.1 Methodology

Each month the surface level of the regular grid of 25 km×25 km show a good spatial distribution of nodes with data values of temperature and salinity. However, many depth levels had a considerable amount of nodes with missing values.

To avoid this difficulty, a sparser grid of 50 km×50 km was derived from the previous existing grid. Only the four closest points from the original grid, within a distance of 100 km from the new grid node, were used to calculate the new data value. A weighting corresponding to the inverse of the distance was used in the interpolation.

A set of vertical profiles of temperature and salinity without gaps, located in the nodes of a grid of 50 km×50 km was obtained. Regions with poor definition in the original grid remain without vertical profiles, but all the profiles have values at all the selected depths. This processing implies the smoothing of the original temperature and salinity fields, but considering the diverse origin of the original data from the NODC data base, the final result still reflects the large scale picture of the region.

---

[1] The southeasterly wind events during Autumn are locally called 'levante' and are well known to the local people. A warming of the seashore waters, a rise in the turbidity of the water and locally rough sea are associated with these events.

Based in the temperature and salinity profiles, the dynamic height (geopotential anomaly) at the surface relative to 500 dbar was computed by employing the standard algorithms recommended by *UNESCO* [1991]. The choice of 500 dbar as the reference surface was dictated by the objective of building a picture of the seasonal flow patterns of the near-surface layers. In the coastal transition regions the physical processes reflected in seasonal pattern changes occur in general above 500 dbar. Below this level, the density changes are negligible compared with those above. Similar references levels have been chosen in the coastal transition zone off California (e.g. *Huyer et al.* [1991]; *Ramp et al.* [1991]). The presence of the Mediterranean outflow in the region does not affect the choice of a reference level because the main cores develop at deeper levels [*Zenk and Armi*, 1990; *Hinrichsen et Al.*, 1993]. The shallowest core of Mediterranean water detected in the region flows close to the continental slope between 400 and 700m [*Ambar*, 1983], but its spatial scale is too small to affect the surface dynamic height pattern relative to 500 dbar in such a large region.

No extrapolation was done into shallow waters, thus, the continental shelf and upper continental slope regions were not considered. Due to the nature of the original NODC data, features with interannual variability, such as eddies, jets and meanders are not expected to appear in the representations. The dynamic height fields computed from this grid tend to be somewhat smoothed versions of the mean fields. The grid spacing used, together with a bidimensional cubic spline function, appears to be a reasonable compromise between spatial resolution and data reliability for the time and space scales of interest in this part of the study.

### 3.4.2 Dynamic topography

The mean fields of the surface geopotential anomaly relative to 500 dbar representative of winter (December/January), early summer (June/July) and late summer (September/October), are displayed, in dynamic meters ($\Delta D_{0/500}/g$), in Figure 3.8. The con-

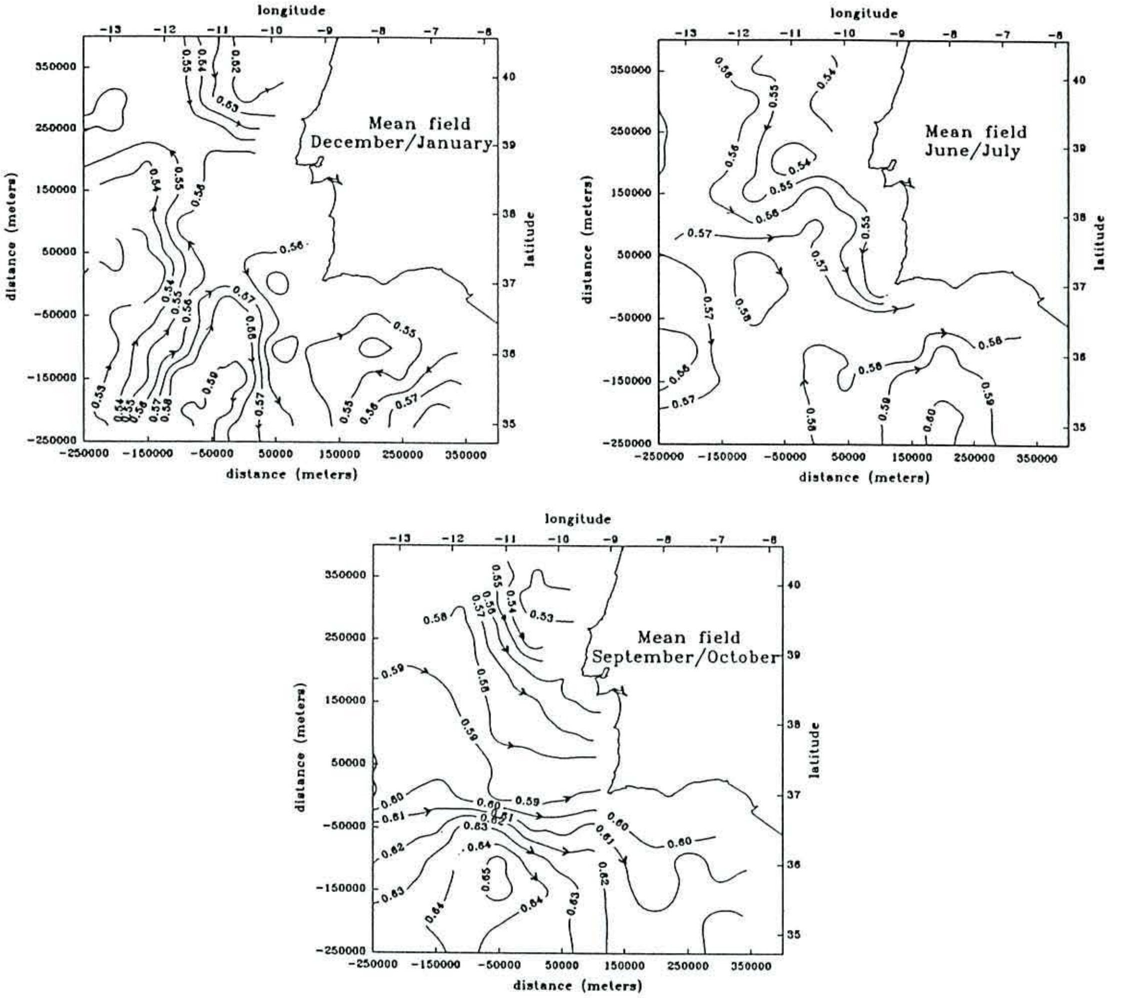

Figure 3.8: Mean dynamic height (in dynamic meters) of the surface relative to 500 dbar for three periods: December/January, June/July and September/October. Contour interval is 0.01 dyn m.

tour maps show, to some degree, the variations in relative strength of near-surface flows. The contours of the geopotential anomaly (dynamic topography) would represent the streamlines of the geostrophic flow, vertically integrated between 500 dbar and the surface, if the velocity at 500 dbar were everywhere zero. The intensity of the geostrophic flow is proportional to the dynamic height gradient, leaving the higher values to the right in the Northern Hemisphere.

The winter pattern is dominated by a northward flow offshore of the southwest tip of Iberia. The bulk of the flow is located about 200-250 km offshore, that means away from the continental slope, and the speeds are of the order of 5 cm/s. Part of this northward flow curves eastward at the latitude of Cape São Vicente and turns southward, still distant from the continental shelf and slope. In the Cape São Vicente region and off the south coast of Algarve the mean dynamic height field is not so organized. In the region the spatial gradients of the dynamic height are smaller, and consequentially weak flows dominate the current pattern. A signal of a southward flow appears in the northern part of the represented region.

The represented poleward flow occurs in a region where the flow field is poorly defined, because few data points in the original data exist in the area (see January/December data points in Figure 3.5). Anyway, this poleward flow cannot be identifiable as the surface poleward current referred in recent works as a characteristic feature of the winter circulation off the western coast of Iberia [*Frouin et al.*, 1990; *Haynes and Barton*, 1990]. These previous works indicate, by direct measurements carried out off the northern half of western Iberia and by satellite imagery, the existence of a warm and salty poleward flow of the order of 50 km in width along the continental shelf and slope, with speeds of about 20 to 30 cm/s. The winter pattern showed in Figure 3.8 reveals a weaker poleward flow further offshore, with some continuity from south, and a direct connection between those two flows cannot be established.

Further to the south of the study region, along the coast of Africa, the Canaries Current flows southward as part of the eastern limb of the anticyclonic North Atlantic subtropical gyre [*Stramma and Siedler*, 1988]. North of this system, the upper ocean circulation is not clearly defined, but most of the results suggest a weak eastward flow [e.g., *Saunders*, 1982; *Pollard and Pu*, 1985]. The geostrophic adjustment of this large scale oceanic zonal flow as it interferes with the continental slope of the western Iberia, can contribute to the poleward flow along Iberia. However, a meridional sea surface tilt may occur along the eastern North Atlantic boundary, providing a significant contribution to a northward regime too. The configuration of the dynamic height field presented here, suggests that the winter circulation regime is northward further offshore and southwest of the continental slope of Iberia, probably as part of the larger scale circulation. Similar winter surface patterns are also observed in the region as results of recent numerical models simulations [*Johnson and Stevens*, 1994; *Neves et al.*, 1996].

A different situation is observed during early summer. The mean dynamic height field show a weak southward flow which intensifies as it reaches the Cape São Vicente region. Apparently the flow turns around the Cape São Vicente and continues eastward. The southward flow off the western coast is a characteristic feature of the summer months in the region, in response to the coastal upwelling regime, forced by the northerly winds dominant during this time of the year. Further offshore off the Cape São Vicente region, the dynamic topography is roughly flat, without any predominant flow. Off the southern coast the dynamic topography pattern suggests a weak flow towards the Gulf of Cadiz.

The early summer dynamic height pattern off the western coast remains in the September/October field, reflecting the permanence of a coastal upwelling regime off the western coast. However, a general rise of the mean dynamic height occur in most of the displayed region. The meridional trend of the isolines of the dynamic topography shown in the northern part of the region is lost as we progress towards the southern region. South of the Cape São Vicente latitude the trend is zonal and is continuous from west to east. The flow is clearly eastward, probably included in the large scale thermohaline circulation of the upper ocean of the Northeast Atlantic Ocean [*Pollard and Pu*, 1985], spreading oceanic surface and subsurface waters into the Gulf of Cadiz. In the Cape São Vicente region, the waters advected equatorward along the western coast merge with the oceanic offshore waters advected from west. A recirculation pattern towards south, similar to those observed in the winter field, appears further offshore, southwest of Cape São Vicente.

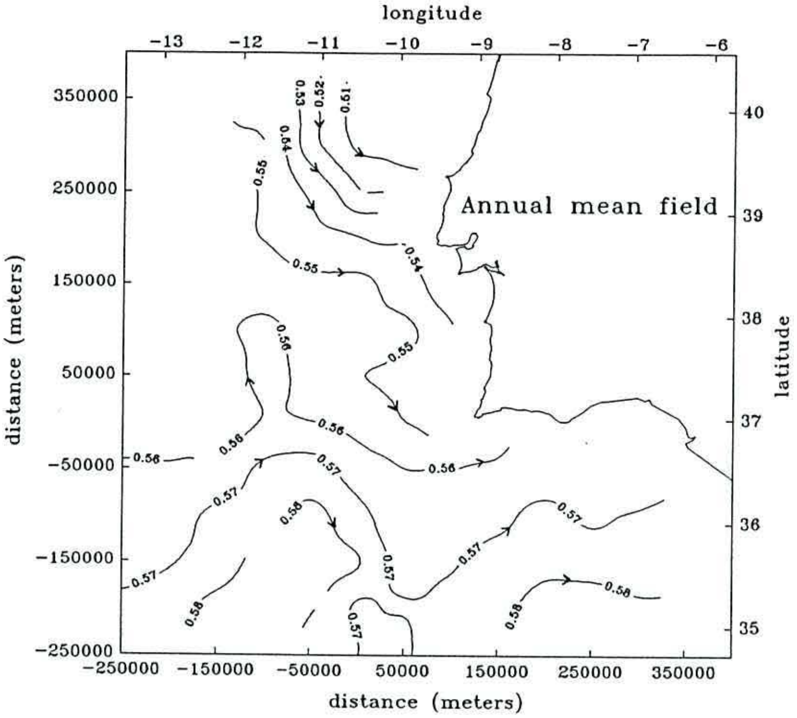

Figure 3.9: Annual mean dynamic height (in dynamic meters) of the surface relative to 500 dbar. Contour interval is 0.01 dyn m.

The annual mean field of the dynamic topography is represented in Figure 3.9. The annual field reflects the main features of the region: a southward flow along the western coast of southern Iberia, and a weak eastward flow south and southwest of Iberia, advecting oceanic waters towards the Gulf of Cadiz. This picture show a good agreement with the previous ideas of the mean circulation pattern of the region.

## 3.5 Summary

Analysis of historical hydrographic data shows that there is a marked seasonality in the surface patterns of the coastal transition region off the southwest tip of the Iberian Peninsula. The definition of the monthly mean surface fields of temperature, salinity and density, based on the NODC data, show relatively uniform fields during the winter season, with an overall positive gradient of temperature and salinity from north to south. The summer is characterized by the appearance of strong horizontal gradients. Although the general meridional gradients are maintained, isolines tend to follow the coastline, turning eastward around the Cape São Vicente, leaving colder and fresher water inshore. Such pattern reveals the establishment of an upwelling regime during the summer, associated with the equatorward winds that prevail during this time of the year along the western coast of Iberia. The configuration of the isolines related to the upwelling regime is not seen to extend far to the east along the southern coast of Iberia.

The seasonal evolution of the near surface vertical structure of the temperature reflects the annual heating cycle, with the seasonal thermocline developing above 50-100 meters depth during summer in contrast with the development of a surface mixed layer of about 100 meters thick during the winter. Evidence of the summer upwelling regime is observed when the evolution of the thermocline in nearshore and offshore locations are compared. Different characteristics of the upwelling regime along the coast are discernible, suggesting the decay of the upwelling intensity, or the occurrence of upwelling episodes with shorter time scales, further south and off the southern coast.

The flow fields suggested by the analysis of the geostrophic circulation relative to 500 dbar show different patterns in winter and summer. The dynamic topography suggests that the circulation is dominated by a northward flow off the western continental shelf in winter, while the summer pattern is characterized by an equatorward flow along the western coast, in response to the coastal upwelling regime. Such flow turns eastward around the Cape São Vicente, and apparently merges with oceanic waters advected from the west by the zonal flow south of the Cape latitude.

# Chapter 4

# Sea level and related variables

## 4.1 Introduction

This part of the study analyses the observed sea level at several sites along the southwest coast of Iberia and its relation to wind and coastal temperature. The analysis is done in terms of mean sea surface conditions and seasonal variation, before examining aspects involving the interannual variability.

Factors contributing to the mean and seasonal sea level elevation include freshwater effluent forcing, atmospheric pressure, evaporation and precipitation, seasonal heating and cooling, wind forcing, and oceanic currents. Any spatial variation of these factors will generate a sea level slope. If the forcing is on very long or seasonal time scales, then a mean or seasonal-varying sea level slope will be established.

Land movement, by changing the position of the recording instrument, affects the sea level height. However, records from Instituto Hidrográfico, the Portuguese institution responsible for the national tide gauge chain, indicate no significant changes during the period of interest. Also short term tidal effects are not considered for the present study.

### Freshwater effluent forcing

Freshwater effects of river inflow alter the density of the near shore waters, thereby affecting the sea level height. The freshwater effluent forcing is a direct function of the river runoff and the way the freshwater plume spreads into the ocean relative to the location of the tide gauge. In mid-latitudes, such as the Iberian Peninsula region, any sea level elevations generated by river effluent are expected to have an extremely time-dependent nature, due to the high variability and high seasonality of the river runoff. In general terms, for these latitudes, a seasonally varying sea level slope might be generated or affected by the freshwater effluents, rather than a permanent mean sea level slope.

### Atmospheric pressure

The atmospheric pressure effect on the sea level results from the downward force on the sea surface due to the mass of the overlying atmosphere. The water can be expected to respond to the local atmospheric pressure changes as an 'inverted barometer', standing at a low level when the atmospheric pressure is high and *vice versa.* This results not from compression of the water, but from a horizontal redistribution of water mass in response to horizontal variations of the atmospheric pressure at the sea level.

The change in sea level, $\Delta h$, in response to a change in the atmospheric pressure at the sea level, $\Delta p$, is given by:

$$\Delta h = -\frac{1}{\rho g} \Delta p \tag{4.1}$$

where $\rho$ is the water density and $g$ is the acceleration of the gravity. With $\Delta p$ expressed in millibars (mbar) and $\Delta h$ expressed in centimetres, the response to an increase of 1 mbar in the atmospheric pressure at sea level, will be a decrease of approximately 1 cm in the sea level (a more precise relation is 1 cm decrease for every rise of 1.005 mbar in atmospheric pressure [*Lizitzin*, 1974]). The term 'adjusted' sea level is commonly used to refer to the sum of tide gauge height plus atmospheric pressure minus a standard atmosphere. This corresponds to removing the effect of the variations of the atmospheric pressure at sea level from the tide gauge records. Although the general applicability of this correction for the whole ocean remains questionable [e.g., *Pattullo et al.*, 1955; *Saur*, 1962; *Roden*, 1965], observations support its validity everywhere, except the tropics and western current extentions [*Wunsch and Stammer*, 1997].

### Evaporation and precipitation

Evaporation and precipitation do not seem to be a strong factor in sea level changes, unless they occur in very localised or enclosed circumstances, which is not the case in the southern Iberia region. The process of evaporation involves a decrease of the total water in the oceans and seas, while precipitation involves an increase. Since the total water masses in the world ocean remain practically unchanged over a prolonged period, evaporation and precipitation (including river discharges) must be in balance. Their significance in sea level variation is not very pronounced and becomes significant only in enclosed or semi-enclosed basins.

### Seasonal heating and cooling cycle

Variations of the long term sea level elevation are related to changes in the density (or specific volume) of the upper ocean. These so called steric sea level changes are mainly determined by the annual heating and cooling cycle associated with seasonal changes in solar insolation, through the induced thermal expansion or contraction of the water column. The steric sea level is high when the water is warm, low when it is cold. Salinity variations make a small contribution to steric sea level changes [*Pattullo et al.*, 1955], due to their small influence on the density determination in the open ocean. Thus, vertical temperature and salinity distributions are enough to compute the steric sea level and to estimate the relative sea level height in the open ocean.

### Wind forcing

Wind forcing is one of the most important factors determining sea level changes on a variety of scales. The direct effect of wind stress upon the sea surface produces short period, short spatial scale variations of sea level, such as surface waves and oscillations generated by transient winds which are associated with rapidly moving storm formations. However, due to their short time scale, these events are not significant for the determination of the mean and seasonal sea level changes.

Significant sea level changes occur through dynamical effects of the wind stress due to the induced Ekman transport. This mechanism is very efficient in coastal regions (where tide gauges usually are): Alongshore wind regimes in the northern hemisphere, blowing with the coastline on the left hand side (upwelling conditions), will result in an offshore transport of surface waters and a consequent vertical transport of colder subsurface water at the coast, in order to conserve mass. The upwelled water, being more dense, replaces a smaller volume than the original water, and therefore a drop in the sea level height at the coast will take place. Conversely, an alongshore wind regime blowing with the coast at the right hand side (downwelling conditions) will lead to a sea level rise, due to the onshore transport in the surface waters. In coastal upwelling regions, sea level depends seasonally on the magnitude of the alongshore component of the wind [*Hickey*, 1975].

Propagation of the upwelling or downwelling responses, and associated sea level disturbances, by coastal waves into regions where the local wind is not upwelling or downwelling favourable, is an effective mechanism for sea level changes. However, the relatively short time-scale of those events (several days) should allow a great reduction of its effect on mean and seasonal sea level height by low-pass filtering the data.

## Oceanic currents

Dynamical effects of geostrophic currents contribute largely to the sea level height. Geostrophic motion results from the balance between the Coriolis force and the pressure gradient force. Both forces act perpendicularly to the direction of the current. With $x$ aligned in a right angle to the right of the direction of the geostrophic velocity $v_g$, the balance is written as:

$$f v_g = \frac{1}{\rho} \frac{\partial p}{\partial x} \tag{4.2}$$

where $f$ is the Coriolis parameter, $\rho$ is the water density and $p$ is the total pressure. Applying the hydrostatic equilibrium, $\partial p = \rho g \partial h$, where $p$ is the pressure in the water column due to the elevation $h$, the cross-stream sea level slope is written as:

$$\frac{\partial h}{\partial x} = \frac{f v_{gs}}{g} \tag{4.3}$$

where $v_{gs}$ is the geostrophic velocity at sea surface. Thus, the sea level height slope is proportional to the velocity of the near surface geostrophic flow, which flows in the northern hemisphere with the higher sea level on its right hand side.

In coastal regions, nearshore geostrophic currents would provoke a coastal sea level rise when the flow increases in the northward sense (a drop when decreases) with the coast on the right hand side, and a drop when the flow increases (a rise when decreases) with the coast on the left hand side. Therefore, geostrophic current variations will be associated with signals in tide gauge records that would affect the mean or seasonal sea level elevation.

## 4.2 Seasonal cycle of the sea level in the Eastern North Atlantic

Generally, the dominant signal observed in low-frequency time series of sea level height is a seasonal cycle. The nature of the seasonal cycle varies with geographic location, but generally (with exceptions) has an annual period. Sea level is generally lower in spring and higher in autumn [*Pattullo et al.*, 1955].

Along the Atlantic European coasts, sea level data records have shown that the seasonal variations are fairly regular. Maximum sea level is observed in Atlantic European waters during the latter part of the year, and there is a retardation of the occurrence of the maximum when progressing from the south towards the north [*Lisitzin*, 1974]. Mean monthly data of recorded sea level height presented by *Pattullo et al.* [1955] show for the Iberian Peninsula, the high sea level in October and the low sea level in February. Further south, in the Canarian Island region, the high sea level occurs in August/September and the low sea level occurs in February/March [*Navarro-Pérez*, 1996].

## 4.3 Data and processing

### 4.3.1 Sea level data

Sea level data recorded hourly at four tide-gauges along the southwest coast of Iberia were obtained from Instituto Hidrográfico, Lisbon, the Portuguese national office responsible for the operation and maintenance of the tide-gauge national chain and the correspondent data acquisition and validation. The tide-gauges are located at Sines, in the western coast, and at Lagos, Faro and V.R.S. António, along the southern coast. The Lagos tide gauge is a GLOSS (Global Sea Level Observation System) station. According to Instituto Hidrográfico (personal communication) Sines is a recent tide gauge and one of the most reliable of the national net. The V.R.S. António records

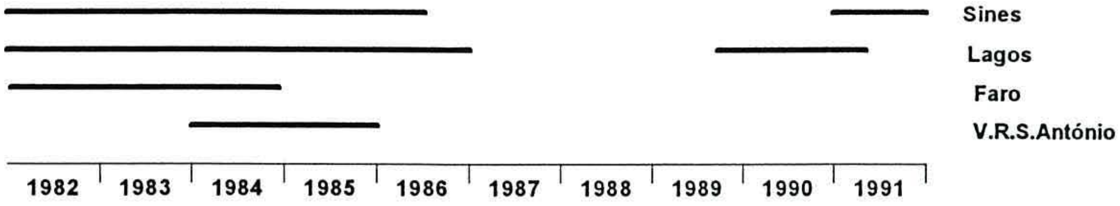

Figure 4.1: Duration of the available tide gauge time series.

correspond to a temporary installation of a tide gauge device and the data were checked and validated. Faro records are raw data that were made available without validation.

The sea level time series provided represent all the available tide gauge data for the region in the Instituto Hidrográfico data base, between January 1982 and December 1991. Unfortunately, none of the tide gauges provided a complete ten years time series. Apart from small gaps, the duration of the sea level time series is shown in Figure 4.1. Faro tide gauge has three consecutive years of records, but the time series showed a significant drift in the records, probably due to malfunction of the device. The data set was not suitable for seasonal and mean analysis of sea level height, but could be a relevant source of information for short term analysis.

The raw hourly data time series were split into sets without gaps and filtered to eliminate tidal and higher frequencies by means of a Cosine-Lanczos low-pass filter with half power point at 40 hours (0.6 cpd) spanning 121 hours. The time series data were then resampled at six hour intervals and small gaps in the data, typically less than ten days, were filled with linearly interpolated data.

Standard procedures of the Instituto Hidrográfico include the inspection of the tide gauge levelling. All tide gauges of the national net are levelled with a maximum error of 0.5 cm (personal communication from Instituto Hidrográfico), and all departures are referred to the national hydrographic zero. The hydrographic zero was defined by the Instituto Hidrográfico as the reference level for the tide gauge records and is located two meters below the benchmark established for the country, in such a way that it is below the lowest computed astronomic tide [*Instituto Hidrográfico*, 1996].

### Atmospheric pressure adjustment

Available records of atmospheric pressure at Sines, Sagres and Faro, corresponding to the ten years period of the sea level time series (1980-1991) were obtained from the Instituto de Meteorologia, Lisbon. Sines station is located on the west coast at an altitude of 16 meters, Sagres station is located on the Cape São Vicente cliffs, the intersection point of the western and southern coasts, at an altitude of 38 meters and Faro station is located on the seashore on the south coast, at an altitude of 9 meters. All the altitudes are referred to the mean sea level. A reduction to the mean sea level of all the atmospheric pressure data was done using the hydrostatic equilibrium for a standard atmosphere ($\partial p/\partial z = -\rho g$, giving 1mbar $\approx$ 8m in altitude).

A visual inspection of the time-varying plots of the atmospheric pressure raw data (not presented here) of all locations, revealed that the absolute values are almost the same in all the three meteorological stations, and that atmospheric pressure variations are basically the same at all stations even for high frequencies. Thus, atmospheric pressure should not affect sea level differences between tide gauges, but could have some influence in the definition of the seasonal cycles, because larger amplitude variations of the atmospheric pressure occurs in winter time, associated with the transient atmospheric fronts that cross the Iberian Peninsula during that time of the year.

The atmospheric pressure time series were then demeaned with the mean atmospheric pressure of the period 1960-1989 at each meteorological station, reduced to the mean sea level. The low passed sea level time series were then combined with the contemporaneous atmospheric pressure residuals of the nearest meteorological station. Distance between the tide gauge and the meteorological station was never larger than 100km.

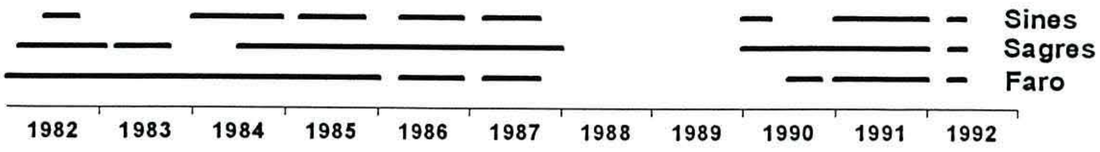

Figure 4.2: Duration of the available wind time series.

### 4.3.2 Wind data

By courtesy of the Instituto de Meteorologia, at Lisbon, wind data during a ten years period, between 1982 and 1991, at three different meteorological stations along the southwest coasts of Iberia (Sines, Sagres and Faro) were made available. The location of the meteorological stations is the same as described for the atmospheric pressure data.

The duration of the time series are displayed in Figure 4.2 and reveal a considerable amount of gaps, with no data recorded during 1988 and 1989 at any location. The original data were recorded every hour at Faro, every three hours at Sagres and every day at Sines.

### 4.3.3 Sea surface temperature data

Daily nearshore surface temperature at three locations along the southwest tip of the Iberian Peninsula was also provided by the Instituto de Meteorologia, Lisbon. The locations correspond to Sines, on the western coast, Portimão, on the western part of the south coast, and Faro, on the south coast about 80km further east. Time series cover also the period between 1982 and 1991. The duration of the coastal temperature time series is shown in Figure 4.3. Small gaps were filled with interpolated values.

Daily data were collected directly from the seashore, in shallow water, at nine o'clock every morning, in order to avoid the effect of the daily heating cycle. Despite

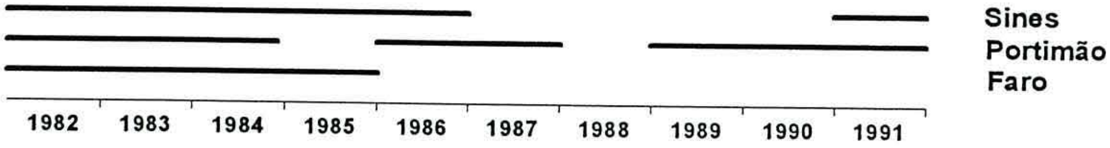

Figure 4.3: Duration of the available nearshore sea surface temperature time series.

the rudimentary procedure on the collection of these data, they should provide relevant information about the annual heating and cooling cycle at different locations.

## 4.4 Seasonal and interannual variability

### 4.4.1 Wind pattern

The long-term average for each calendar month over the entire multiyear time series was calculated in order to obtain the 'mean year' during the period of the wind measurements. These average monthly curves at Sines, Sagres and Faro are displayed for each component in Figure 4.4, along with the observed maximum and minimum monthly values in the time series. Error bars for the monthly standard deviation are also displayed, representing the variability with time scales less than a month. Alongshore winds are represented by the meridional component (V) in Sines and Sagres, in the western coast, and by the zonal component (U) in Faro, in the southern coast. Positive values are towards north and east.

Along the western coast, the alongshore is predominantly from the north, upwelling favourable, through most of the year. This northerly wind regime is weak in winter and reveals an intensification during the summer season, in particular in the southernmost station (Sagres). The wind regime in the southern coast show a different pattern. The wind is predominantly zonal blowing from the west, upwelling favourable, during the summer season. This different summer wind pattern observed in western and southern coast is mainly due to the establishment of a thermal low pressure centre

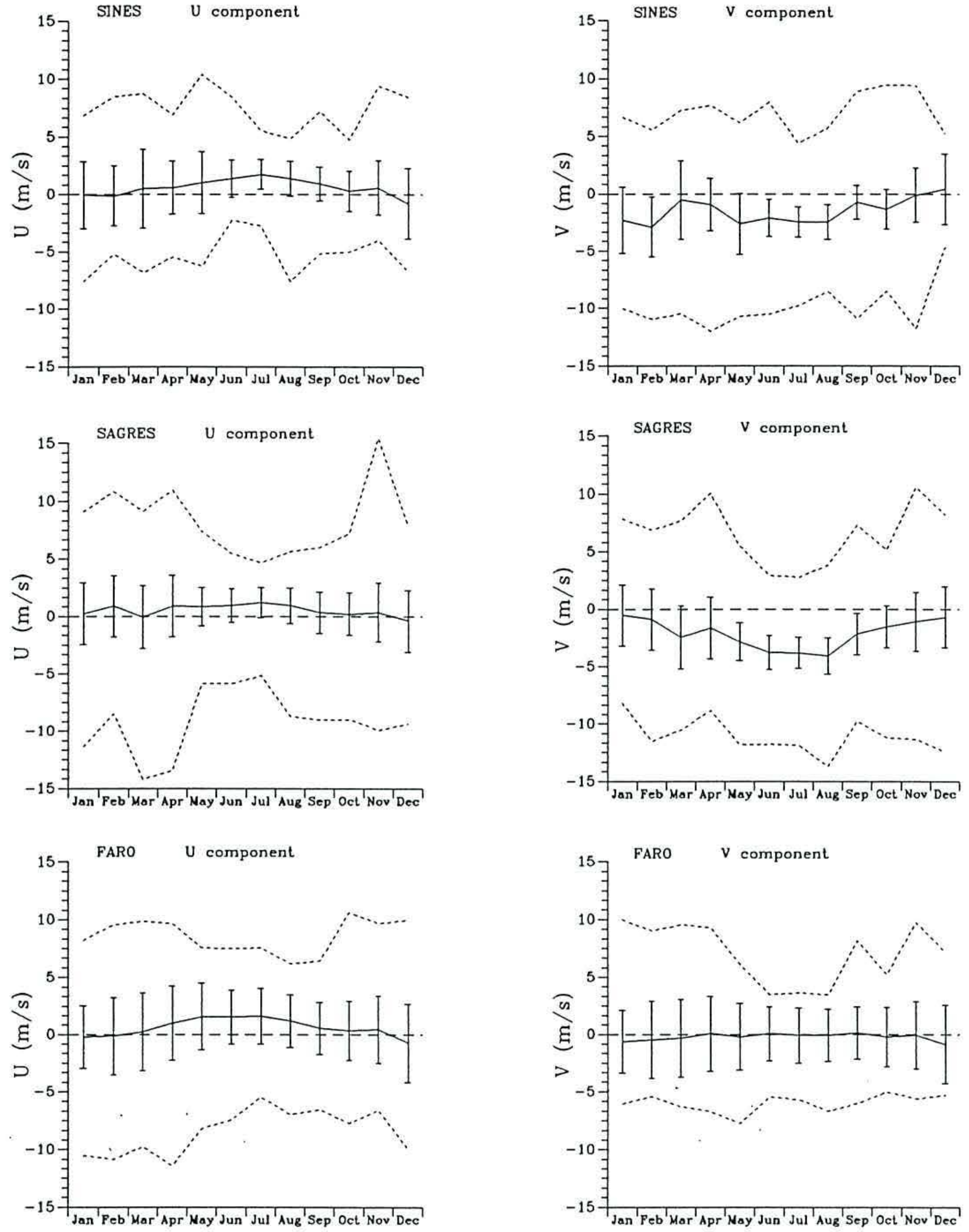

Figure 4.4: Average monthly curves for zonal and meridional wind at Sines, Sagres and Faro (solid line). Dashed lines represent the maximum and minimum wind velocities observed each month and error bars represent the standard deviation within each month. Positive values are towards north and east.

over the Iberian peninsula during the summer, forcing the geostrophic winds to curve eastward along the southern coast following the pressure field. The rising orography of the Algarve also contributes to deform zonally the wind field. However, the upwelling favourable mean winds are stronger in the western coast than in the southern coast. Also, the standard deviations of the summer months wind measurements are smaller at the western coast than at the southern coast, showing a smaller variability of the upwelling favourable wind regime during the summer off the western coast when compared to the southern coast. The winter regime is characterized by weak average monthly winds. However, the strongest winds (maximum and minimum envelop curves in Figure 4.4) occur in winter. Also the highest monthly standard deviations of the alongshore wind are observed in winter, due to the atmospheric fronts that cross the region during this season.

In order to visualize the interannual variability of the wind time series at each location, a recursive Butterworth digital filter working in the frequency domain [*Hamming*, 1983] was built, and the wind data were low-passed to eliminate periods less than 60 days. The applied filtering retains the year to year variability but makes the time series less dominated by single events, making the seasonal nature of the data more evident. The filtered time series of the zonal and meridional wind at Sines, Sagres and Faro are displayed in Figure 4.5.

The seasonal nature of the alongshore wind component time series is evident at Sagres. The summer of 1982 was marked by anomalously strong northerly winds. The Sines time series does not allow a comprehensive picture of the seasonal nature because the time series are interrupted. Intermittent periods of weak wind reversal to southerly are observed during the winter along the western coast. The seasonal nature of the alongshore wind component in the southern coast, represented by the Faro station, is less apparent than in the western coast. Year to year variability is higher there even for

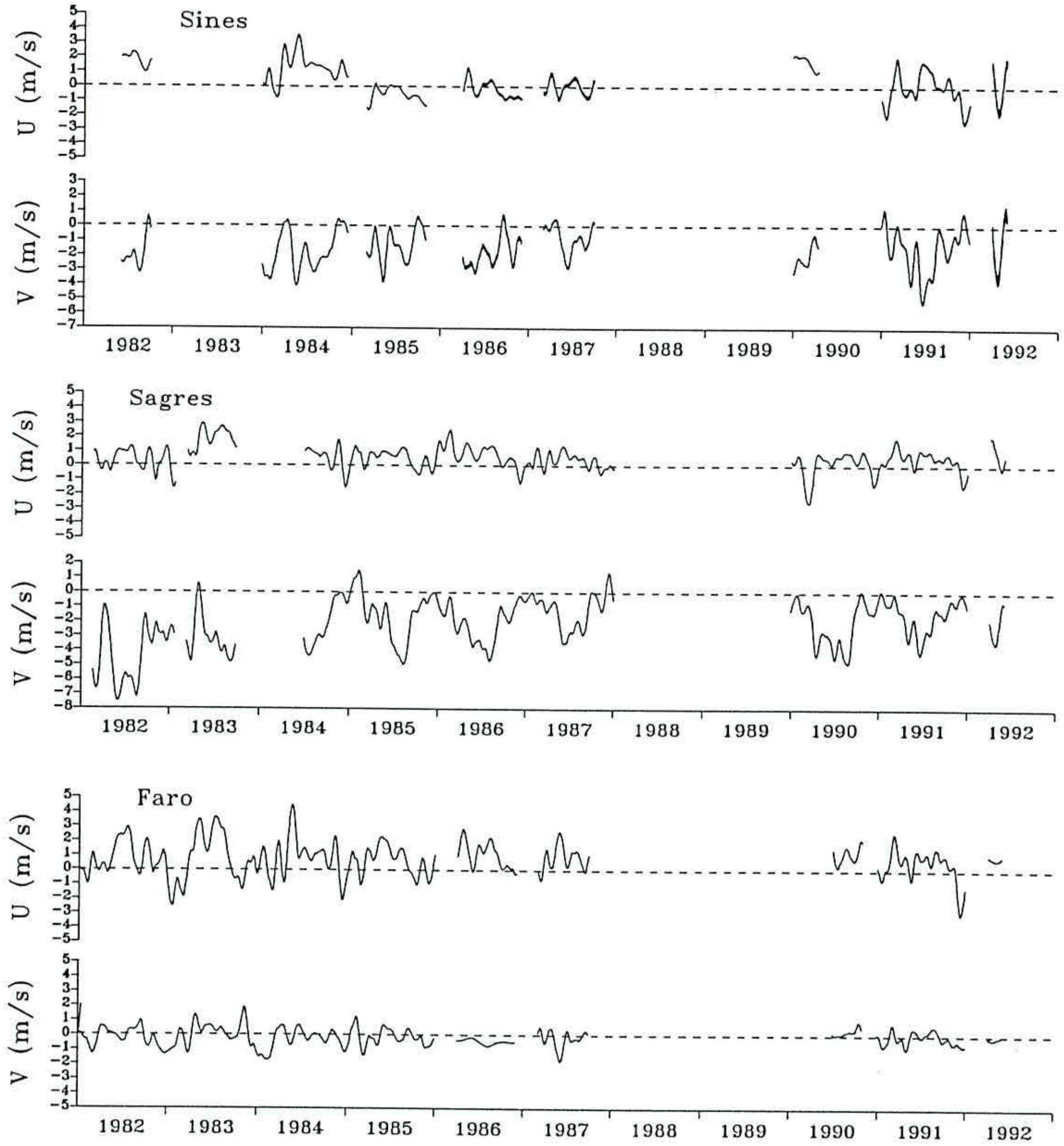

Figure 4.5: 60 days low-pass-filtered wind time series at Sine, Sagres and Faro. Positive values are towards north and east.

these time scales with periods more than two months. Upwelling unfavourable winds are observed in the winter season.

The different patterns of the upwelling favourable winds in the western and southern coasts suggest some differences in the upwelling regimes of the two coasts. Conditions for upwelling intensification and maintenance appear to be more characteristic of the western coast, while in the southern coast upwelling seems to be a more transient phenomena. On both western and southern coasts, the winter wind pattern is unfavourable to the establishment of an upwelling regime, even showing downwelling conditions dur-

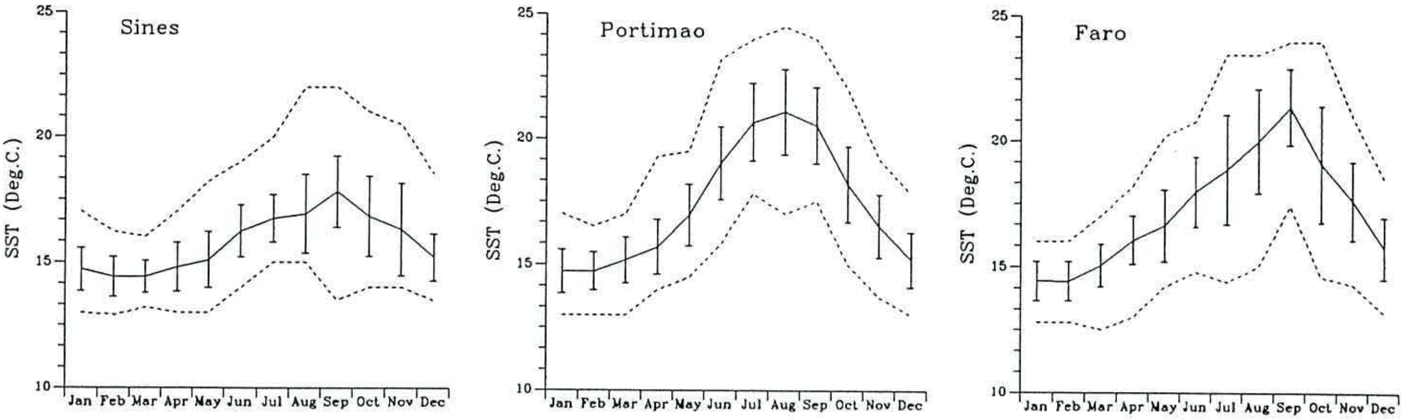

Figure 4.6: Average monthly cycles of the coastal sea surface temperature at Sines, Portimão and Faro (solid line). Dashed lines represent the maximum and minimum temperatures observed each month and error bars represent the standard deviation within each month.

ing some periods. This does not mean that short upwelling events, limited in time, do not occur on both coasts in winter, since short events are masked by the lowpass filtering applied.

### 4.4.2 Surface temperature pattern

The seasonal cycle of the nearshore sea surface temperature at Sines, Portimão and Faro, was calculated by computing the long-term average for each calendar month over the entire time series. These average monthly curves are displayed in Figure 4.6, along with error bars for the monthly standard deviations and dashed lines for the observed maximun and minimum temperatures observed each month in the entire time series.

In this set, Sines is the only station in the western coast, and reveals a relatively low amplitude in the annual cycle. High amplitudes are observed in Portimão and Faro. The range of maximum monthly mean temperatures is greater than that of minimum monthly mean temperatures, thus the different amplitudes of the annual cycles are due mainly to the maximum monthly mean temperatures. However, the plots show that the heating and cooling annual cycles are in phase in all the three locations. The maximum monthly mean coastal temperatures are reached in late summer (August/September) and the minimum in winter (January/February). The larger values of the monthly standard deviation occur in the summer months, indicating a higher variability of the coastal temperature with time scales less than one month during the months of more active upwelling. During the summer season, the average monthly curve and standard deviations are closer to the curve of the minimums at Sines comparatively with Portimão and Faro, revealing that the occurrence of high nearshore temperatures is more sporadic off the western coast than off the southern coast during the this season. This evidence suggests that during the summer the upwelling regime is more persistent and intense off the western coast, while off the southern coast the upwelling events seems to be more episodic.

The interannual variability of the coastal temperature time series at Sines, Portimão and Faro was analysed. For this purpose, the low-pass Butterworth digital filter was applied to the time series, removing oscillations with periods less than 60 days, in the same way as was done for the wind data. The filtered seashore temperature time series in the three locations are represented in Figure 4.7.

The seasonal nature of the coastal temperature is better defined in the southern coast stations (Portimão and Faro) than at Sines, in the western coast, where a higher interannual variability of the coastal temperature is observed. The temperature time series at Portimão and Faro are characterized by larger-magnitude abrupt transitions, especially in spring and autumn. The annual cycle is not symmetrical in time and in general the heating/cooling transition is faster than the cooling/heating transition. Although time series were low passed filter at 60 days, upwelling signals are observable in most of the years, represented as relative minimums of the temperature pattern during the summer period. The development of the sea surface heating in the annual cycle is delayed in Sines, on the west coast, because of the persistent northerly winds

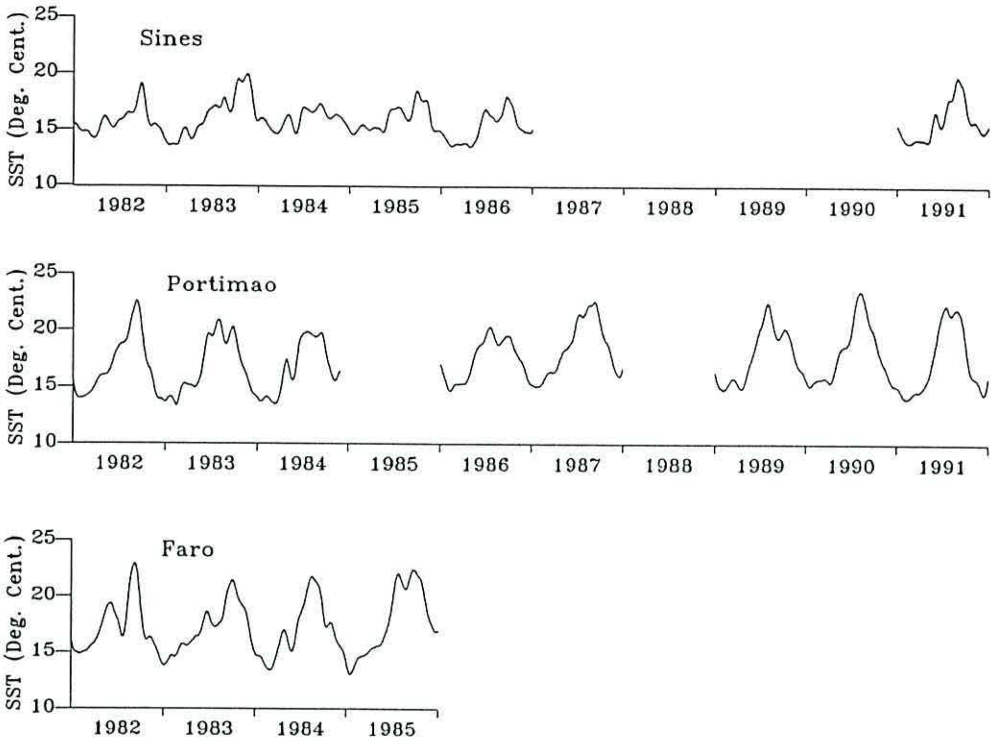

Figure 4.7: 60 days low-pass-filtered nearshore sea surface temperature time series at Sines, Portimão and Faro.

and establishment of upwelling. In the southern coast locations, in some years, the upwelling signal is quite tenuous or does not appear at all. The year of 1984 is rather interesting: in Sines, the heating part of the annual cycle does not develop at all because of a northerly wind regime throughout the year, and associated upwelling establishment. The development of the heating cycle does appear at Portimão, and seems normal at Faro.

### Inshore/offshore temperature comparison

A comparison between the seasonal cycle of the coastal temperature at Sines and Faro with the seasonal cycles of oceanic surface temperatures computed from the historical data is shown in Figure 4.8. The compared locations (**A** and **B** in Figure 4.8) correspond to nodes of the temperature grid previously computed from the NODC data

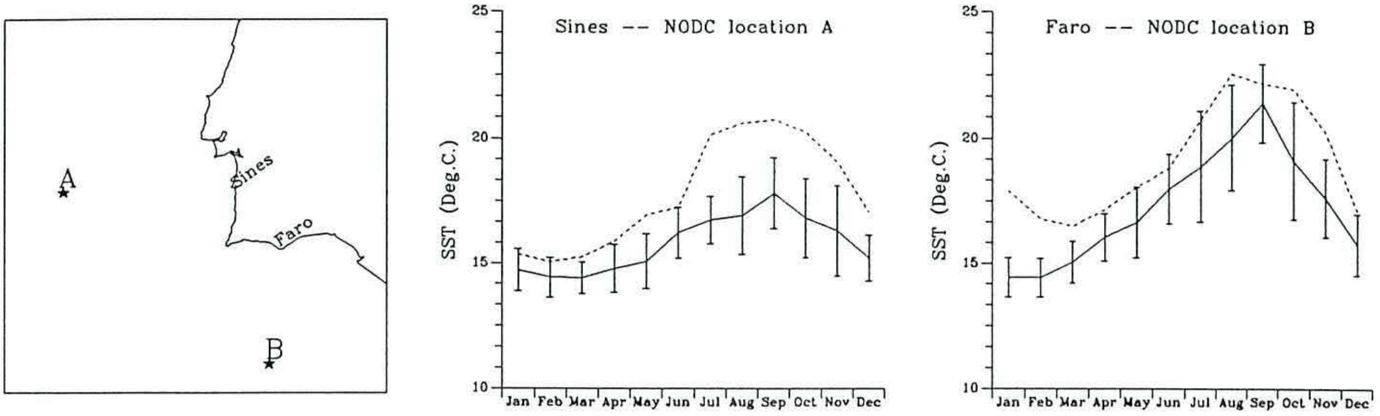

Figure 4.8: Comparative plots between the average monthly cycles of the coastal sea surface temperature at Sines and Faro (solid lines) and the mean sea surface temperature at the offshore locations **A** and **B** respectively (dashed lines), computed from historical data. A sketch shows the position of the oceanic locations **A** and **B**. Error bars represent the standard deviation of the coastal temperature within each month.

base, and represent oceanic positions straight offshore Sines and Faro. The complete methodology used to compute the monthly mean surface temperature in the offshore locations is described in Chapter III.

Despite the different nature of the compared data, a qualitative analysis of the plots emphasises the different upwelling characteristics observed along both coasts. If taken as an upwelling index, the difference between the coastal temperature at Faro and the oceanic surface temperature at location **B** does not reveal any intensification of an upwelling regime in the southern coast during the summer season. Upwelling off the southern coast is characterized by episodic events, limited in time, and are not revealed in a monthly time scale basis. Off the western coast, increased differences between offshore and inshore surface temperatures are observed during the summer and autumn, revealing the existence of a well established upwelling regime.

### 4.4.3 Sea level pattern

After removing tidal and other near diurnal effects from the sea level data and correcting the data for the inverted barometer effect, monthly mean six hourly sea level values were computed for the Sines, Lagos and V.R.S. António. The annual cycle of the sea level height is shown in Figure 4.9, along with the adjusted sea level height range at each location, represented by the maximum and minimum records found within all the six hourly low-passed values of each month (dashed lines), and the standard deviation within each monthly set of values (arrows), representing the variability with time scales less than one month. The labels denote the number of values in each monthly set of values.

The V.R.S. António tide gauge is located close to the mouth of the river Guadiana. However, the location does not seems to be a relevant factor for the long term sea level height. The river Guadiana has several dams and the outflow is generally weak all around the year. Any occasional rise of the outflow, due to any dam discharge or heavy rain has a time scale that would have been removed by the low-pass filter.

A common pattern is observed in the three tide gauges, and the spatial variations of the sea level patterns are minimal. Monthly mean sea level increases towards the end of the year when the highest values are reached, and then drops into the lowest values of the year, which occur during spring. The annual pattern observed in these tide gauges on the southwest tip of the Iberian Peninsula, show a close agreement with the sea level annual cycle of the eastern North Atlantic.

Both southern tide gauges (Lagos and V.R.S. António) show a stronger variability than the northern tide gauge (Sines) located in the western coast. In all the three tide gauges the maximum sea level height is further deviated from the mean sea level than the line of the minimum sea level height, especially in the southern locations. Also particularly evident in the southern tide gauges is the stronger variability of the

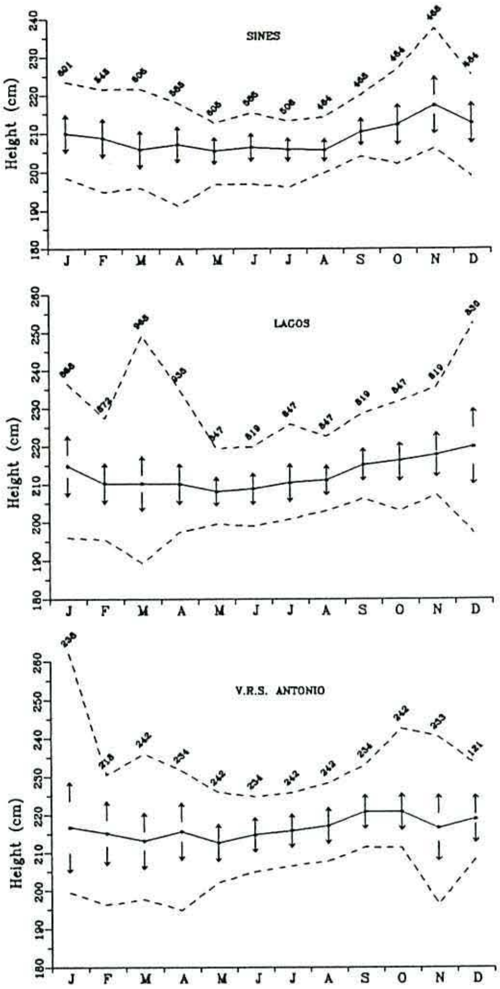

Figure 4.9: Seasonal variation of the sea level height, adjusted for the inverted barometric effect, at Sines, Lagos and V.R.S. António. Arrows denote the standard deviations, dashed lines denote extreme values, and labels denote the number of records in each monthly set of values.

envelope of maximums compared with the envelope of minimums. These patterns suggest the occurrence of short periods of positive sea level fluctuations, more intense in the southern coast.

The largest differences between the maximum and the minimum values occur in winter, decreasing towards the summer months. Standard deviation patterns follow this trend, revealing the higher short scale variability during the summer. The large range of observed sea level heights in winter is mainly due to high maximum values, again more evident in the southern tide gauges. This empirical evidence suggests a stronger activity of the coastal ocean during the winter months and in the southern coast, inducing transient fluctuations in the sea level height, in contrast with a relative undisturbed sea level behaviour during the summer.

Since the sea level records were corrected for the inverted barometric effect, the high variability in winter cannot be attributed to pressure variations associated with the atmospheric fronts that cross Iberia during this time of the year, although strong winds related to this fronts may be responsible for short scale variation in the sea level. Also transient variations of the rivers outflow, due to variable rainfall in winter, does not seems to account for the observed sea level variability: although the V.R.S. António tide gauge is located close to the mouth of a river, Lagos and Sines tide gauges are far away from any significant river discharge.

The coastal ocean off both western and southern coasts is subject to upwelling events during the summer. Thus, variability of the sea level elevation occurs during summer, associated with the activity of coastal mesoscale features induced by the upwelling, specially in the southern coast where all the evidence suggest a more intermittent behaviour of the upwelling episodes. However, the results presented here indicate an even higher activity of the coastal ocean during the winter time. This high activity is coincident in time with a weakening, or even a reversal, of the wind forcing, and with the smaller variability of the coastal sea surface temperature.

The few previous investigations in the region were based in thermal infrared satellite images, thus reporting summer patterns [*Fiúza*, 1983; *Sousa and Bricaud*, 1992; *Barton and Haynes*, 1995]. The absence of thermal signature in the winter ocean due to an uniform sea surface temperature field, and the lack of *in situ* observations during winter, does not allow yet any explanation of this evidence.

The low-pass Butterworth filter, removing periods less than 60 days, was applied to the sea level time series of Sines, Lagos and V.R.S. António, in order to assess the interannual low frequency variability of the time series, after removing the effects of

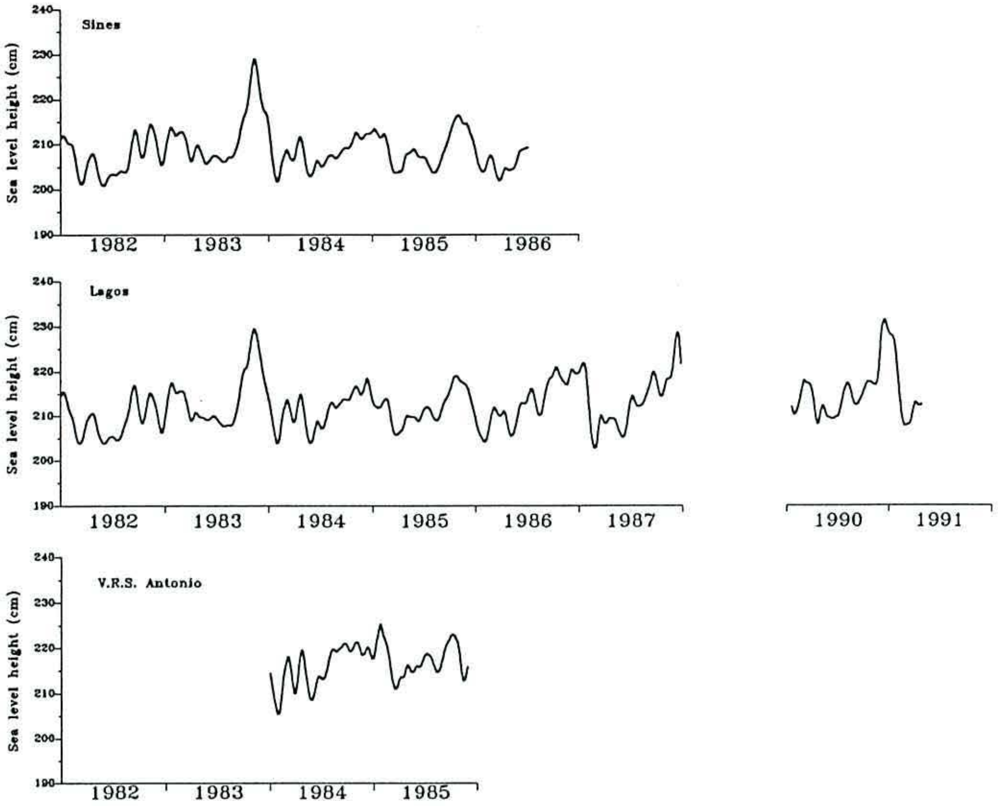

Figure 4.10: Interannual variability of the sea level height at Sines, Lagos and V.R.S. António. All periods less than 60 days were removed by low pass filtering. Sea level heights are referred to the national hydrographic zero (see text for explanation).

single short scale variations. The resulting time series of the sea level at each tide gauge is represented in Figure 4.10.

One of the most important features in the filtered time series of the sea level height is the significant interannual variability of the annual cycle apparent at all locations. However, the displayed plots suggest that the sea level cycle has a seasonal nature. In most years a significant sea level rise occurs in the last months of the year, followed by a substantial sudden drop into the lowest values of the year. V.R.S. António tide gauge does not show any annual pattern particularly distinct from the other two tide gauges, confirming the small influence of the river Guadiana outflow.

The highest annual oscillations observed in the long term time series occurred in 1983, both in Sines and Lagos, with an amplitude of about 27 cm. Striking is the fact that the drop occurred in a span of time less than three months. The smallest annual range was of the order of 12 cm, at Sines in 1984.

After the processing applied to the sea level time series, it is considered that the only significant remaining signals in the long term variation represented in Figure 4.10 are due to the wind forcing, heating and cooling cycle and advection by oceanic currents.

### Measured sea level and dynamic height

The steric contribution to the seasonal variation of the mean sea level was analysed by comparing the seasonal variation of the monthly mean sea level height observed at the three tide gauge stations with the seasonal variation of the dynamic height relative to 500 dbar calculated from the historical NODC hidrographic data. Monthly mean sea level data of each individual tide gauge, adjusted for the inverted barometric effect, along with error bars for the standard deviation, are plotted in Figure 4.11 superimposed on the mean monthly dynamic height computed at the nearest node of the 50km×50km grid described in the previous chapter. Location of the grid nodes used are also displayed.

Given the different nature and the slightly different location of the compared data series, only the general features of the seasonal variation should be considered significant. A visual inspection of Figure 4.11 indicates that the dynamic height data series agree fairly well with the measured sea surface elevation data series in all three stations. Generally, dynamic height monthly mean values fall inside the monthly standard deviation of the sea level height. The steric effect makes a mean contribution of 69% to the seasonal signal observed in the tide gauge data, and no striking differences occur between the tide gauges pattern. Such a percentage arises largely from the seasonal heating cycle, and is a common pattern in these latitudes [*Pattullo et al.*, 1955]. Since the effects of the variations of the atmospheric pressure were removed prior to mean sea level computations, this result also suggests that *nonisostatic* processes (other fac-

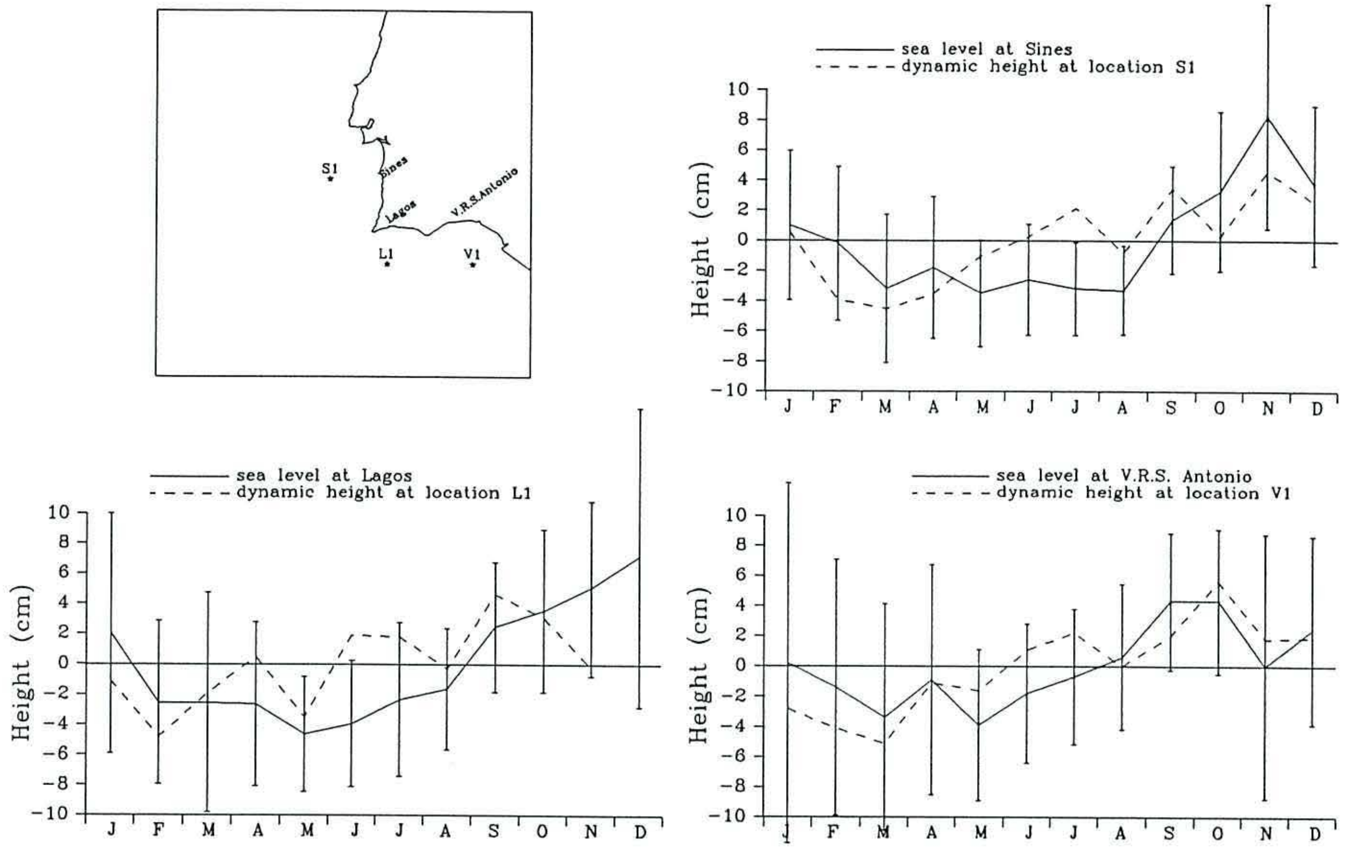

Figure 4.11: Dynamic height ($\Delta D_{0/500}/g$) (dashed lines) and sea level monthly mean seasonal variation (solid lines). Error bars represent the monthly standard deviations of the sea level. Dynamic height and sea level values were demeaned. Location of the tide gauges and position of the compared grid nodes are also displayed.

tors than atmospheric pressure and steric effects) contribute to the observed seasonal changes of the sea level. Although over the open ocean areas the seasonal variation of the sea level is mainly *isostatic*, large discrepancies frequently appear along continental coasts [*Lisitzin and Pattullo*, 1961].

The relatively good agreement between the seasonal variation of the measured sea level at V.R.S. António and the dynamic height pattern further offshore at the closest grid node confirms the negligible influence of the river Guadiana outflow.

## 4.5 Influence of the wind and coastal temperature on the seasonal sea level variability

A comparative analysis of the sea level behaviour with the two main governing factors, wind and sea surface temperature, is presented here on a seasonal time scale. Some aspects involving individual years and interannual differences are discussed qualitatively, but aspects involving short-term fluctuations are not presented. For this purpose, simultaneous time series, low pass filtered at 60 days, of alongshore wind, nearshore sea surface temperature and sea level, adjusted for the atmospheric pressure effect, for the southern and western coasts are displayed in a comparative form in Figure 4.12 and Figure 4.13 respectively. Sea level at the Lagos tide gauge is compared with the zonal wind at Faro and the nearshore sea surface temperature at Portimão, and is assumed to be representative of the conditions in the southern coast (Figure 4.12). Positive values of the zonal wind are towards east. Sea level at Sines tide gauge is compared with the meridional wind at Sagres and the nearshore sea surface temperature also at Sines, and is assumed to represent the conditions in the southern part of the western coast (Figure 4.13). Positive values of the meridional wind are towards north.

A visual inspection of the displayed data suggests a significant seasonal relationship between alongshore wind, sea surface temperature and sea level, more evident in the southern coast than in the western coast.

For the southern coast (Figure 4.12), alongshore wind and sea level are strongly related, and are seen to be in opposed phase (the maximum negative correlation, -0.61 significant at the 97.5% level, occurs at near zero lag). This suggests a strong degree of influence of the seasonal alongshore wind on the sea level fluctuations, compatible with the offshore Ekman transport associated with the upwelling favourable westerly wind. A similar behaviour is observed in the western coast. Despite the intermittent character

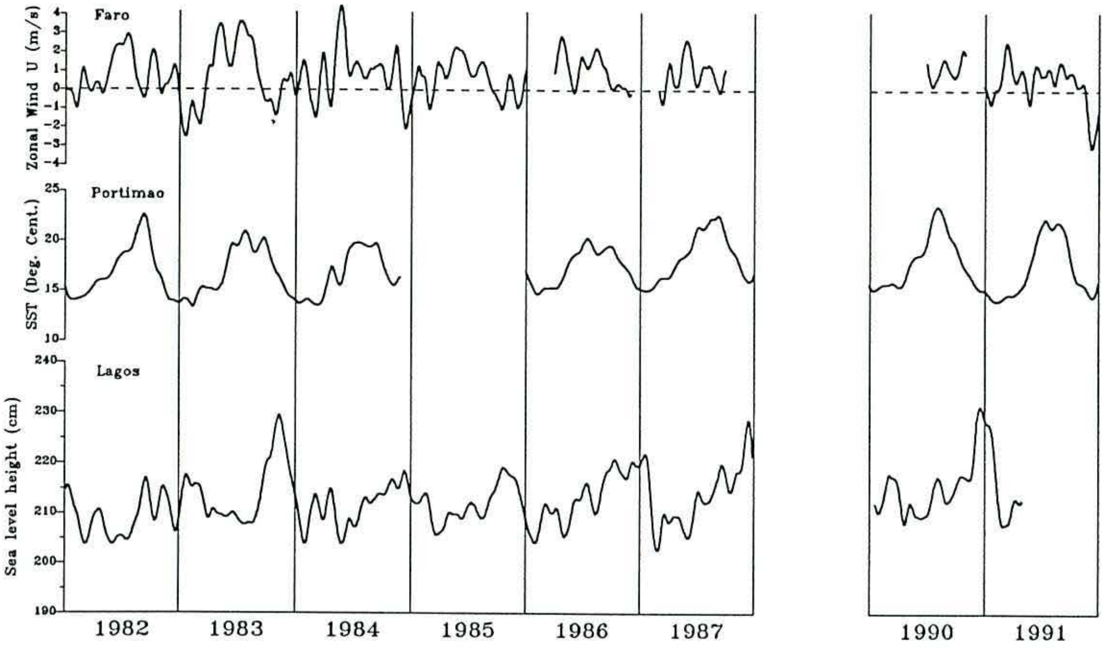

Figure 4.12: Long term variation of the sea level height at Lagos (bottom), sea surface temperature at Portimão (middle), and zonal component of the wind at Faro (top). All periods less than 60 days were removed by low pass filtering.

of the wind time series, a correlation between the upwelling favourable northerly wind and the sea level variations is visually evident in Figure 4.13.

The nearshore sea surface temperature at the southern station (Portimão) reflects mainly the seasonal solar heating, but is also strongly influenced by the onset of upwelling. Comparison between sea level and sea surface temperature (Figure 4.12) suggests that, although solar heating can account for a portion of the observed sea level variation, it is not significant in the determination of the maxima of the sea level signal (the maximum positive correlation between the two time series, 0.82 significant at the 97.5% level, occurs at a lag of about four months).

A positive trend of the sea level through most of the year, consistent with a temperature rise, is observed in the years where the westerly winds were not so strong during the summer season. However, the sea level rise continues after the temperature starts to decrease, reaching its maximum value nearly four months after the sea surface tem-

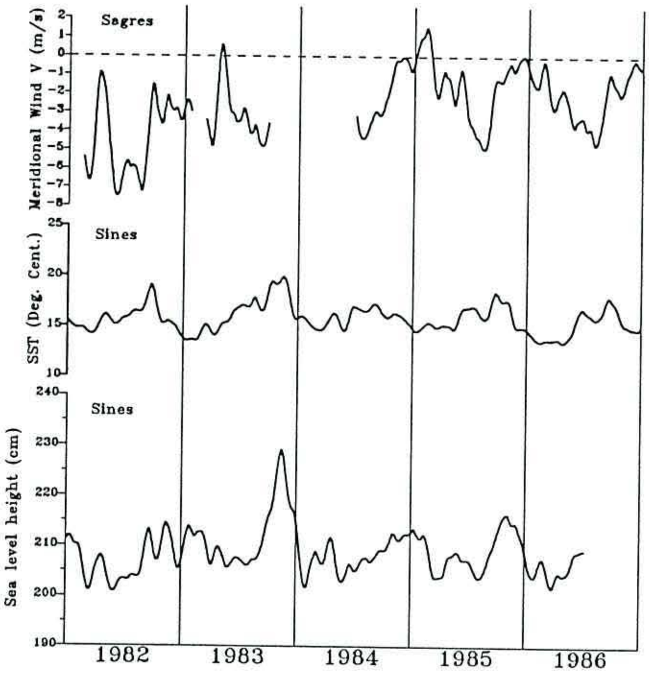

Figure 4.13: Long term variation of the sea level height at Sines (bottom), sea surface temperature at Sines (middle), and meridional component of the wind at Sagres (top). All periods less than 60 days were removed by low pass filtering.

perature maximum, on average. In years when a strong westerly wind regime occurs (1983 is a good example), a sharp increase of the sea level is observed late in the year, after the drop of the sea surface temperature, but simultaneous with decreasing wind. The maintenance of the sea level rise after the drop of the sea surface temperature, and its sharp increase in the years when the westerly winds were strong, cannot be completely attributed to surface convergence of the water against the coast (pile up) forced by an easterly wind. The observed large sea level increase could be explained in terms of an accumulation of water in the Gulf of Cádiz at the end of the summer period of westerly winds, causing enhanced general eastward flow south of the Iberian peninsula. When westerly winds relax, the increased sea level travels west along the Algarve.

A similar situation occurs in the western coast. Due to the northerly wind regime prevailing for most of the year, with stronger intensity during the summer season forcing the establishment of coastal upwelling, the rise of the nearshore sea surface temperature due to the solar heating cycle is not so well defined as it is in the southern coast. Thus, the wind forcing prevents the nearshore sea surface temperature from fully reflecting the annual solar heating cycle.

On average the maximum of sea level follows the maximum of coastal temperature by more than one month (the maximum correlation, 0.78 significant at the 97.5% level, occurs when the temperature curve leads the sea level curve by a lag of 1.3 months), considerably less than what occurs in the southern coast, and occurs simultaneously with the relaxation of the upwelling favourable northerly winds.

On both southern and western coasts, evidence shows that the wind forcing prevents any sea level rise in the summer season. The weakening of the alongshore upwelling favourable wind component corresponds to a rise in the sea level. However, the annual maximum of the nearshore sea surface temperature occurs prior to the maximum of the sea level height, specially in the southern coast. Thus, the sea level behaviour is determined primarily by the wind forcing, and upwelling strongly modifies the annual thermal cycle nearshore.

## 4.6 Alongshore sea surface slope

Accepting the levelling of the tide gauges, realistic comparison of absolute sea level height at the different tide gauges stations is possible. A comparative plot of the seasonal variation of the absolute mean sea level at Sines, Lagos and V.R.S. António tide gauges is represented in Figure 4.14.

The most important feature apparent in Figure 4.14 is the indicated alongshore coastal elevation slope, with sea level rising from Sines towards Lagos along the west-

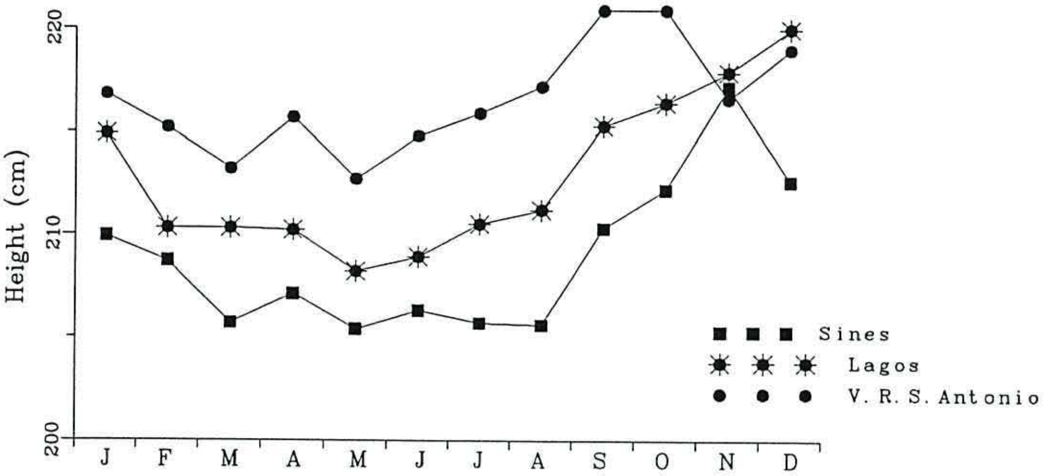

Figure 4.14: Mean sea level computed from tide gauge measurements, corrected for the inverted barometric effect, at Sines, Lagos and V.R.S. António.

ern coast, and from Lagos towards V.R.S. António, along the southern coast. This pattern occurs throughout most of the year, with exceptions in the months of November and December. The maximum alongshore sea level slope occurs in summer, with maximum values in August. This maximum monthly mean slope is 5.6 cm between Sines and Lagos (142.5 km distance) and 6.0 cm between Lagos and V.R.S. António (120 km distance), which are strong when compared with sea surface slopes off California [e.g. *Ramp and Abbott*, 1998].

The absolute alongshore pressure gradient is important to the circulation dynamics of the coastal region. The total pressure gradient consists of a barotropic and a baroclinic contribution. For a coastline parallel to the $x$ axis, the total alongshore pressure gradient at a depth $D$ (positive $z$ upward) is given by [*Chelton*, 1984]:

$$\frac{\partial p}{\partial x} = \rho_0 g \frac{\partial \eta}{\partial x} + g \int_D^0 \frac{\partial \rho}{\partial x} dz \tag{4.4}$$

where $p$ is the pressure, $g$ the gravitational acceleration, $\eta$ the sea surface elevation, $\rho$ the water density, and $\rho_0$ the surface water density. For shallow waters over the continental shelf, $D$ is small and if it is assumed that the vertically integrated alongshore

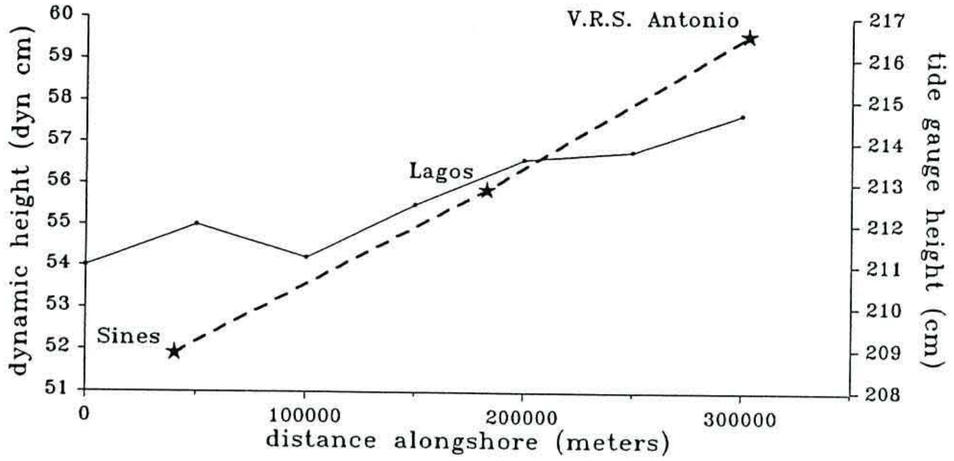

Figure 4.15: Alongshore mean annual slope observed in the tide gauges (dashed line) and alongshore dynamic height slope relatively to 500 dbar (solid line).

density gradient is small, the barotropic mode is dominant and the pressure gradient is proportional to the surface sea level slope. The presence of any baroclinic component due to alongshore density gradient will tend to compensate the surface flow with depth.

An independent check to the tide gauge levelling can be done by comparing the mean annual slope observed in the tide gauges with the dynamic height slope relatively to 500 dbar computed from the NODC data (Figure 4.15). Dynamic heights were taken from the grid built to define it mean annual field (Figure 3.9). The grid nodes closest to shore were chosen, but those nodes are located off the shelf. The estimated slopes from the dynamic height and from the tide gauges have the same sense and similar order of magnitude. However, the slope of the dynamic height has three sources of errors: sparse sampling may affect the result at any node; the choice of the 500 dbar as the reference level near the slope, where a shallow Mediterranean water vein occur, may not be completely correct; the assumption that the sea level slope in the same offshore and at the coast.

Thus, it seems evident that an alongshore monthly mean pressure gradient force acts during most of the year, with particular incidence during summer, causing a coastal circulation westward along the southern coast and northward along the western coast of the southwestern Iberia. The strongest pressure gradient occurs in summer, when upwelling favourable intense winds blow, and the forcing is small, or even vanishes, in winter time, when the sea level shows more short term variability.

## 4.7 Discussion

For a coastline parallel to the $x$ axis, the vertically averaged alongshore component of the linear momentum equation for a barotropic ocean can be written as [*Gill*, 1982]:

$$\frac{\partial u}{\partial t} = -fv - g\frac{\partial \eta}{\partial x} + \frac{\sigma_s}{\rho H} + \frac{\sigma_b}{\rho H} \tag{4.5}$$

where $u$ and $v$ denotes the vertically averaged alongshore and cross-shore components of velocity respectively, $f$ denotes the Coriolis parameter, $\sigma_s$ and $\sigma_b$ denote the surface stress imposed by the wind and the bottom stress due to friction respectively, and $H$ denotes the water depth.

Accepting the geodetic levelling of the tide gauges, during summer, from July till September, a mean sea level elevation of 4.5 cm is observed from Sines to Lagos along the western coast (142.5 km distance), and a mean elevation of 5.7 cm is observed from Lagos to V.R.S. António along the southern coast (120 km distance). The alongshore barotropic acceleration forced by the alongshore pressure gradient, if acting alone, is given by:

$$\frac{\partial u}{\partial t} = -g\frac{\partial \eta}{\partial x} \tag{4.6}$$

For the observed alongshore pressure gradients, the barotropic acceleration is about 0.26 $\mathrm{ms^{-1}day^{-1}}$ between Lagos and Sines, along the western coast, and about 0.40 $\mathrm{ms^{-1}day^{-1}}$ between V.R.S. António and Lagos, along the southern coast. However, other effects retard the acceleration, in particular friction. Assuming now that a steady state is reached when the bottom stress equals the alongshore pressure gradient, the balance equation can be written as:

$$-g\frac{\partial\eta}{\partial x} = \frac{C_b}{H}|\vec{V_w}|u_w \tag{4.7}$$

with the bottom stress written as a quadratic stress law $\sigma_b = \rho C_b|\vec{V_w}|u_w$ [*Gill*, 1982], where $\vec{V_w} = (u_w, v_w)$ represents the near-bottom current vector, and $C_b$ the bottom drag coefficient. An order of magnitude for the alongshore velocity in the steady state can thus be found from equation 4.7. Taking $C_b = 3.0 \times 10^{-3}$ [*Wang* 1993b] and considering the water depth of 100 meters over the continental shelf, an equilibrium velocity of about 0.32 m/s is obtained for the western coast, and of about 0.39 m/s for the southern coast. These values represent upper limits for the alongshore current velocities, westward along the southern coast and poleward along the western coast, when no surface friction is acting. Regarding the large barotropic accelerations computed before, such velocities are reached in short time scales, of the order of days.

However, the important role that the surface wind stress plays was not considered here. As was observed before, alongshore northerly winds and alongshore westerly winds blow during the summer season along the western and southern coasts respectively, opposing the alongshore pressure gradient forcing and slowing down the alongshore current. The estimates computed here suggest a quick response of the coastal ocean to the wind relaxation events, indicating a strong short scale variability of the alongshore current field in this region.

Recalling equation 4.5, it can be expected that the vertically averaged Coriolis term is small, because the depth average cross shelf flow is close to zero. The bottom stress will act to reduce any flow and when the current due to the alongshore pressure gradient is exactly balanced by an opposing wind stress, the bottom friction is zero. In this case, for a steady state flow, the vertically averaged alongshore flow is determined principally by the relative magnitude of the wind stress and the vertically integrated pressure gradient force for a given water depth, and so the balance equation 4.5 is reduced to:

$$g\frac{\partial \eta}{\partial x} = \frac{\rho_a C_s}{\rho H}|\vec{V_a}|u_a \tag{4.8}$$

with the wind stress written in it explicit form, $\sigma_s = \rho_a C_s|\vec{V_a}|u_a$, where $\rho_a$ represents the air density, $\vec{V_a} = (u_a, v_a)$ represents the wind vector, and $C_s$ the surface wind stress drag coefficient.

The local alongshore wind stress and the alongshore pressure gradient force act in opposite directions. Simple calculations of Equation 4.8 using a finite difference approximation, with $\rho_a = 1.225\,\mathrm{Kgm^{-3}}$, $\rho = 1027\,\mathrm{Kgm^{-3}}$, $C_s = 1.2 \times 10^{-3}$, and assuming a water depth of 100 meters over the continental shelf, will imply a northerly alongshore wind velocity of 14.5 m/s in order to balance a mean sea level slope of 4.5 cm between Sines and Lagos, and a westerly alongshore wind velocity of 17.8 m/s in order to balance the mean sea level slope of 5.7 cm between Lagos and V.R.S. António. Thus, in mean terms, the observed alongshore pressure gradient forces a vertically averaged alongshore flow, westward along the southern coast and northward along the western coast, unless the wind velocity exceeds the above values and forces the alongshore flow to reverse.

On a long time scale such alongshore wind velocities is unlikely to occur Figure 4.5, despite small scale transient events of strong wind, well above the computed thresholds, in particular in the western coast. However, previous works show observations of a southward coastal current over the shelf and continental slope off the western coast of Portugal during summer [*Fíuza*, 1983; *Fíuza*, 1984]. Circulation patterns off the southern coast are unknown.

A source of subjectivity on the computation of a wind threshold to reverse the direction of the coastal flow is the assumed value of the water depth, H. In fact, H is the depth of the layer over which the wind stress acts. Here, H was assumed to be constant and to represent the depth of the fluid over the continental shelf. Thus, a well mixed coastal ocean was assumed, in which all the water column was dragged by the wind. However, in a stratified ocean the wind stress acts only in the upper layer above the pycnocline.

Observations carried out in the region during the early summer [*Relvas and Barton*, 1995], and fully reported later on this work (Chapter VI and VII), revealed the existence of a pycnocline in the region. A realistic estimate of the mean depth of the pycnocline will be about 30 meters. Analysis of the vertical distribution of the temperature field based on the historical NODC data (not shown here), also suggests the existence of a pycnocline during the summer at that depth. Assuming a stratified ocean and taking $H = 30$ m, solutions of Equation 4.8 indicate alongshore wind velocities of about 7.9 m/s and 9.7 m/s in order to reverse the near surface flow off the western and southern coasts respectively. The pattern assumed here implies the presence of vertical velocity shear in the water column. Such alongshore wind velocities seems more realistic estimates since they are more likely to occur and persist during longer time periods, in view of the observed wind variations in Figure 4.5. This is especially true for the western coast, where there is observational evidence of southward flow in the upper ocean layer over the continental shelf during the summer (upwelling) season [*Fíuza*, 1983; *Fíuza*, 1984].

Assumptions made here are somewhat subjective. Apart from the mentioned uncertainties in, for example, thickness of the mixed layer and surface drag coefficient, a major possible source of error lies in the levelling of the tide gauges. However, the agreement within a factor of two with the estimated dynamic height slope is encouraging and, as will be shown later, the results are strongly supported by remote sensing and *in situ* observations. The goal was to demonstrate that the wind forcing, under certain conditions, could drive the coastal flow against the observed vertically averaged alongshore pressure gradient, which forces an alongshore flow from V.R.S. António towards Cape São Vicente and then northward off the western coast. Such conditions of upwelling favourable wind are characteristics of the summer season on both western and southern coasts, but the threshold necessary to drive the coastal flow is more easily reached on the western coast, due to the smaller magnitude of the alongshore pressure gradient and the stronger favourable winds prevailing during summer. The response of the coastal ocean to the wind relaxations, re-establishing the alongshore flow, seems to be rather quick. Implications of the different balance conditions between the western and southern coasts will be the object of analysis later on this work.

The situation found here seems to have some similarity with that observed off the Peru coast, where the alongshore pressure gradient plays an important role. There, the alongshore velocity field over the shelf and slope is not strongly driven by the local alongshore component of the wind stress, although when wind stress increases in magnitude it gains importance as a driving mechanism [*Brink et al.*, 1978].

The presence of a meridional pressure gradient off western Iberia all year, balanced during the summer by the southward wind stress, was already hypothesized by *Frouin et al.* [1990]. However, no driving mechanism has been suggested for the southern (zonal) coast of Iberia. Based in satellite imagery and large scale meteorological considerations, *Fiúza* [1983] mentioned that without westerly winds, the coastal circulation off southern Portugal seems to be predominantly westwards. Evidence from cruise observations carried out by *Haynes and Barton* [1990] during September 1986 off western Iberia in a situation of post upwelling, showed a poleward flow on the continental shelf, associated with the northward advection of anomalously warm and salty water with water mass characteristics similar to waters from the Gulf of Cádiz. This fact suggests a continuity of the flow along the southern coast of Iberia, bending northward around Cape São Vicente. The magnitude of the observed sea surface tilt, leading to an alongshore barotropic current, suggest that the pressure gradient force may be of primary importance to the generation of such flow, although during winter its influence is reduced. During the summer season off the western coast, this flow is balanced, at least in the upper layers, by the equatorward geostrophic current resulting from local upwelling forced by the northerly winds. Off the southern coast such balance occurs only occasionally during the summer, when favourable strong westerly winds blow locally. Presumably, due to the different time scales of the forcing conditions necessary to reverse the flow, conspicuous phenomena occur in the Cape São Vicente region when the southward current off the western coast encounters a westward flow along the southern coast of Portugal.

## 4.8 Conclusions

The seasonal evolution of the sea level height in the considered region shows a pattern consistent with the sea level seasonal cycle of the eastern North Atlantic. The variation of the sea level height is influenced by the local wind regime, which prevents the sea level from closely reflecting the seasonal nearshore sea surface temperature signal. However, the steric effect is shown to contribute to the seasonal variation of the monthly mean sea level, as elsewhere in these latitudes.

The empirical evidence presented here suggests that the coastal circulation along the southwestern tip of the Iberian Peninsula is dominated by an alongshore pressure gradient, forcing the flow westward along the southern coast of Portugal and northward along the southern part of the western coast. This forcing is stronger during summer and weaker in winter (or even vanished in early winter). Intense wind, blowing northerly along the western coast and westerly along the southern coast during the summer season, opposes the pressure gradient force and is able to reverse the surface flow during this season.

Requirements necessary to reverse the surface flow are more easily reached in the western coast than in the southern coast: during the summer season, a weaker pressure gradient force occurs on the western coast relative to the southern coast, and also the northerly wind blowing along the western coast is stronger than the westerly wind blowing along the southern coast. For those reasons, the summer southward surface flow along the western coast, associated with the upwelling set-up, is more permanent than the summer eastward surface flow along the southern coast, which has a more intermittent character. This means that the empirical evidence for the western coast suggests a pattern consistent with the behaviour of an eastern boundary current system during the summer, but that this characteristic is somewhat attenuated in the southern coast.

Although the bulk of this work is focused in the summer situation, observational evidence shows that the winter season is characterized by a higher variability of the sea level elevation, suggesting a high mesoscale activity of the coastal ocean off the southwestern Iberia during this season.

The upper ocean circulation of the northeast Atlantic is not clearly defined, but the consensus is that the flow is directed eastward in a broad band north of 33°N, associated with a meridional pressure gradient [e.g.,*Saunders*, 1982; *Pollard and Pu*, 1985]. Upon reaching the western Iberian continental margin, this flow forces local downwelling and consequently a northward surface coastal current, which is reversed during summer due to the northerly wind forcing [*Frouin et al.*, 1990; *Haynes and Barton*, 1990]. Presumably, the large scale pressure gradient is present all year long.

This picture is compatible with the observed alongshore sea level slope off the southern part of the western coast of Iberia, and can also explain the observed sea level slope off the southern coast of Portugal. A possible mechanism for the observed slope along the southern coast would be that part of the broad eastward flow enters the Gulf of Cádiz where it impinges against the eastern coasts near the Strait of Gibraltar, so increasing sea level there. Some flow enters the Mediterranean Sea through the Strait, but some can only be relieved by recirculating westward along the Algarve coast. Thus, this recirculated water would be part of the poleward coastal flow observed on the western Iberian continental shelf and slope. This picture is consistent with the observation, off western Iberia, of water with water mass characteristics similar to waters from the Gulf of Cádiz [*Haynes and Barton*, 1990]. Of course during summer, alongshore wind stress is superimposed on this pattern, reversing the surface coastal flow.

# Chapter 5

# Mesoscale patterns

## 5.1 Introduction

Eastern ocean boundary regions are recognized to be areas of eddy activity, often dominated by mesoscale features associated with complex flow patterns with strong variability in time and space [*Wooster and Reid*, 1963]. Over the last few decades, since early 1980's, the great improvement of the spatial and temporal resolution provided by satellite imagery has revealed the inhomogeneous and complex nature of the transition zone between coastal and offshore waters at the eastern ocean boundaries, particularly during the occurrence of coastal upwelling. Infrared satellite images allowed a synoptic description of the sea surface temperature pattern over an extensive portion of a coastal region, and revealed that, rather than forming an upwelling front oriented roughly parallel to the coast, the upwelled front is contorted and stretched into a series of thin tongues or filaments of colder water, as mentioned in Chapter II. The formation and development of cold filament structures extending offshore from spatially intermittent locations along the coast have been observed off the coasts of California, southwestern Africa and Iberian Peninsula [*Brink and Cowles*, 1991]. In this last case, evidence from satellite imagery suggests that the filaments are associated with the major topographic features of the region, in particular prominent capes [*Haynes et al.*, 1993].

At the southwestern tip of the Iberian Peninsula, the zonal southern coast and the meridional western coast of the Iberian Peninsula meet together almost in a right angle, with Cape São Vicente forming a prominent protrusion. The Cape is itself an upwelling center under wind favourable conditions, and is the origin of one of the major cold filaments observed along the western coast of Iberia [*Haynes et al.*, 1993]. This filament has a singular behaviour because, at different times or at different years during the upwelling season, it is observed to extend in different directions, even bending round eastwards into the Gulf of Cadiz, unlike the other filaments along the western coast which extend generally westward. A particular full development of the Cape São Vicente filament with a north-south orientation and an offshore limit developing into a dipole eddy pair is reported by *Barton* [1991].

It is assumed that the coastal region off western Iberia follows the classical understanding of the circulation near eastern boundary regions, which is that upwelling favourable winds force a near-surface offshore transport, leading to upwelling of cold subsurface waters at the coast and the generation of alongshore currents, namely a poleward undercurrent and an equatorward surface jet. Under such conditions, cold filaments are observed to grow from the cool upwelled coastal water. The establishment of coastal upwelling seems to be a previous requirement for the formation of cold filament structures but, since the offshore transport in the filament structures is much higher than the local Ekman transport [*Kosro and Huyer*, 1986; *Ramp et al.*, 1991], other factors must cooperate in the formation and development of such structures. Present hypotheses of filament formation, summarized by *Strub et al.* [1991] and presented here in Chapter II, always involve the deformation of the equatorward surface jet. The fact that Cape São Vicente is associated with the root of a major and singular cold filament feature, and represents a discontinuity in the eastern boundary region, thus in the equatorward jet, makes it an interesting region to investigate such features. In addition, in the Cape São Vicente coastal region the equatorward surface jet interacts at times with the coastal circulation off the southern coast of Portugal, which seems to be dominated by an alongshore pressure gradient, as the empirical evidence presented in the previous chapter suggests.

Depending on atmospheric conditions, satellite infrared imagery can provide extensive information, in time and space, on the horizontal gradients of the sea surface temperature, a valuable index for tracking the evolution of features. In this chapter the variability and kinematics of the mesoscale field of the coastal transition zone off Cape São Vicente during the upwelling season, observed from advanced very high resolution radiometer (AVHRR) satellite imagery, is described. Characteristic features and patterns of the region are identified and attention is given to the formation, evolution and persistence of the Cape São Vicente filament, and the contrasting generation of poleward flow. Wind, sea level and nearshore sea surface temperature data measured at local stations are used to analyse and discuss the possible forcing mechanisms associated with the formation and development of the major mesoscale features observed in the region.

## 5.2 Satellite data and processing

The sea surface temperature satellite data used in this investigation were collected by the advanced very high resolution radiometer (AVHRR) carried onboard the NOAA-series polar orbiting satellites. The ground resolution provided by these satellites is 1.1 km × 1.1 km at nadir increasing to 2.5 km × 7.0 km at maximum scan angles. Satellite data consists of an archive of over 1200 monochrome prints representing brightness temperature scenes of relatively cloud free AVHRR images provided by the University of Dundee satellite ground receiving station, corresponding to the period 1981-1995. This photographic form only allows a qualitative analysis of the temperature patterns. For this reason, selected images of particularly interesting scenes were obtained in digital form from the University of Dundee. These images were processed at the NERC

Remote Sensing Data Analysis Service, Plymouth Marine Laboratory, U.K., using the semi-automated *Panorama* (Processing and Automatic Navigation Of ReAl-time iM-Ages) satellite image processing system [*Miller*, 1996], and then edited for attributes, annotations and composition at University of Algarve, Portugal, allowing a quantitative analysis of the sea surface temperature fields.

The AVHRR is a scanning radiometer sensitive in five spectral channels, two of them (channel 1 and 2) operating in the visible wavelengths. The radiance measured by the sensors is directly related to the sea surface temperature. For the determination of sea surface temperatures only the infrared channels 4 (10.3-11.3$\mu$m) and 5 (11.5-12.5$\mu$m) are used in the atmospheric correction algorithm. However, in satellites NOAA 6,7,8, and 10 the AVHRR channel 5 is a copy of the channel 4 sensor and therefore existing atmospheric correction algorithms were not considered reliable enough for the computation of the sea surface temperature. Images from these satellites were only calibrated for channel 4 brightness temperature, which can then be used as a rough indication of temperature gradients and differences across the area of the sea being viewed.

The atmospheric correction was performed using the split window algorithm of *McClain et al.* [1985], which combines the brightness temperatures for channels 4 and 5. Because the atmospheric contributions are different at night from the day-time, it was necessary to use different algorithm coefficients for night-time and day-time images. The brightness temperature measured by each independent channel is therefore a skin temperature, thus reflecting the temperature of the very top layer of the sea at the sea-air interface, subject to the influence of surface processes such as heat fluxes through the air sea interface, wind stirring or diurnal thermocline development. Clearly it may be different from what is normally measured as sea surface temperature, which is generally the temperature at some depth within the top few meters of the ocean. However, the operational atmospheric correction algorithms are based on a match between satellite infrared observations and *in situ* measurements from buoys, which record bulk sea surface temperatures within the top one or two meters, no account being taken of the diurnal thermocline or the skin layer temperature deviation due to the vertical heat flux. This means that the temperature product generated by the algorithms truly represents the bulk sea surface temperature rather than the skin sea surface temperature [*Robinson*, 1985]. Nevertheless particular attention has to be taken with the interpretation of infrared images obtained during the afternoon, unless it is known that a wind strong enough to destroy the diurnal thermocline was blowing at the time. Anyway, possible errors have a significance depending on the application of the data. The study of spatial temperature structure in the sea requires accurate measurement of temperature gradients, whilst absolute values of the sea surface temperature are less important.

Another possible source of errors in the satellite measurements of the sea surface temperatures are the cloud contaminated data. The large cold uniform cloud masses are clearly identifiable in the processed AVHRR images due to the generated low brightness temperature. The problem arises when clouds with a sub-pixel size are present within the field of view, too small to resolve but nonetheless enough to biase the retrieved temperature. Analysis has to be done subjectively by identifying cool regions superimposed on strong sea surface temperature patterns and any remaining errors will be contained within acceptable bounds and will not have influence in the interpretation of temperature patterns. Furthermore, most of the interpretations in this chapter are based in sequences of images and any cloud contamination would then be easily identified.

## 5.3 Interannual variability

A detailed and systematic analysis of all the individual cloud free images from the AVHRR imagery archive between 1982 and 1991 was carried out, corresponding to over 900 scenes. All images collected between 1992 and 1995, while this study was under way, were also observed and analysed but not systematically sampled. The complete set of analysed AVHRR images include over 1200 brightness temperature scenes, the large majority of them collected from May till October. Image analysis was limited to the region 35°30′N—38°30′N and 10°30′W—7°00′W, corresponding to what it was considered to be the Cape São Vicente region.

From the detailed analysis of the archive of brightness temperature scenes, it was possible to analyse separately the temporal evolution of four particular mesoscale features of the sea surface temperature field of the region.

- The occurrence of upwelling off the western coast of Iberia in the Cape São Vicente region.
- The occurrence of upwelling off the southern coast of Iberia in the Cape São Vicente region, corresponding to the southern coast of the Algarve.
- The appearance of a filament of cold water, developing seaward from Cape São Vicente.
- The development of a narrow band of warm water along the southern coast of Algarve, spreading from east to west and occasionally turning around Cape São Vicente towards the north.

The observed seasonal evolution of these features between 1982 and 1991 is represented in Figure 5.1, along with the record of the sampled cloud free AVHRR images. The features mentioned above occur mainly during summertime. Most of the imagery collected during winter time shows a quite uniform sea surface temperature field, revealing a lower activity of the coastal ocean during this time of the year. Exceptions occured during the winter of 1986/87, although the observed features show a weak surface temperature signal.

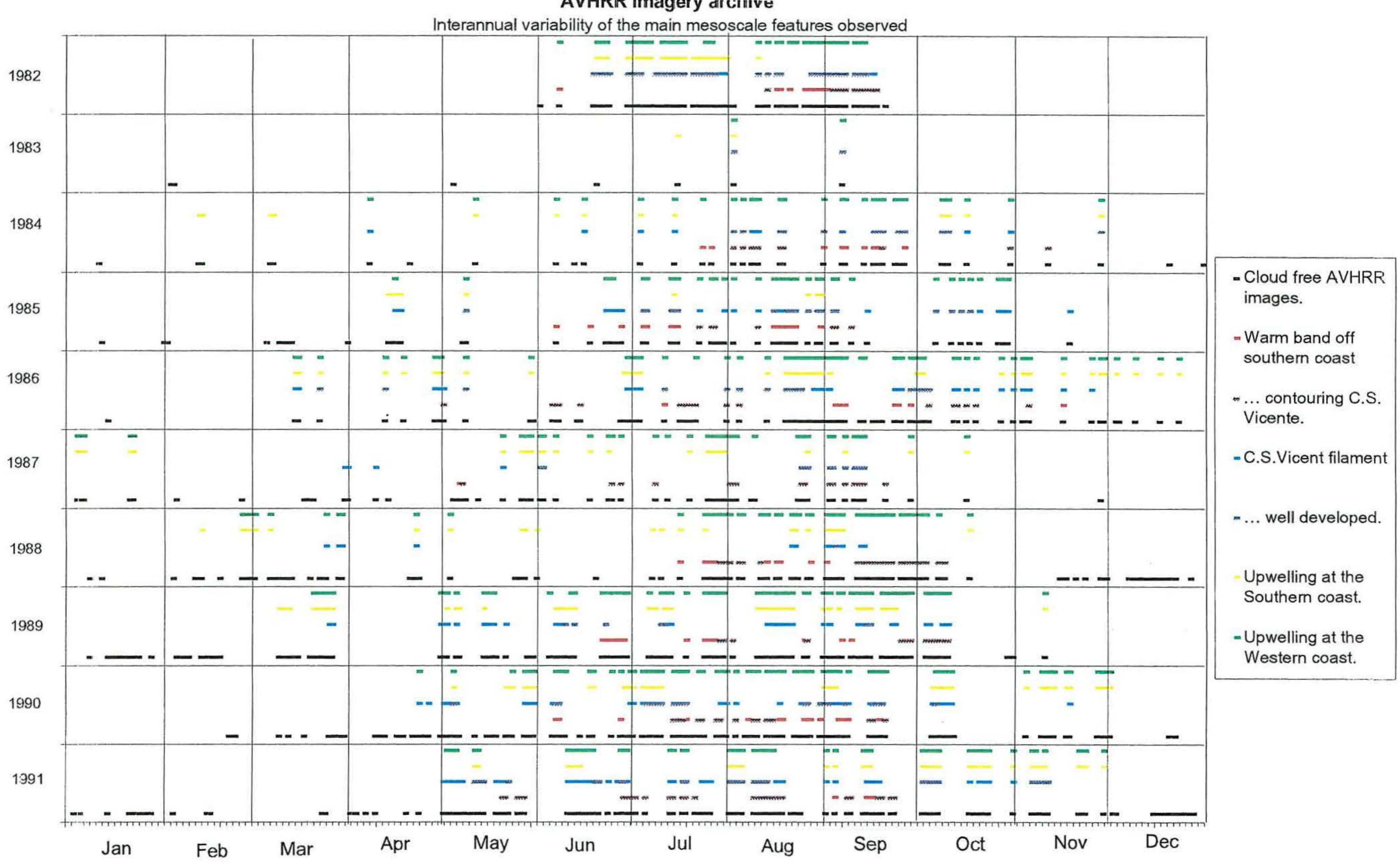

Figure 5.1: Comparative temporal evolution of the main features observed in the sea surface temperature field in the Cape São Vicente region between 1982 and 1991. Information about the sampled AVHRR images is also displayed.

The analysis of the AVHRR imagery archive, summarised in Figure 5.1, reveals that the occurrence of upwelling is more frequent in the western coast than in the southern coast. Also, the upwelling regime in the western coast has a marked seasonality, with upwelling concentrated in the summer months, while in the southern coast upwelling events are more distributed through the year, showing a weak seasonal signal. The upwelling in the southern coast is, most of the times, most intense or limited to near Cape São Vicente. The development of upwelling conditions farther east than Cape Santa Maria (Faro) is sporadic.

The development of the Cape São Vicente filament, with various orientations, is a frequent feature from late Spring till early Autumn. However, the filament is intermittent and its continuous presence during all the season is exceptional. The appearance of the filament, in its initial stages of development, is associated with the establishment of upwelling in the western coast. Its continued development requires persistent upwelling in the west coast. This evidence leads to the hypothesis that the filament is primarily fed by waters upwelled farther north and advected equatorward by the coastal jet associated with the upwelling. However, upwelling on the western coast can occur without growth of the filament, as was observed during part of the summers of 1987 and 1989 and almost all the summer of 1988.

Analysis of Figure 5.1 reveals that the development and evolution of the Cape São Vicente filament is independent of the occurrence of upwelling in the southern coast of Algarve, suggesting that the filament is not supplied by the cold water upwelled in the southern coast.

One of the most recurrent features observed during the period of stronger coastal activity (end of May/June till October) is the development of a narrow band of warm water along the southern coast of Algarve, leaving cooler water offshore over the continental slope. Analysis of Figure 5.1 show that the development of this coastal warm feature occurs whenever coastal upwelling is absent from the southern coast. Satellite imagery shows the evolution of this warm band begins in the east, near the Gulf of Cadiz, and progresses westward along the Algarve. Similar features have been observed off California during upwelling relaxation [*Send et al.*, 1987; *Harms and Winant*, 1998]. Sometimes, when upwelling is absent for a long period, this warm feature turns around Cape São Vicente and extends poleward. In extreme conditions, the warm water can reach the Cape of Sines, about 100 km to the north.

The presence of this coastal warm feature is somewhat independent of the presence of the Cape São Vicente filament. If the filament is present when the warm water reaches the Cape São Vicente, then the cold west coast coastal upwelling jet that supplies the filament is forced to separate from the coast, and the filament loses it connection with Cape São Vicente itself, being apparently fed with cold water upwelled farther north.

## 5.4 Observed parameters and mesoscale features

Measurements of wind, sea level and nearshore sea surface temperature during summer 1982, collected in three regions along the southern and western coasts of the southwest Iberian Peninsula, were analysed together with relevant information about the evolution of mesoscale features in the region observed in the AVHRR imagery. This period was chosen because it shows development of a typical mesoscale pattern and an excellent set of observations were available. Upwelling along the western coast, development of the Cape São Vicente filament and the setup and progression of the band of warm water along the southwest coast were all observed.

The wind, sea level and nearshore sea surface temperature time series are represented in Figure 5.2, along with a summary of the evolution of the mesoscale features taken from the satellite images. The nearshore surface temperature was collected every morning at 0900, sea level time series are based in hourly observations, corrected for the inverted barometer effect, and the wind time series are based in hourly measurements at Faro, 3-hours interval data at Sagres and 8-hours interval data at Sines. Wind and sea level time series were low-pass filtered at 40 hours. The time series correspond to three distinct regions. At Sines and Faro the three parameters were measured at the same geographical location. For the Cape São Vicente region, the wind was measured at Sagres, on the Cape São Vicente cliffs, the sea level at Lagos, about 27 km eastward, and the surface temperature was collected at Portimão, another 13 km eastward from Lagos in the southern coast.

The displayed time series representing the evolution of the orientation and length of the Cape São Vicente filament was taken from *Haynes* [1993]. These filament parameters were measured from the monochrome prints of AVHRR images available between June and September of 1982. A degree of subjectivity was involved in the measurements, but an accuracy better than ±20 km in the location of the offshore end of the filament and of ±5° in the orientation of the filament was estimated. Time series showing the occurrence of other features observed in the imagery, such as upwelling in the western and southern coast and the development of the warm water band around the coast, are represented in Figure 5.2 by different symbols. A rise in the symbols sequence means an intensification of the event. An index of the sampled images is also displayed.

Figure 5.2 shows that a northerly wind was blowing along the western coast, almost uninterruptedly, from the beginning of June till about 13 September (julian day 257). Velocities over 5 m/s were common in Sines, the more northern site, but they exceed frequently 10 m/s in Sagres, near Cape São Vicente. An intensification of the northerly wind as the season progressed was observed in Sagres, reaching the absolute maximum velocity of 14.8 m/s about 20 September (day 233). The velocities recorded during this period were the highest velocities observed in all the available wind time series at Sagres, from 1982 to 1992 (Figure 4.5, Chapter IV). In response to this wind pattern, upwelling occured on the western coast, and led to the growth of the Cape São Vicente

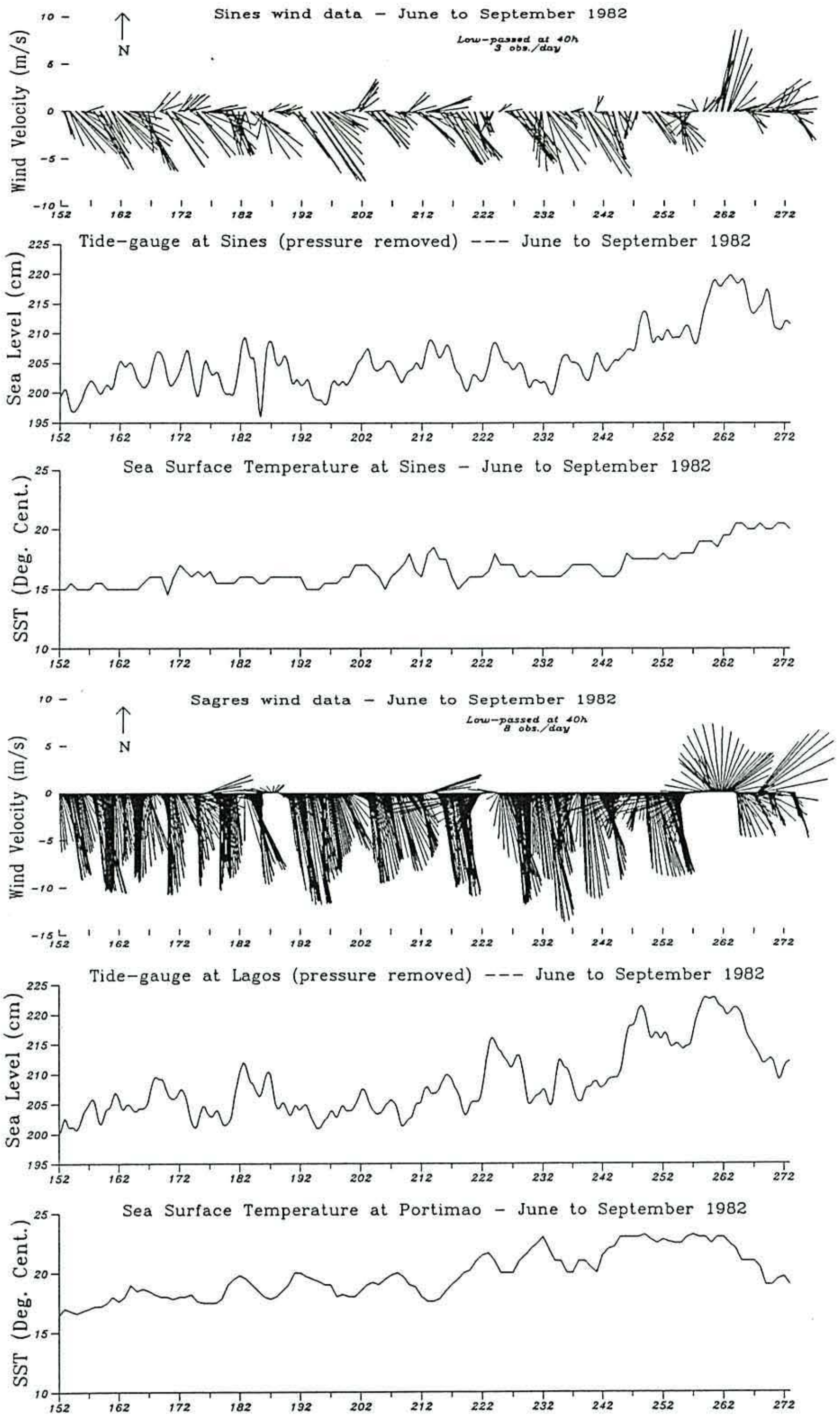

Figure 5.2: Comparative temporal evolution of the wind, sea level and nearshore sea surface temperature observed along the coast with the main features observed in the brightness temperature scenes of the Cape São Vicente region between June and September 1982. A rise in the symbols representing the features means its intensification. Information about the sampled AVHRR images is also displayed. A detailed description is given in the text.

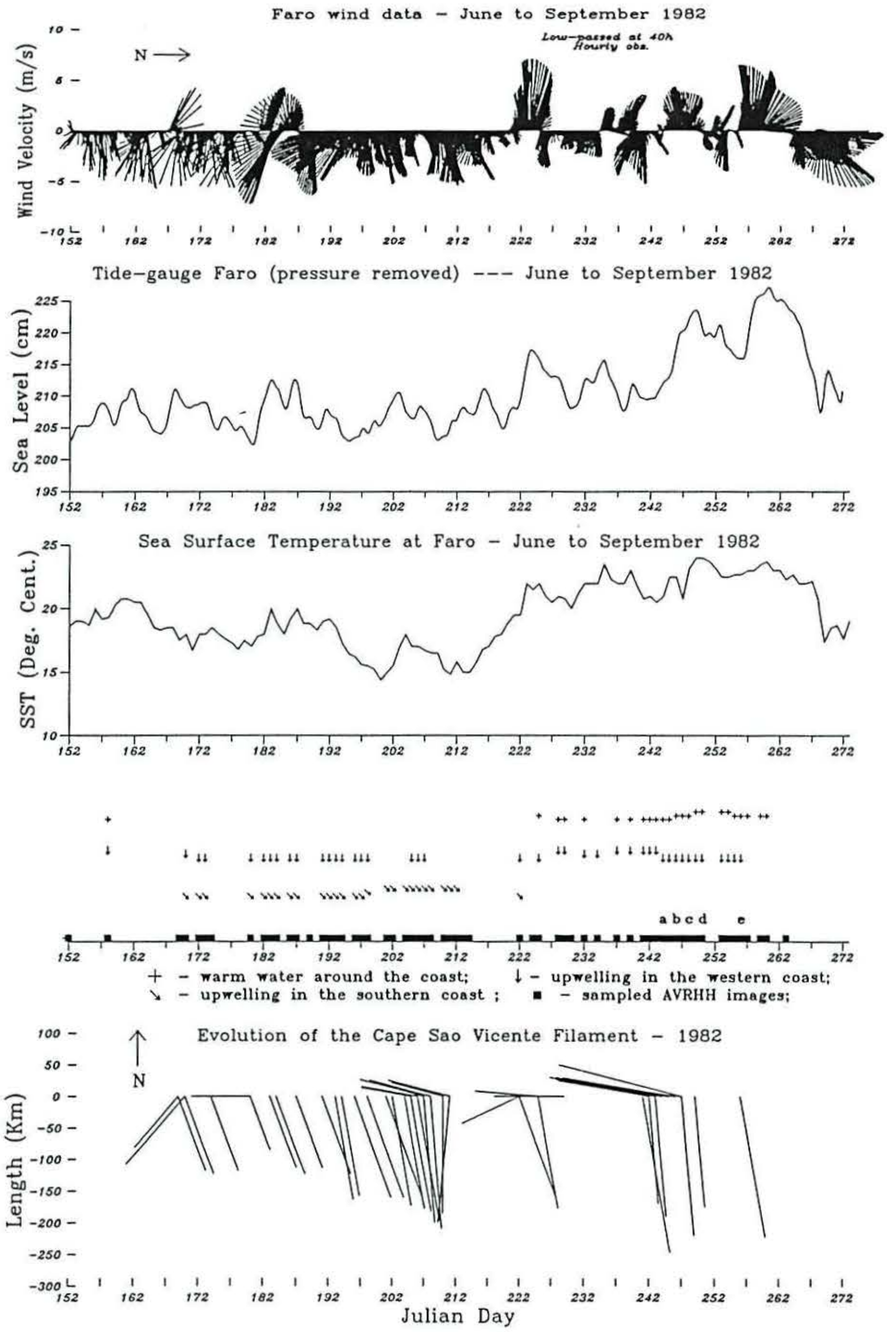

Figure 5.2: *continued*

filament, with a southward configuration. The maximum development of the filament occurred on 30 August (day 242), when a southward extent of about 250 km was observed, coincident with the final stage of a strong upwelling event off the western coast. This was the maximum length of the Cape São Vicente filament observed in the imagery archive. During this period a weaker westward branch of the filament also developed.

In the southern coast, represented by the Faro meteorological station, a more variable wind regime was observed (Figure 5.2). Typically, the summer wind pattern is affected by a thermal low over the Iberian Peninsula, forcing the northerly wind circulation observed along the western coast of Portugal to turn towards the east at the latitude of the Algarve. This typical situation is illustrated by the surface meteorological chart of 16 July 1982 presented in Figure 5.3. The orographic constraint caused by the ridge that extends zonally along the Algarve also contributes to rotate the wind into a more east-west alignment. Thus, the summer wind regime along the southern coast has a prevailing westerly component. Following this general pattern, the wind was blowing eastward, upwelling favourable, till the beginning of August (about day 220), but much more weakly than on the west coast. In response, an upwelling regime was present, although two short relaxation events were observed during this period. After the beginning of August, variable easterly winds were dominant till mid September (about day 262). By the end of the displayed period, the wind reversed to westerly again. Coincident with the occurrence of easterly winds, the upwelling regime ceases and the narrow band of warmer water starts to develop from east along the southern coast of Algarve.

With the onset of the easterly winds a significant rise in the sea level was observed in Faro. The relative maximums were well correlated with the stronger episodes of downwelling favourable winds. A rise in the sea level, with a similar pattern, is also observed in Lagos, 72 km west of Faro. The lagged correlation between the two sea

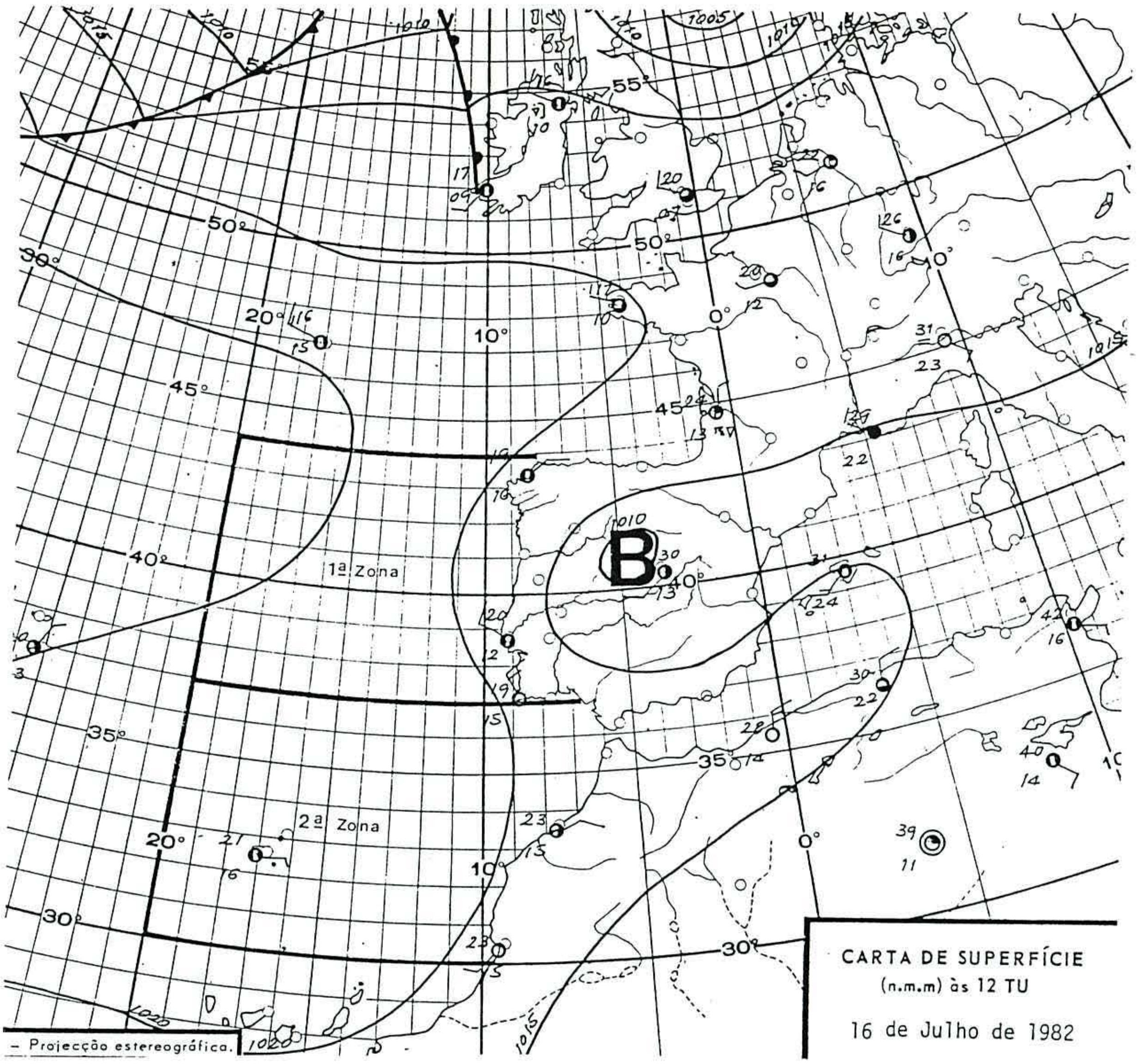

Figure 5.3: Surface meteorological chart of 16 July 1982 at 12:00 showing a thermal low centred over the Iberian Peninsula, which corresponds to a typical summer pattern in this region.

level time series gives a maximum of 0.90, significant at the 97.5% level, with the sea level curve at Faro leading the sea level curve at Lagos by a lag of 18 hours, meaning a progression of the signal of 96 km/day. From the analysis of consecutive available AVHRR images, the warm water band is seen to progress along the southern coast 31 km from day 244 at 0320 till day 246 at 0256 and 33 km from this day till day 248 at 0412, representing a steady flow with a speed of about 16 km/day. The raw AVHRR images, scanned from the monochrome prints, are displayed in Figure 5.4, **a**, **b**, and **c**, and the arrows represent the edge of the coastal warm water. Although there is some uncertainty in these estimates, because of the difficulty of tracking features from one image to the next, this evidence suggests that the observed rise in the sea level is primarily due to the decline of the upwelling rather than to the progression of the warm water. With the end of the upwelling regime and the westward progression of the warm water, an increase in the nearshore surface temperature of about 5°C in Faro and 3°C in Portimão is observed. By the end of the displayed time series, a drop in the sea level and in the nearshore temperature occurred, apparently in response to the re-establishment of westerly wind and the related upwelling regime. However, no satellite images were available for that time.

The coastal warm intrusion advanced about 60 km between day 248 at 0412 and day 250 at 0337 (Figure 5.4, **c** and **d**), turning around Cape São Vicente and advanced northward along the western coast, with a progression of about 30 km/day, almost the double of the progression speed in the southern coast. This event occurred during a relaxation of the northerly wind at both Sines and Sagres. At that time, the upwelling was limited to the part of the western coast north of 37.5°N, and the filament near Cape São Vicente was not directly connected to the Cape itself, but with the water upwelled further north. Subsequently, a short time span of northerly wind intensification occurred and the warm water ceased its northward progression along the coast. Instead it was diverted westward as an offshore prolongation of the flow along the

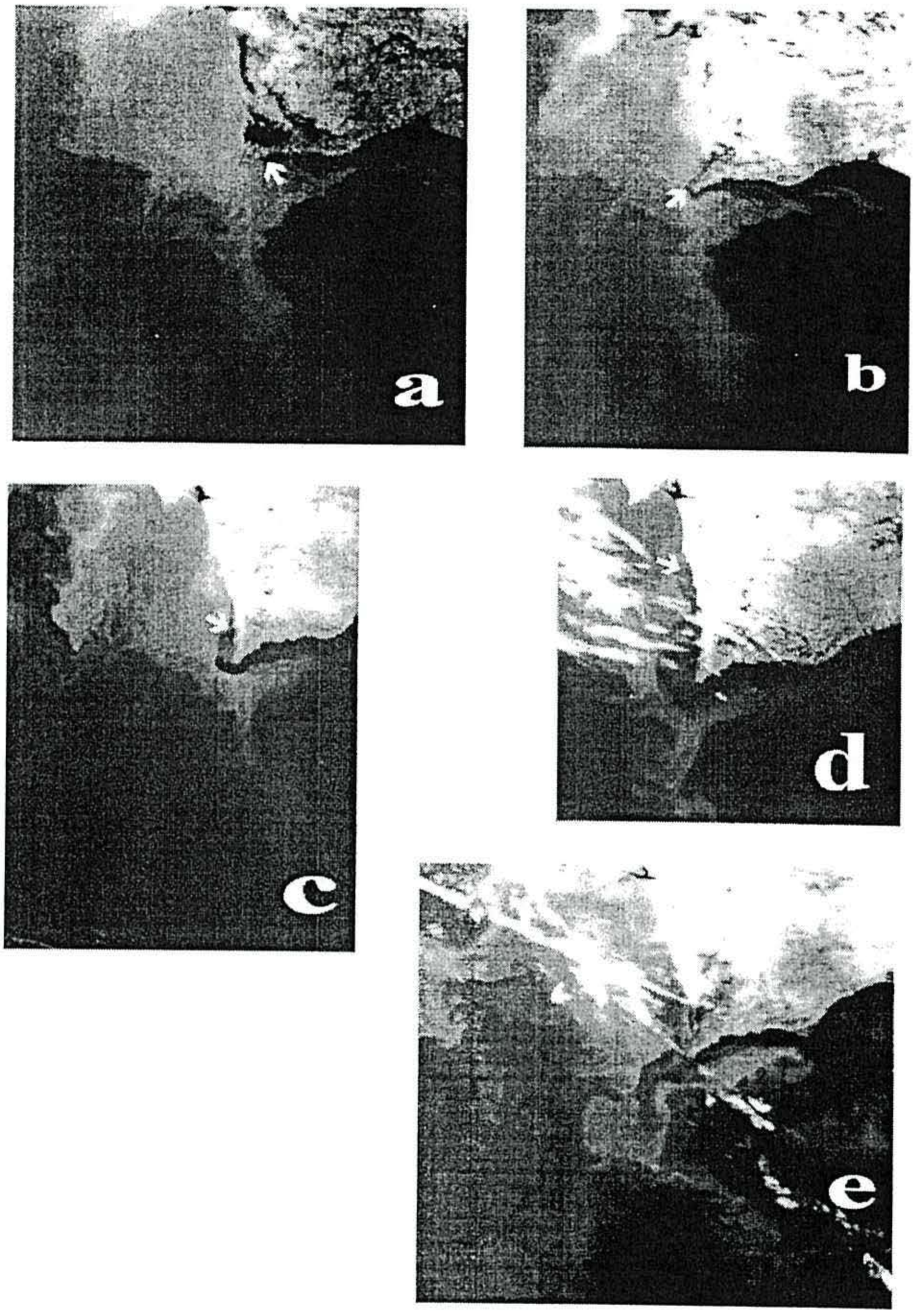

Figure 5.4: Raw AVHRR satellite images, scanned from monochrome photographic prints, showing the westward progression and 'breakthrough' of the coastal warm counterflow. Arrows point the edge of the warm counterflow. Images correspond to: (a) — 1 September at 0320 (day 244); (b) — 3 September at 0256 (day 246); (c) — 5 September at 0412 (day 248); (d) — 7 September at 0337 (day 250); (e) — 13 September at 0417 (day 256), all from 1982.

southern coast of Algarve. This can be seen in Figure 5.4, **e**, which corresponds to 13 September (day 256). The warmer water crossed the bathymetry into deep water and broke through the surrounding cold filament, which became separated from the cold upwelled water off the western coast. Consequently, the separated filament lost definition and began to decay. Also the cold water over the southern coast continental slope became separated from the water upwelled on the western coast. Simultaneously, a pronounced relative minimum in the tide gauge records of Faro and Lagos, on the southern coast, suggested the sudden release of the warm water accumulated in the southern coastal region over the cold denser offshore water. This pattern of warm water 'breakthrough' was observed several times during the 14 years covered by the satellite imagery archive. Another of these events occurred in September 1988, although the cold Cape São Vicente filament was not present at the time. A digital format AVHRR was available for that time and is displayed in Figure 5.9 as an additional illustrative example.

By mid September (day 259), a wind reversal occurred at all three wind stations and southerly downwelling favourable winds of about 8 m/s were observed on the western coast. As upwelling ceased off the western coast, the warm intrusion developed northward as a coastal counterflow, reaching Sines by the end of the analysed period. A rise in the sea level and a significant warming of the nearshore surface temperature was then observed at Sines, clearly out of phase with those observed in the southernmost stations.

Similar analyses were made for the summers of 1985, 1990 and 1991, although the sets of observations were not so complete. The observed patterns were consistent with those observed in 1982.

## 5.5 Sea surface temperature patterns in the Cape São Vicente region

Some AVHRR images available in digital format were used to clarify and analyse the sea surface temperature patterns in the Cape São Vicente region. Relevant sequences of images, or individual images, showing the characteristic features and their evolution were selected. The aim is to illustrate and examine the typical patterns, rather than to study individual cases. However, when wind measurements contemporaneous with the images are available, they will be plotted for a better understanding of the constraints and forcings. Wind vectors representing the mean winds in the 72 hours prior to the image time are overlaid at the Sines, Sagres and Faro locations. Images were processed for sea surface temperature as described above, and the 100, 200 and 500 meters depth contours were overlaid. Off the zonal Algarve coast and to about 10 km north of Cape São Vicente, the 100 meters contour can be understood as the shelf edge, which is very sharp and lies at about 100-130 meters depth, followed by a steep slope down to about 700 meters depth.

### 5.5.1 Upwelling patterns

A set of images from the summer of 1988 is displayed in Figure 5.5 (the NOAA-10 image from July was only processed for brightness temperature). Upwelling occurred off the western coast all summer 1988 in response to prevailing northerly winds. On 25 July a wide band of cooler upwelled water was situated along the western coast. The thermal front between the upwelled water and the warmer offshore waters was contorted by small scale disturbances. A major filament structure was present, but with no evident relation with the Cape São Vicente. The coastal southward jet associated with the upwelling regime appears to advect cold water along the depth contours eastward around Cape São Vicente. Although a similar pattern could be generated by shelf edge upwelling, this mechanism is not likely to be present. Clearly, non-upwelling conditions were present in the southern coast due to the weakness of the winds and the cooler waters advected by the jet after turning Cape São Vicente stretch along the shelf break/upper slope area, leaving warmer water on both sides. This pattern is a very frequently observed in the imagery archive.

By the end of August upwelling was still present off the western coast. The temperature anomaly due to upwelling was about 5°C but the thermal front is rather diffuse. A not very developed filament is observed to extend westward from Cape São Vicente and a weak upwelling is seen to set-up in the western part of the southern coast. By the beginning of September a filament formation is seen to extend about 80 km southward from Cape São Vicente. Further west the offshore warm water migrates poleward obscuring the thermal signature of the westward filament formation. However, by 5 September the upwelling in the western coast had decreased in intensity due to the wind relaxation, the equatorward filament structure weakened, and the extent of cold water along the southern coast had decreased. Scenes from 30 September and 1 October show a pattern similar to that from the end of July.

The Cape São Vicente cold filament did not grow into a full developed structure during the upwelling season of 1988, although upwelling was present in the western coast during most of the season. In all the years covered by the imagery archive, this was the only one without a consistent development of the Cape São Vicente filament.

A set of cloud free images from late summer and early autumn of 1993 are displayed in Figure 5.6, representing a typical upwelling regime off the southern coast of Algarve in response to prevailing westerly winds. As seen before, upwelling in the southern coast is less frequent, and usually weaker, than in the western coast. Apparently a pattern like this is sporadic, because it was seldom observed in the 14 years archive of images. Upwelling was intensified during the second half of September, reaching a strong temperature contrast with the offshore waters of about 5°C. The outer limit of the upwelled waters does not extend far beyond the continental slope, in contrast

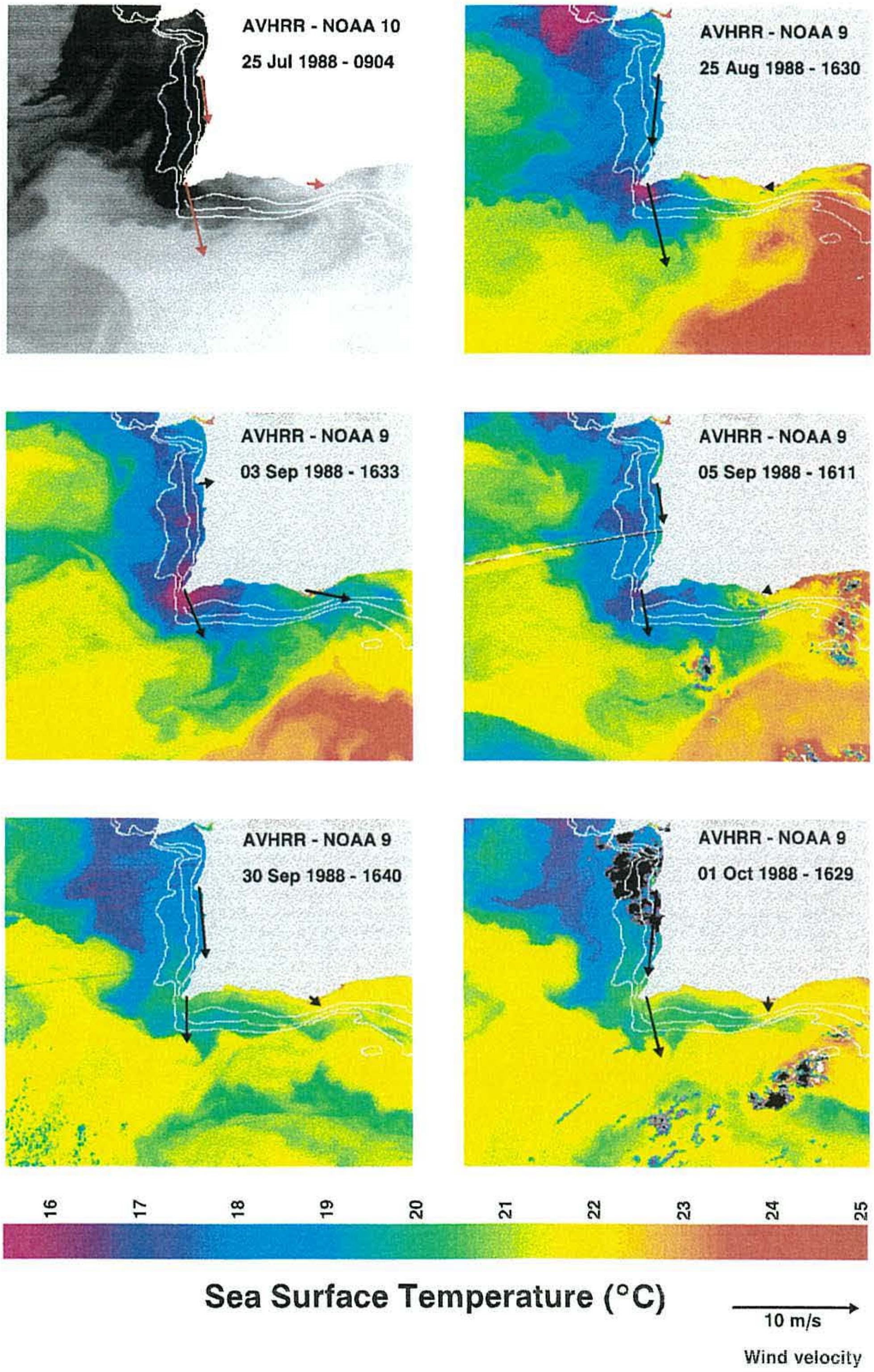

Figure 5.5: Set of thermal infrared NOAA-AVHRR images for the summer of 1988, when upwelling occurred off the western coast. The first image (NOAA 10) was processed only for brightness temperature. The other images (NOAA 9) were processed for sea surface temperature. The 100m, 200m, and 500m depth contours are overlaid to the images. Wind vectors, computed as explained in the text, are plotted at Sines, Sagres and Faro.

with what occurs off the western coast. Seaward off the western coast, the northward migration of warmer water is evident, apparently supplied also by the warm water lying further south off the Algarve coast. By the end of October a wind reversal is observed at Faro and upwelling starts to decay in the eastern half of Algarve. A generalized cooling of the surface waters occurred and a small cold plume is seen to grow with a strong westward component from Cape São Vicente, apparently in consequence of the intensification of the upwelling off the western coast.

### 5.5.2 Non-upwelling patterns

The non upwelling pattern observed in the imagery corresponds always to the development of a warm water band along the coast. The extent of the development of the warm band depends on the occurrence of upwelling and, in this way, is related to the wind regime. A good example, showing the progression and retraction of this feature between 27 July and 12 August 1992 is presented in Figure 5.7.

In the initial stage (27 July), upwelling was present off the western coast but not off the southern coast, where the warm coastal feature starts to emerge corresponding to winds blowing with an easterly component along the south coast of Algarve. A zonal tongue of cold waters extends eastward along the Algarve shelf edge and slope, apparently due to the continuation around Cape São Vicente of the equatorward coastal current off the western coast. By 4 August the narrow coastal structure is clearly distinguished, with a temperature signal of about 3.5°C. As the upwelling regime decays on the western coast due to the weakening of the prevailing winds, the leading edge of the coastal warm intrusion turns around Cape São Vicente, progressing about 110 km in 8 days ($\approx$14 km/day). The tongue of cooler water reduces its extension while further south offshore warmer waters progressed to the west.

The full development of the warm band was reached on 8-9 of August, when it passed the Cape of Sines. Although the appearance of this feature along the southern

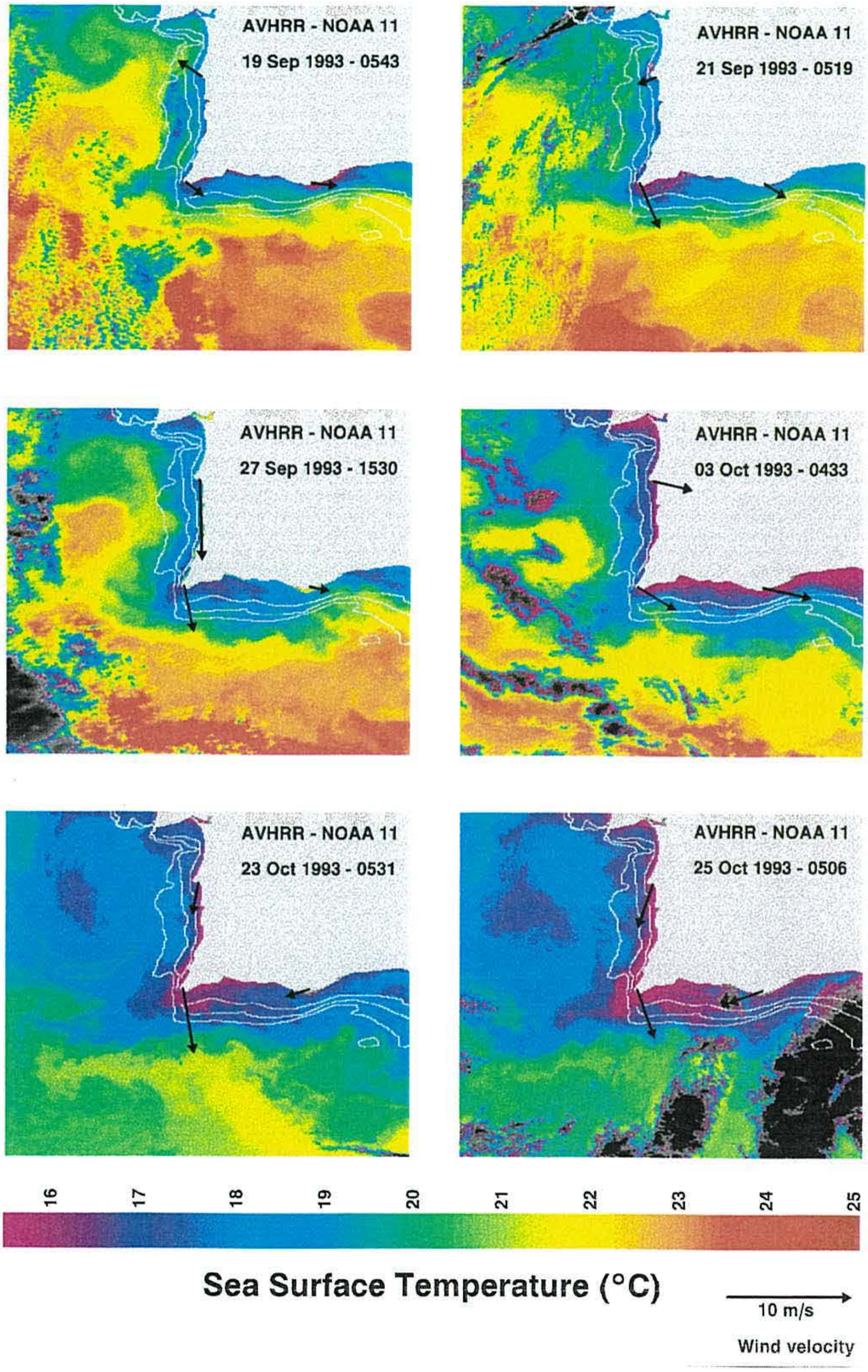

Figure 5.6: Set of thermal infrared NOAA-AVHRR images showing an upwelling episode in the southern coast of Algarve. Images were processed for sea surface temperature. The 100m, 200m, and 500m depth contours are overlaid to the images. Wind vectors, computed as explained in the text, are plotted at Sines, Sagres and Faro.

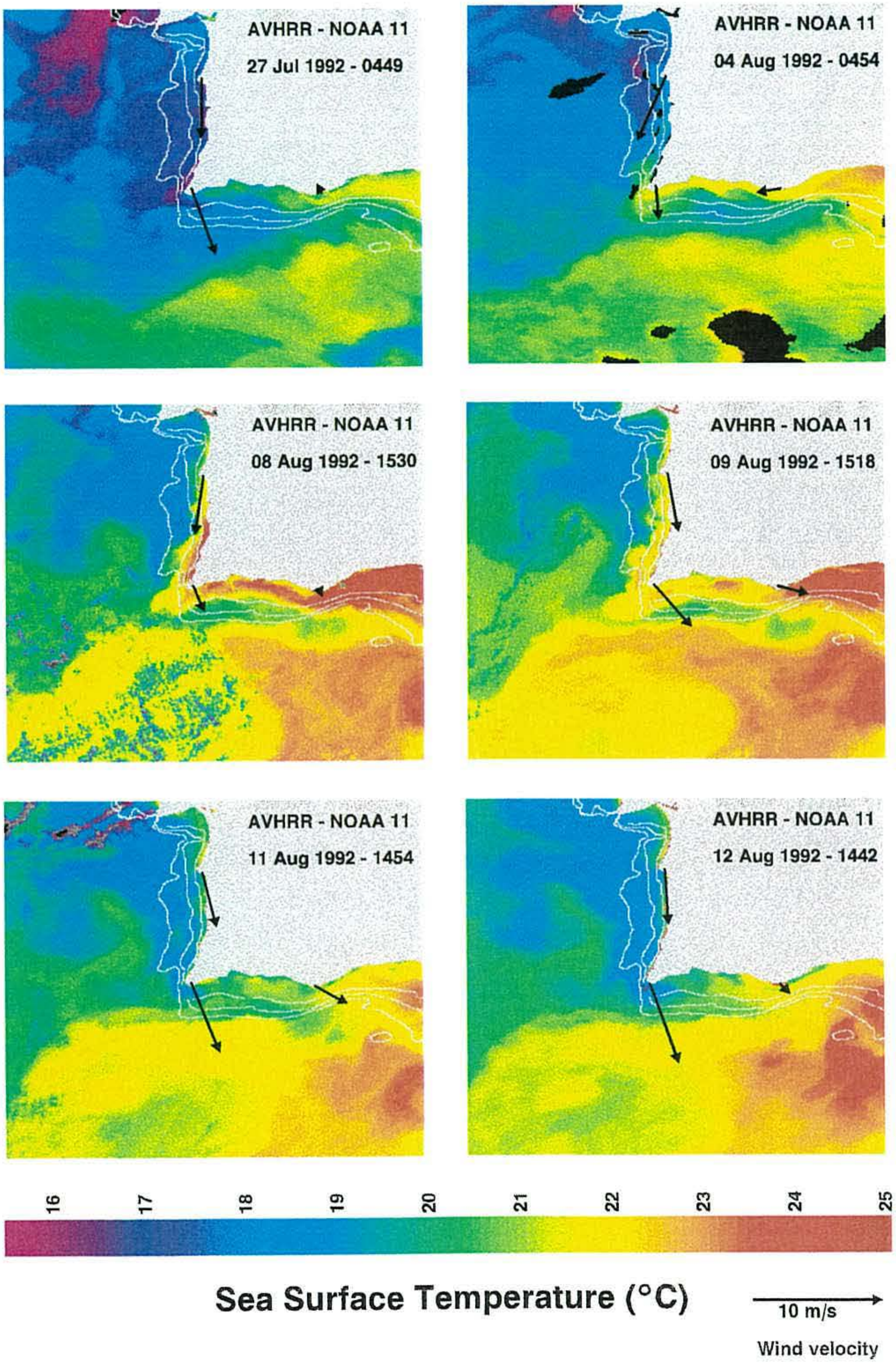

Figure 5.7: Set of thermal infrared NOAA-AVHRR images for the summer of 1992 showing the progression and retraction of a warm intrusion close to the coast in the Cape São Vicente region. Images were processed for sea surface temperature. The 100m, 200m, and 500m depth contours are overlaid to the images. Wind vectors, computed as explained in the text, are plotted at Sines, Sagres and Faro.

coast was systematically observed in the imagery whenever upwelling was absent, the evolution of the warm band along the western coast is more sporadic due to the higher persistence of upwelling on the western coast, and it reaches the most northward regions only in the final stage of its evolution. From 4 August at 0454 till 8 August at 1530 the progression of the warm water along the western coast can be estimated as 125 km (≈28 km/day). The coastal warm water is confined to the continental shelf, roughly limited by the 100 meters contour, suggesting a bathymetric control of the feature. It is observed to have a width of 15-25 km, which decreases northward, and a significant warming is observed to occur nearshore. Cooler water still remains over the continental slope and warmer offshore waters are seen to migrate, first westward, and then starting to flow northward off the western coast. By 11-12 of August the coastal warm feature had disappeared, due to the re-establishment of upwelling in the western coast induced by stronger favourable winds, and colder water is once again seen to turn cyclonicaly, close to shore, around Cape São Vicente. Also off the southern coast winds are observed to reverse westerly and the warm feature is seen to start to retreat.

The speeds of the coastal alongshore migration of the warm water, either off the southern coast or off the western coast, are remarkably similar to those estimated earlier in this chapter for the summer of 1982. In addition, other estimations of the kinematics of the coastal warm counterflow, possible from cloud free AVHRR monochrome prints sequences, showed very consistent values: between 19 July at 0359 and 20 July 1986 at 0348 (Figure 5.8) it progressed 14 km (≈14 km/day) and between 11 August at 0322 and 13 August 1991 at 0303 (Figure 5.10) it progressed 32 km (≈16 km/day), in both cases turning around Cape São Vicente, and between 18 September at 0104 and 19 September 1988 (Figure 5.9) it progressed 39 km along the western coast (≈33 km/day). Accepting the surface temperature as a non-conservative tracer of the flow path, it is possible to presume that the non-upwelling pattern in the Cape São Vicente region is dominated by a coastal warm countercurrent, flowing with surface speeds of the order of 16-18 cm/s westward along the southern coast and of the order of 32-38 cm/s poleward along the western coast.

An explicit example of the coastal warm feature turning clockwise around the Cape São Vicente is shown in Figure 5.8, corresponding to 20 of July 1986 (julian day 202). Low passed wind vectors at Sines, Sagres and Faro, available for July 1986, are also displayed. Sagres wind is shown twice, unrotated and rotated to the east-west direction, as was done with the Faro data. The "nose" of the warm feature is very narrow but well defined, with a width about 10 km and a surface thermal signature of about 2°C. The pattern observed in the satellite scene corresponds to the end of a short period of easterly downwelling favourable winds, blowing along the southern coast with relatively weak alongshore velocities (about 3 m/s at Faro and 2 m/s at Sagres). The warm feature turns poleward around the Cape crossing the bathymetry and leaving some amount of cooler water inshore. This occurred during a relaxation of the northerly winds observed at Sagres and Sines. Further north along the western coast upwelling was still present, and the usual pattern with cold water extending along the continental slope was observed off the southern coast.

A pattern observed in the imagery at times when upwelling is absent from the southern coast and the warm coastal countercurrent is setup, is exemplified by the AVHRR image of 19 September 1988 in Figure 5.9. Part of the warmer water flows poleward along the western coast, but the main part of the coastal warm water is seen to continue directly west from Cape São Vicente. It breaks through the body of cooler water that was previously established off the western coast and along the shelf edge and slope east of the Cape. The warm lighter water crosses over the denser colder water and connects with the offshore warm water, apparently due to a weakening of the cooler equatorward jet or to the excess of water of the coastal warm flow. Cooler water stays isolated over the southern continental slope.

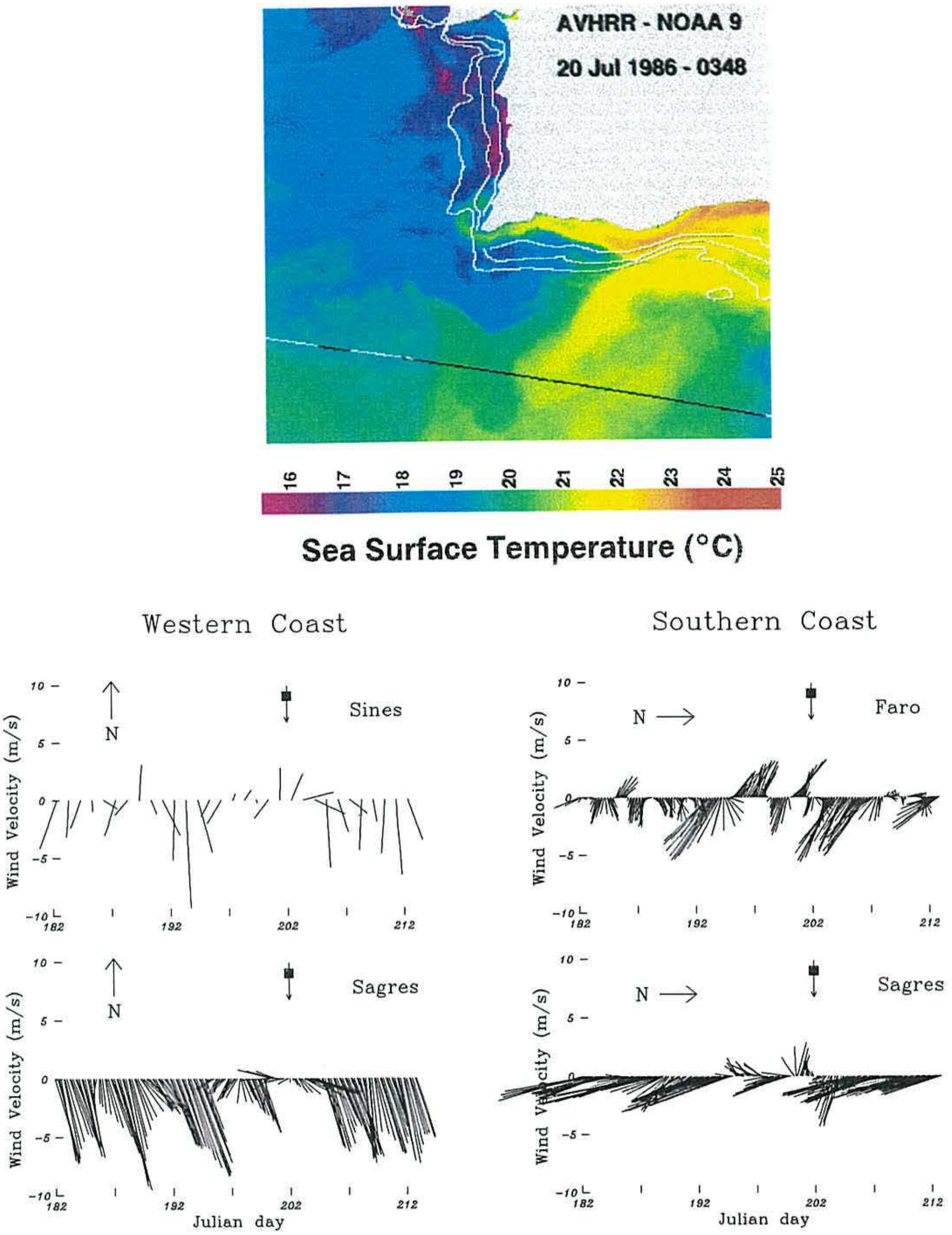

Figure 5.8: Thermal infrared NOAA-AVHRR image of 20 of July 1986 (julian day 202) showing the development of the coastal warm feature the Cape São Vicente region and the wind vectors (low pass filtered at 40 hours) for July 1986 at Sines, Sagres and Faro, rotated alongshore for the western and southern coasts. Image date is marked in the stick diagrams. Image was processed for sea surface temperature. The 100m, 200m, and 500m depth contours are overlaid to the image.

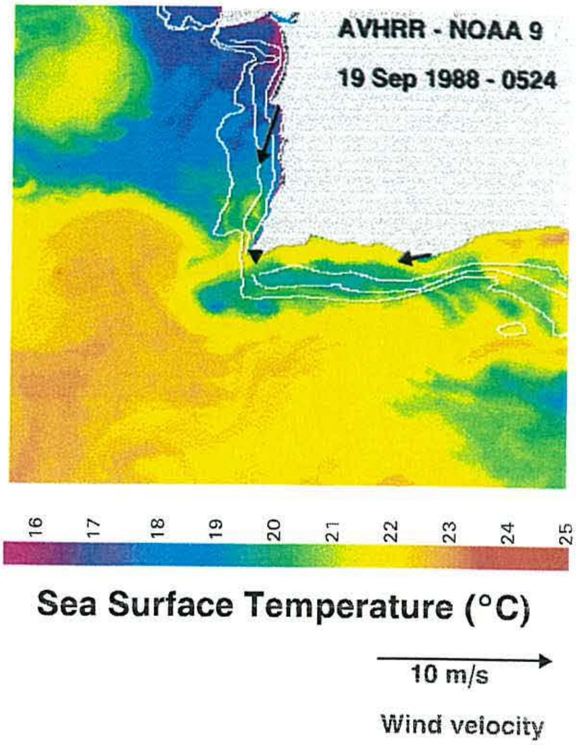

Figure 5.9: Thermal infrared NOAA-AVHRR image of 19 of September 1988 showing the offshore release of the warm coastal feature near the Cape São Vicente. Image was processed for sea surface temperature. The 100m, 200m, and 500m depth contours are overlaid to the image. Wind vectors, computed as explained in the text, are plotted at Sines, Sagres and Faro.

### 5.5.3 Filament patterns

Selected images are used to illustrate the characteristic patterns of the cold filament that are often observed during the upwelling season, apparently related with Cape São Vicente itself. Images are displayed in Figures 5.10, 5.11 and 5.12, along with the corresponding time series of the low pass filtered wind vectors at Sines, Sagres and Faro. Wind vectors are represented so that the ordinate represents the alongshore wind component, with negative values indicating an upwelling favourable wind component.

It is observed that the filament formation is always preceded by periods of upwelling along the western coast, driven by relatively intense alongshore northerly wind, and that the filament persists until the wind weakens. For instance, in the sequence of thermal images of the first half of August 1991, shown in Figure 5.10, upwelling was

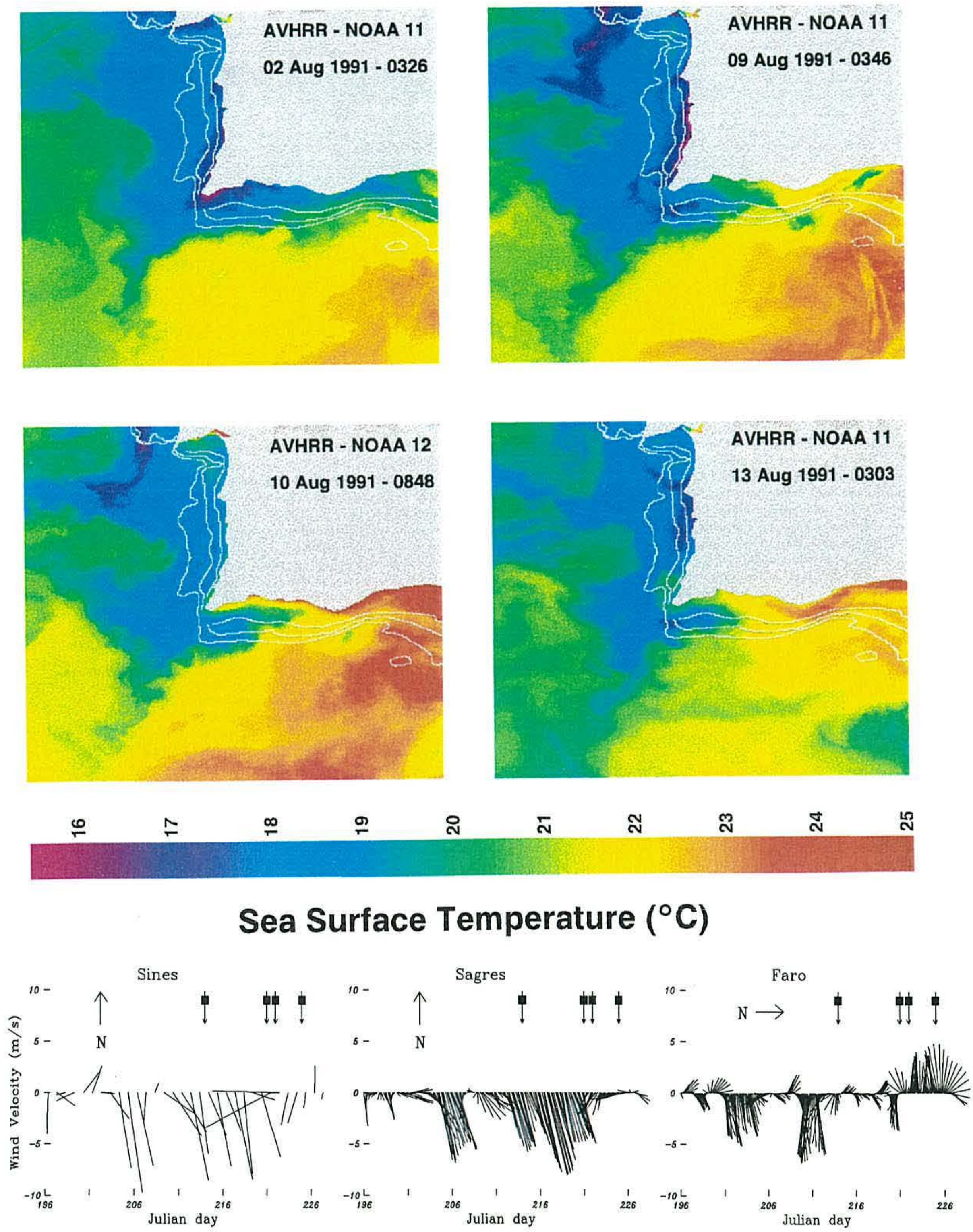

Figure 5.10: Set of thermal infrared NOAA-AVHRR images for the first half of August 1991, when the Cape São Vicente filament structure was developing. Images were processed for sea surface temperature. The 100m, 200m, and 500m depth contours are overlaid to the images. Stick vectors time series of the wind field measured at Sines, Sagres and Faro from 15 of July till 15 of August are also displayed. Wind vectors are represented so that the ordinate always represent the alongshore wind component. Image dates are indicated in the stick diagrams. ( 2 of August - day 214; 9 of August - day 221; 10 of August - day 222; 13 of August - day 225)

established along the western coast during early August, in response to relatively intense southward wind. The Cape São Vicente filament develops with a surface thermal signature of about 3°C and is seen to grow with a southward orientation, reaching a length of about 110 km by 2 August (day 214) and 160 km by 9 August (day 221). Similar wind patterns associated with the filament formation are observed in Figure 5.11 (26 August 1985 — day 238 and 4 September 1985 — day 247) and Figure 5.12 (16 September 1984 — day 260).

Coming back to Figure 5.10, upwelling is observed along the southern coast by 2 of August (day 214), in response to a short event of intense westerly wind recorded at Faro. Upwelling is later seen to retreat along the southern coast as a consequence of the relaxed winds recorded at Faro, in the southern coast, and coastal warm water is seen to progresses westward, even turning clockwise around the cape by 13 of August (day 225), profiting from easterly winds blowing at that time along the southern coast. Also, in 4 of September 1985 (day 247 — Figure 5.11) and 16 of September 1984 (day 260 — Figure 5.12) upwelling is absent from the southern coast and the coastal warm water band is seen to expand westward, despite some weak unfavourable easterly wind, leaving cooler water offshore over the continental slope.

In all the above mentioned situations, the southward filament was present, showing a clear independence between upwelling on the southern coast and the filament growing from the Cape São Vicente. This filament apparently constitutes the southward continuation of the equatorward coastal jet associated with the west coast upwelling overshooting the Cape.

In Figure 5.10, apart from the southern end of a filament from further north, another cold filament apparently related to Cape São Vicente is seen to grow roughly westward from the Cape. By 10 August (day 222) it has a length of about 130 km. Such westward filament structure is also observed in the satellite images displayed in Figures 5.11 and 5.12. This filament formation might result from the meandering flow of the geostrophic southward current associated with the upwelling, instigated by the presence of Cape São Vicente, and it would represent the offshore trending limb of a meander of the geostrophic flow. Another possible mechanism would be the presence of an eddy drawing cold water offshore, although no clear evidence of the presence of such an eddy is observed in the sea surface temperature field. An onshore return flow located to the south of the filament jet, much weaker than the jet itself, seems to be a characteristic feature of the filament structures [*Strub et al.*, 1991; *Ramp et al.*, 1991]. Such return flow would partially feed the southward filament.

The sea surface temperature structure shown in Figures 5.10, 5.11, and 5.12 illustrate the most typical upwelling pattern of the Cape São Vicente region observed in the imagery archive: Two cold filaments related to the Cape São Vicente, one equatorward and another westward, and a 'tongue' stretching eastward, roughly over the southern continental slope. These are particularly evident in the image of 16 of September 1984 (Figure 5.12). The cool 'tongue' is very stable and persistent, sometimes very narrow, having a length that ranges between 20 and 150 km, reaching occasionally as far as the Gulf of Cadiz. This cool water often results from the advection of coastal water along the depth contours around the Cape São Vicente, due to the conservation of potential vorticity. These waters often merge with waters upwelled off the Algarve, which were separated from the coast by the westward progression of the warm coastal counterflow. Occasionally frontal disturbances are observed in the offshore boundary of the cool eastward 'tongue'. The westward filament has a large variation in direction and development and occasionally rolls cyclonicaly in the offshore end. Sometimes it is very undefined or does not even appear. The southward filament is very frequent, well developed and with variations in configuration and a small degree of variation in direction. Frequently it is observed to roll cyclonicaly or to grow into a vortex pair structure with an inverted mushroom like shape.

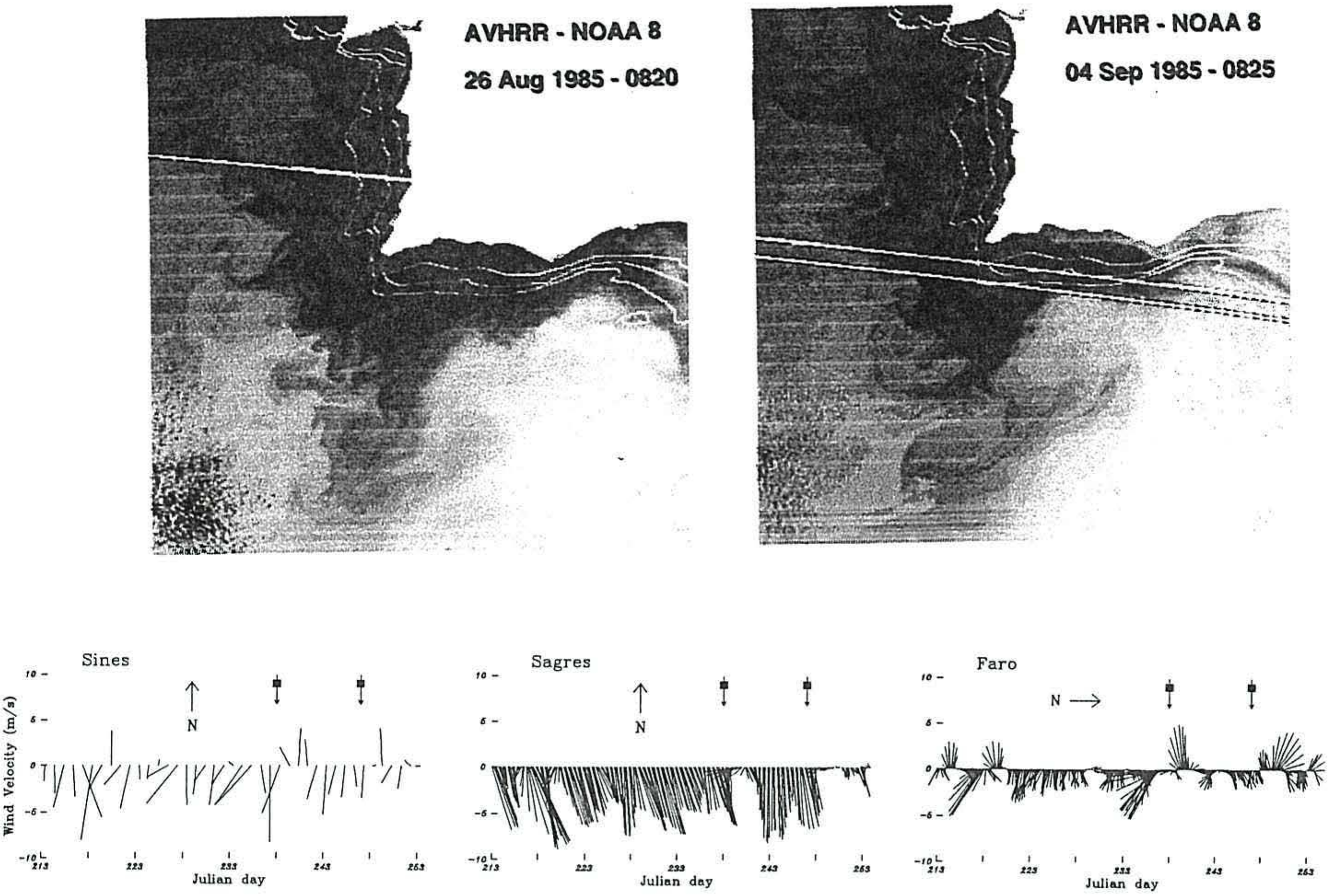

Figure 5.11: Thermal infrared NOAA-AVHRR images of 26 of August (day 238) and 4 of September (day 247) of 1985. Images were processed for brightness temperature. The 100m, 200m, and 500m depth contours are overlaid to the images. Stick vectors time series of the wind field measured at Sines, Sagres and Faro from 1 of August till 10 of September are also displayed and the image dates are indicated. Wind vectors are represented so that the ordinate always represent the alongshore wind component.

During the upwelling season, the most persistent feature of the pattern is the cool eastward 'tongue' stretching over the southern continental slope, followed by the southward filament and by the westward filament as the least persistent. However, east, south and west are the three privileged directions of development of the cold features. It is very rare that a filament grows with a southwestern or southeastern directions, although its particular form changes in time.

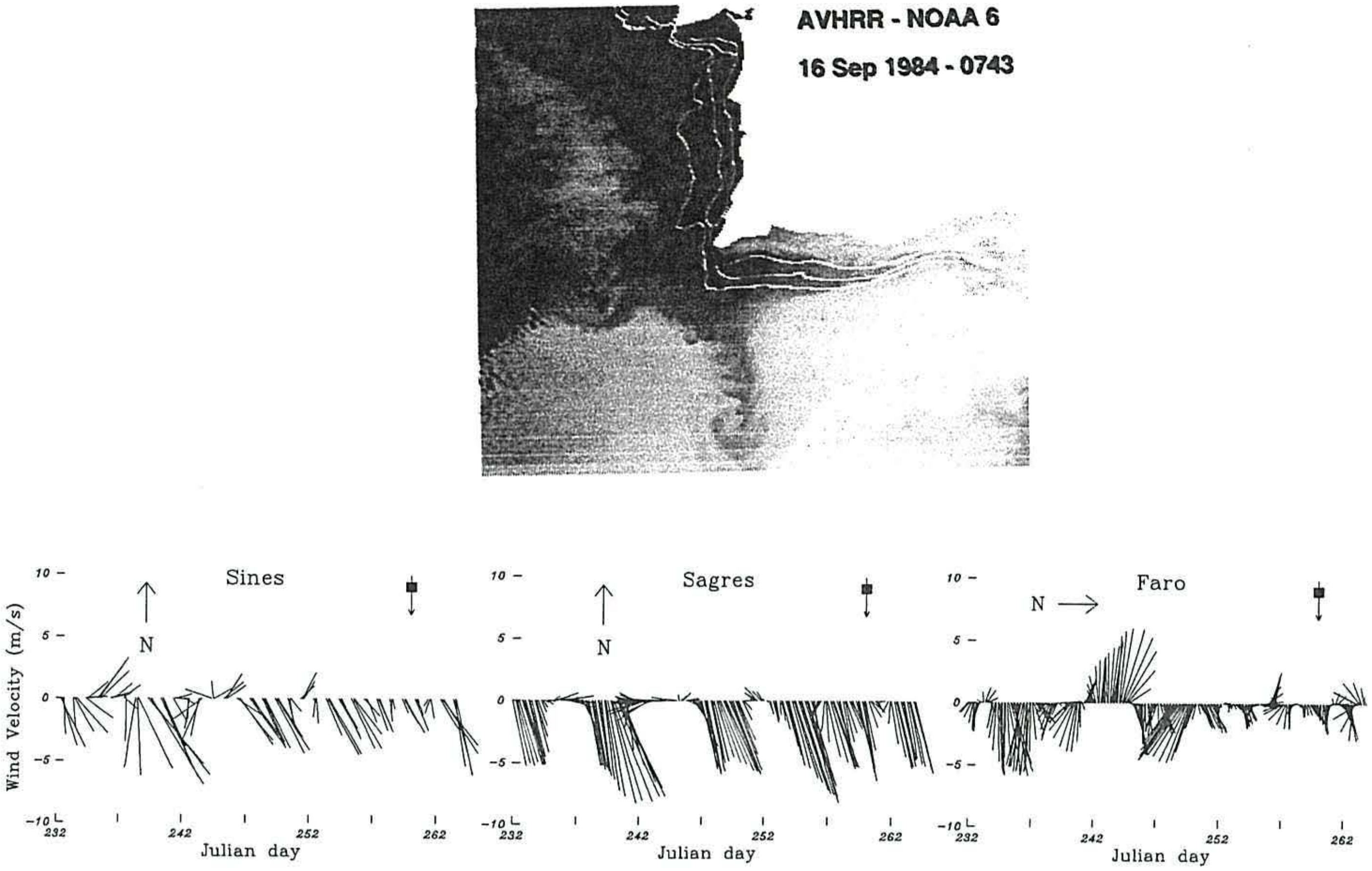

Figure 5.12: Thermal infrared NOAA-AVHRR image of 16 of September (day 260) of 1984. Image was processed for brightness temperature. The 100m, 200m, and 500m depth contours are overlaid to the images. Stick vectors time series of the wind field measured at Sines, Sagres and Faro from 20 of August till 20 of September are displayed, and the image date is indicated. Wind vectors are represented so that the ordinate always represent the alongshore wind component.

The frontal region that separates the cold filament waters from the surrounding warmer waters is almost always populated by conspicuous small scale disturbances. Those are particularly evident in the filament presented in Figure 5.12, suggesting the instability of the southward jet inside the filament. Also in the satellite image of 26 August 1985 presented in Figure 5.11, a well defined series of regularly spaced small perturbations oriented outwards is seen to contort the western boundary of the filament. These perturbations bend cyclonically in their outer edge resembling small scale replicas of filament features.

## 5.6 Conclusions

The analysis of the satellite thermal infrared imagery archive revealed that the coastal ocean in the region of Cape São Vicente has a marked seasonality, with the stronger activity occurring during summertime. This activity is characterized in the western coast by an almost permanent upwelling regime, while in the southern coast it is characterized by the eastward progression over the continental shelf of a coastal band of warm water, intercalated by upwelling episodes, strong at times.

In summertime the kinematics of the Cape São Vicente region is dominated by two main flows: A flow of warm waters progressing westward off the southern coast, with a probable origin in the Gulf of Cadiz, and an equatorward flow of cold waters off the western coast, with origin in the upwelled waters along the coast. Those two flows converge in the region of southwestern Iberia, where the southern and western coast meet.

The dynamics of the westward flow along the southern coast is likely driven by the alongshore pressure gradient discussed in the previous Chapter, and the observed westward progression of warm waters over the shelf represents a surface manifestation of this forcing. The wind forcing plays also an important role in the circulation off the southern coast by augmenting or diminishing the effect of the pre-existing alongshore pressure gradient. As is observed, strong westerly winds are able to induce coastal upwelling along the southern coast and to reverse the alongshore flow.

The dynamics of the equatorward flow off the western coast is presumably driven by the predominant northerly winds that, in accordance with Ekman theory, force near-surface offshore transport. This gives rise to coastal upwelling and to the associated southward current jet, due to geostrophic adjustment. During northerly wind relaxation events, the coastal warm feature seen to progress along the southern coast turns clockwise around Cape São Vicente and continues northward as a coastal countercurrent, occasionally progressing over 120 km along the western coast.

Strong and uninterrupted upwelling conditions off the western coast will imply a persistent energetic equatorward jet along the coast. The Cape São Vicente represents the southern limit of the western coast, where the constraint imposed by the presence of the meridional coastline disappears. Three privileged directions of spreading of the cold upwelled water advected southward along the coast are identified in the Cape São Vicente region, through the analysis of satellite imagery: eastward along the southern shelf break and slope, directly southward in the prolongation of the western coast, and westward around the latitude of the Cape São Vicente.

Although there is a lack of *in situ* observations of the cold mesoscale features developing in the coastal ocean off Cape São Vicente, it is possible to hypothesize qualitative explanations of the major processes involved in their formation and development, consistent with the satellite observations and with the previous understanding of the coastal transition zone processes.

- The westward cold filament observed to grow from the upwelling front roughly at the Cape São Vicente latitude in an approximately perpendicular direction, represents a typical filament structure, similar to those observed further north at the western Iberian coast [*Haynes et al.*, 1993] and off the coasts of California [*Brink and Cowles*, 1991]. Three main theoretical hypothesis for the filament formation were summarised by *Strub et al.* [1991], as discussed in Chapter II: 1) the pre-existence of a mesoscale eddy field which interact with the coastal upwelled water; 2) one-way jets, transporting coastally upwelled water seaward ('squirts'); 3) offshore and onshore meandering of the unstable continuous equatorward jet. Observation of the satellite imagery does not suggest that mesoscale eddies are the primary cause of the filament.

The pure one-way offshore jet hypothesis hardly admits the existence of the observed equatorward filament. Furthermore, when warmer water is seen to turn clockwise around Cape São Vicente, the westward filament is seen to be supplied by coastal waters upwelled further north. The 'squirt' hypothesis, topographically forced by the cape, implies that the cold water advected offshore in the filament was upwelled locally, which is not suggested by the observations of the imagery archive.

The hypothesis of an unstable equatorward jet, meandering offshore and onshore, instigated by the prominent protrusion of the Cape São Vicente, is suggested by the imagery observation. Additionally, some surface cold water of the filament jet could result from *in situ* upwelling due to ageostrophic divergence of the current flow, as it is suggested by *Strub et al.* [1991] for filaments off the Californian coast. This scenario is coherent with the development of the southward filament, which shall be fed partially by the onshore return flow, much weaker than the jet, located to the south of the filament jet. The meandering model forced by the coastal topography was already hypothesized by *Haynes et al.* [1993] as the primary mechanism for the formation of filaments along the western coast of Iberia. Observations presented here confirm that, at least for the westward filament related to the Cape São Vicente, it is the most likely mechanism. However, the coupling of this mechanism with the interaction with an offshore eddy can also be envisaged as a secondary process.

- The southward filament represents a particular case, because it occurs at a discontinuity of the western coast, represented by Cape São Vicente. The filament is fed by the cold waters upwelled further north, off the western coast, and advected equatorward by the coastal jet associated with the upwelling. Cold waters proceeding from upwelling episodes off southern coast are not likely to be present in the filament, because they would flow east under the geostrophic constraint.

Apparently the filament forms the southernmost edge of the intense coastal upwelling jet which overshoots Cape São Vicente and the jet itself represents the primary source of energy for the filament formation. The flow regime of the offshore warmer waters off the zonal coast of Algarve provides the energy to modulate the filament configuration or even inhibit its formation in the case of a less energetic equatorward jet.

In addition to mixing processes, the observed near-surface warming as water is advected seaward in the filament is due to the rapid sinking of waters in the filament as they flow offshore, as is suggested by observations in filaments in the California Current system [*Kadko et al.*, 1991; *Flament et al.*, 1985].

- The most frequent cold feature observed in the region is the eastward 'tongue' seen to extend over the southern shelf break and slope, leaving warmer water on both the inshore and offshore sides. This water apparently results from the eastward advection around Cape São Vicente of cold waters upwelled off the western coast, due to conservation of potential vorticity. They possibly merge with waters upwelled locally under westerly favourable winds, which migrated offshore due to the progression of the warm coastal counterflow.

In the initial stages of the upwelling regime, or during events of weak upwelling on the western coast, the equatorward jet is not strong enough to form a southward filament, and only the cold eastward 'tongue' develops, constrained by the conservation of potential vorticity. If upwelling is occurring at that time on the southern coast, the 'tongue' will merge with the cold upwelled waters. A stronger jet with higher kinetic energy, induced by a more intense upwelling regime on the western coast, will result in the formation of the southward cold filament. In the case of a persistent equatorward jet, it may meander triggered by the Cape São Vicente interaction with the ambient regime offshore, to produce the eastward filament. This picture is consistent with the order of occurrence and the relative persistence of the three cold features identified.

# Chapter 6

# The oceanographic experiment in the Cape São Vicente region

## 6.1 Introduction

A physical oceanography experiment was realized during the Cruise nº 201 of RV POSEIDON, leg 9 (POS 201/9) between 11 and 22 of June 1994, as part of the present study of the dynamics of the Cape São Vicente upwelling region. The field work was a collaboration of the Unidade de Ciências Exactas e Humanas/Universidade do Algarve and School of Ocean Sciences/University of Wales, Bangor with the EUROSQUID project AIR 1 CT 92 0573. It was a joint cruise with biological and physical oceanography components. The biological component was related with the environmental characterization of possible cephalopod spawning sites near the Portuguese coast.

The overall aim of the physical oceanography component was to investigate the hydrographic and flow regimes in the area around Cabo São Vicente in relation to the mesoscale features revealed in satellite sea surface temperature imagery. The analysis of the AVHRR imagery archive had been done prior to the cruise, so we had in advance a general overview of the behaviour of the coastal ocean in the region during this time of the year. Specific goals for the cruise were:

i) to study the three dimensional structure, dynamics and evolution of the Cape São Vicente filament during upwelling favourable winds.

ii) to improve our knowledge of the nature of the coastal warm counter-flow and to understand the physical processes involved in its formation and development.

iii) to understand how the equatorward jet off the western coast interacts with the apparent westward flow off the southern coast of Algarve.

## 6.2 Cruise plan and execution

The initial plan for the physical oceanography experiment was very broad, including only the transects 1,2,3,4,5 and 13 (Figure 6.1). However, it was our intention that the detailed cruise planning should be continually modified during the experiment as satellite images were received and processing of *in situ* data was carried out on board the ship.

During most of the cruise the winds were, against our expectation, weak except around 20 June. We expected strong winds with components from north and west, more typical of the wind regime in this region during this time of the year. We also expected an intensification of the equatorward flow around Cape São Vicente and the development of a coastal upwelling front, both due to the wind forcing. With those conditions, the development of the Cape São Vicente filament of upwelled water would be probable. Since 1982 the spatial and seasonal development and evolution of the upwelling front and filaments of Iberian Peninsula have been observed and analysed with regularity using AVHRR imagery. It was possible to conclude that upwelling generally starts in late May or early June, although the major filament structures generally appear in late July or August. However, one of the most impressive developments of the Cape São Vicente filament was observed in June [*Barton*, 1991]. The dates of the cruise seemed appropriate to reach the objectives of the experiment and sample

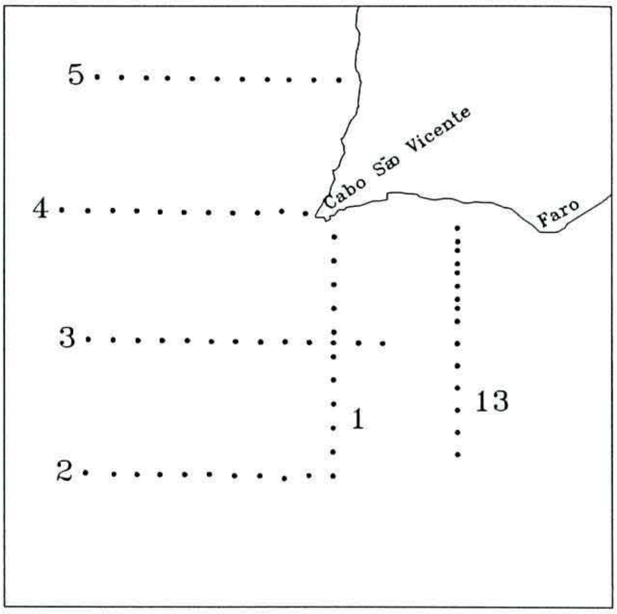

Figure 6.1: Initially planned transects

the upwelling filament off Cape São Vicente. Furthermore, the analysis of the AVHRR satellite images for the days just before the beginning of the cruise, showed the presence of an upwelling front off the western and southern coasts of Portugal.

During the cruise, available images received by the University of Dundee reception facility were processed and analysed by colleagues in the School of Ocean Sciences in near real time. When a clear image was available, it and a simplified sketch of its main features were transmitted to ship by telefax. During the first days of the cruise the presence of clouds did not allow the guidance of the oceanographic sampling by the AVHRR satellite images of the sea surface temperature. After sampling the initially planned transects, some clear days allowed us to confirm with the AVHRR images that the previously present upwelling fronts had disppeared and there was no well defined filament development. Obviously, this situation was evident from the weakness of the wind and from the analysis of the vertical profiles from the first transects.

In consequence, it was planned to sample on a 10×10 km grid off the western coast, a similar grid off the southern coast and an oblique transect from near Cape São Vicente towards open ocean. The objective of this pattern was to focus the sampling more in the coastal dynamics and circulation of the apparent poleward warm flow around Cape São Vicente, essentially concentrating on the two last objectives of the experiment. This sampling pattern would reveal in any case the presence of even a weak upwelling front, if present.

## 6.3 Environmental data

Throughout the cruise environmental data were collected. These comprised the ship speed components, wind components, air temperature of the dry bulb and wet bulb, irradiance, air pressure and water temperature at three meter hull intake. The readings were taken every four minutes. Because meteorological sensors on both sides of ship were not functioning, the data are not always from the exposed side of the vessel. The port air temperature sensors failed. Starboard wind direction was not functioning and, as the mast may alter the wind flow, some directional errors can appear in the records. Wind speed was taken as the maximum of port and starboard sensors before calculating the components. Ship speed components were added to wind components to obtain values of wind velocity relative to earth.

For the cruise period, by courtesy of the Instituto de Meteorologia in Lisbon, we obtained also the wind observations from the meteorological station located at Sagres. The speed and direction measurements were realized every three hours.

All the environmental data collected during the cruise are displayed in *Relvas and Barton* [1995], along with some additional information concerning the data presentation.

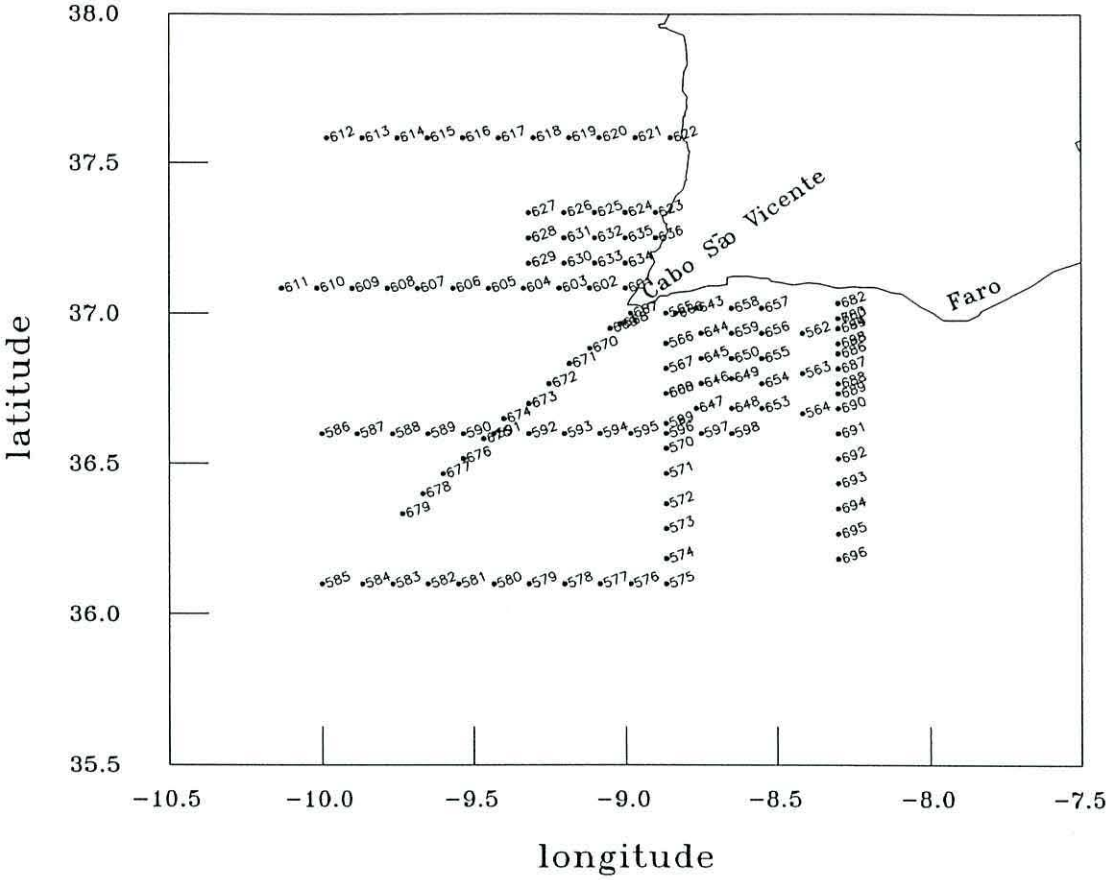

Figure 6.2: CTD stations of Poseidon cruise 201/9 (11 of June to 22 of June 1994)

## 6.4 CTD data

During the cruise 132 CTD stations were executed. The location and the station numbers of the CTD stations are presented in Figure 6.2 and the temporal distribution of the sampling stations are shown in Table 6.1. Inserted between the CTD stations, there were 16 biological stations where CTD casts were not performed, so that station numbering is not always consecutive. The distance between CTD stations was 10 km, except nearshore in two of the transects, where the distance was 5 km. The casts were limited between the surface and 500 meters depth in the majority of the stations. In the case of shallow water, the samples were limited to 5 meters above the bottom depth.

| **Poseidon cruise 201/9** | |
|---|---|
| **Date** | **CTD Stations** |
| 11 June | 562 to 568 |
| 12 June | 569 to 584 |
| 13 June | 585 to 598 |
| 14 June | 599 to 610 |
| 15 June | 611 to 625 |
| 16 June | 626 to 636 |
| 17 June | 643 to 650 |
| 18 June | 653 to 659 |
| 19 June | 666 to 679 |
| 20 June | 682 to 696 |
| 21 June | 698 to 700 |

Table 6.1: Performing dates of the CTD stations

The CTD measurements were made with a new Sea-Bird Electronics instrument, model SBE 19 *Seacat Profiler* belonging to the UCEH/Universidade do Algarve. The instrument was equipped with an 512K bytes of static RAM memory. All the other features were standard, without optional configurations or equipment. The sampling rate was adjusted to 1 scan every 0.5 seconds and the used lowering speed was 1 meter/second at all the stations. The CTD worked perfectly throughout the cruise.

Just after each CTD station the raw data obtained in the profile were downloaded to a personal computer. A basic processing was carried out and a quick display and a draft plot of the profile was printed using the Sea-Bird software (Seasoft). Initial processing included, among other details, removing those scans recorded out of water, excluding scans associated with pressure reversals due to the ship oscillation and averaging the data in bins of two decibars. With this procedure it was possible to have a quick look at the data shortly after finishing the station. A few minutes after finishing each transect, the vertical fields of the temperature, salinity and density were plotted. The objective was to detect as soon as possible the crossing of any front and for that goal these representations based in uncalibrated data were enough.

Subsequent stages of the processing and the calibrations were carried out later in the School of Ocean Sciences/University of Wales at Menai Bridge, using locally developed Fortran programmes to produce final graphics and summary listings of derived parameters. These include plots of the vertical profiles of temperature, salinity and density ($\sigma_t$), a table of these values at standard depths plus the dynamic height anomaly, a T-S diagram and the station identification. The calibrated values of temperature and salinity were used to derive the density and dynamic height anomaly. All the derived information was calculated by employing the standard algorithms recommended by UNESCO [1991]. The complete set of the stations summaries plus the observed vertical and horizontal fields of temperature, salinity and density were published in a data report [*Relvas and Barton*, 1995].

### 6.4.1 Calibration and correction of T-S data

The Sea-Bird CTD instrument was calibrated with the original manufacturer's calibration, dated from 25 of March 1993. The cruise was the first time this instrument was used. During the cruise, water samples and temperature readings were taken on 29 stations to calibrate the sensors. The majority of the samples was taken near the maximum cast depth. Salinity samples were collected from a Nansen bottle clamped to the wire, just above the CTD. Due to the CTD guard cage, the distance between the conductivity sensor and the Nansen bottle was more than one meter. Temperature readings were taken from a digital reversing thermometer secured to the Nansen bottle. The water samples were collected in tightly closed bottles and the samples were analysed some time after the cruise in an Autosal salinometer at the School of Ocean Sciences in Menai Bridge. There were 19 temperature comparisons and 25 salinity comparisons after obviously erroneous values were eliminated. In the Figure 6.3 are represented the temperature and salinity differences versus the station number.

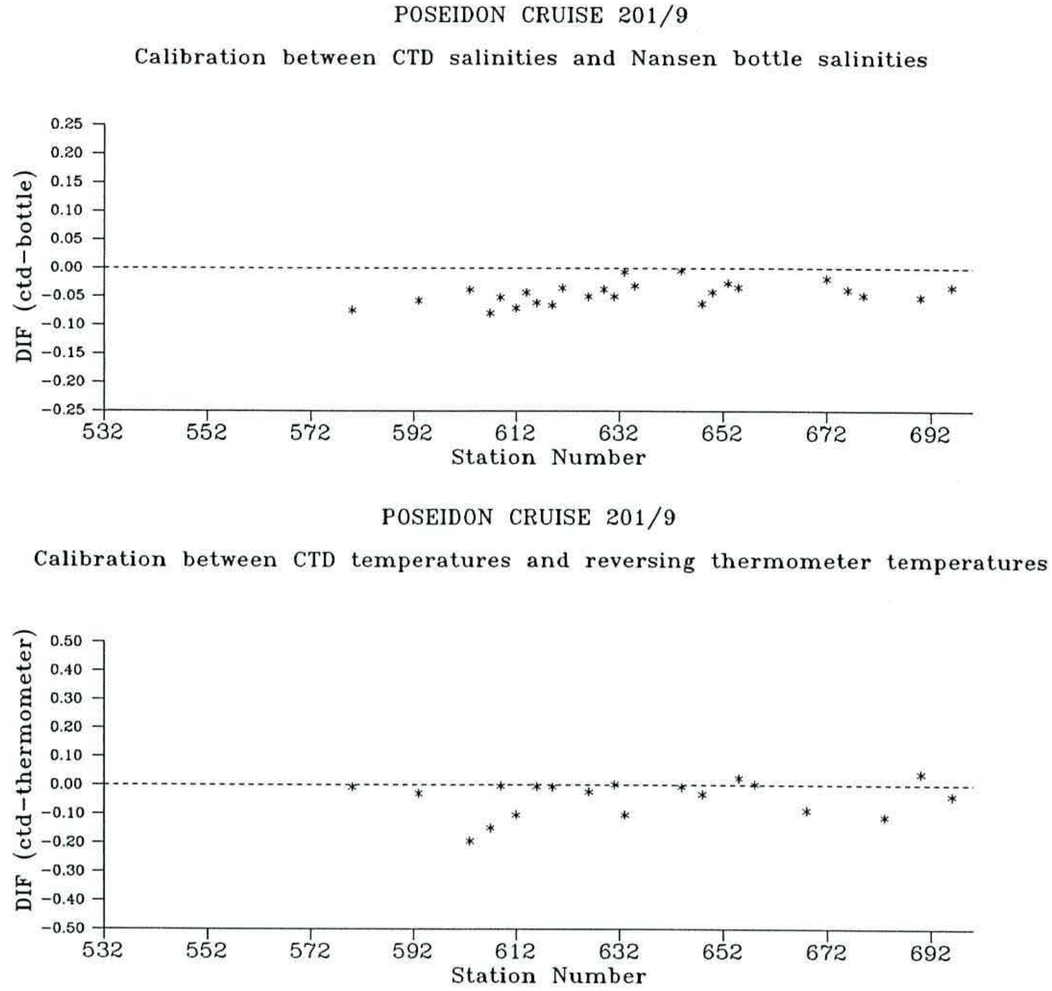

Figure 6.3: Calibration of salinity and temperature

The mean of the differences between the temperatures measured by the CTD and by the reversible thermometer was −0.0441°C with a standard deviation of 0.0627. In the salinity the mean of the differences was −0.0448 psu with a standard deviation of 0.0192. In view of the calibration results and to maintain the coherence among the data, it was decided to adjust to the mean the values of the temperature and salinity. A great part of the scatter in the data is probably explained by the sampling in zones of vertical gradient and not in uniform layers as would be ideal. Indeed, the presence of Mediterranean water near the maximum depth of several casts, where most of the samples were taken, increased the vertical gradients. The delay of about one week, between the sampling and the laboratory analysis of the salinity of the samples, that were kept in bottles as tight as possible, could be another cause for the scatter. To validate the data several comparison were done with the historical data from the region, in the oceanographic data base of the National Oceanographic Data Center (NODC). T-S diagrams for selected regions, based on the historical data, were plotted and compared with the present T-S diagrams for the same regions. The data collected during the cruise fall well inside the limits defined by the NODC data for this region. Comparison between the actual CTD data and SeaSoar data obtained during a previous survey in the same region [*Haynes*, 1993] also showed a good agreement.

## 6.5 Acoustic Doppler Current Profiler Data

During the campaign, the data from the ship mounted Acoustic Doppler Current Profiler (ADCP) were continuously recorded, in conjunction with the navigational data provided by the GPS (Global Positioning System) of the ship. An additional GPS was carried on board, but the existing system seemed very reliable. The complete results provided by the processing of this data were published in a separate report dedicated to the velocity fields in the Cape São Vicente region [*Relvas and Barton*, 1996].

### 6.5.1 Data acquisition

The measurements were made from the R/V Poseidon through a hull-mounted RDI narrow band Acoustic Doppler Current Profiler operating at 150 kHz. The ADCP transducer transmitted sound pulses with 16 meters length in four independent beams oriented at a 30° angle from the vertical axis of the ship.

The data acquisition system consisted of an IBM-PC compatible computer running the RDI DAS program version 248. The software automatically recorded the navigation data provided by the Global Positiong System (GPS) of the ship into the ADCP data files (ping files). The averaging time interval was set to 5 minutes in order to decrease inherent system noise and the effect of surface wave motion on the measured velocities, though the raw data was recorded for post-processing. The vertical bin size was set to 8 meters of water column. All the measurements with more than 25% of pulses returned were recorded into the ADCP datafile.

Data were collected continuously from 1353 UT on 11 June 1994, until 1910 UT on 21 June 1994. However, a malfunction of the navigation system at the beginning of the cruise was detected later in the post processing of the data, and reliable data were obtained only from 0200 UT on 12 June. The cruise track, given by the edited GPS measurements, is shown in Fig. 6.4, along with the longitude and latitude displacements.

### 6.5.2 Data processing: editing, calibration, and navigation

The ADCP data processing was carried out in the School of Ocean Sciences, University College of North Wales using the Common Oceanographic Data Access System (CODAS) software, developed at the University of Hawaii.

A preliminary processing step was to scan the raw data (binary ADCP ping data files) in order to ensure the data were readable and to detect bad sections. The ping files were then loaded into a CODAS database, suitable for processing and analysis. The database is hierarchical in form and the processing is done through control files and programs for accessing, manipulating, archiving and plotting the database. The displaying of the database is accomplished using MATLAB routines. After creating the CODAS database, the next processing steps are the editing, calibration, navigation and plotting the database.

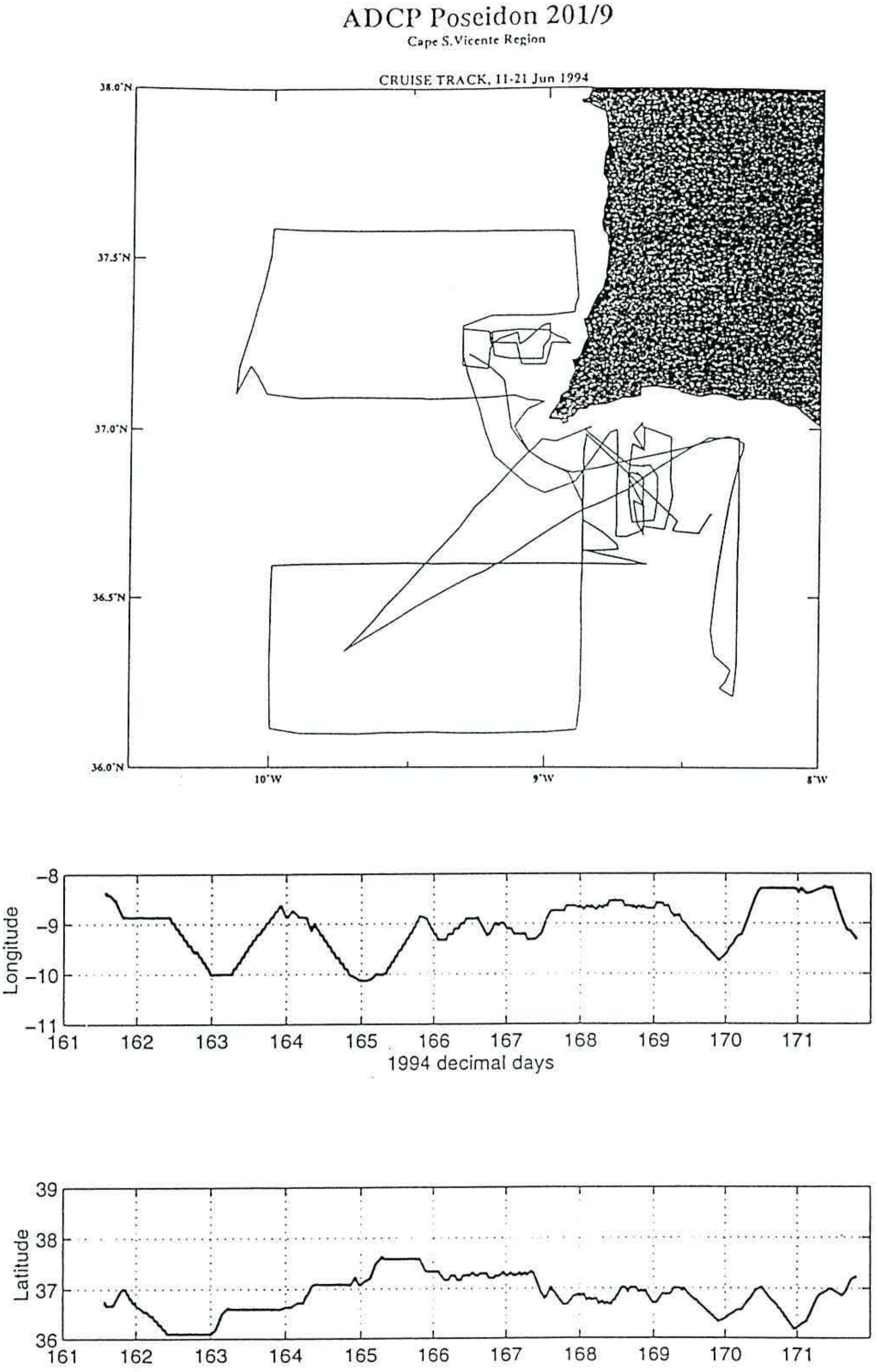

Figure 6.4: Cruise track and longitude and latitude displacements of the ADCP experiment during the Poseidon Cruise 201/9

### Editing

In this processing step an interactive scanning of the individual profiles was carried out, in order to identify the profiles with reflection of the acoustic beams from the bottom, and to detect contaminated bins.

After setting acceptance thresholds for the quality test control parameters (percentage of good return, amplitude, variance of the vertical velocity, error velocity and second derivates of U,V and W), all the profiles were edited by a combination of automated and manual screening. Each profile was scanned for several parameters (relative velocities, return signal amplitude, error velocity and percentage of good return) on staggered profile plots which automatically flag signals that deviate beyond the thresholds. The flagged bins and profiles were inspected to decide whether the data were flagged due to natural noise, such as scattering layers, or due to bottom reflections, isolated interference from the CTD wire or other anomalies. Then, the CODAS database was updated by setting the top good bin, maximum depth good bin (or bottom) and deleting the rejected depth bins or profiles.

Apart from the profiles sampled in shallow waters close to shore, which showed a strong reflection from the bottom, the Poseidon 201/9 cruise data were clean, with a good return signal to more than 400 meters. Few bins were deleted due to interference signals from the CTD wire and no profiles showed anomalies due to malfunction of the instrument. Close to the coast, the data from the last 15% of the range were rejected to account for the contamination due to the geometry of the beams relative to the bottom.

### Calibration

The aim of this processing step was to correct the measured velocities relative to the ADCP for the orientation of the transducer beam pattern relative to the gyrocompass and to check any inaccuracy in the behaviour of the transducer beam pattern. This is achieved through the computation of correction factors for the amplitude and for the angle between the gyrocompass forward axis and the transducer forward axis.

Due to the small amount of bottom track data collected during the Poseidon 201/9 cruise, a water track calibration was used to compute the amplitude and angle errors. In this method accelerations relative to the water as measured by the ADCP are compared to the accelerations over the ground measured by the navigation system. The absolute water velocity is assumed to remain constant through the calibration period.

Available good quality navigation information is essential to derive accurate calibration parameters using the water track method. The navigation data from the GPS were copied directly into the structure of the CODAS database and, at this stage of the processing, a time shift of 146 seconds was detected between the ADCP time (which comes from the PC clock) and the GPS fix times. A constant offset correction was applied to the ADCP time and the CODAS database was updated. An assessment of the quality of the GPS fix data was done by calculating and plotting absolute currents for the reference layer [*Relvas and Barton*, 1996]. This reference layer, used for the computation of the ship's relative velocity as it will be described in the next section, was calculated using a bin range of 5–20 (about 50–170 meters).

Calibration points were obtained during substantial accelerations of the ship, most of then occurred when the ship stopped on CTD stations and then got back underway. For the Poseidon 201/9 cruise the estimation of the amplitude and phase calibration coefficients was performed using 7 profiles (each profile is a 5 minute ensemble) around each major change in velocity, as this set produced the best results for the standard deviations. The calculated amplitude factor was 0.987 with a standard deviation of 0.019 and the misalignment angle was -0.69° with a standard deviation of 1.03. The standard deviations are well inside the limits suggested by the authors of the CODAS processing system [*Firing and Ranada*, 1995]. However a rotation was applied to the data in agreement with the angle offset. The phase and amplitude for all the estimates and for an edited subset as well as the frequency histogram are shown in Fig. 6.5

### 6.5.3 Navigation

This stage of the ADCP data processing was to calculate the ship velocity and finally the absolute current velocities. The ADCP measures the relative velocities between the ship (ADCP transducer) and scatterers that are advected by the currents. In order to obtain the absolute currents, the velocities of the ship relative to the earth, which are determined by the GPS fixes, must be subtracted out.

Relative ADCP velocities of a reference layer were computed. The reference layer is expected to be smoothly varying along the cruise track. Hence, it was chosen as the thickest layer containing good data, omitting the first few bins near the surface. Due to the good ADCP range and good weather conditions during all the cruise time, the reference layer was set as the average between bins 5-20, corresponding to about 50-170 meters. The reference layer velocity data were smoothed with a Blackman filter with a half-width of 1/2 hour. An estimate of the reference layer velocity and ship position were plotted as a function of time, and a few anomalous GPS fixes were detected and eliminated to obtain the final absolute reference layer velocity and earth coordinates of the GPS fixes [*Relvas and Barton*, 1996]. GPS coverage was good for most of the survey except for a short period in the beginning of the cruise.

Data on ship velocity relative to the reference layer was extracted from the CODAS database (this is done by the CODAS program ADCPSECT) and added to the absolute reference layer to obtain the absolute ship velocity. The calculated ship positions and velocities were then stored in the CODAS database.

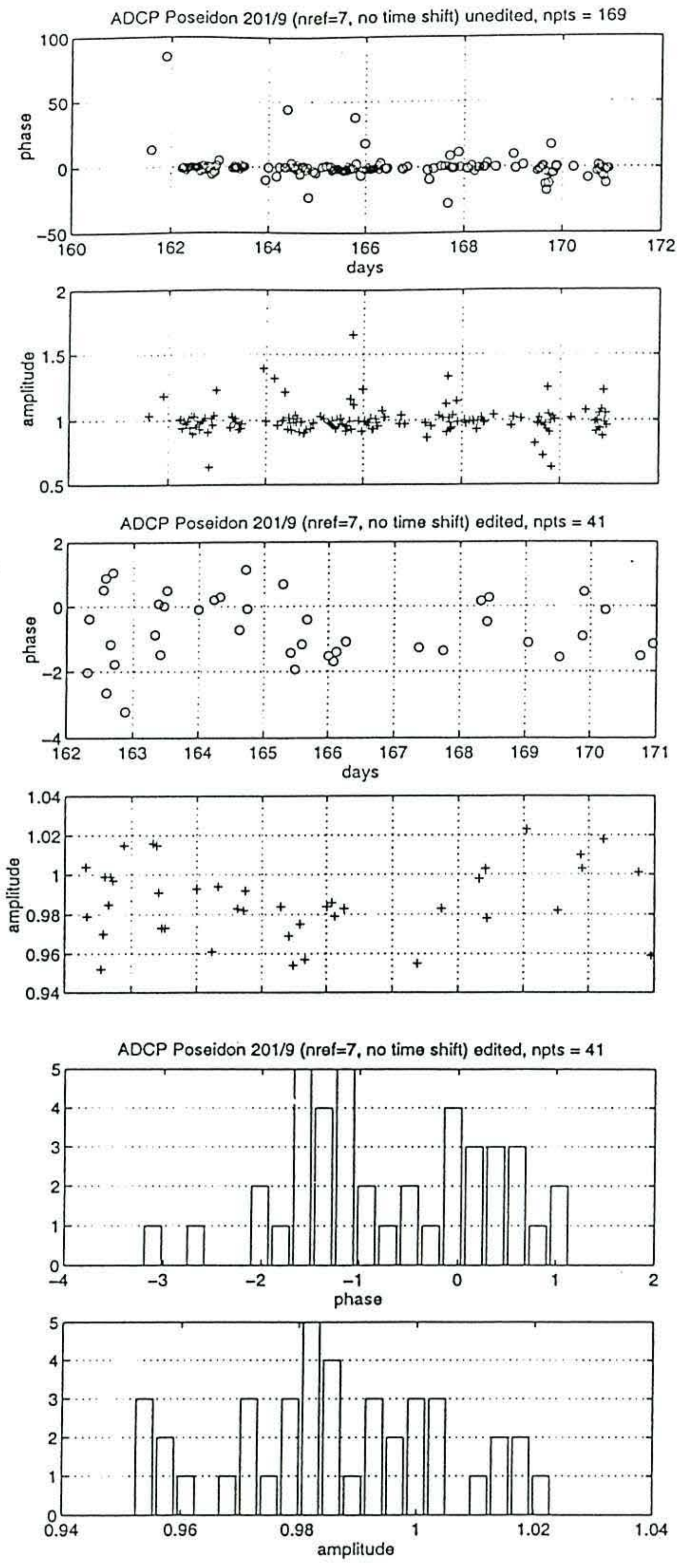

Figure 6.5: Calibration parameters for the Poseidon 201/9 ADCP data as explained in the text

### 6.5.4 Assessment of the Data Quality

An assessment of the data quality was made through the plotting of average profiles of the velocity components and various ancillary parameters, separately for the periods when the ship was on station and underway. The on-station data correspond to the time periods when the ship was on the 132 CTD stations plus a few biological stations.

Plots of the average value and standard deviation between the 5 minute ensembles of the amplitude and percentage of good return, vertical velocity component and error velocity, and the first vertical difference of the zonal and meridional velocity components versus depth are shown in Figure 6.6.

The on station curve and the underway curve show an appreciable agreement for all depths in the profiles of the returning signal amplitude and percentage of good return. The return signal amplitude was higher at shallow depths, dropping to the noise level around 300 meters depth. Both on station and underway, the data show a high percentage of pings with a good return till very deep. The percentage was close to 100% till around 250 meters, better on station than underway. The threshold to accept data as good was set to 30% of good return, which corresponds to a depth of about 475 meters.

The computed $w$ component velocity is the mean of the two independent estimates of the vertical velocity given by the ADCP. The error velocity is a function of the difference between the two estimates. Inside the depth range of reliable ADCP data, the vertical velocity was very small, as it is normally in the ocean, with slightly positive values for depths below 100 meters. The error velocity was very close to zero (less than 0.4 cm/s) over the depth range. The zonal component and meridional component first differences were very small, both on station and underway.

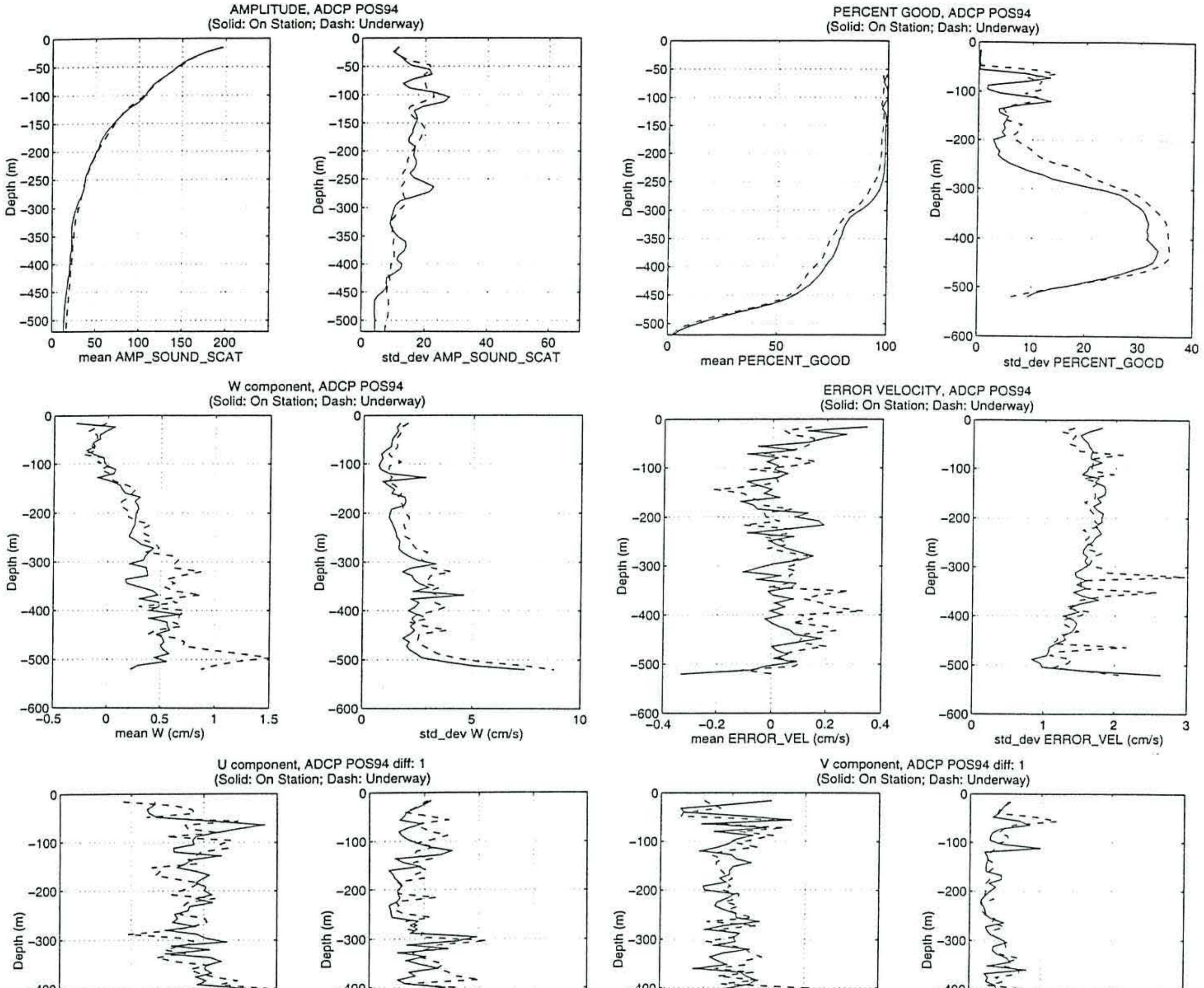

Figure 6.6: Plots of the average value and standard deviation between the 5 minute ensembles of the amplitude and percentage of good return, vertical velocity component and error velocity, and the first vertical difference of the zonal and meridional velocity components versus depth. The $w$ component velocity represented in the plot is the mean of the two independent estimates of the vertical velocity given by the ADCP. On each plot the solid line represents the data collected on station and the dotted represents the data collected while the ship was underway.

## 6.6 Satellite Data

With the goal of guiding the oceanographic sampling, the available brightness temperature images from the Advanced Very High Resolution Radiometer (AVHRR) sensor on board the polar orbiting satellite NOAA-11, covering the region of the cruise, were acquired. The images were provided by the University of Dundee satellite receiving station and transferred electronically to colleagues at the School of Ocean Sciences at Menai Bridge for analysis. If any oceanographic structure of interest was identified, the scene and a sketch of the scene prepared by our colleagues at Menai Bridge, with the coastline and temperature fronts enhanced, was sent to Poseidon by telefax. With this strategy it was possible to have a good quality satellite information on board with a lag of few hours after the satellite pass. Unfortunately, due to the presence of clouds during part of the cruise and the absence of defined temperature fronts, few images were transmitted, although a larger number were analysed at the School of Ocean Sciences.

## 6.7 Summary

Although the performed field work did not correspond to our expectations of sampling the Cape São Vicente cold filament, due to the absence of upwelling conditions during most of the cruise time, a set of valuable data were acquired in a coastal transition region where observations are sparse and the knowledge of the ocean behaviour is rather undefined.

A complete coverage of the region was obtained with ADCP data, 132 CTD casts and supporting environmental data and thermal infrared satellite images. This data set revealed detailed features of the mesoscale hydrographic structure of the region, contributing to the understanding of the dynamics of the coastal ocean in the Cape São Vicente region, as discussed in the next Chapter. Although the Poseidon cruise (POS 201/9) was not exclusively dedicated to physical oceanography and included a biological component, measurements carried out exceeded our initial expectations, and all the work attempted was completed successfully. The post-processing of the data involved mainly minor corrections, and only a small amount of data had to be rejected. The assessment of the data set showed it was of good quality, thus reliable for the proposed objectives.

# Chapter 7

# The upper-ocean structure observed in June 1994

## 7.1 Introduction

In this Chapter the results from the observations during the Poseidon 201/9 survey are presented and discussed. An assessment of the observed water masses, hydrographic fields, and kinematics is made, and the implications for the knowledge of the dynamics and energetics of the coastal transition zone in the Cape São Vicente region are discussed. The relation with the larger scale circulation is also considered.

Initially, the experiment strategy was developed to sample the Cape São Vicente cold filament, but it soon was evident that the cold filament was absent, due to the weak winds along the western coast. The strategy was re-assessed to concentrate on the coastal dynamics of the region, with particular emphasis in the coastal warm counterflow apparent in the satellite imagery. Thus, two fine scale nearshore grids, off the western and southern coasts, were carried out.

The focus of these survey was mesoscale processes in the upper layers, where the wind forcing, upwelling, and related phenomena are dominant. Thus, the analysis and discussion produced in this Chapter refers only to the upper layers, above 400-500 me-

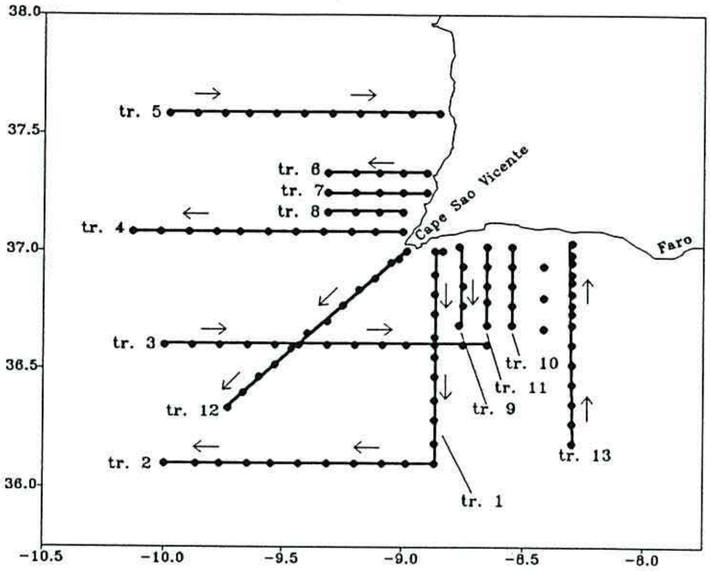

Figure 7.1: Transects carried out during the Poseidon 201/9 cruise. Arrows represent the steaming direction.

ters. The deeper Mediterranean water is beyond the scope of the present investigation, although it appeared frequently in the deeper limit of the data.

The Cape São Vicente region was covered with a set of 13 CTD transects, represented in Figure 7.1, between 11 and 20 of June 1994. The transects were sampled sequentially, except transect 7 and 8 in the nearshore grid off the western coast and transect 10 and 11 in the nearshore grid off the southern coast, where the sampling was alternating within each pair of transects. Arrows in Figure 7.1 represent the sampling succession. Table 7.1 indicates the timing of each transect. A more complete sampling of the current field was carried out, since the water velocity was measured continuously during the cruise track (Figure 6.4) through the hull mounted ADCP.

## 7.2 Wind conditions

During the summer months the wind regime along the coastal region of Portugal is characterized by winds blowing from the north, associated with the northward displacement of the Açores high pressure cell and the weakening of the Iceland low. Thus, we expected to encounter a northerly wind regime during the cruise time. This wind

| Poseidon cruise 201/9 | First St. | Last St. | Start time | Finish time |
|---|---|---|---|---|
| transect 1 | st565 | st575 | 11 June 19:42 | 12 Jun 10:30 |
| transect 2 | st575 | st585 | 12 June 10:30 | 13 Jun 00:08 |
| transect 3 | st586 | st598 | 13 June 06:24 | 13 Jun 22:32 |
| transect 4 | st601 | st611 | 14 June 08:59 | 15 Jun 00:00 |
| transect 5 | st612 | st622 | 15 June 08:23 | 15 Jun 19:24 |
| transect 6 | st623 | st627 | 15 June 21:44 | 16 Jun 01:47 |
| transect 7 | st628 | st636 | 16 June 02:53 | 16 Jun 11:13 |
| transect 8 | st629 | st634 | 16 June 04:08 | 16 Jun 09:40 |
| transect 9 | st643 | st647 | 17 June 14:53 | 17 Jun 19:30 |
| transect 10 | st653 | st657 | 18 June 10:02 | 18 Jun 13:47 |
| transect 11 | st648 | st658 | 17 June 20:00 | 18 Jun 14:47 |
| transect 12 | st667 | st679 | 19 June 10:09 | 19 Jun 21:58 |
| transect 13 | st682 | st696 | 20 June 12:14 | 20 Jun 23:10 |

Table 7.1: Sampling period of each transect and the number of the first and last station in each transect during the Poseidon 201/9 survey.

pattern induces upwelling off western Iberia and an associated southward circulation in the upper layers. However, the winds observed during the cruise period were in general weak and variable.

The wind was measured on board the ship every four minutes. The data were low pass filtered to remove oscillation of period less than one hour. The temporal evolution of the wind components are represented in Figure 7.2 and the distribution along the track is represented by means of stick diagrams in Figure 7.3. During the first half of the cruise the winds were generally light and variable, with a southward trend. A period with a higher amplitude of the wind variations occurred after 17 June with the maximum pulses reaching 10 m/s. By 20 June, after an episode of weak northeasterly winds, the wind rotated to westerly, upwelling favourable off the southern coast, remaining steady above 10 m/s for about 14 hours. Then, rotated again to northeasterly and variable. The last part of the cruise track was covered under relatively strong (about 15 m/s) northeasterly wind.

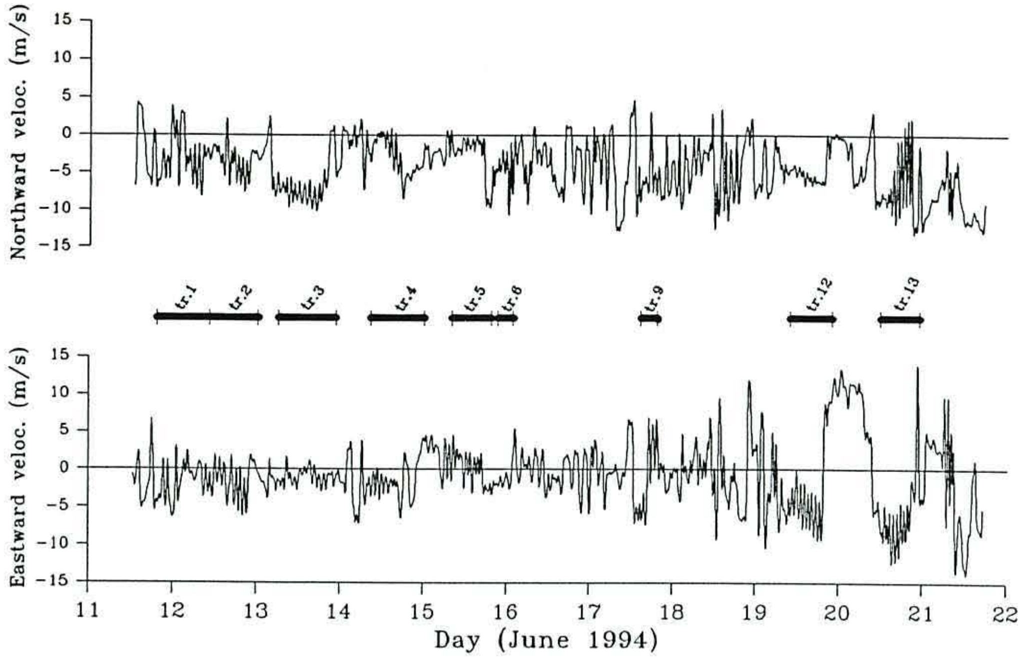

Figure 7.2: Temporal evolution of the northward and eastward wind components measured on board the ship. Readings were taken every four minutes and the data were low pass filtered to remove oscillations with periods less than one hour. The periods of the transect casts are represented.

The temporal evolution of the wind components measured on land at the nearby meteorological station of Sagres, located in the Cape São Vicente cliffs, is represented in Figure 7.4. The data represent eight daily observation and are displayed without any filter. Winds measured at the Sagres station show a considerable difference from the ship measured winds. The differences may be explained in part because only the starboard direction sensor on the ship was functioning. The greater of the speeds measured by the two ship speed sensors was combined with the starboard direction to provide the relative wind velocity estimate as eastward and northward components. The components of the ship speed were then subtracted to provide the estimate of absolute wind velocity. Because of the possible effects of interference with the wind flow by the ship superstructure the wind velocity is less reliable than normal. However, real differences due to the spatial inhomogeneity of the wind field as the ship worked around the area of Cape São Vicente are probably the major factor that originates the difference. The shore data confirm the weakness of the wind and the occurrence

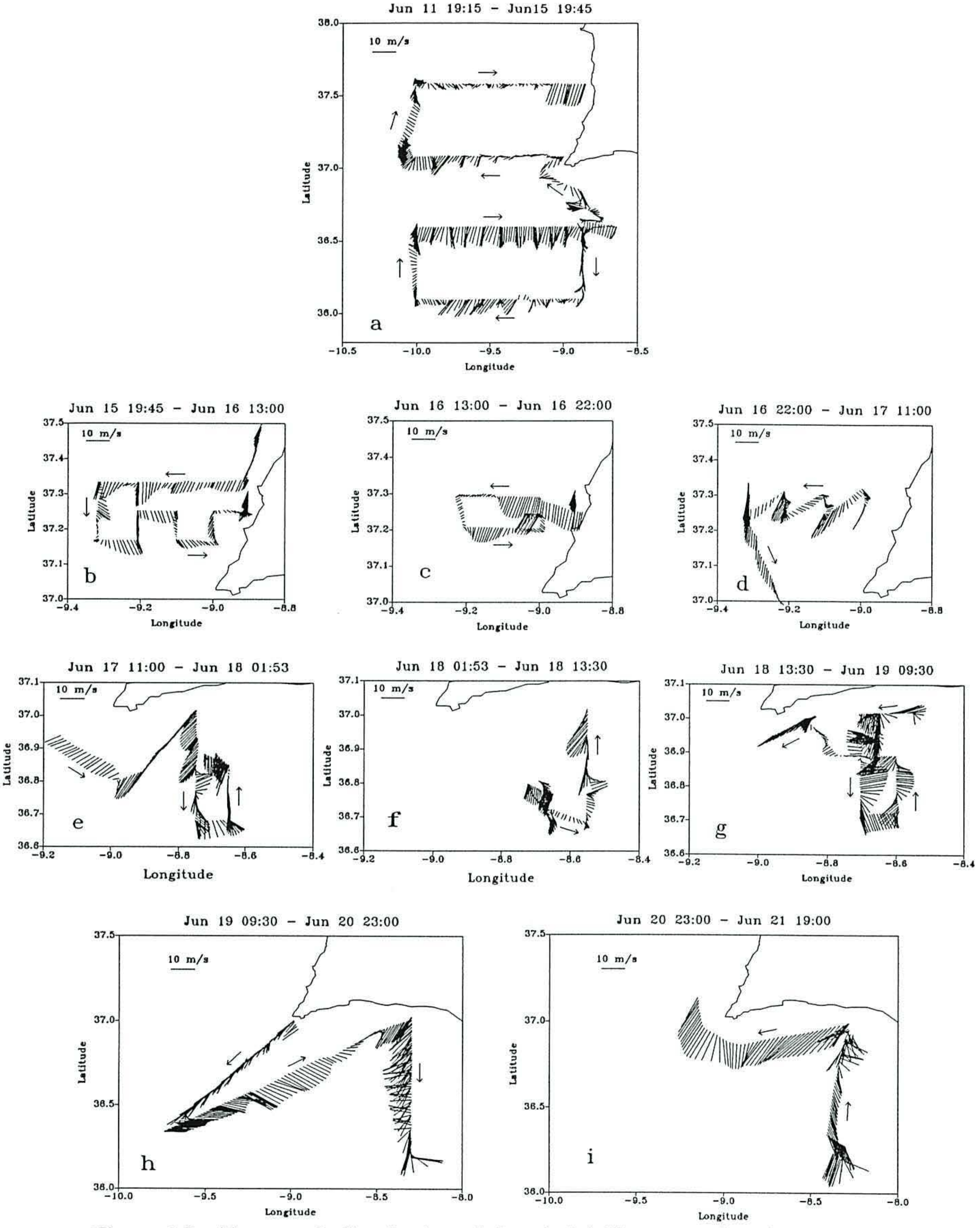

Figure 7.3: Along track distribution of the wind field measured on board. The data were low pass filtered to remove oscillations with periods less than three hours. For clarity the track was subdivided in consecutive subsets.

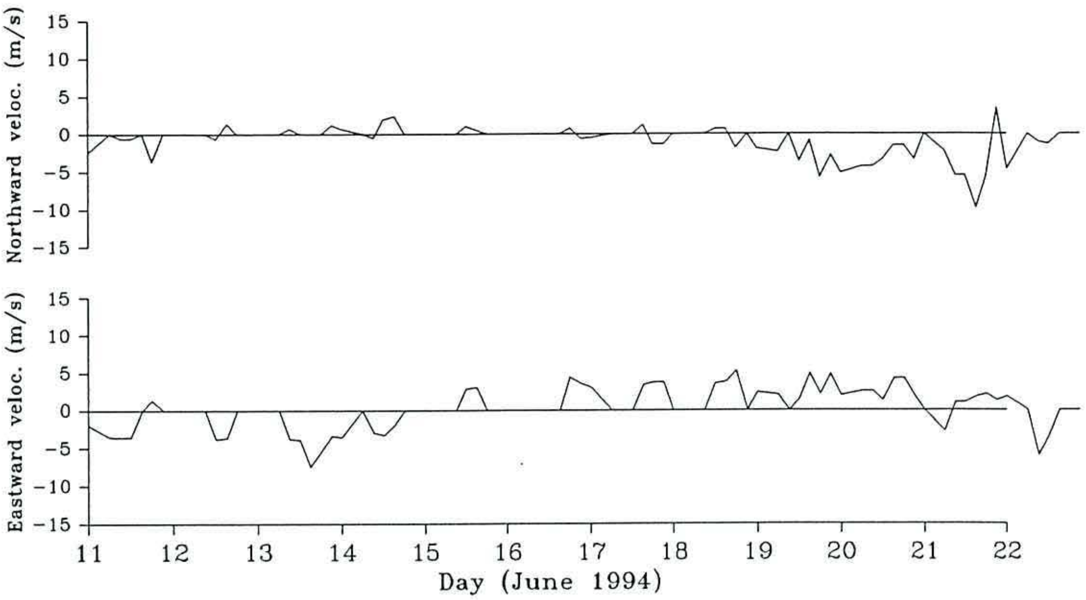

Figure 7.4: Time series of the northward and eastward wind components measured at the coastal station of Sagres. The curve represent the raw data of the eight daily readings taken at the station.

of northerly winds in the last part of the cruise. However, the variability of the zonal component, in the final stages of the survey, was not recorded at Sagres.

## 7.3 Water mass structure and variability

### 7.3.1 Observed water masses

Typically two sub-layers can be defined in the upper layer of the Portuguese coastal ocean: i) a surface layer in which ocean-atmosphere interactions take place, comprising the surface mixed layer and the seasonal thermocline and extending to 100-200 meters depth, and ii) a sub-surface layer corresponding to the permanent thermocline, occupied by 'Central Water' typical of the eastern basin of the North Atlantic, and characterized by a roughly linear relationship between temperature and salinity. Below this upper layer begins the influence of the Mediterranean outflow.

The central water masses in the northeast Atlantic are dominated by the North Atlantic Central Water (NACW) [*Sverdrup et al.*, 1942], which are known to have a weak eastward circulation offshore of Iberia [*Pollard and Pu*, 1985]. More recently

NACW has been subdivided according to its formation and region of origin. The thermohaline characteristics of the sub-surface central water west of Portugal coincide with those of the Eastern North Atlantic Water (ENAW), defined by *Fiúza and Halpern* [1982]. According to *Fiúza* [1982] the thermohaline characteristics of ENAW correspond to a straight line in the T-S plane and it definition does not conform to the classical definition of North Atlantic Central Water (NACW). It is this water that is observed to upwell off the Atlantic coast of Portugal during the summer months [*Fiúza*, 1984]. ENAW can be taken as a subdivision of NACW, and is found to have a decreasing influence as we progress northward along Iberia. ENAW is apparently formed by mixing of Subtropical Water and remnants of Antarctic Intermediate Water in the southwest of Açores [*Fiúza*, 1982]. The T-S characteristics of this subtropical mode of ENAW are defined as 12.2°C, 35.66psu and 18.5°C, 36.75psu [*Fiúza and Halpern*, 1982; *Ríos et al.*, 1992]. A subpolar mode of ENAW, formed during winter ventilation in the Atlantic sub-polar gyre north of 46°, characterized by temperatures and salinities between 4°C, 34.96psu and 12°C, 35.66psu [*Harvey*, 1982] is observed to dominate further north, off the northern tip of Iberia [*Ríos et al.*, 1992]. These two central waters with different water masses characteristics were termed by *Ríos et al.* [1992] as $\mathrm{ENAW}_T$ for the subtropical mode and $\mathrm{ENAW}_P$ for the subpolar mode. $\mathrm{ENAW}_P$ and $\mathrm{ENAW}_T$ constitute two different water bodies of NACW in the Iberian region, whose demarcation in a T-S plane was defined by *Ríos et al.* [1992] as the point 12.2°C, 35.66psu. Beneath the central water the complex spreading pattern of waters of Mediterranean origin is characterized by spatially variable relative maxima in the vertical distribution of temperature and salinity [*Zenk and Armi*, 1990].

In Figure 7.5 are represented the T-S scatter plots for the entire Poseidon cruise, divided into three groups of CTD stations, corresponding to the regions off the western coast, southwest of Cape São Vicente and off the southern coast. In all regions the

T-S plots show clearly the presence of central waters beneath the surface waters, corresponding to the near linear region roughly between 11°, 35.6psu and 16.5°, 36.5psu.

The waters found in the subsurface layer conform to the definition of ENAW, as indicated in Figure 7.5. Actually, the central waters are observed to be slightly cooler and saltier than the definition, but the shift fall within the limits of the thermohaline decadal changes of the ENAW reported by *Pérez et al.* [1995]. Most of the water is observed to correspond to the subtropical mode (ENAW$_T$), but a small amount of waters of the subpolar mode (ENAW$_P$) is still observed in the region (in Figure 7.5 the point **H** represents the limit between ENAW$_T$ and ENAW$_P$). However, a smaller portion of the deeper ENAW$_P$ is observed off the southern coast compared with the western coast, following the understanding of an increasing influence of ENAW$_P$ northwards along Iberia [*Haynes*, 1993]. Also the maximum temperature and salinity of the central waters are slightly higher off the southern coast when compared with the western coast stations. T-S characteristics of ENAW observed in the region southwest of Cape São Vicente are closely similar to those observed off the southern coast.

Below the central waters the presence of Mediterranean Water (MW) is clearly evident in the T-S diagrams, corresponding to increasing values of temperature and salinity (Figure 7.5). These correspond to the vein of MW along the continental slope of Iberia between 400-500 meters depth, which was identified by *Ambar* [1983]. This shallower vein is distinct from the two main outflow cores of MW found further offshore at $\approx$ 750 meters and $\approx$ 1250 meters [*Zenk and Armi*, 1990]. The T-S plot of the region southwest of Cape São Vicente shows a smaller signal of MW because only a few CTD stations were over the continental slope. The path of the nearshore MW vein from the Algarve to north of Cape São Vicente was clearly defined in these survey data.

The surface layers of the waters in the Cape São Vicente region exhibit two preferred salinities separated by a gap of about 0.4psu with fairly similar temperature patterns, indicating the existence of a strong salinity front at near-surface levels. The

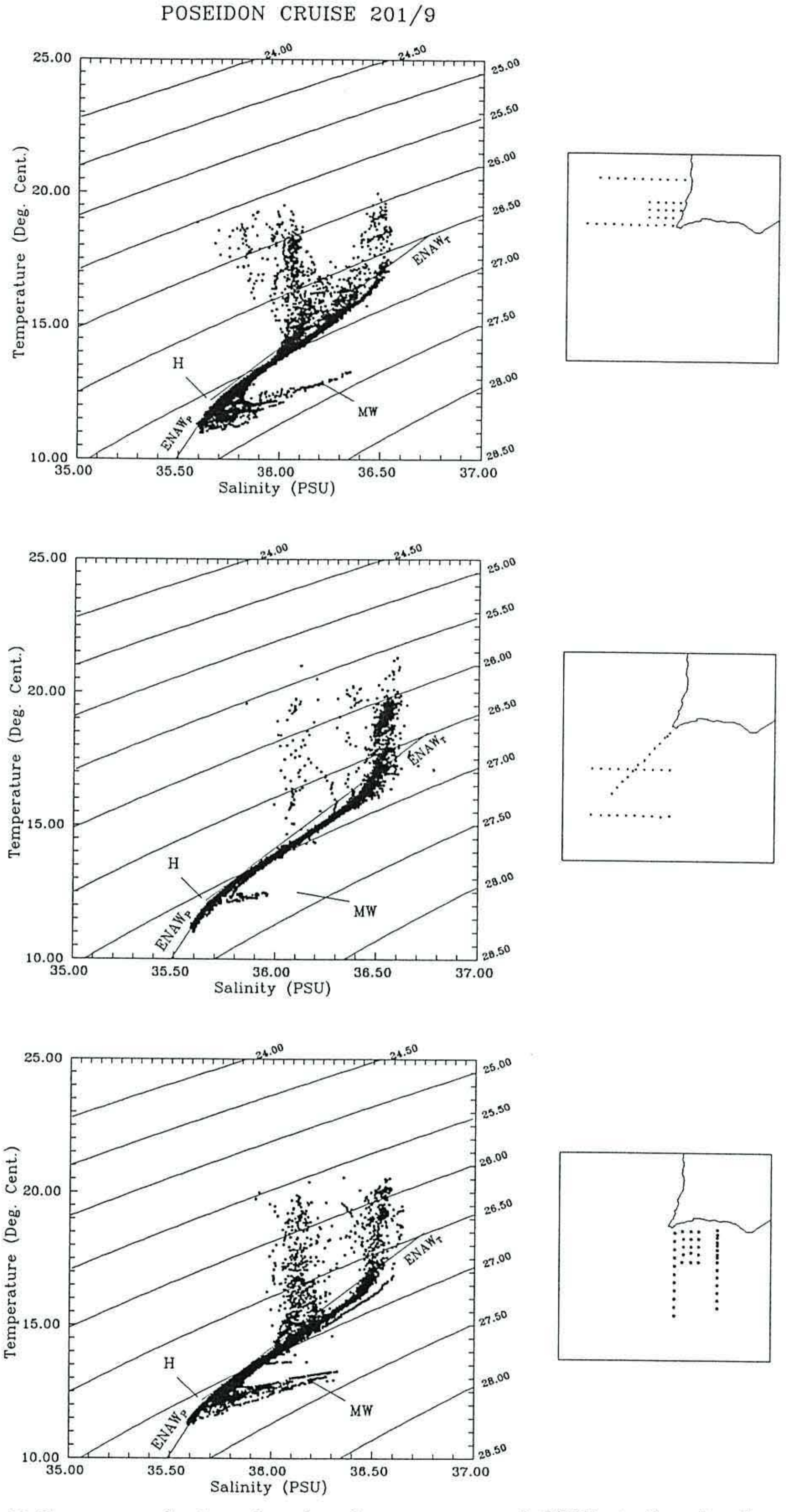

Figure 7.5: T-S scattered plots for the three groups of CTD station in the Cape São Vicente region. Definitions of ENAW$_T$ and ENAW$_P$ are shown and H represents the limit between the two waters. Maximum depth of the casts was 520 meters. Diagrams are shown along with a sketch of the location of the CTD profiles in each plot.

lower salinity values correspond to the coastal regions, over the continental shelf and upper slope, and all of transect 5, located further north along the western coast (Figure 7.1), where all profiles show low salinities in the surface layers. In Figure 7.6 some representative profiles of nearshore and offshore stations are shown. The location of the strong near surface salinity gradient will be discussed later. The T-S plot of the region southwest of Cape São Vicente exhibits a small number of profiles with lower salinity in the surface layers because relatively few stations were near the coast in that sector. Offshore upper layer waters, represented by the higher salinity branch in the T-S plots, show a fairly constant salinity pattern with values similar to the uppermost underlying central waters ($\mathrm{ENAW}_T$). This is the consequence of surface warming of the upper levels of $\mathrm{ENAW}_T$ under conditions of weak wind.

Nearshore surface waters, represented by the lower salinity branch in the T-S plots, show a more constant salinity pattern off the southern coast than off the western coast. However, in both regions, salinities of the nearshore surface waters are similar to those of deeper layers of $\mathrm{ENAW}_T$. In fact, until just prior to this survey, strong upwelling was taking place around Cape São Vicente, as can be observed in Figure 7.7. Analysis of the T-S diagrams suggests that these coastal surface waters were formed as a consequence of the surface warming of deeper $\mathrm{ENAW}_T$ waters upwelled previously to the cruise in the coastal regions.

The nearshore surface waters off the western coast exhibit a salinity pattern with lower values and higher variability than the pattern observed off the southern coast. The low salinity values suggests that the waters upwelled off the western coast before the cruise have their origin at deeper $\mathrm{ENAW}_T$ levels than the waters upwelled off the southern coast. This agrees with the general view of more intense upwelling events off the western coast than off the southern coast, as discussed earlier in Chapter V. Also, the comparison of individual profiles of nearshore station 619 and offshore station 614 (Figure 7.6) shows a lower surface salinity at station 614, suggesting that surface waters

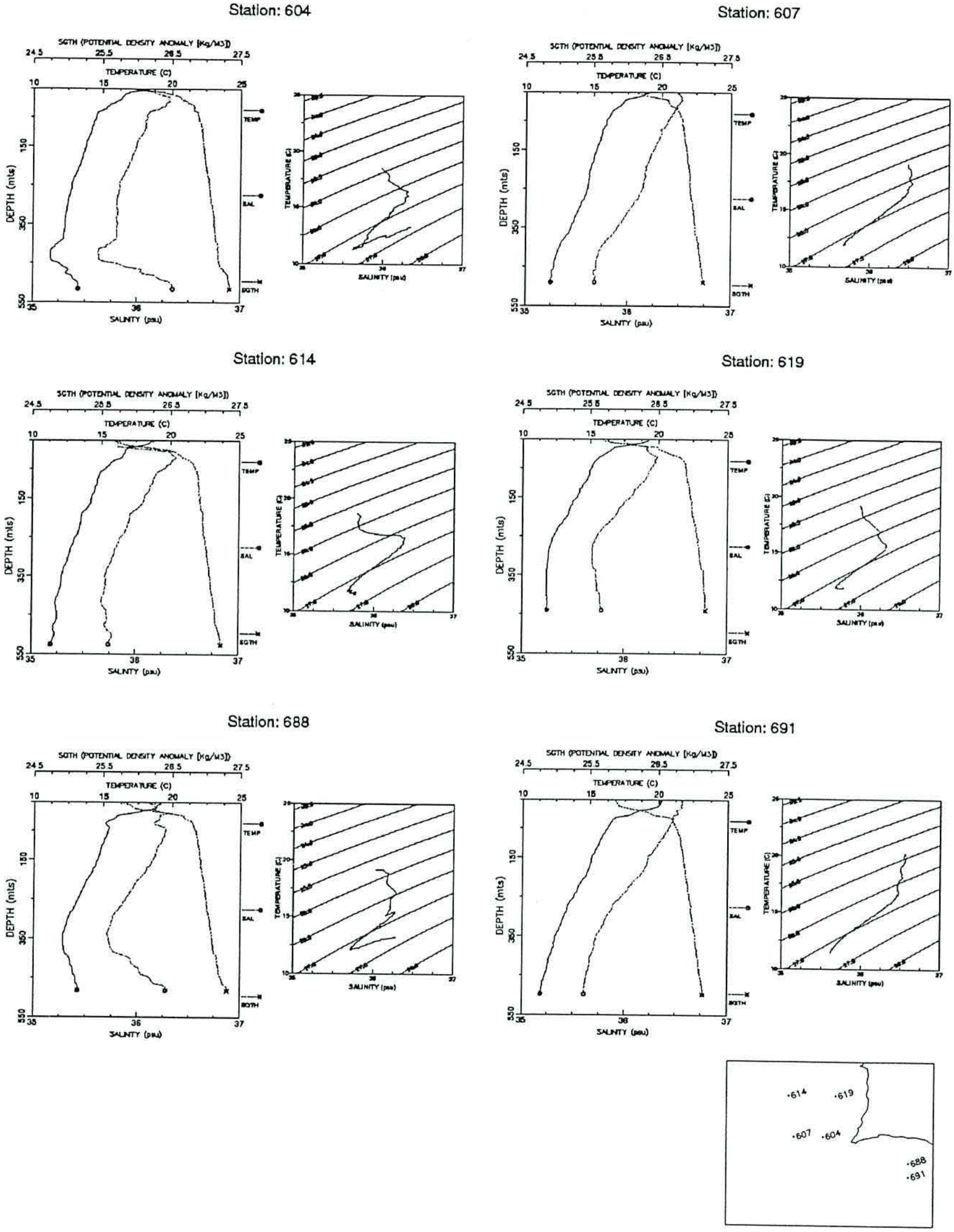

Figure 7.6: Summaries of some nearshore and offshore CTD stations sampled in the Cape São Vicente regions. The T-S diagram and the vertical profiles of temperature, salinity and $\sigma_t$ are displayed. Location of the stations is represented.

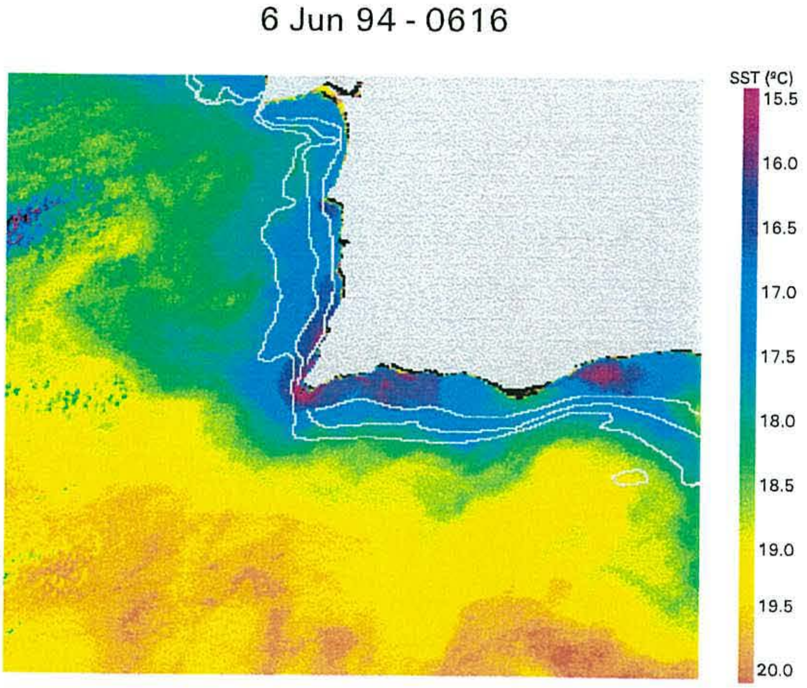

Figure 7.7: AVHRR satellite sea surface temperature image for 6 June 1994, showing the upwelling event in Cape São Vicente region a few days before the beginning of the Poseidon 201/9 cruise.

found offshore in the northern part of the studied region proceed from deeper ENAW$_T$ layers, which were spread offshore during the upwelling event before the survey.

### 7.3.2 Hydrographic structure

#### Horizontal fields

The near surface (5 meters depth) horizontal fields of temperature, salinity and density ($\sigma_t$), inferred from the CTD sampling, are displayed in Figure 7.8. Although there is a considerable time span between the start and the end of the ship survey, during which some changes occurred in the wind forcing conditions, relevant information can be obtained by displaying the horizontal fields as though they were truly synoptic.

Temperature and salinity fields show a zonal, rather than meridional, trend with the isolines following the continental slope off the southern coast, contouring the Cape São

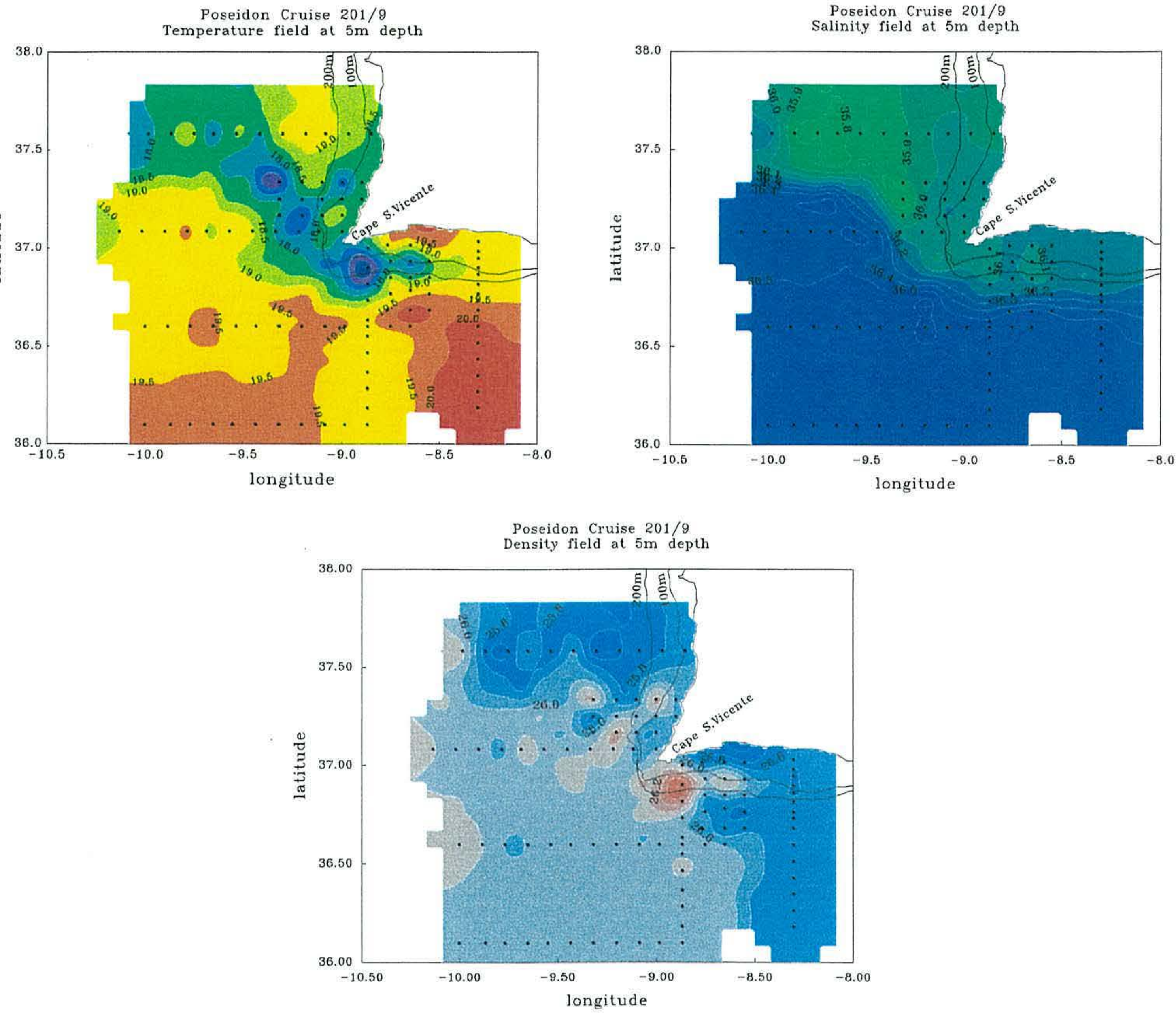

Figure 7.8: Horizontal fields of temperature, salinity and density ($\sigma_t$) at 5 meters depth, observed during the Poseidon 201/9 survey. Individual conductivity-temperature-depth profiles are denoted by dots along the ship track. 100 and 200 meters bathymetric lines are also represented.

Vicente and then turning offshore, not following the bathymetry off the western coast. Farther off the southern coast and southwest of Cape São Vicente all fields, including density, exhibit a rather uniform behaviour, revealing remarkably homogeneous surface waters in those regions. Gradients of the surface fields were restricted to the continental slope and shelf off the southern coast and around Cape São Vicente, and off the western coast. Although upwelling occurred off the western coast prior to the cruise start, as is observed in the AVHRR images (e.g. 6 June 1994, Figure 7.7), no surface signal of the presence of a Cape São Vicente cold filament was found in the survey data.

Results deduced from the T-S plots are supported by features observed in the horizontal distribution of salinity. The most striking feature revealed in the surface fields is the sharp salinity front, reaching over 0.5 PSU contrast, lying off the shelf break along the southern coast, following around the Cape São Vicente to the north and then turning westward at about 37.3°N, separating lower salinity inshore waters over the shelf and upper slope from higher salinity offshore waters. This surface salinity pattern is consistent with the trend shown in the mean monthly surface salinity fields for the summer months computed with the historical data, displayed in Chapter III, Figure 3.3. The observed values are within the range of the mean historical values in the region, suggesting that possibly this observed feature is not transient and is characteristic of the summer pattern in the region. Low salinity waters (less than 35.9 PSU) are also found in the northern part of the study region. To the west of about 8.7°W longitude, the salinity front is accompanied by a near-surface temperature front, with about 1°C contrast between cooler waters to the north and warmer waters to the south. In the northern edge of the study area, centred at 9.2°W, the surface water temperature increases again, forming a temperature valley progressing from the northwest corner of the study region till the Cape São Vicente region.

The salinity front is seen to be largely compensated by the temperature, in terms of the surface density field. This shows a region of homogeneous surface waters in the

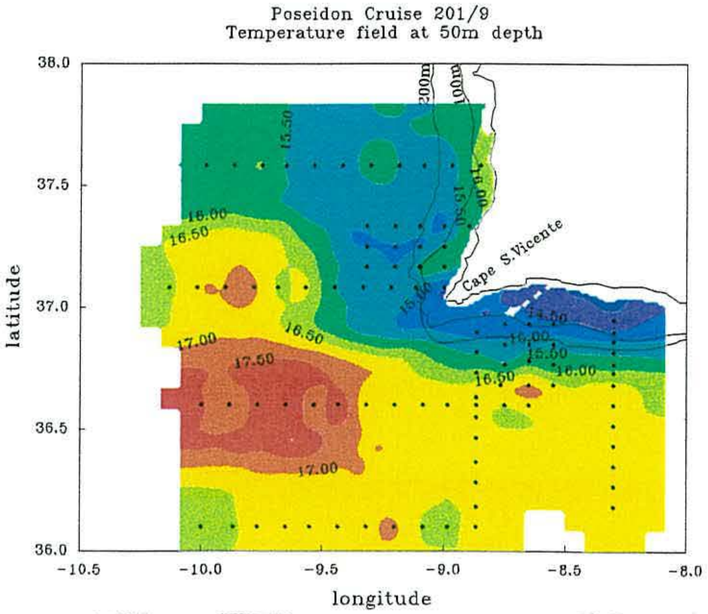

Figure 7.9: Horizontal fields of temperature at 50 meters depth, observed during the Poseidon 201/9 survey. Individual conductivity-temperature-depth profiles are denoted by dots along the ship track. 100 and 200 meters bathymetric lines are also represented.

southwest, and a region of a rather undefined pattern in the northern limit of the study area, where the isopycnals meander zonally. There is an overall weak density gradient with lower density waters to the north.

Another feature of interest observed in the near surface temperature field, with influence in the density field, is the 'tongue' of cold water, with a temperature signal over 2°C cooler than the surrounding waters, spreading eastward centred over the shelf break off the southern coast. No salinity signal is observed in the area of this cold water tongue, which constitutes the eastern limit of the temperature valley mentioned above, suggesting the continuity of these waters. The NW-SE cool temperature patch off the western coast, culminating in the zonal cool tongue off the southern coast, develops parallel to the salinity front and just north of it. The cold tongue is clearly a near surface feature, as no signal is observed in the temperature field at 50 meters depth (Figure 7.9). A 'band' of warmer water is seen to extend inshore, over the shelf, along the southern coast. Also, a relative temperature maxima is observed close to shore off the western coast, just north of Cape São Vicente, at about 37.1°N. The continuity of these waters cannot be excluded, since there are only relatively sparse measurements just in front of Cape São Vicente.

### Vertical fields

The vertical field of temperature, salinity and density observed along transects 3, 4 and 5, located zonally to the west of Cape São Vicente, are represented in Figure 7.10. The three transects were sampled sequentially, starting with transect 3 at 0624 on 13 June and finishing at 1924 on 15 June. During this time interval, weak northerly winds (about 8 m/s) were blowing during the first hours, decaying then to a virtually calm pattern (mean speeds of around 3 m/s) intercalated by short and weak pulses with variable directions.

The transects show a stratified ocean in the upper layers, with a northward intensification and rise of the pycnocline. In transect 3, the southernmost transect of this set, all vertical fields are zonally uniform. The pycnocline is seen to be at about 75 meters depth in the western half of the transect, rising to 50 meters in the eastern half. Below the 26.9 isopycnal, which corresponds to about 200 meters depth, the isopycnals show a weak negative slope till station st589 and then a positive slope till station st593.

The vertical patterns observed in transect 4, which extends west from Cape São Vicente, show some features of interest. The first point is the well pronounced depression of the temperature and salinity fields, below 100 meters depth, centred in stations st607 and st608. Due to the preponderance of temperature in the density definition, a depression of the isopycnals is also observed. A second feature of interest is the upward slope of the fields, very significant in the sub-surface layers, generating between stations st603 and st605 the surface gradients observed previously in the temperature and salinity surface fields. At the surface this front is density compensated. The inclined isosurfaces and the location of these strong surface gradients separated from the near coastal region, possibly constitute the hydrgraphic pattern of the upwelling event that occurred prior to the survey. A third important feature is the significant deepening of the isopycnals observed in the surface layers over the continental shelf due to the nearshore presence of warmer water in a region where the vertical distribution of salin-

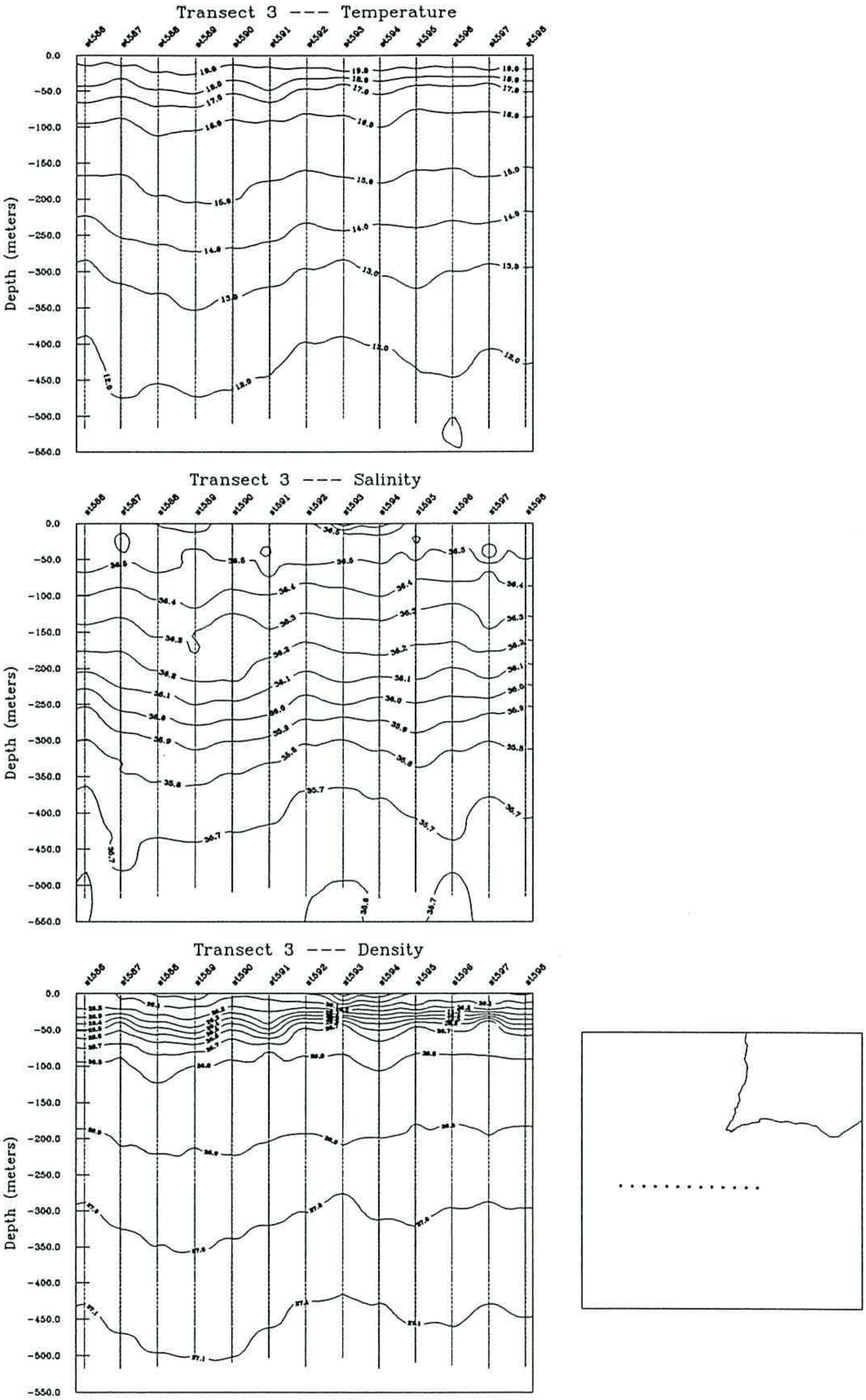

Figure 7.10: Vertical fields of temperature, salinity and density ($\sigma_t$) along transects 3, 4 and 5. A sketch with the location of each transect is displayed. Vertical columns of dots with labels on top indicate the location of the CTD stations.

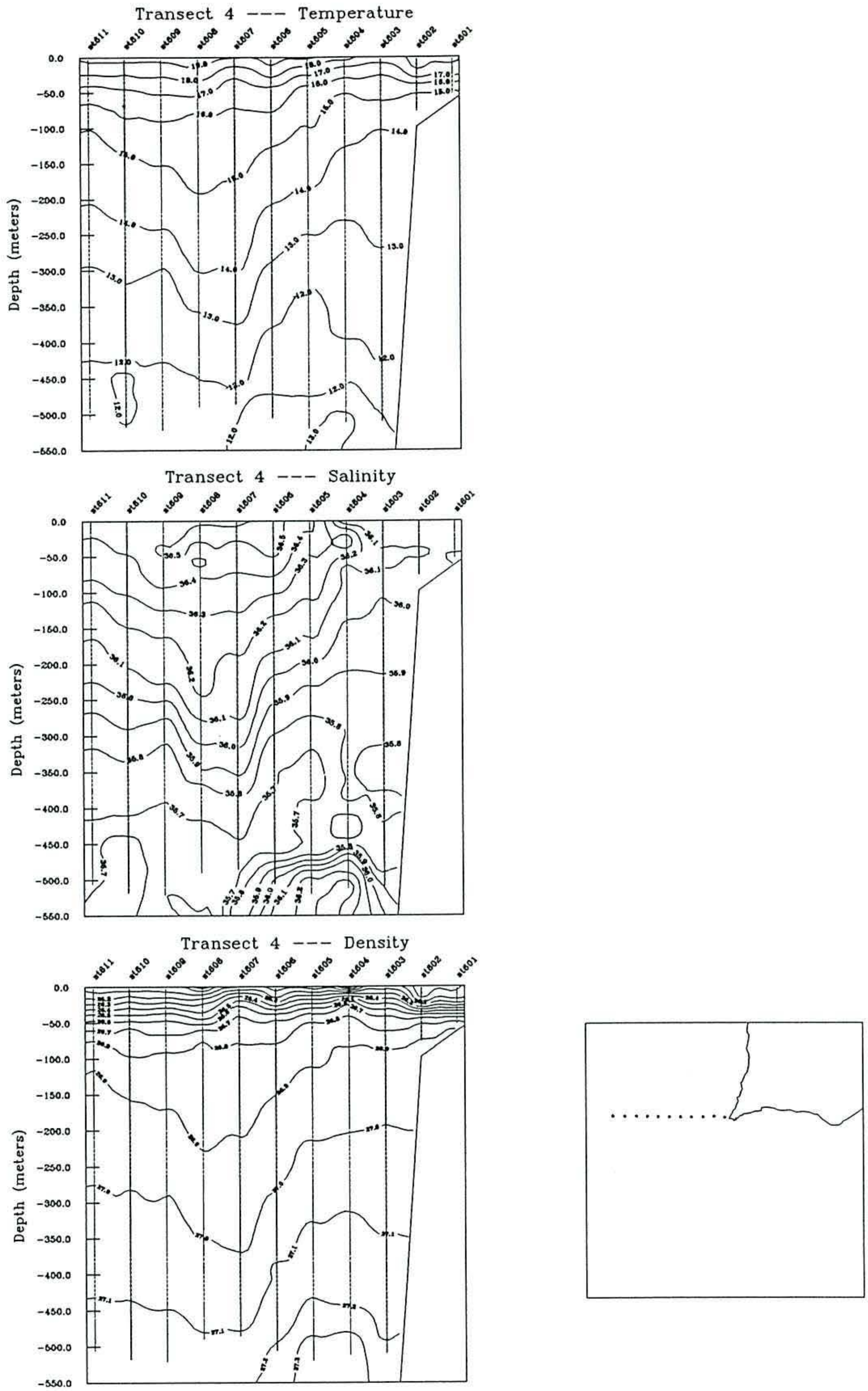

Figure 7.10: *continued*

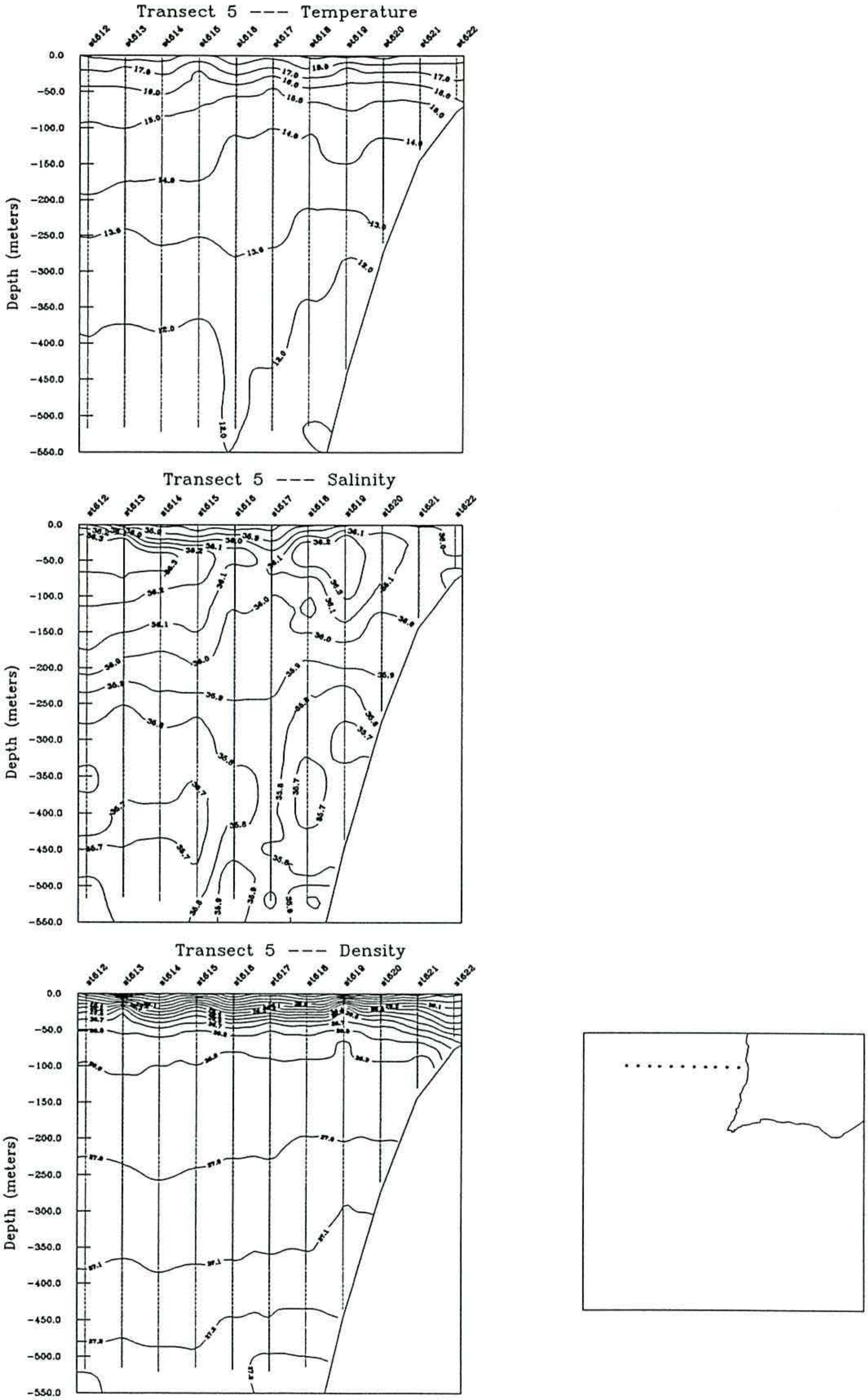

Figure 7.10: *continued*

ity is rather uniform. This feature will be seen in more detail in transects 6, 7 and 8. Also of interest is the downward tilt of the isotherms below 200 meters depth over the continental slope, generating a divergent pattern towards the slope, characteristic of a poleward flowing undercurrent. Finally, a vein of warm and saline Mediterranean Water is clearly discernible below 450 meters depth, close to the continental slope. This feature observed here is consistent with the location of a shallow core of MW reported earlier by *Ambar* [1983].

Most of the features revealed in transect 4 changed dramatically in transect 5, located further north. The offshore surface waters are relatively cool and a downward slope of the isotherms and isopycnals over the upper continental slope is strongly evident, since the shelf is virtually absent here. The shoreward rise of the isolines is not observed in this transect, and a region of reduced vertical gradient of temperature and salinity is observed centred in stations st616 and st617. Two relative maxima of salinity are observed in the subsurface waters and two relative minima are observed bellow 250 meters depth, surrounding the region of relatively homogeneous salinity and temperature. However, this feature is compensated in the density field, which is seen to be relatively uniform in the zonal direction, with a strong intensification of the vertical gradient in the near surface layer forming a pronounced pycnocline.

The small inshore sampling grid off the western coast, just north of Cape São Vicente, comprises the zonal transects 6, 7 and 8. The stations were sampled sequentially along transect 6, but alternated between transect 7 and 8. During the sampling period (from 2144 on 15 June to 1113 on 16 June) very weak northerly winds prevailed (mean speeds of around 4 m/s). The vertical fields of temperature, salinity and density along these transects are displayed in Figure 7.11. In this region the continental shelf is very narrow. A significant overall shoreward drop of the isotherms and isopycnals towards the coast is observed in the three sections, suggesting a mean northward geostrophic flow over the slope. However, in the upper layers further offshore the opposite slope of the isotherms and isopycnals is observed. This feature is particularly evident in transect 8, and is located closer to shore as we progress northward (transect 7 and 6). A shoreward divergent pattern of the isotherms, centred at about 200 meters depth, is evident in transects 6 and 8. This feature, which is also seen in transects 4 and 5, could be interpreted as the signal of a poleward slope current. As elsewhere in the region, below 50 meters depth the salinity decreases with depth, but below 450 meters a sudden increase is observed due to the presence of the Mediterranean water vein.

Off the southern coast, two long meridional transects and three short inshore meridional transects were performed during the cruise. The two long transects (transect 1 and 13) were the first and the last transects to be sampled during the cruise and a considerable time span exists between them during which the wind conditions changed considerably.

Transect 1 was performed prior to the zonal transects examined above (start on 11 June at 1942 and finish on 12 June at 1030), under very weak winds (less than 5 m/s), first from the east quadrant rotating then to northerly. The temperature, salinity and density fields are displayed in Figure 7.12. In the offshore region of the transect, the fields are horizontally uniform and the ocean is stratified. However, over the continental slope and shelf, a rise of the isolines towards the coast is observed, followed by a nearshore drop of the isotherms and isopycnals. Thus, on the temperature and density sections there are prominent fronts close to shore with cool dense water reaching the sea surface, with a configuration similar to that observed around Cape São Vicente, in transect 4 (Figure 7.10). In this region close to shore the salinity field is rather homogeneous, but further offshore and coincident with the offshore edge of the temperature front, the isohalines intersect the surface raising from depths as deep as 200 meters, forming a strong surface salinity front, leaving the less saline waters inshore. Again, this pattern is similar to that observed in the salinity field of transect 4, on the other side of Cape São Vicente, revealing a continuity of the nearshore

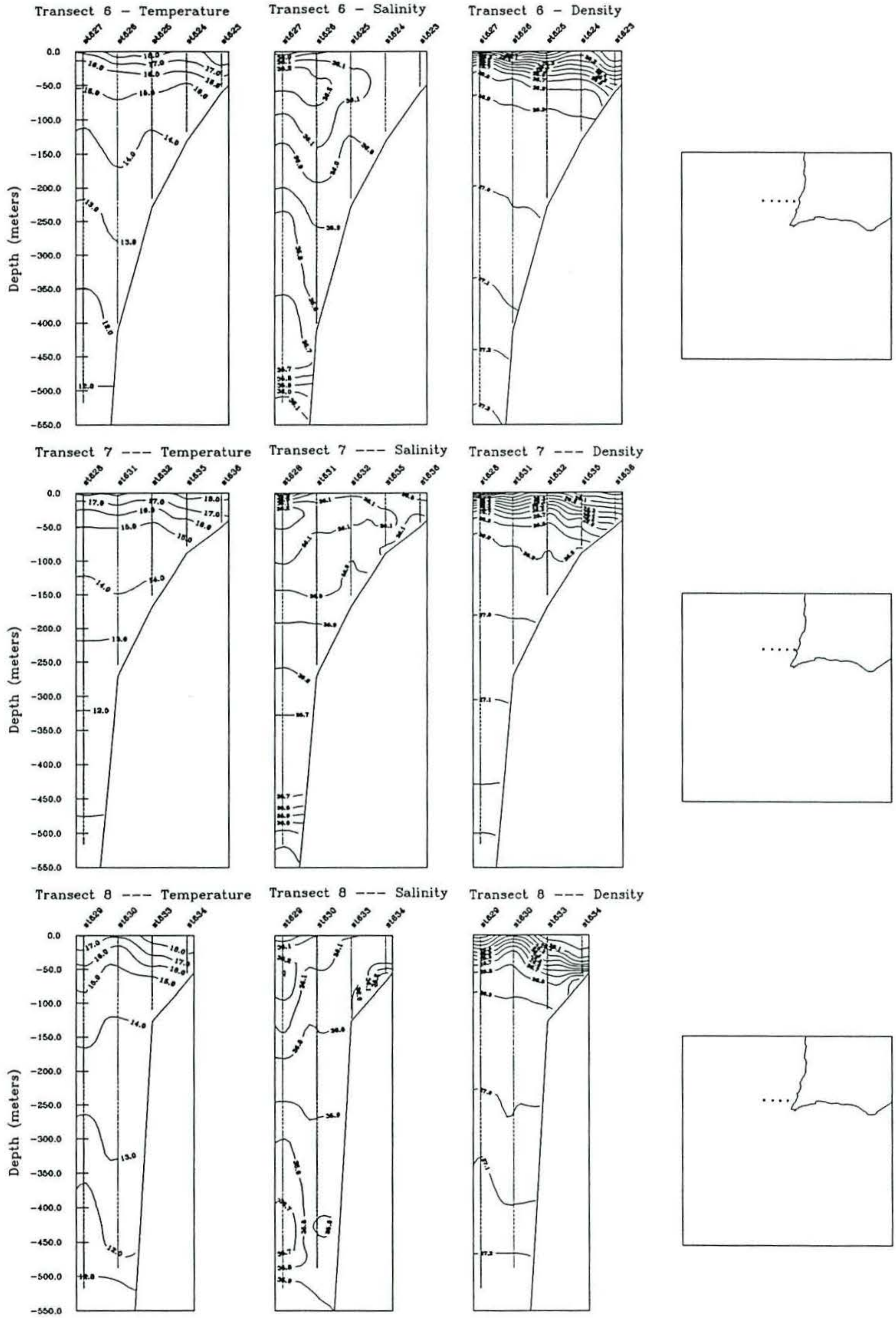

Figure 7.11: Vertical fields of temperature, salinity and density ($\sigma_t$) along the inshore transects 6,7, and 8. A sketch with the location of each transect is displayed. Vertical columns of dots with labels on top indicate the location of the CTD stations.

water mass around the cape in the surface layers. The divergent configuration of the isotherms towards the coast observed at about 200 meters depth in the zonal transects off the western coast and interpreted there as a slope poleward current, is not noticeable here. Close to the continental slope below 450 meters depth the presence of the Mediterranean water vein is evident.

The vertical fields observed along the small meridional transects 9, 10 and 11, which constitute the nearshore grid performed off the southern coast close to Cape São Vicente, are displayed in Figure 7.13. The grid sampling took place between 17 of June at 1453 and 18 of June at 1544. During this period the wind remained weak, blowing from northeast during the first hours with speeds about 6 m/s, turning then to northwesterly wind, decaying then to less than 3 m/s from the north quadrant. Despite the time interval of a week between these transects and transect 1, as the wind did not change dramatically, the structure of the coastal waters shown in this transects is similar to that observed in transect 1: a general tendency of the isolines to rise against the coast, resulting in surface fronts, and a drop of the isotherms and isopycnals in the surface layers over the shelf, leaving lighter and warmer water nearshore, with no signal in the salinity field. A general warming of the surface layer waters relatively to transect 1 is observed. In the deeper layers below 400-450 meters, the presence of Mediterranean water is observed hold to the continental slope.

The last two transects of Poseidon 201/9 cruise (transect 12 and 13, Figure 7.14) were realized between 19 of June at 1009 and 20 of June at 2310, with the winds blowing with some intensity. Transect 12 was performed just off Cape São Vicente in a northeast-southwest direction with the wind blowing from northeast with speed about 11 m/s turning to northwesterly wind of 10 m/s. The isotherms and ispycnals rise nearshore to the surface as a consequence of the renewed upwelling, in contrast to the situation found 8 days before in transect 1, approximately in the same position. However, near surface waters over the upper slope are warmer than in transect 1 as

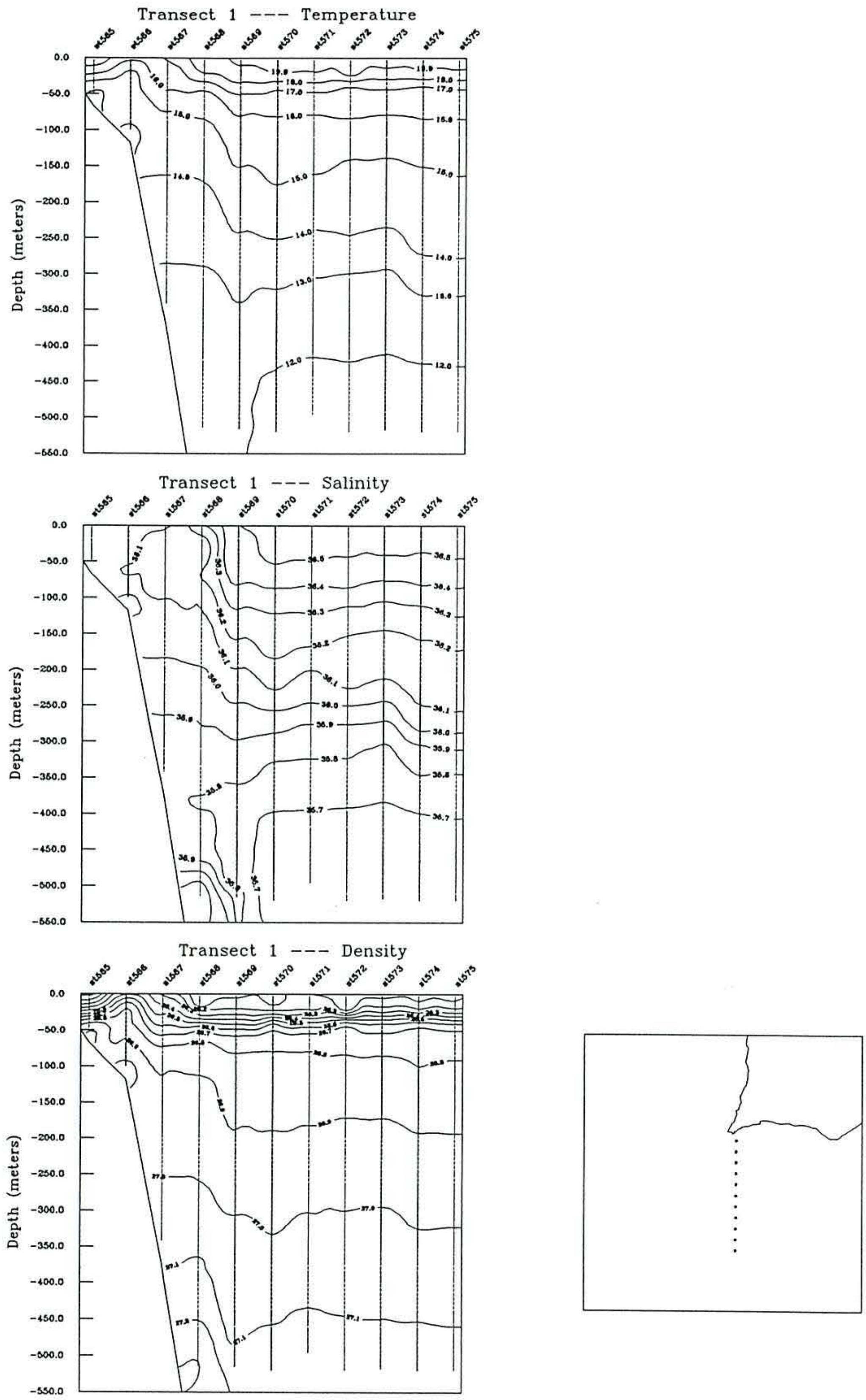

Figure 7.12: Vertical field of temperature, salinity and density ($\sigma_t$) along transect 1. A sketch with the location of the transect is displayed. Vertical columns of dots with labels on top indicate the location of the CTD stations.

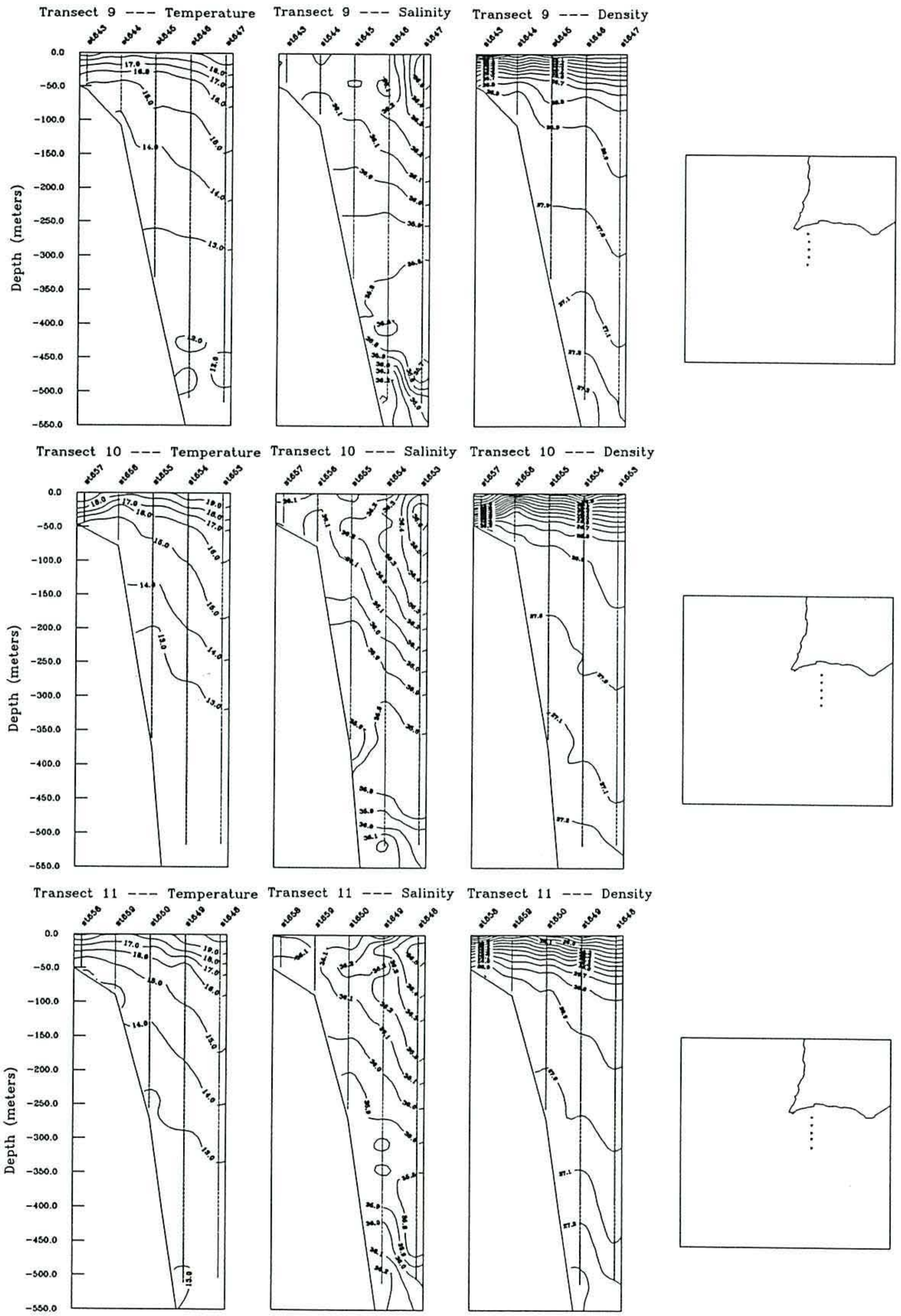

Figure 7.13: Vertical fields of temperature, salinity and density ($\sigma_t$) along the inshore transects 9, 10, and 11. A sketch with the location of each transect is displayed. Vertical columns of dots with labels on top indicate the location of the CTD stations.

a result of the intervening period of warming. The divergent pattern of the isotherms against the coast at 200 meters depth is evident and the presence of Mediterranean water is well marked in the salinity field.

Transect 13 was the easternmost transect of the cruise and was carried out under northeasterly to easterly winds with speeds about 10 m/s. However, a period of about 17 hours of intense wind with a strong westerly component ($\approx$12 m/s) occurred just before the sampling. Thus, the nearshore drop of the isotherms observed before in transects 9, 10 and 11 is not evident now. A continuous tilt of the isotherms along the slope from more than 200 meters depth is observed, indicative of weak upwelling. The rise of the isohalines from more than 200 meters deep to form a strong surface salinity front is observed, consistent with what was observed before in other transects. Mediterranean waters are seen to be constrained to the slope below 400 meters.

## 7.4 Flow field

### 7.4.1 Dynamic height

Data from the entire cruise were used to compute quasi-synoptic maps of dynamic height, which was normalized by the acceleration of gravity in order to obtain $\Delta D_{p_{sup}/p_{ref}}/g$ in dynamic meters. The resulting distribution of dynamic height of the sea surface relative to 500 dbar, 100 dbar and 30 dbar, and of the 100 dbar surface relative to 500 dbar are shown in Figure 7.15. For the shallower stations in the $\Delta D_{0/500}$ and $\Delta D_{100/500}$ maps, $\Delta D_{0/p_{max}}$ or $\Delta D_{100/p_{max}}$ were calculated directly and $\Delta D_{p_{max}/500}$ was calculated by linear extrapolation from the next offshore pair of stations, following the technique described by *Reid and Mantyla*, [1976]. The other two maps were prepared using only data from CTD casts to at least the reference depth. The 500 dbar level seems to be a reasonable choice for the maximum reference level. This pressure level is deep enough to suppose a level of no motion and shallow enough to avoid the

Transect 12 --- Temperature

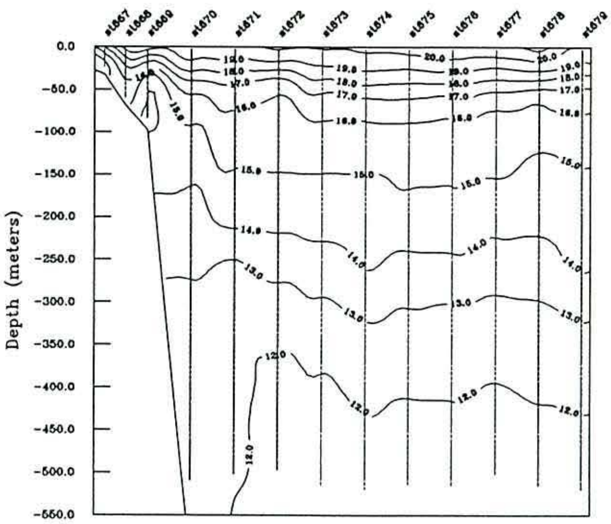

Transect 12 --- Salinity

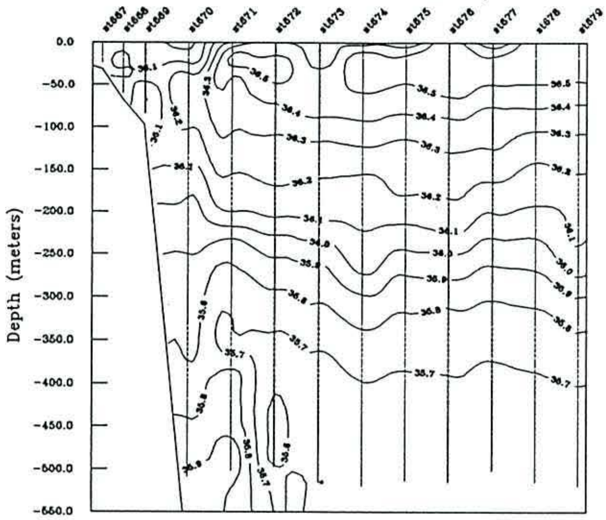

Transect 12 --- Density

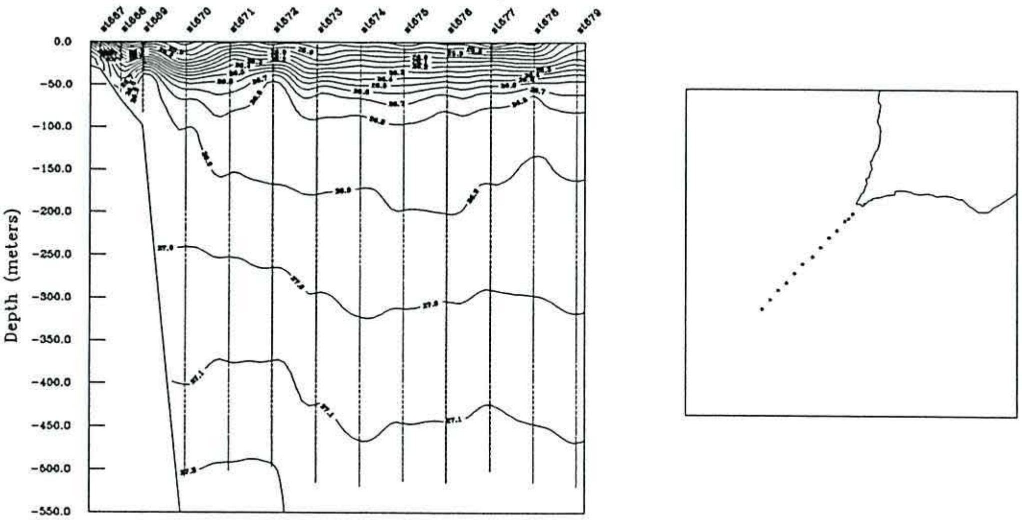

Figure 7.14: Vertical fields of temperature, salinity and density ($\sigma_t$) along the inshore transects 12 and 13. A sketch with the location of the transects is displayed. Vertical columns of dots with labels on top indicate the location of the CTD stations.

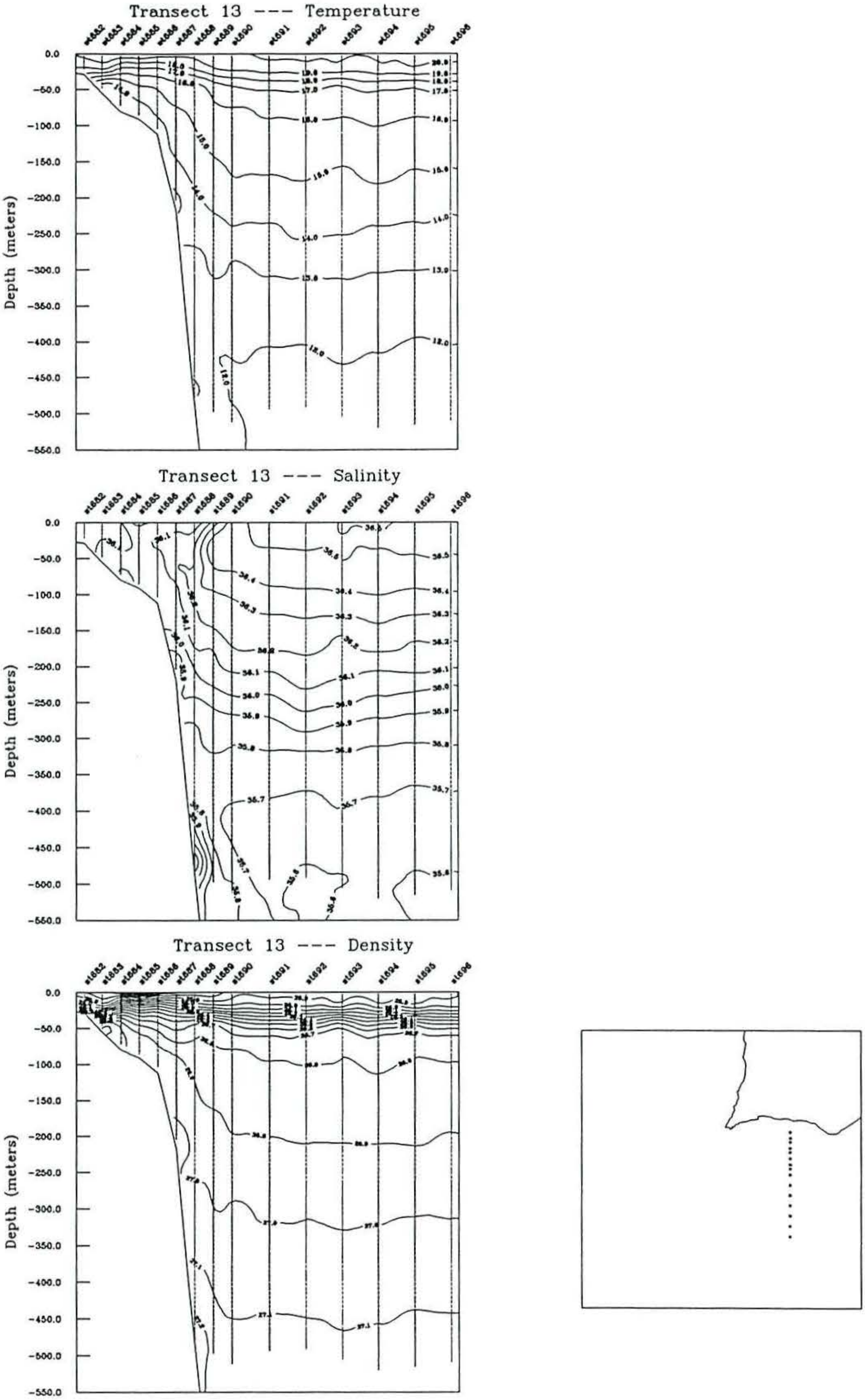

Figure 7.14: *continued*

influence of the main paths of the Mediterranean outflow. The contours of the dynamic height would represent streamlines of the geostrophic flow if the velocity at 500 dbar were everywhere zero. This level corresponds to the depth limit of the data collected during the survey. A similar pressure level has proved to be an acceptable reference level off California [e.g., *Ramp et al.*, 1991]. However, in the Iberian region care must be taken because if strong motion occur at MW depths it might influence the surface topography, in particular during the occurrence of meddy features.

In the distribution of the dynamic height of the sea surface relative to 500 dbar (Figure 7.15, top left), a tongue-like feature of low geopotential anomaly is evident extending southward off the western coast, centred at about 9.3 W. The centre of this feature is characterized by a relative minimum, at 37.3 N. The presence of a low geopotential anomaly region nearshore in the top of the displayed area, reveals that part of the equatorward geostrophic flow coming into the region from the north turns onshore, and part enters into the tonge-shaped feature. Near Cape São Vicente, over the shelf and upper slope, higher dynamic height values are observed. This configuration corresponds to a cyclonic geostrophic flow, integrated to 500 dbar, around the dynamic minimum in the tongue-like feature. A second feature, running from northwest to southeast, is a strong dynamic height gradient, roughly coincident with the temperature and salinity fronts mentioned before (Figure 7.8). To the east, the geostrophic streamlines converge over the south coast continental slope. Higher dynamic height values are observed in the coastal region off the southern coast, indicating an overall eastward flow between the surface and 500 dbar. However, is important to notice that the CTD stations that define the fields in this region were carried out already with an upwelling favourable wind blowing with some intensity. Also, the assumption that the eastward flow extends to the nearshore regions is somewhat ambiguous due to the extrapolation into shallow waters applied to the data. Another feature of interest is the large anticyclonic eddy centred at 36.6 N; 9.7 W, where the highest dynamic height

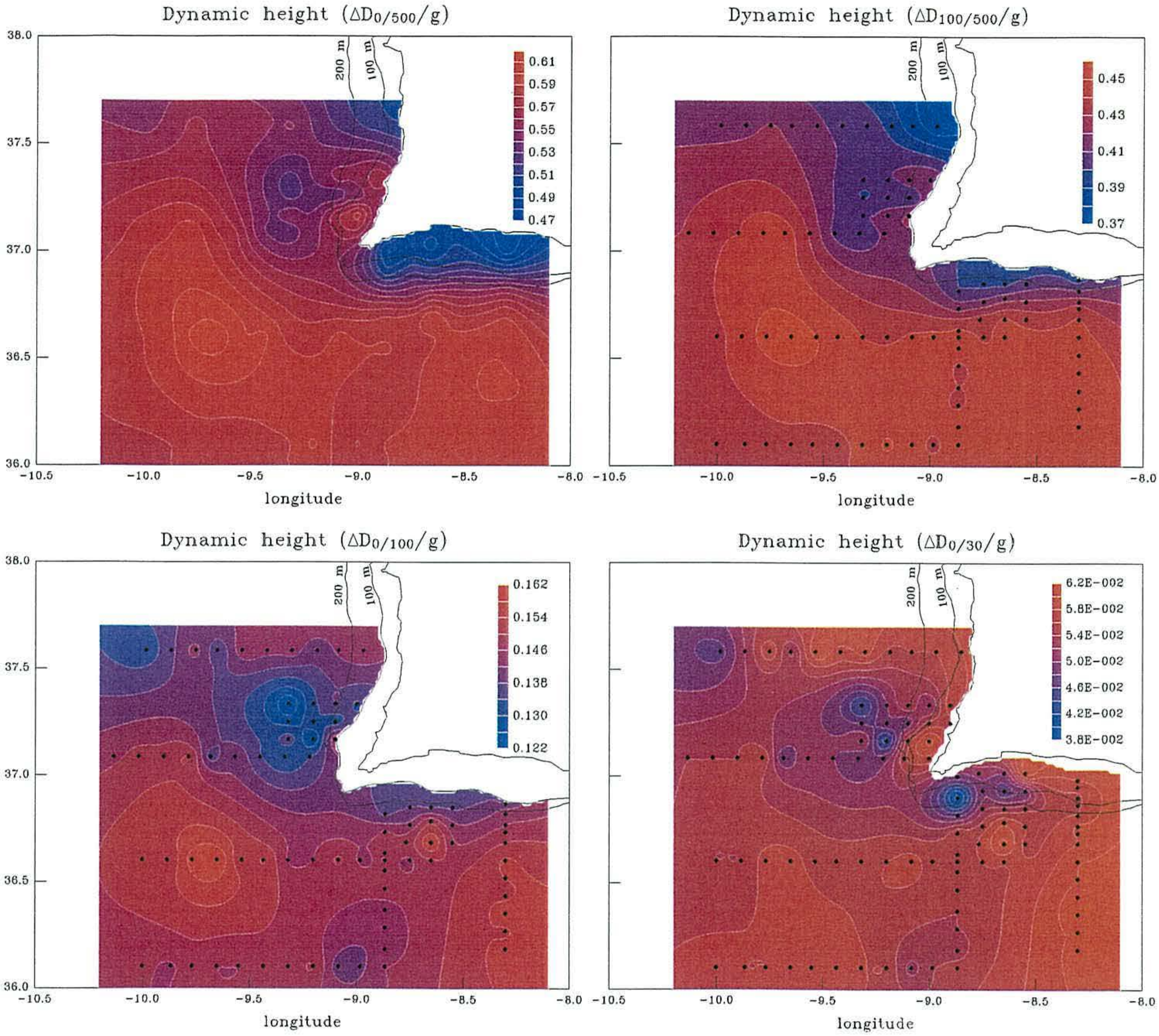

Figure 7.15: Contour maps of dynamic height normalized by the acceleration of gravity at the surface relative to 500 dbar (top left), at 100 dbar relative to 500 dbar (top right), at surface relative to 100 dbar (bottom left) and at surface relative to 30 dbar (bottom right), from the Poseidon 201/9 survey. Individual conductivity-temperature-depth profiles are denoted by dots along the ship track. 100 and 200 meters bathymetric lines are also represented.

values of the studied region are observed. The hypothesis that this feature corresponds to the surface signature of a deeper mesoscale eddy structure of Mediterranean water (meddy) can not be excluded, since meddies are seen to be correlated with surface height anomalies [*Hinrichsen et al.*, 1993] and can be related to positive altimeter anomalies in the surface topography [*Stammer et al.*, 1991].

The main features observed in the $\Delta D_{0/500}$ map remain defined in the $\Delta D_{100/500}$ surface (Figure 7.15, top right). However, the surface geostrophic streamlines relative to 100 dbar, $\Delta D_{0/100}$ (Figure 7.15, bottom left), where no extrapolation into shallow waters were done, show two well defined eddy features, the anticyclonic one centred at 36.6 N; 9.7 W, and a cyclonic eddy off the western coast, corresponding to the centre of the tongue-like feature of low geopotential anomaly observed in the $\Delta D_{0/500}$ map. Notice that this eddy feature is well resolved by the sampling CTD grid, which is dense in this region. The geopotential anomaly isolines for the 0/100 surface do not show a continuity with the regions further north. The 100 dbar level is unlikely one of no motion, implying that the cyclonic eddy feature is energetic in the upper layers, while the continuity with the regions further north occurs mainly at the subsurface. Off the southern coast, off the 100 meters isobath, the geostrophic flow relative to 100 dbar is eastward.

An attempt to resolve the geostrophic circulation over the shelf and to investigate the origin of the high dynamic height anomaly observed nearshore off the western coast was done by computing the surface dynamic height map relative to 30 dbar, $\Delta D_{0/30}$ (Figure 7.15, bottom right). Close to Cape São Vicente, off the southern coast, a tongue-like feature of low dynamic height values extends eastward over the continental slope, coincident with the cold protrusion observed before in the surface temperature field (Figure 7.8), leaving higher dynamic height values inshore. This pattern complies with the view presented in previous chapters that a narrow surface coastal counter-current flows westward along the coast of Algarve, turning northward around the Cape.

In the $\Delta D_{0/30}$ pattern shown here the geostrophic coastal counter-current is seen to roll anticyclonically after turning around the Cape São Vicente. Another feature revealed in the $\Delta D_{0/30}$ map is that while the cyclonic eddy off the western coast is still observed, the anticyclonic eddy centred at 36.6 N; 9.7 W and still defined in the $\Delta D_{0/100}$ map, almost disappeared. This means that while the cyclonic eddy is intensified at surface, the anticyclonic eddy is not intensified at the surface relatively to 30 dbar depth, supporting the explanation that this is a deeper meddy feature. Further support for this idea is the strongest perturbations of the hydrographic fields in the anticyclonic eddy area occur at the deeper levels, below 200 meters (see Figure 7.10, transect 3).

### 7.4.2 Acoustic Doppler profiler velocity observations

Vector plots representing the horizontal velocity field in the Cape São Vicente region measured by means of the shipboard Acoustic Doppler Current Profiler (ADCP) are presented and analyzed in this section. The data were extracted from the edited and calibrated CODAS database, described in the preceding Chapter, using a built in software (ADCPSECT). The data were extracted for particular time ranges and then averaged over selected intervals along the track and over 50 meters depth bins, except for the shallowest good bin which was from 16 to 25 meters. Data above 16 meters depth were not used. Current vector maps corresponding to consecutive subsets of the cruise track were built. Maps showing the time ranges corresponding to transect 1 to 5 and transect 12 to 13 were averaged horizontally on 0.05° intervals, while the maps showing the detailed sampling of specific regions to the west and south of Algarve (transect 6 to 8 and transect 9 to 11) were averaged horizontally on 0.025° intervals.

The lack of any extended time series stations precluded the use of the ADCP data for accurate evaluation of the degree of contamination of the recorded data by tidal currents. However, subsets of the data were confined to relatively small areas, and so could be treated as if they did form time series. Harmonic analyses of these subsets provided estimates of the tidal amplitudes for the main constituents. A separate assessment of the effect of tides in the ADCP velocities was done by means of a tidal model for six major constituents (M2, S2, K2, O1, P1 and Q1) run specifically for the Cape São Vicente region, by courtesy of MARETEC, Instituto Superior Técnico, Lisboa. The results show maximal tidal currents of the order of 7 cm/s in a restricted nearshore region to the south of the Cape and less than 4 cm/s elsewhere. Also, results from simulations of seven major harmonics derived from TOPEX/POSEIDON data sets carried out by *Fanjul et al.* [1997], gave tidal currents of the order of 5 cm/s for the M2 component off Iberia at about 40°N, the closest region to Cape São Vicente represented in the paper. These estimates were in agreement with the results from the harmonic analyses. The typical velocity signal measured by the shipboard ADCP was much greater, therefore the tidal signal would have negligible influence in the main features revealed in the observed velocity field. Moreover, subsequent analysis showed that the main features observed in the ADCP data were closely related with the observed hydrographic features and environmental conditions. Because of these reasons the original ADCP data set was left unaltered. Similar conclusions were reached in studies in the coastal transition zone off California, where the effect of tidal currents on the measured ADCP data was systematically neglected [e.g. *Huyer and Kosro*, 1987; *Ramp et al.*, 1991; *Huyer et al.*, 1991], and when it was evaluated the authors concluded that the effect was very small [*Barth and Brink*, 1987].

The horizontal vector plots of ADCP velocities for the long transects to the west and southwest of Cape São Vicente (transect 1 to 5), averaged for the 16-25 meters and 75-125 meters depth bins, are shown in Figure 7.16. The $\Delta D_{0/500}$ and $\Delta D_{100/500}$ fields are shown underlying the respective vector plot. Recalling that this first part of the cruise was carried out under calm conditions, wind driven currents will be negligible. The velocity vectors show a complex flow pattern that seems dominated by small scale instabilities. Since the spacing between adjacent transects is about 40-50 km, we cannot expect the dynamic topography to resolve eddies or meanders with meridional scales of less than 80-100 km, except in the nearshore region close to the Cape São Vicente where the small grid was sampled (transects 6 to 8). There, the dynamic topography can resolve features with alongshore scales of about 15-20 km, as seen later.

With reference to the upper layer (Figure 7.16, top), a narrow southward flow with velocities up to 0.3 m/s is observed off the shelf on the western coast (transect 4 and 5), limited on both sides by northward velocities. This flow is coincident with the gradient of dynamic height that turns eastward around the Cape, off the continental shelf. Evidence of the large eddy feature located on the southwestern part of the displayed region is observed in the ADCP data, although the centre of the feature may not be exactly coincident. In the top left corner of the survey region, relatively strong northwestward velocities ($\approx 0.3\,\mathrm{m/s}$) are observed, which are not resolved in the dynamic topography. Those features are common to the 75-125 layer (Figure 7.16, bottom).

The southward flow seems to penetrate into a region with an opposed flow regime, while turning eastward around the Cape. Inshore, over the steep continental slope close to the Cape São Vicente, a strong poleward counterflow, sometimes exceeding 0.4 m/s, is observed. The configuration of the ADCP velocity vectors to the west of this counterflow suggests that part of the southward flow is getting separated from the main flow, turning cyclonically following the dynamic topography. Possibly, a similar situation occurs further north, as observed in transect 5, where a strong horizontal shear occurs at -9.4° of longitude. Horizontal shear also occurs to the west of the southward flow, which is not only a near surface feature.

The vertical distribution of the alongshore meridional velocity along transect 4 and 5 is shown in Figure 7.17, with the poleward velocities as positive. In the northernmost transect (transect 5, Figure 7.17, **a**) a southward current is observed through the entire water column roughly between 9.4 and 9.8° W, with the bulk of the jet approximately

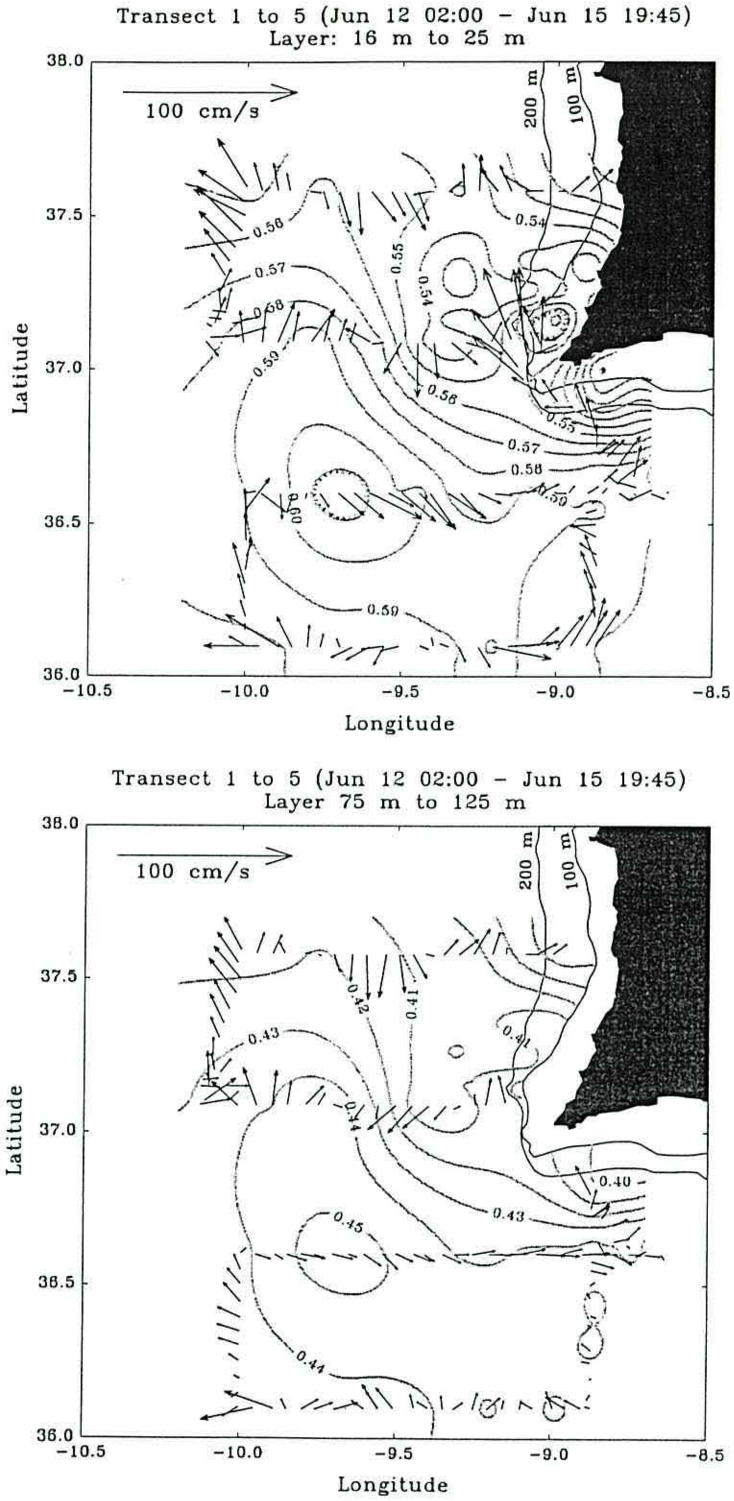

Figure 7.16: Maps of the ADCP current vectors for transect 1 to 5 (Jun 12 02:00 - Jun 15 19:45). **Top**: Velocities averaged for the 16-25 m depth bin superimposed on the $\Delta D_{0/500}$ field; **Bottom**: Velocities averaged for the 75-125 m depth bin superimposed on the $\Delta D_{100/500}$ field. The scale of the ADCP vectors is shown in the panels. Units of the dynamic topography are dyn m. The 100 and 200 meters bathymetric contours are represented.

in the centre between 75 and 300 meters depth, reaching velocities over 0.25 m/s. Inshore and also throughout the water column, a northward flow is observed with velocities about 0.10-0.15 m/s. The southward flow is closer to the coast in transect 4 (Figure 7.17, **b**). There, it is broader and less intense, with the highest velocities (>0.20 m/s) at the surface. Over the shelf and slope, the coastal counterflow is seen with the stronger velocities (>0.40 m/s) near the surface, decreasing rapidly with depth. Offshore on both transects the flow is northward at all depths. Further to the south, along transect 3 (Figure 7.18), the flow was observed to be mainly eastward at all depths, with appreciable southward flow limited to the near surface layers.

As noticed before, the coastal region between transects 4 and 5 was sampled with a finer grid, allowing a better definition of the fields in the region. Thus, the cyclonic feature centred at 37.3 N; 9.3 W was resolved by the dynamic topography. The ADCP velocity vectors, averaged for the 16-25 meters bin, observed in this region (transect 6 to 8) are displayed in Figure 7.19 in an enlarged scale, along with the $\Delta D_{0/30}$ field. The ADCP data show the near surface counterflow curling against the coast over the shelf, with velocities up to 0.4 m/s, consistent with the field of dynamic height ($\Delta D_{0/30}$). The 30 dbar reference is not a level of no motion, but the feature observed in the ADCP data is discernible in the $\Delta D_{0/30}$ field. Further offshore the velocity vectors are weaker ($< 0.25$ m/s) and are seen to point northward, curling slightly westward, also following the dynamic topography.

The vertical distribution of the meridional velocity observed along transect 6 is represented in Figure 7.20. Transect 6 is the northernmost transect of this fine grid, sampled zonally along 37.33°N, and was the only that was sampled consecutively allowing a reliable vertical representation. This transect lies just north of the cyclonic feature and shows northward velocities (>0.30 m/s) nearshore over the shelf, in a similar pattern to that observed in transect 4. A northward intensification occurs at about 200 m depth, over the slope. Such intensification is also observed further north at the

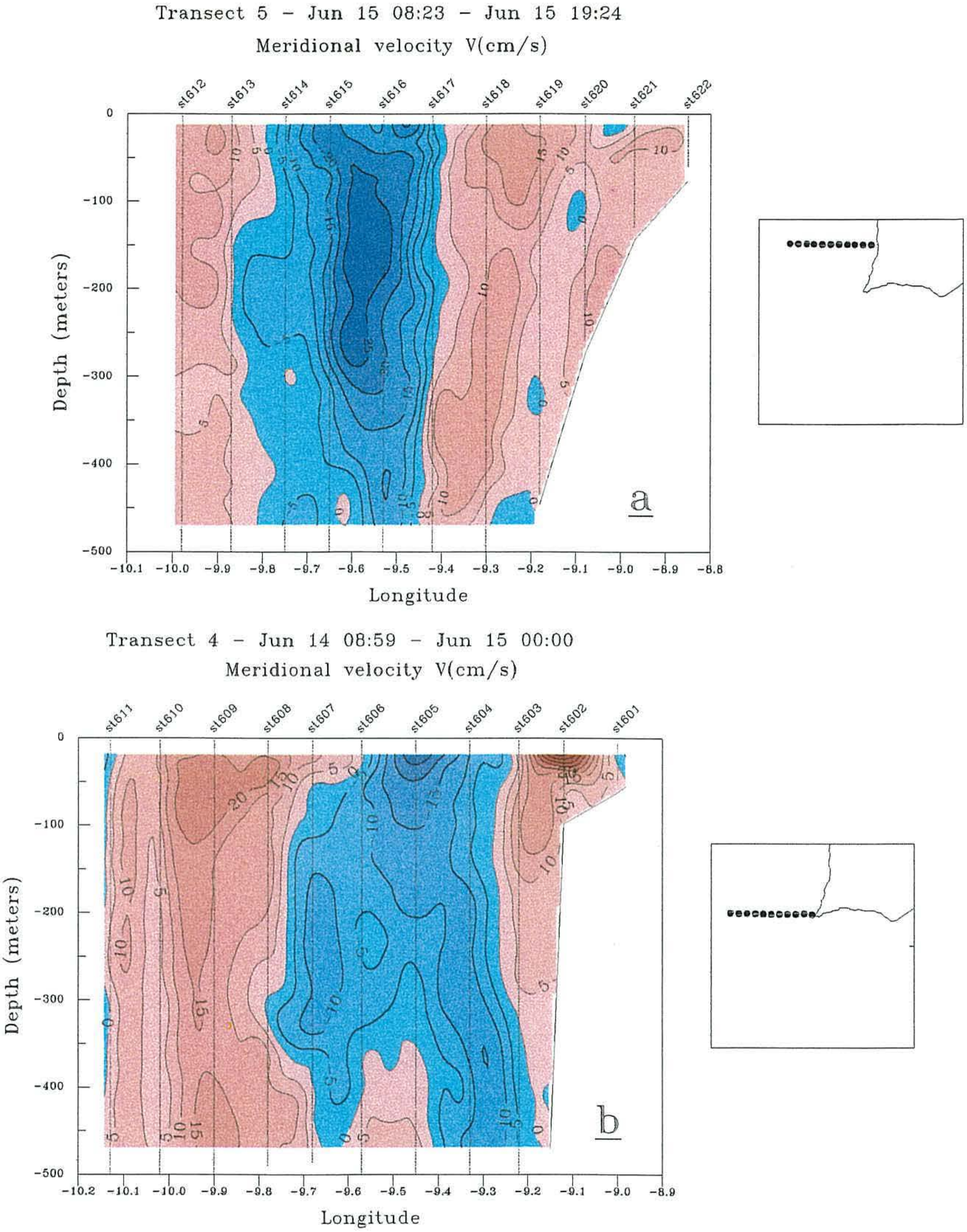

Figure 7.17: Vertical distribution of the meridional velocity in (**a**) transect 5 and (**b**) transect 4, objectively mapped from the ADCP data. Positive velocities are northward. CTD station are also indicated. For clarity a sketch shows the locations of the transects.

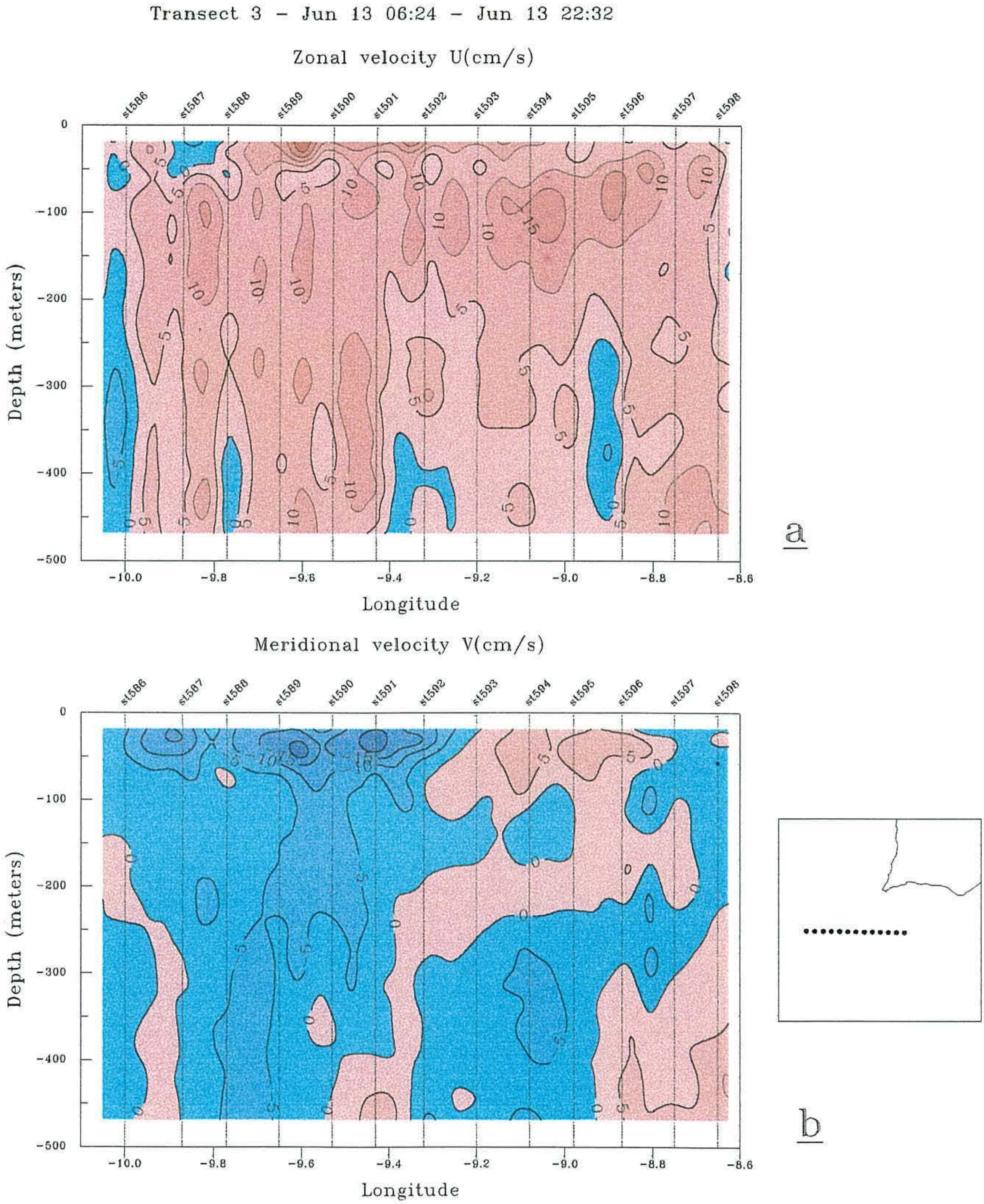

Figure 7.18: Vertical distribution of the (**a**) zonal and (**b**) meridional velocity in transect 3, objectively mapped from the ADCP data. Positive velocities are eastward and northward. CTD station are also indicated. For clarity a sketch shows the locations of the transect.

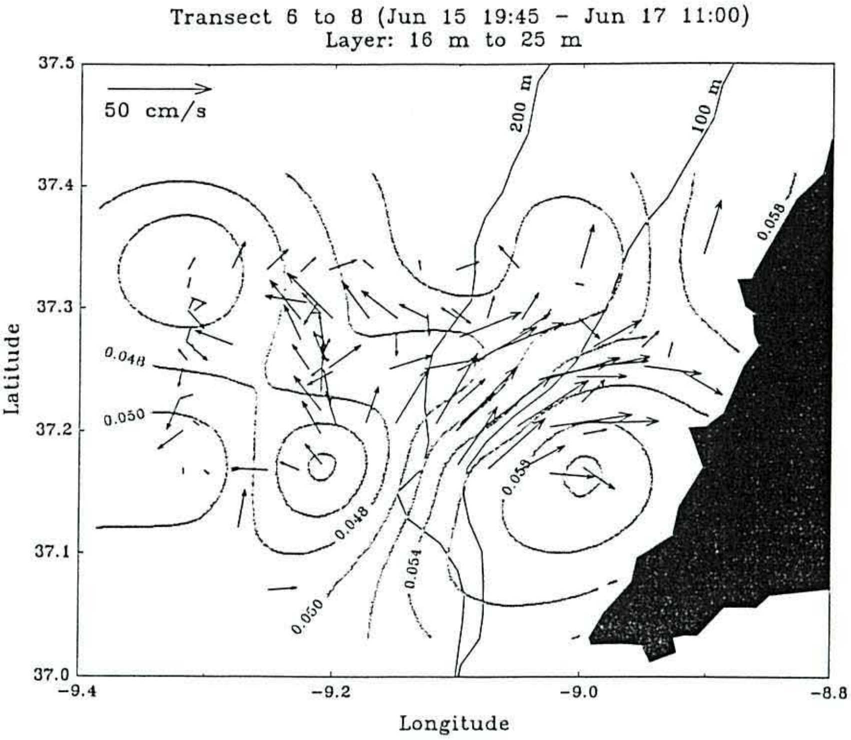

Figure 7.19: Map of the ADCP current vectors for transect 6 to 8 (Jun 15 19:45 - Jun 17 11:00), averaged for the 16-25 m depth bin and superimposed on the $\Delta D_{0/30}$ field. The scale of the ADCP vectors is shown in the panels. The dynamic topography is in dyn m. The 100 and 200 meters bathymetric contours are represented.

same depth, in transect 5 (Figure 7.17, **a**), consistent with the onshore drop of the isotherms observed before (Figures 7.10 and 7.11) and interpreted there as a signal of the poleward slope current.

Off the southern coast close to the Cape, at least part of the near surface eastward flow was seen to curl cyclonically (Figure 7.16) and contribute to the shallow coastal counterflow. Further to the east off the southern coast of Algarve, where a finer sampling grid was carried out (transect 9 to 11), the near surface velocity field from the shipboard ADCP (Figure 7.21 **a**) shows also a tendency for a cyclonic rotation offshore, and a rather undefined flow pattern inshore. In this region, where the evidence suggests that horizontal shear and instabilities dominate, the geostrophic circulation and the ADCP current field are not consistent because factors other than the Coriolis force and the horizontal pressure gradient are acting. Moreover the assumption of 500 dbar as a level of no motion may not be correct here, because of the presence of the shallow vein of Mediterranean water. However, the vertical distribution of the zonal velocity along transect 9 (Figure 7.22) shows a signal of a shallow westward flow

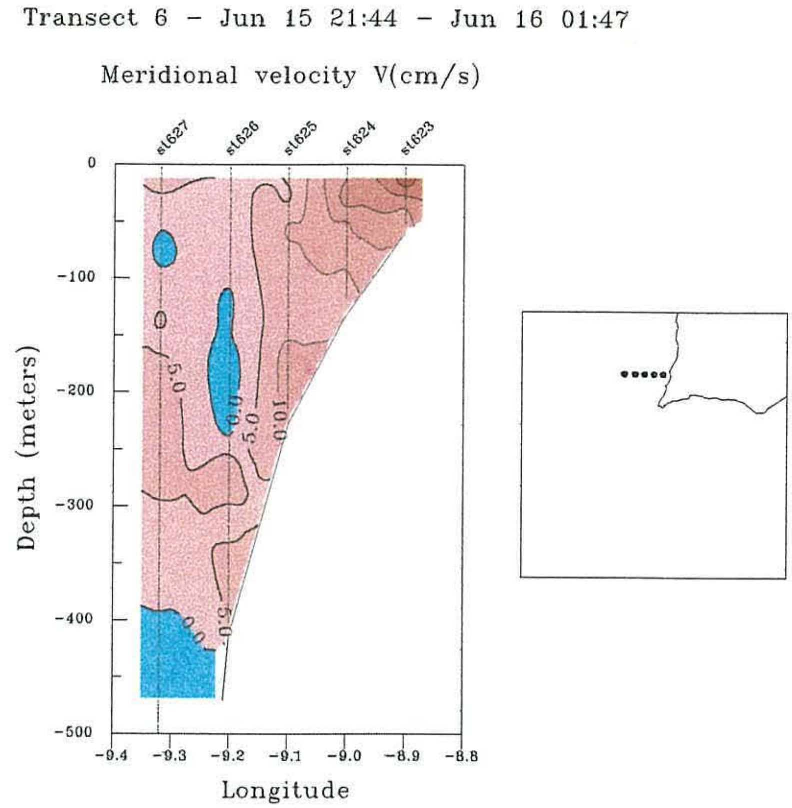

Figure 7.20: Vertical distribution of the meridional velocity in transect 6, objectively mapped from the ADCP data. Positive velocities are northward. CTD station are also indicated. For clarity a sketch shows the locations of the transect.

close to shore. Due to the sampling strategy this was the only transect of this fine grid sampled sequentially, allowing the objective mapping of the alongshore velocity. At deeper levels a small scale cyclonic eddy acquires definition (Figure 7.21 **b,c,d,e**), with the westward velocities increasing with depth. Figure 7.22 shows this feature at about 200 m depth, with the bulk of the westward flow trapped to the slope. At the deepest layer with reliable data (425-475 m depth layer, Figure 7.21 **f**), the averaged ADCP velocity vectors show a westward flow with velocities up to 0.30 m/s, which presumably is already the signal of the shallow westward flow of Mediterranean water.

The last part of the cruise was undertaken with intensifying variable winds, reaching more than 10 m/s at times, and the effects of the wind stress were observed in the upper layers. The shipboard ADCP velocity vectors, averaged for different bin depths are displayed is Figure 7.23. The velocity vectors show a complex flow pattern, with an overall eastward flow over the continental slope off the southern coast, consistent with the field of dynamic height. The anomalous near surface flow feature centred around

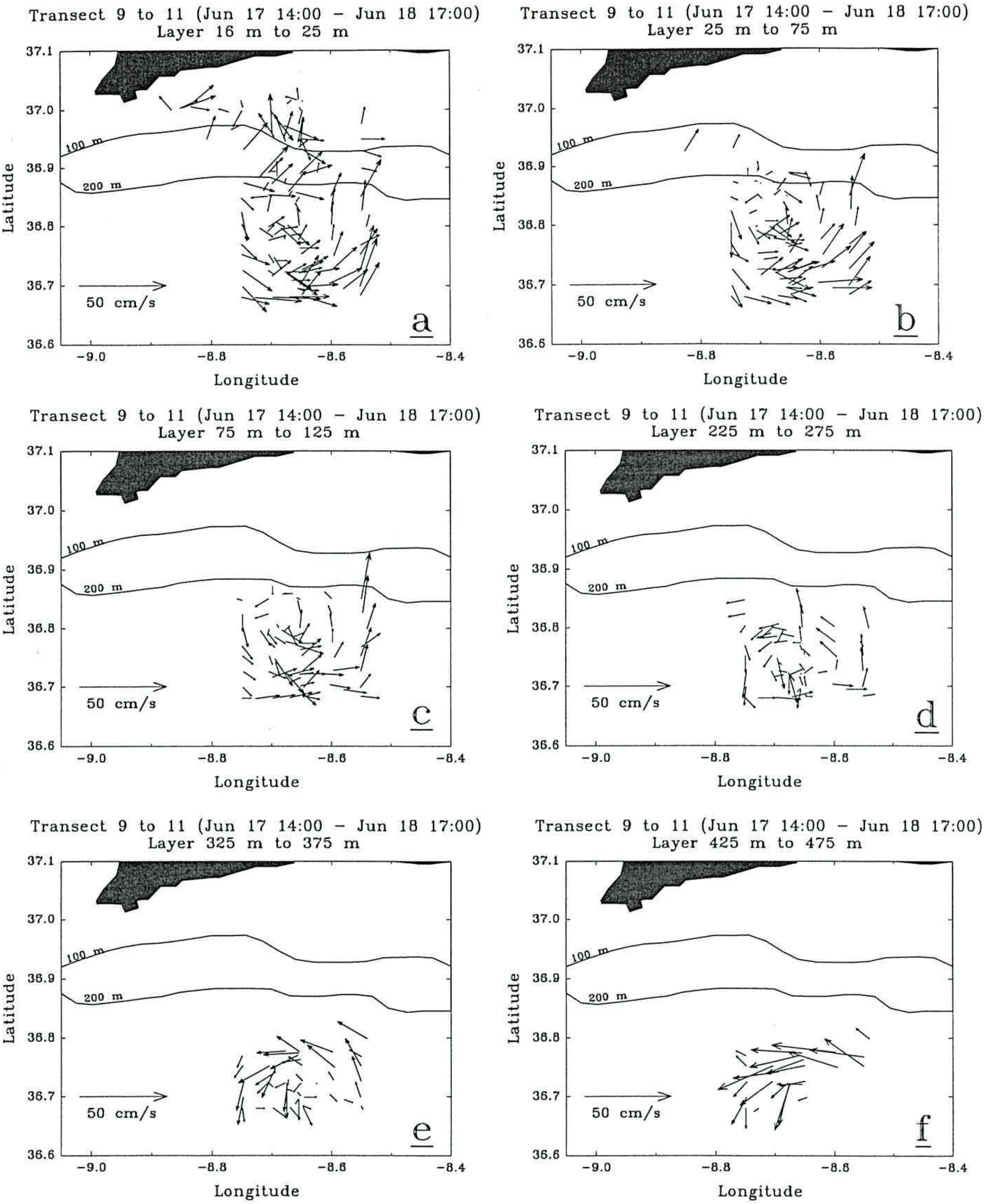

Figure 7.21: Maps of the ADCP current vectors for transect 9 to 11 (Jun 17 11:00 - Jun 19 09:30), averaged for the (**a**) 16-25, (**b**) 25-75, (**c**) 75-125, (**d**) 225-275, (**e**) 325-375, and (**f**) 425-475 meters depth bins. The scale of the ADCP vectors is shown in the panels. The 100 and 200 meters bathymetric contours are represented.

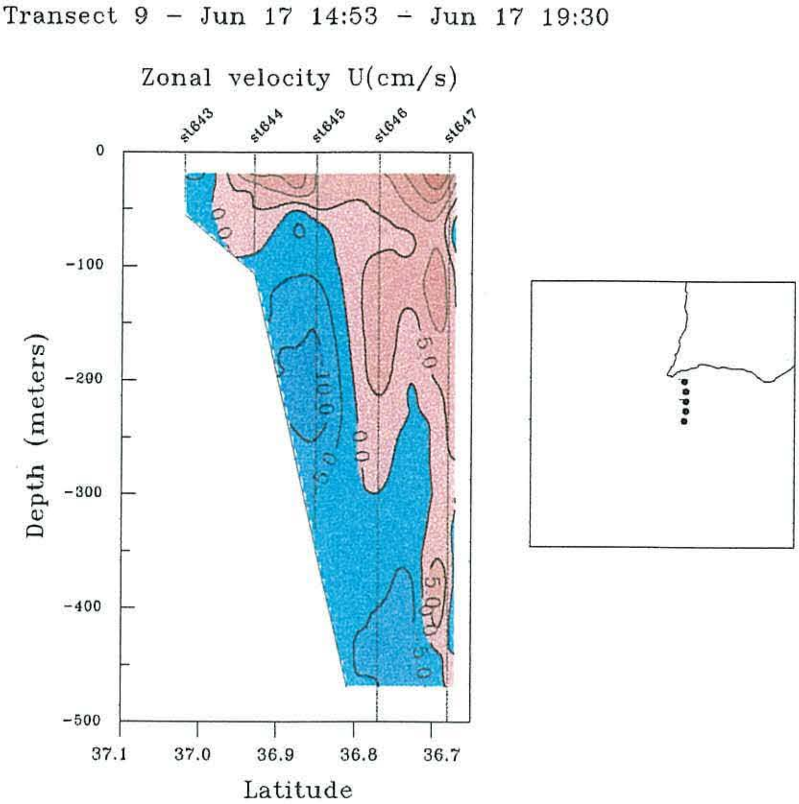

Figure 7.22: Vertical distribution of the zonal velocity in transect 9, objectively mapped from the ADCP data. Positive velocities are eastward. CTD station are also indicated. For clarity a sketch shows the locations of the transect.

8.4°W will be analyzed later. In the 25-75 meters depth bin a weak westward averaged flow is observed nearshore over the shelf, due to the coastal counterflow pointed out before in this section. Such counterflow was not apparent in the upper 16-25 bin because it was masked by the wind stress acting above the thermocline, which was seen to be at about 30-40 meters depth in the region [*Relvas and Barton* 1995]. Small scale eddies and meanders could be present and not resolved by the ADCP data. For instance, the flow pattern observed in the western half of the area suggests the presence of such features. This part of the survey was begun with northeasterly winds blowing at about 8 m/s, that rotated then to stronger (> 10 m/s) persistent westerly winds. The vertical distribution of the alongshore ADCP velocities while sampling southward along transect 13 (Figure 7.24) shows an eastward flow in the upper layers centred at about 36.75°N that diminishes towards the coast. No clear signal of the coastal counterflow is observed here, due to the forcing by the prevailing westerly winds, via Ekman transport and geostrophic adjustment. Below the eastward flow (>300 m depth) and offshore,

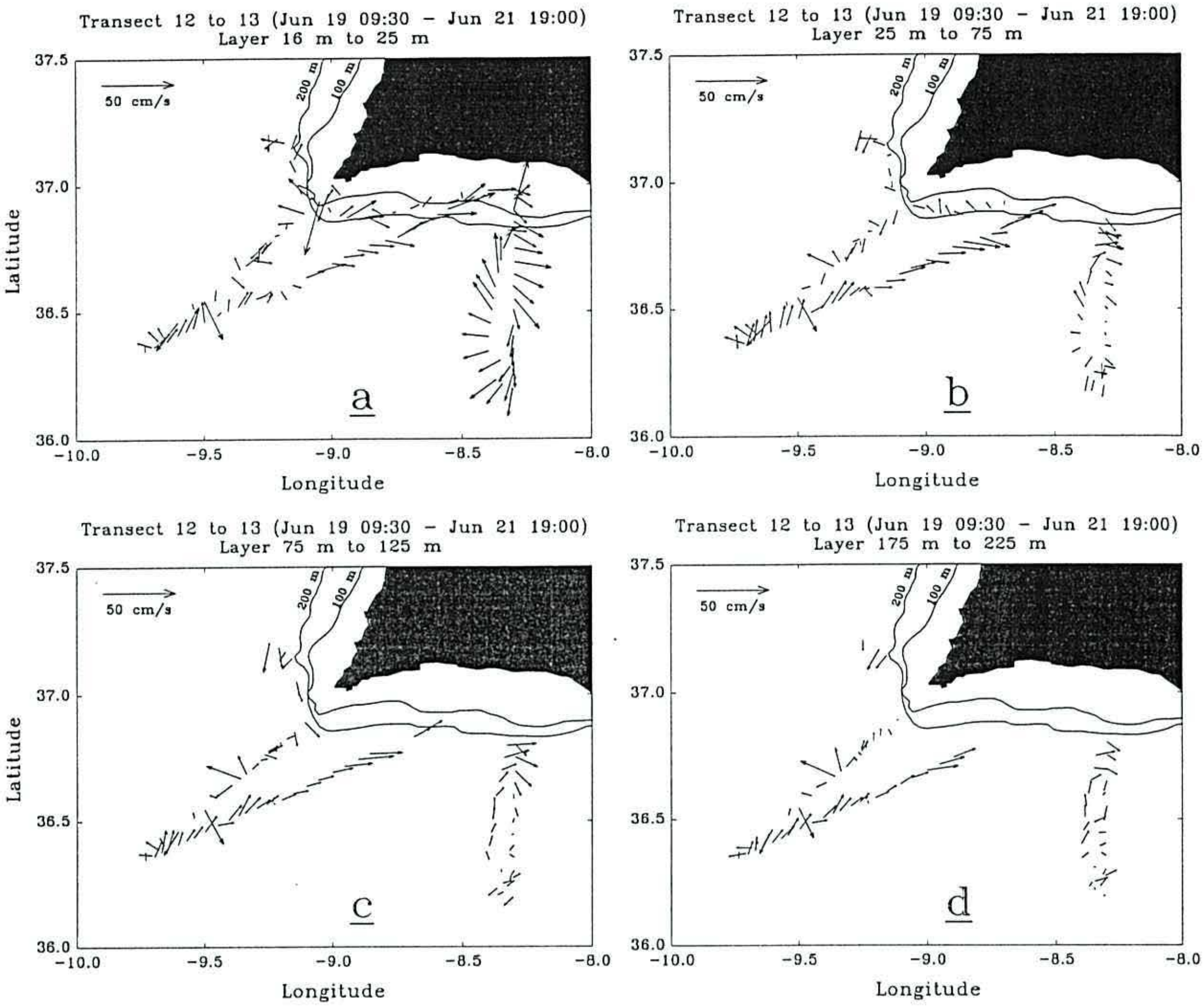

Figure 7.23: Maps of the ADCP current vectors for transect 12 to 13 (Jun 19 09:30 - Jun 21 19:00), averaged for the (a) 16-25, (b) 25-75, (c) 75-125, and (d) 175-225 meters depth bins. The scale of the ADCP vectors is shown in the panels. The 100 and 200 meters bathymetric contours are represented.

the flow is weak towards west. The intensification of the westward current over the slope below 350 m depth is likely to be related with the shallow vein of Mediterranean water.

Transect 13 was carried out from north to south at 8.3°W and then a return track back to the coast was made (Figure 7.23). During the return the surface velocities changed dramatically. The strong velocity variations were limited to the surface layers above the pycnocline, which was seen to be at about 30-40 meters depth in the region (Figures 7.6 and 7.14). The comparison between measured ADCP profiles of zonal velocities and profiles of geostrophic velocities relative to 500 dbar computed from con-

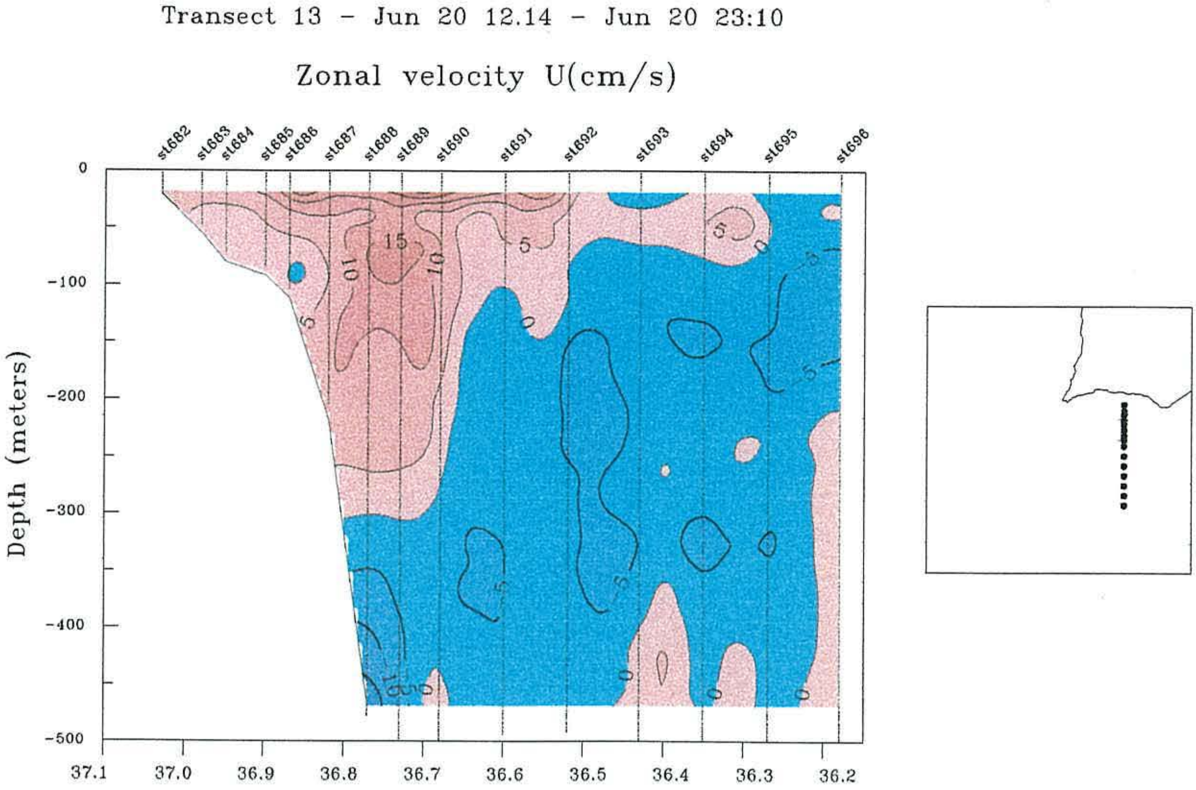

Figure 7.24: Vertical distribution of the zonal velocity in transect 13, objectively mapped from the ADCP data. Positive velocities are eastward. CTD station are also indicated. For clarity a sketch shows the locations of the transect.

secutive CTD stations along transect 13 show a reasonable agreement except in the surface layers (Figure 7.25). There, the flow is eastward with the measured ADCP velocities much higher than the computed geostrophic velocities. This difference could be attributed to the wind stress acting above the pycnocline, inducing an ageostrophic component in the velocity. The ADCP measures this contribution but the geostrophic method does not.

The shipboard measurements of the wind (Figure 7.26**a**) show a strong westerly event with velocities up to 13.5 m/s just before the start of transect 13 (note vectors are drawn so winds from east are up the page). Then, during the CTD sampling, the wind rotated to easterly and the return track was done under weaker variable winds. The pseudo-time series of the measured ADCP velocities, starting and finishing at the coastal end of transect 13 (Figure 7.26**b**), show a clockwise rotation during this time span. For this latitude (36.5°N) the inertial motion would have a period of $\frac{2\pi}{f} \approx 20.2$ hours. The period of the flow variations observed in the ADCP data coincide

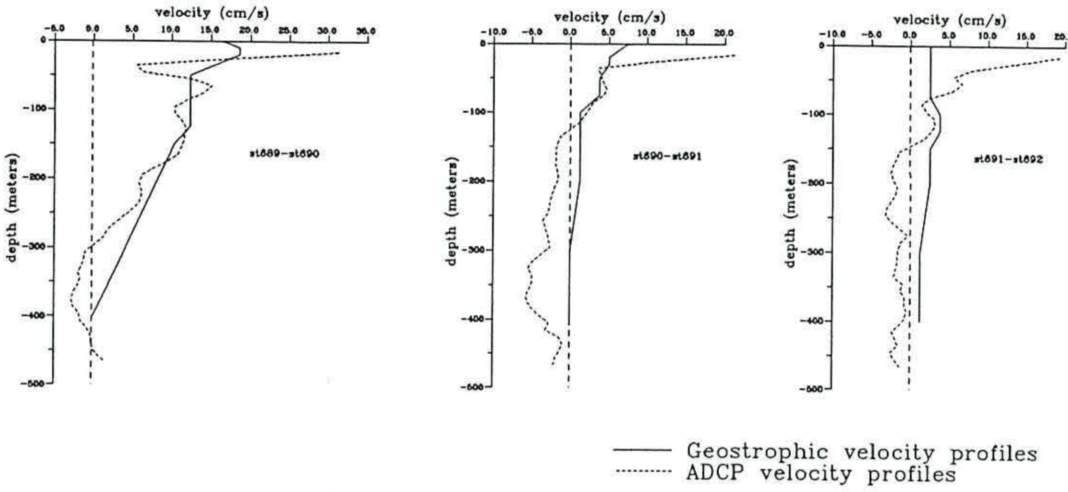

Figure 7.25: Comparative plots between the profiles of geostrophic velocities relative to 500 dbar computed from consecutive CTD stations (solid lines) and the measured ADCP profiles of zonal velocities (dashed lines) along transect 13.

with the inertial period for this latitude. The pseudo-trajectory represented through a progressive vector diagram in Figure 7.26**c** shows clearly the anticyclonic rotation, superimposed on a drift of to the southeast. The dashed line represents a least square fit of an inertial oscillation with a period of 20.2 hours. The hodograph, represented in Figure 7.26**d** along with the fitted inertial circle (dashed line), shows a complete revolution although higher frequency oscillations were also evident. For the observed velocity of about 0.15 m/s the inertial radius is about 1700 meters, which agrees with the simulated trajectory (Figure 7.26**c**).

## 7.5 Discussion

### 7.5.1 Sea surface temperature and ADCP velocities

The Poseidon 201/9 cruise took place a few days after the cessation of an upwelling event off the western coast of Portugal and around Cape São Vicente, as was observed in Figure 7.7. At that time cold upwelled water surrounded the southwestern coasts of Portugal and an equatorward near surface current off the western coast turning eastward around the Cape should be established through the geostrophic adjustment mech-

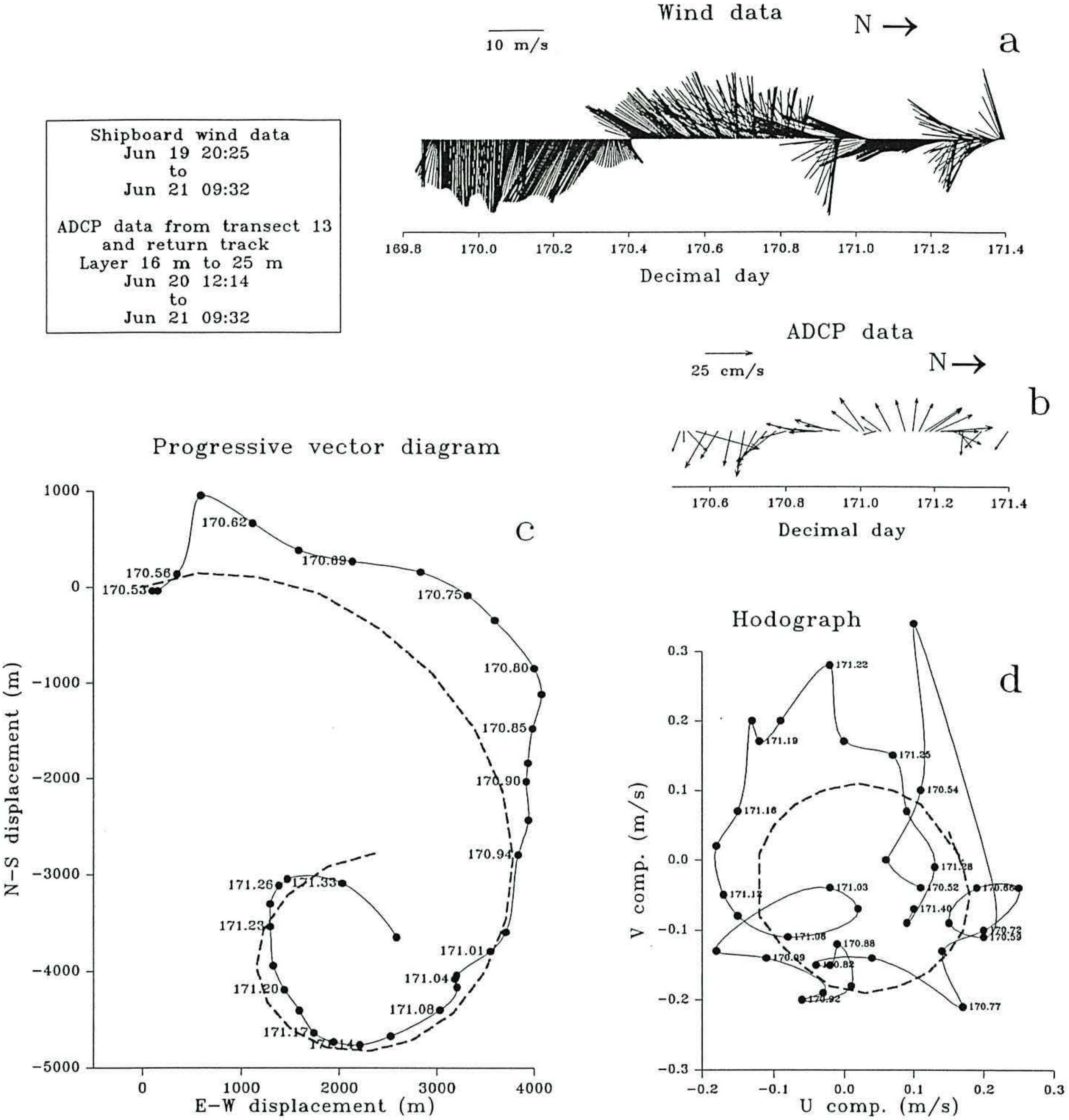

Figure 7.26: Vector plots of the pseudo-time series (**a**) of the shipboard wind measurements and (**b**) of the ADCP velocities for the 16 to 25 m layer, related with the inertial motion event. (**c**) represents the simulated trajectory of a control particle trough a progressive vector diagram and (**d**) the correspondent hodograph. Dashed lines represent the least square fit of an inertial oscillation for 36.5°N and the labels represent the decimal days

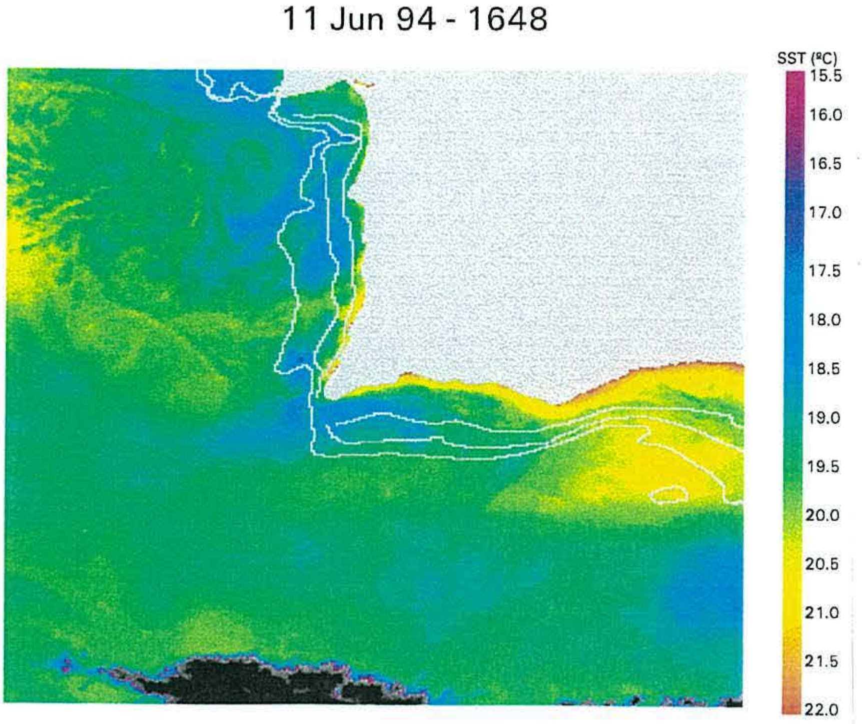

Figure 7.27: AVHRR satellite sea surface temperature image for 11 June 1994, showing the absence of upwelling in Cape São Vicente region at the start of the survey.

anism. However, by the start of the cruise no upwelling was evident in the AVHRR satellite images (Figure 7.27). In a typical non-upwelling situation a westward flow along the southern coast, turning poleward around the Cape São Vicente, should prevail in the region, forced by the alongshore pressure gradient, as discussed previously in Chapter IV and V. The situation that was observed during the Poseidon cruise corresponded to this post upwelling pattern, with typical warm coastal counterflow and colder water over the Algarve continental slope.

Such a situation can be observed in the sea surface temperature field revealed by the AVHRR image of 16 June 1994 (Figure 7.28), where the ADCP near surface current vectors (15-26 meters) were overlaid. There, the warmer water around the Cape is seen to be coincident with the stronger northward surface velocities, while cooler water is seen to lay offshore, where the flow is predominantly to the south. An enlarged view of the satellite image, with the near surface current vectors of the detailed sampling grid off the western coast superimposed is displayed in Figure 7.29. The warmer water that

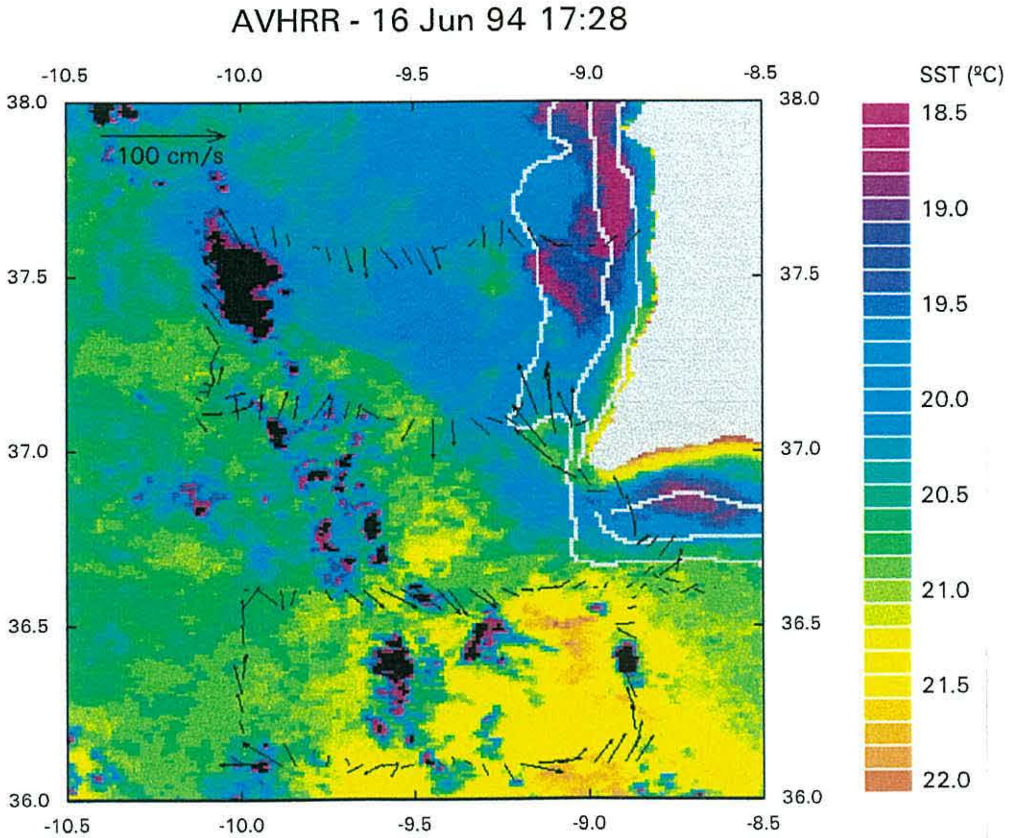

Figure 7.28: AVHRR satellite sea surface temperature image of 16 June 1994 with the near surface (16-25 meters) ADCP current vectors for transect 1 to 5 superimposed. The velocity scale is shown in the panel. The 100, 200 and 500 meters bathymetric contours are represented. Dark patches represent clouds.

turns around the Cape encounters a patch of cold water, presumably originated during the upwelling event prior to the cruise time, curling anticyclonicaly against the coast and progressing nearshore to the north. Also some of the warmer water preceding from the southern coast seems to go round the cold patch by the offshore side.

The larger scale features revealed in the AVHRR image of the sea surface temperature of 16 June 1994 are in close agreement with those observed in the sea surface temperature field sampled during the survey (Figure7.8). However, while the sea surface temperature contours were objectively mapped over a limited region based on discrete observations, the AVHRR image gives an almost continuous representation of the surface temperature, limited only by the pixel size (about 1.1 × 1.1 km). Thus, features such as the warm water turning around the Cape and the patch of cold water

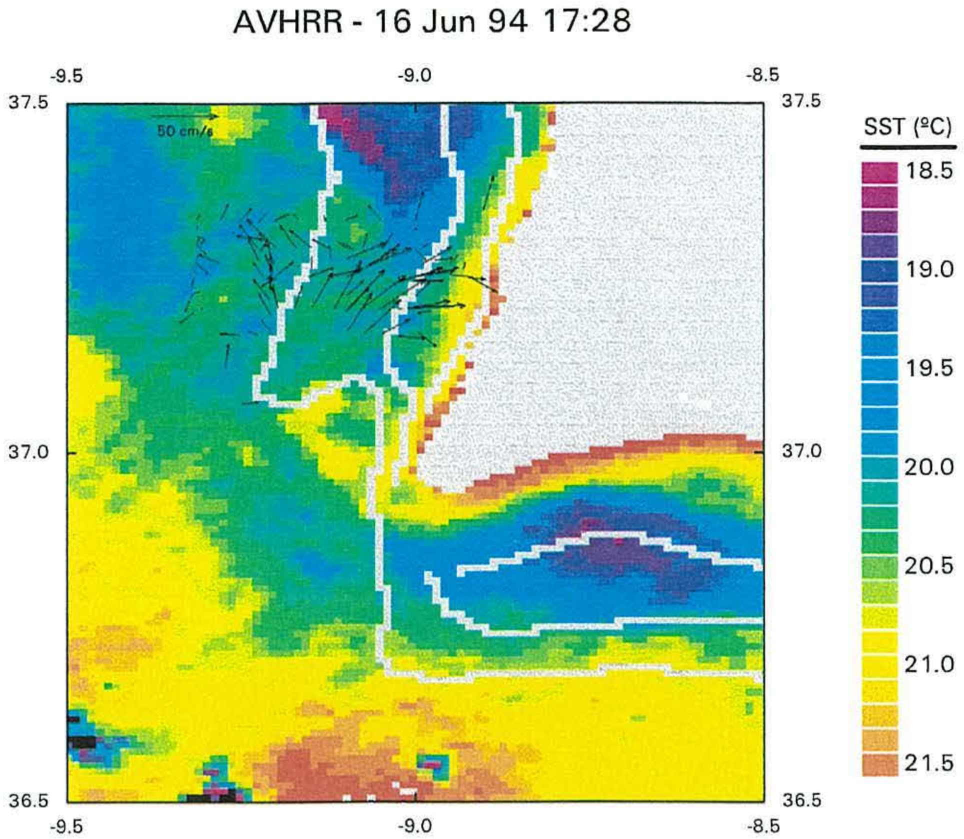

Figure 7.29: Enlarged view showing the Cape São Vicente region of the previous AVHRR image (16 June 1994) with the near surface (16-25 meters) ADCP current vectors for transect 6 to 8 superimposed. The velocity scale is shown in the panel. The 100, 200 and 500 meters bathymetric contours are represented.

off the western coast, evident in the satellite image, were not completely resolved by the sampling grid. Also note that the images are truly synoptic, while the surveys are only quasi-synoptic. Thus, some discrepancies are expected due to the transient characteristics of the surface thermal features and flow field. The choice of the image of 16 June to overlay the ADCP data, which is relatively biased with the time interval of sampling between transect 1 and 5, was dictated by the cloud cover that contaminated the earlier images.

An enlarged view of the AVHRR infrared image of 18 June 1994 is shown in Figure 7.30, covering the nearshore region off the southern coast where a fine sampling grid was carried out between 17 June 14:00 and 18 June 17:00. The near surface (16-25 meters) ADCP current vectors were superimposed to the image showing the cold water

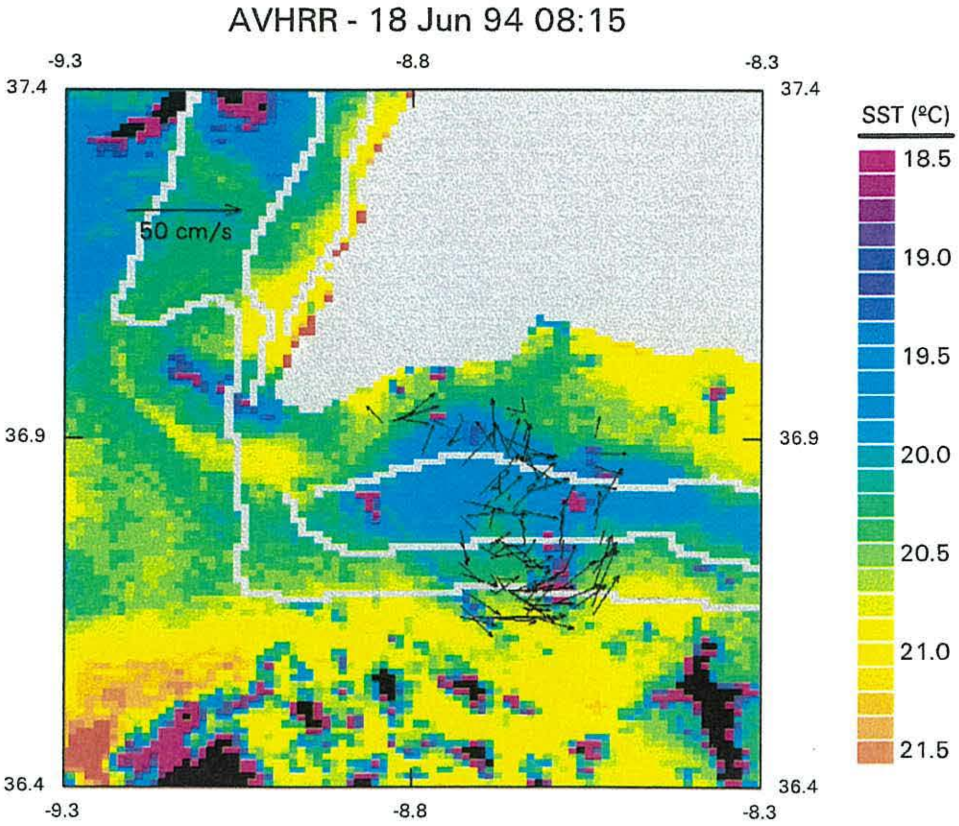

Figure 7.30: Enlarged view of the AVHRR satellite image of 18 June 1994 showing the sea surface temperature pattern observed in the nearshore region off the southern coast, close to the Cape São Vicente, with the near surface (16-25 meters) ADCP current vectors for transect 9 to 11 superimposed. The velocity scale is shown in the panel. The 100, 200 and 500 meters bathymetric contours are represented. Dark patches represent clouds.

intrusion proceeding from the western coast, and possibly merged with cold water upwelled locally before the cruise, curling cyclonically on its offshore limb. This cyclonic tendency seems to coincide with a wave-like perturbation in the offshore front with warmer oceanic waters. A similar cyclonic pattern had been observed in the region during the initial stages of the cruise (see Figure 7.28). Nearshore, the warm water, with a thermal contrast of more than 1.5°C, is seen to progress westward along the southern coast, turning anticyclonicaly around Cape São Vicente and almost breaking the connection between the colder waters off the southern and western coasts. A complex and undefined flow pattern is observed in the region of horizontal shear between the two currents.

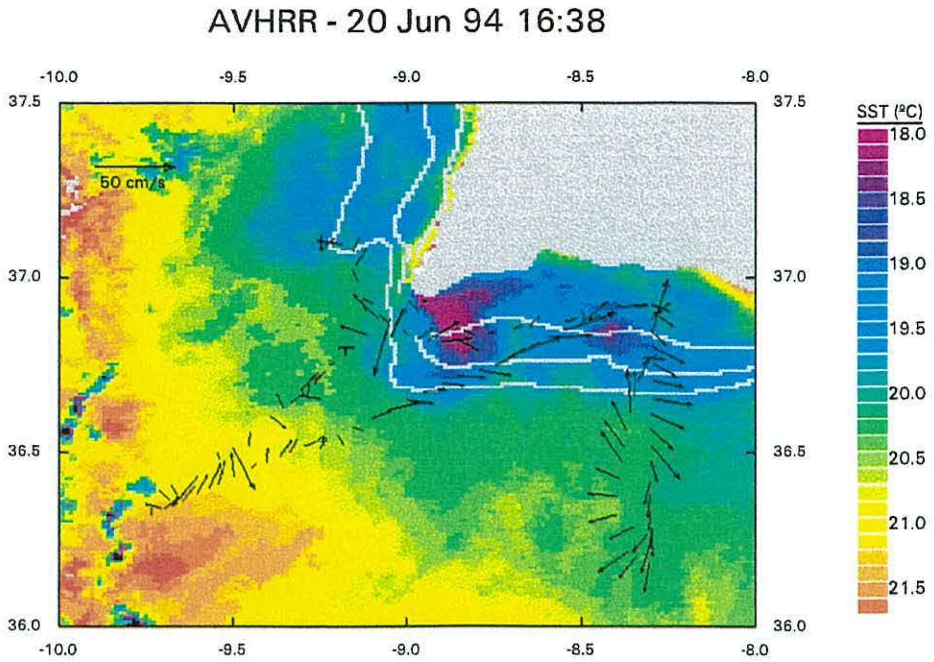

Figure 7.31: AVHRR satellite sea surface temperature image of 20 June 1994 with the near surface (16-25 meters) ADCP current vectors for the last part of the survey superimposed. The velocity scale is shown in the panel. The 100, 200 and 500 meters bathymetric contours are represented. Dark patches represent clouds.

Later, forced by a pulse of favourable winds, an upwelling event started off the southern coast, as was evident in the AVHRR image of 20 June 1994 (Figure 7.31). Over the continental shelf and slope the cold upwelled water was now flowing eastward, due to geostrophic adjustment, as is seen in the near surface (16-25 meters) ADCP current vectors measured between 19 June 09:30 and 21 June 19:00 and superimposed on the satellite image. After the cruise, upwelling continued off the western and southern coasts in the Cape São Vicente region (Figure 7.32**a**). By 1 July warm water was progressing again along the southern coast of Algarve and, associated with the upwelling off the western coast, a cold filament structure was growing in the region (Figure 7.32**b**), which had been, in fact, the main initial objective of this study.

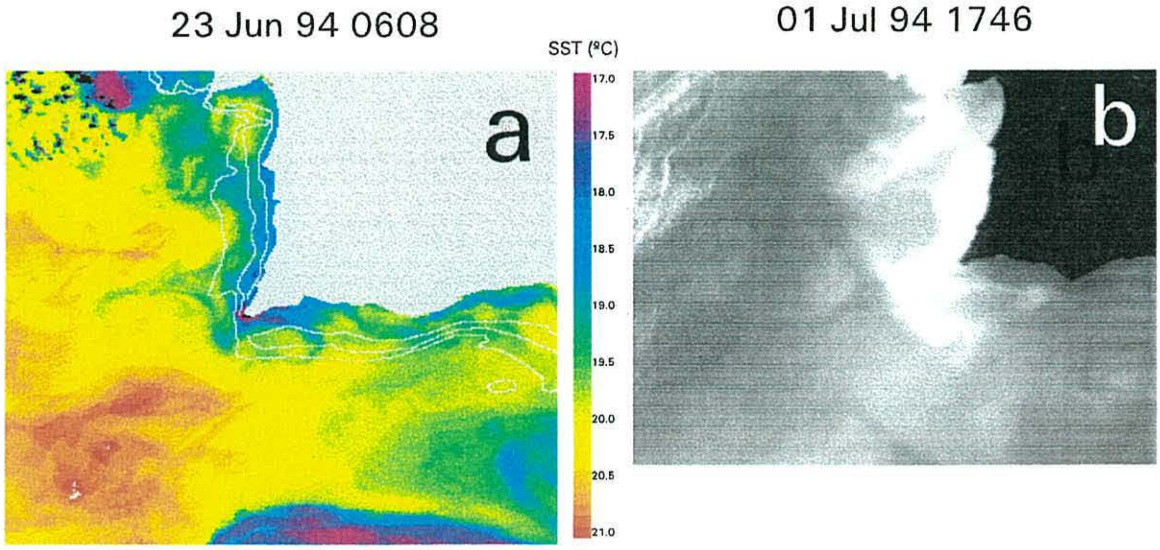

Figure 7.32: **(a)** Processed AVHRR satellite image of 23 June 1994 and **(b)** raw AVHRR satellite image of 1 of July 1994, scanned from monochrome print, showing the evolution of the sea surface temperature pattern after the cruise finish in the Cape São Vicente region.

### 7.5.2 Spiciness

The cold feature off the western coast that turns to the east around Cape São Vicente, along the continental shelf break and slope, evident in AVHRR image (Figure 7.28) and in sea surface CTD temperature field is compensated in the density field by the strong related salinity front (Figure 7.8). It is useful to combine the two observed state variables, temperature and salinity, to compute another state function, the 'spiciness' ($\pi$), conceived to be most sensitive to isopycnal thermohaline variations and least correlated with the density field. Spiciness is a measure of thermohaline properties defined to be higher for warmer and saltier water, and it is a tracer conserved by isentropic motions. Spiciness was computed using the algorithm provided by *Flament* [1986]:

$$\pi(\theta, s) = \sum_{i=0}^{5} \sum_{j=0}^{4} b_{ij} \theta^i (s - 35)^j \tag{7.1}$$

where $\theta$ is the potential temperature and $s$ the salinity. The coefficients $b_{ij}$ are found by requiring that the weighted mean square error on the conditions imposing a generalized orthogonality between the iso-$\pi$ lines and the density on the entire $\theta - s$ domain of existing open ocean water to be minimum. Spiciness has the same physical dimensions as $\rho$. Spiciness has demonstrated to be a useful state variable to study water mass distributions in the California Current region [*Simpson and Lynn*, 1990; *Huyer et al.*, 1991; *Barth et al.*, 1997].

The near surface (5 meters depth) field of spiciness, calculated from the CTD data and objectively mapped, is represented in Figure 7.33, showing that the cool anomaly mentioned above is identifiable as a distinct water body proceeding from the western coast and leaving different waters either offshore and inshore, off the southern coast. The ADCP velocity vectors for the near surface layer (16-25 meters), superimposed on the spiciness field in Figure 7.33, show that the southward flow turning around the Cape, occurs on the outer limit of the low spiciness water body. The bulk of the low spiciness feature around the Cape seems to have some northward flow, but in the regions where the flow field is better resolved by the ADCP data it is possible to identify small scale eddies rotating cyclonicaly. It seems also reasonable to hypothesize an anticyclonic rotating feature in the offshore limb of the low spiciness feature by analysing the current vectors along the 37.1°N ADCP data line (transect 4) and a cyclonic rotating feature in the inshore side of the southward flow in the centre of the low spiciness water by analysing the current vectors along the 37.6°N ADCP data line (transect 5).

The analysis of the vertical distribution of the spiciness in transect 4 and 5, displayed in Figure 7.34 along with the meridional velocity field in the background, reveal the subsurface structure and kinematics of the region. The vertical distribution of the spiciness in transect 5 (Figure 7.34, **top**) shows a central region of relatively homogeneous water, with an anomalously low vertical gradient of spiciness, extending to more

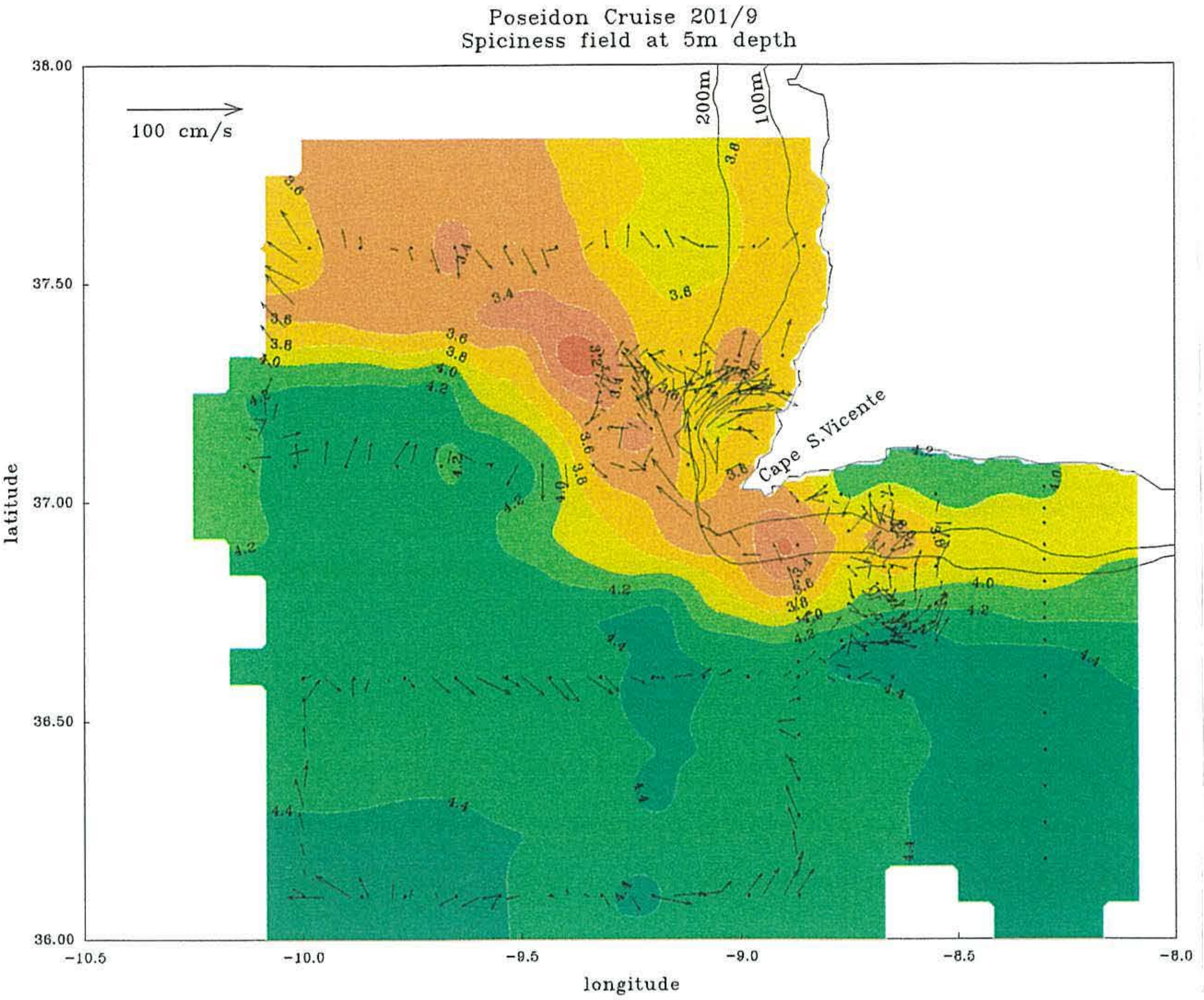

Figure 7.33: Horizontal field of spiciness ($\pi$) at 5 meters depth during the Poseidon 201/9 survey, objectively mapped from individual values computed from the CTD sampling. The mean near surface (16 to 25 meters) ADCP current vectors measured between transect 1 and 11 are superimposed to the map. The velocity scale is shown in the panel. The 100, 200 meters bathymetric contours are represented.

than 350 meters depth. The main part of this feature flows southward, with velocities up to 30 cm/s, while a portion in the eastern side flows northward, suggesting a counter-clockwise rotation of the feature in its eastern boundary. Assuming spiciness as a conservative tracer at subsurface levels, this feature is identified further south, in transect 4 (Figure 7.34, **bottom**), hugging the continental slope and maintaining the counter-clockwise rotation, but with slower southward velocity. To the west, the strong positive tilt of the iso-$\pi$ lines (as well as isotherms and isopycnals, Figure 7.10) agrees with the main southward flow which, in the subsurface layers, extends westward relative to the surface horizontal gradient of spiciness.

The discussion of the thermal infrared AVHRR imagery and of spiciness, along with the observed ADCP velocity data revealed interleaving waters with opposed flows in the Cape São Vicente region during most of the survey. The southward jet-like flow of cold low spiciness water is possibly a remnant of the regime that occurred prior to the cruise start, when an upwelling event with the associated southward regime took place along the coast. At the time of the cruise, after the cessation of upwelling favourable winds, this feature was losing southward momentum through the interaction with the coastal warm counterflow, turning counterclockwise around the Cape to conserve potential vorticity. It can be hypothesized that a more energetic and persistent equatorward flow would have crossed the isobaths originating a cold filament feature straight to the south of the Cape São Vicente, as analysed in Chapter V. The coastal counterflow is forced by the alongshore pressure gradient along the southern coast of the Algarve, as described in Chapter IV. The interaction with this counterflow results in small scale instabilities, whose kinetic energy of rotation must be provided by the main flow through horizontal shear. Kinetic energy is removed from the main flow and transferred to energy of the perturbations, implying the decay of the flow as it proceed to the south and turns around the Cape. Moreover, the forcing factor for the southward flow, that means upwelling favourable winds, ceased while the forcing factor for the alongshore counterflow, that means the alongshore pressure gradient, is persistent during this time of the year.

### 7.5.3 The coastal countercurrent

Evidence from the present data show a narrow coastal countercurrent of warmer waters turning northward around the Cape São Vicente with velocities up to 40 cm/s. Inshore poleward countercurrents seems to be a persistent feature during the upwelling season,

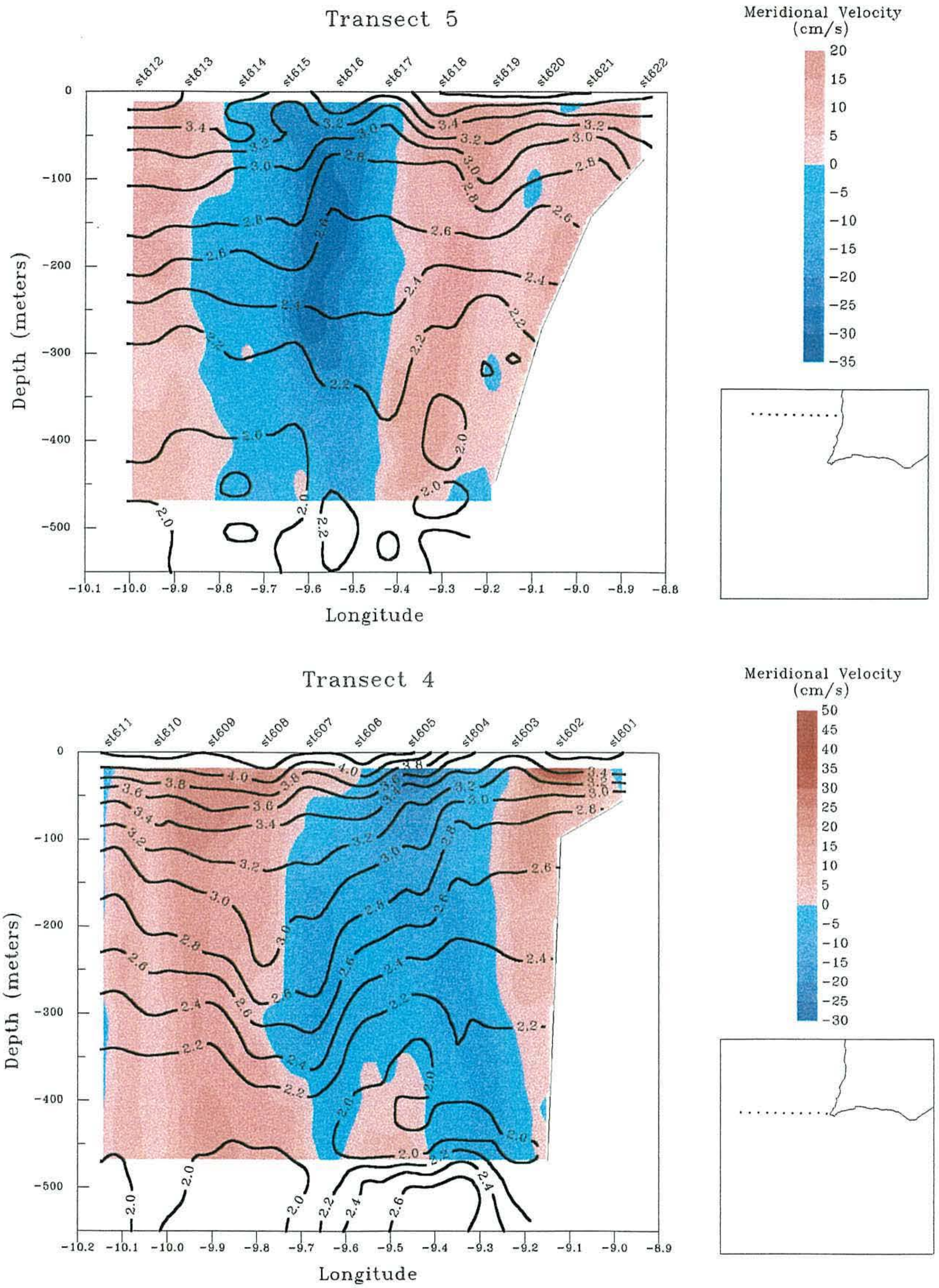

Figure 7.34: Vertical fields of spiciness along transect 5 (**top**) and transect 4 (**bottom**). In the background the vertical fields of the meridional velocity are displayed. Labels indicate the CTD stations. The location of the transects are represented.

at least off central California, as reported by *Chelton et al.* [1988] from observations between Point Sur and Point Conception in two distinct years. For instance, a narrow (<15 km wide) coastal poleward countercurrent was observed off California, near Point Arena, during the local upwelling season [*Huyer and Kosro*, 1987]. Such near surface poleward flow was observed only when strong upwelling favourable winds were absent. This apparent relation between the nearshore counterflow and the wind was also suggested by *Winant et al.* [1987] who, based on data from a moored array off California, showed that currents over the inner shelf are poleward in the absence of wind stress and equatorward when the wind stress is favourable for upwelling. However, the continuity along the coast and the forcing factors associated with this poleward counterflow remain to be investigated. Episodic appearances of poleward coastal near surface countercurrents during the upwelling season, strong at times [e.g., *Kosro et al.*, 1991], were observed during the Coastal Transition Zone program, off northern California. However, those countercurrents were always associated with the kinematics and dynamics of observed mesoscale features, rather than constitute any continuous pattern along the coast.

Assuming an upwelling favourable wind with a large positive curl at one end, *Wang* [1997] shows, through a three-dimensional model simulation, that a strong poleward alongshore pressure gradient is set up by the positive wind curl, driving an inshore poleward current into the upwelling region during active wind forcing, and causing a surge of warm water into the upwelling zone during wind relaxation. The author argues that a positive wind curl induces a cyclonic eddy, which is poleward at the coast. This warm poleward current opposes the cold wind driven equatorward current, and a sharp alongshore temperature front is formed in the confluence zone. The steep density difference across the front creates a poleward pressure gradient, which acts as a remote forcing in the upcoast region. This formulation is able to explain the main circulation features without invoking a particular coastline, although such a wind pattern is commonly found in the vicinity of capes where the synoptic scale wind is disturbed by coastal mountain ranges.

Moreover, *Oey* [1996] suggested that cyclonic eddies can be induced by flows passing around a sharply bent coastline. This implies that a bent coastline, like the Cape São Vicente, may enhance the associated alongshore pressure gradient. This mechanism does not need to impose a pre-existent alongshore pressure force to explain the inshore countercurrent, and is a serious candidate to partially contribute for the observed nearshore counterflow, since all the forcing factors involved may be present at times in the Cape São Vicente region. However, in this hypothesis the pressure gradients are formed locally and the coastal warm countercurrent seems to be a localized feature. The coastal warm countercurrent is seen to extend along all the southern coast of Portugal, progressing from the Gulf of Cádiz and turning northward around the Cape São Vicente, as analysed in Chapter V. Probably, it was the evidence of this larger scale feature that was observed in the limited region covered by the Poseidon 201/9 survey. The effect of a positive wind curl associated with the sharp protrusion of the Cape São Vicente, may cooperate and enhance the observed inshore countercurrent in the region, but does not appear to be its primary driving factor. Moreover, the weak wind observed during the initial stages of the present survey does not support this mechanism as the main forcing.

On the other hand, *Chen* [1989] [*in Wang*, 1997] based on a two-dimensional model and also considering the wind curl, found that the inclusion of a constant large scale alongshore pressure force was necessary to drive the observed coastal warm intrusion. The same author, cited by *Wang* [1997], applied a three-dimensional model to simulate relaxation from upwelling caused by small scale winds. He considered that the coastal ocean is initially forced by an uniform wind which is relaxed sequentially, starting from the south. As the wind subsides, a pool of surface warm waters forms in the south, which eventually intrudes northward into the upwelling zone. However, it was necessary to include a mean poleward alongshore pressure to compel the results to match observations. Evidence of an alongshore pressure gradient in southwestern Iberia during most of the year, emphasized during the summer months, was presented in Chapter IV, and it seems to be the major driving factor for the observed inshore warm countercurrent.

## 7.6 Conclusions

A water mass analysis of the collected CTD data has indicated that, as expected, the major water mass present in the region in the subsurface layers conforms to the definition of ENAW. The subtropical and subpolar modes were identified with a large preponderance of $\mathrm{ENAW}_T$ over the deeper $\mathrm{ENAW}_P$. Beneath this central waters and over limited regions, the presence of Mediterranean water was evident.

The mesoscale structure and kinematics observed in the coastal transition region off Cape São Vicente during the Poseidon 201/9 survey reflects the interaction of the two regimes that dominate the dynamics of the region:

i) Upwelling forced by favourable winds with the associated alongshore flow in the upper layers, southward off the western coast and eastward along the southern coast.

ii) A coastal counterflow, westward along the southern coast and northward along the western coast, forced by the alongshore pressure gradient.

At the time of the cruise signals of both regimes were evident.

The survey took place just after the cessation of an upwelling episode, as was observed in the infrared satellite imagery. During the cruise winds were weak and no upwelling was present. No signal of the Cape São Vicente cold filament was recognized in the data. The observed hydrographic structure revealed a 'tongue' like feature of cold water offshore off the western coast turning eastward around the Cape São Vicente over the continental shelf break and slope, whose offshore boundary was coincident with a strong salinity front and compensated in terms of the surface density field. Analysis of the dynamic height field, ADCP data, satellite sea surface temperature imagery and spiciness, revealed that this feature was advecting cold low spiciness waters around the Cape from regions further north. This feature is interpreted as a remnant of the upwelling regime that occurred prior to the cruise start.

Inshore, a narrow band of warmer water developed along the southern coast as a coastal countercurrent, as observed in the satellite imagery and ADCP data, curling anticyclonicaly around the Cape São Vicente, with velocities up to 40 cm/s, and progressing nearshore to the north. This coastal counterflow is also identifiable in the dynamic height field. This feature was driven by the alongshore pressure gradient characteristic of the region in this time of the year. When a positive wind curl occurs in the region, it may help to force the coastal warm intrusion around the Cape.

The interaction between these two flows generates instabilities of smaller scale in the shear region, removing energy from the main flows and weakening the cold southward flow around the Cape, whose wind forcing had ceased prior to the cruise start.

In the last part of the cruise a pulse of westerly blowing winds induced an upwelling event off the southern coast, and the associated eastward current was able to balance the coastal counterflow, reversing the regime over the shelf against the alongshore pressure gradient. Superimposed on this picture, transient phenomena forced by time varying wind patterns affected the near surface structure. The observed inertial oscillation is a good example.

# Chapter 8

# Conclusion

## 8.1 Dynamics of the Cape São Vicente upwelling region

It is apparent from the analysis of the historical hydrographic data and sea surface temperature satellite images, that the coastal ocean off the southwestern tip of the Iberian Peninsula is characterized by a marked seasonality. During the summer season the region is dominated by an upwelling regime, and the associated kinematics dominates the circulation pattern of the upper ocean. Surface patterns associated with the upwelling regime are observed to weaken towards the east, along the southern coast of Portugal. The winter regime is characterized by relatively uniform surface fields, off both the western and southern coasts.

Results presented in this thesis strongly suggest that the upper ocean around Cape São Vicente is a region where the interaction of two different regimes takes place during the summer season: a cold southward flow off the western coast, that at time turns eastward around the Cape, and a westward coastal warm flow along the southern coast of Portugal, that at times turns northward along the western coast after reaching the Cape São Vicente.

The dynamics of the southward flow off the western coast is driven by the northerly wind stress, predominant during summertime, that in accordance to the Ekman transport theory force near-surface offshore transport, inducing the coastal upwelling of cold denser subsurface waters and the associated southward current jet, through geostrophic adjustment. Reaching Cape São Vicente, at least part of this water turns cyclonically due to conservation of potential vorticity, and flows eastward off the southern coast. Upwelling, and the related physical processes, occur at times off the southern coast, when westerly upwelling favourable winds blow locally. In that situation, waters originating from the western coast merge with cold waters upwelled locally off the southern coast, and flow eastward along the coast.

The warm westward coastal flow off the southern coast is driven by an alongshore pressure gradient, which occurs also off the western coast, near Cape São Vicente, forcing a northward coastal flow there. However, it is more intense along the southern coast than along the western coast. The wind stress is able to balance and reverse this flow, at least in the upper layers. However, due to the weaker alongshore pressure gradient and stronger and steadier upwelling favourable winds, conditions necessary to reverse the near surface flow are more easily reached off the western coast than off the southern coast, where the alongshore pressure gradient is stronger and the upwelling favourable winds weaker and less frequent. This makes the occurrence of the coastal warm counterflow much more frequent off the southern coast.

Analysis of sea surface temperature satellite images show that the two coastal flow patterns in the Cape São Vicente region alternate during the summer season, depending on the wind pattern. In the absence of wind, the coastal flow is "poleward", defined as westward along the southern coast and northward along the eastern coast. The extent of the progression of this warm coastal countercurrent along the southern and western coast is dictated by the the strength of the upwelling favourable wind stress. The setup of a "poleward" coastal flow is rather quick after the relaxation of an upwelling event, when the flow is "equatorward", defined as southward along the western coast and eastward along the southern coast.

The origin of the alongshore pressure gradient is not precisely determined. In regions where the shelf is narrow, deep ocean currents may affect the alongshore elevation slope [*Hickey and Pola*, 1983]. A core of the Mediterranean outflow with an equilibrium depth between 400 and 700 meters, propagates close to the Iberian Peninsula and follows westward along the southern continental slope of Portugal, turning northward around Cape São Vicente [*Ambar*, 1983; *Ochoa and Bray*, 1991]. It cannot be excluded that this Mediterranean vein plays some role in the observed sea surface slope along the southern coast of Portugal. A more probable mechanism for the observed slope is the excess of water entering the Mediterranean Sea through the Strait of Gibraltar, due to the general eastward drift entering the Gulf of Cádiz, that accumulates against the eastern coasts near the Strait and recirculates cyclonically along the coast of the gulf of Cadiz and southern Portugal. The inclusion of this alongshore pressure gradient as part of a larger scale feature can also be hypothesized.

The coastal transition zone off Cape São Vicente is the region where the southward current jet of cold water upwelled off the western coast is freed from the constraint of a coast and where it interacts with the warmer coastal counterflow. Analysis of long series of satellite thermal infrared images revealed the existence of three preferred directions for the spreading of the cold water advected equatorward along the western coast. The first and most persistent throughout the summer season is eastward along the southern shelf break and slope. This eastward cold flow possibly merges with waters previously upwelled locally, which becomes separated from shore by the coastal progession of the warmer counterflow. The second preferred direction of spreading occurs less frequently and results in the southward development of a cold filament feature. It is fed by cold waters upwelled further north and represents the southernmost extent of the intense coastal upwelling jet which overshoots Cape São Vicente. The jet itself represents the primary source of energy for the filament, which develops only when the kinetic energy in enough to break through the offshore waters. The third and least frequent feature to develop is a cold filament that grows westward at the latitude of Cape São Vicente. It appears to result from the meandering of the equatorward jet when it is persistent and intense during the upwelling season. The coastal countercurrent is seen to interact with the equatorward jet at times of relaxation, not only by separating the cold upwelled water from the coast, but also occasionally, when it is energetic enough, breaking westward offshore through the equatorward cold flow and separating the eastward and southward cold features from the upcoast cold waters.

The hydrographic structure and kinematics revealed by the *in situ* measurements carried out in June 1994 support the interpretation of the mesoscale structure and dynamics that was suggested by the measurements taken from land and space. However, the Cape São Vicente cold filament was not observed in the *in situ* data, as the observations were carried out in a non-upwelling situation, just after a short-lived upwelling event. A patch of cold water was observed offshore off the western coast curling eastwards around Cape São Vicente, and extending along the continental shelf break and slope off the southern coast. This feature represented advection of cold waters around the Cape from regions further north, and is likely to be a residual of the equatorward regime associated with the upwelling event that occurred before the period of *in situ* observations. Inshore, a warm coastal countercurrent was observed to curl anticyclonicaly around the Cape with velocities up to 40 cm/s, and stretch northward close to shore. It is identified as the narrow warm coastal counterflow observed in the satellite imagery archive and driven by the alongshore pressure gradient. The boundary between the two opposing flows was populated by small scale instabilities that subtract kinetic energy from the mean flows, weakening the southward flow arround the Cape.

## 8.2 Further work

The completion of this work does not exhaust the subjects related with the oceanography of the southwestern Iberia. On the contrary, it leaves some questions to be addressed, reveals some new points to be investigated and has kindled interest for further research in the frame of larger scales of time and space.

An obvious task to be completed in the future is the detailed definition of the three-dimensional structure and dynamics of the Cape São Vicente cold filament and the investigation of the relationship between its development and the surrounding current field, which could not be carried out because the filament was not present at the time of the *in situ* sampling. Such investigation will allow the comparative anatomy of this filament with other filament formations observed in different coastal transition zones with different physical constraints, contributing to a more general undestanding of filament related processes. The evaluation of the importance of the cross-shelf transport associated with the offshore flow in the filament and its contribution to nearshore-open ocean exchange processes will be an objective too. Also the relation of the Cape São Vicente filament with the equatorward surface current jet associated with the upwelling off the western coast of Portugal will be an issue for future research.

The characterization of the seasonal variability of the flow regime off the western and southern coast of Iberia would provide additional information of the processes involved in the dynamics of the mesoscale circulation of the region, and possibly would have implications in the understanding of the larger scale circulation along the eastern boundary of the North Atlantic.

The observed warm coastal counterflow is still poorly defined and its time scale, seasonal variability and spatial development need further investigation. Results presented in this work suggest that this flow is driven by an alongshore pressure gradient, whose origin and continuity into the Gulf of Cádiz and northwestern Africa, or to the north along the western Iberian coast, needs further investigation in order to evaluate whether it is a localized feature regionally driven or a manifestation of a larger scale pattern, countinuous along the eastern boundary region of the North Atlantic. Coastal trapped waves offer a mechanism for transferring momentum and other properties along coastal boundaries. These occur together with alongshore pressure gradients, but the later are possible without associated trapped waves. The role of coastal trapped waves in the observed alongshore circulation in this region needs thorough investigation. Also the apparent independence of the coastal countercurrent from the summer poleward undercurrent along the eastern boundary region off western Iberia needs further confirmation, since this idea was based only in the results of a single cruise.

Long term observations of the flow regime (over one year), either off the western and southern coasts, along with time series of sea level, wind data and coastal sea surface temperature, would answer most of the questions addressed above. Also, analysis on a comparative basis would have implications for the regional oceanography, establishing the differences between the upwelling regimes off the western and southern coasts and providing important information about the relative importance of the forcing factors acting in the region.

# References

Allen, J. S., Models of wind-driven currents on the continental shelf, *Ann. Rev. Fluid Mech.,* 12, 389-433, 1980.

Allen, J. S., L. J. Walstad, and P. A. Newberger, Dynamics of the coastal transition zone jet, 2. Nonlinear finite amplitude behavior, *J. Geophys. Res.,* 96(C8), 14,995-15,016, 1991.

Ambar, I., A shallow core of Mediterranean water off western Portugal, *Deep Sea Res.,* 30(6A), 677-680, 1983.

Ambar, I., and M. R. Howe, Observations of the Mediterranean outflow — 1. Mixing in the Mediterranean outflow, *Deep Sea Res.,* 26, 535-554, 1979.

Barth, J. A. and K. H. Brink, Shipboard acoustic doppler profiler velocity observations near Point Conception: Spring 1983, *J. Geophys. Res.,* 92(C4), 3925-3943, 1987.

Barton, E. D., The poleward undercurrent on the eastern boundary of the subtropical North Atlantic, in *Poleward Flows Along Eastern Ocean Boundaries*, edited by S. J. Neshyba, C. N. K. Mooers, R. L. Smith, and R. T. Barber, pp. 85-95, Springer-Verlag, New York, 1989.

Barton, E. D., Development of a dipole filament in the Iberian upwelling region, *EOS Transactions, A.G.U.*, 72(44), 274, 1991.

Barton, E. D., A. Huyer, and R. L. Smith, Temporal variation observed in the hydrographic regime near Cabo Corveiro in the northwest African upwelling region, February to April 1974, *Deep Sea Res.,* 24, 7-23, 1977.

Batteen, M. L., R. L. Haney, T. A. Tielking, and P. G. Renaud, A numerical study of wind forcing of eddies and jets in the California Current system, *J. Mar. Res.,* 47, 493-523, 1989.

Batteen, M. L., Costa, C. L., and C. S. Nelson, A numerical study of wind stress curl effects on eddies and filaments off the northwest coast of Iberian Peninsula, *J. Mar Syst.*, 3, 249-266, 1992.

Bernstein, R. L., L. Breaker, and R. Whritner, California Current eddy formation: Ship, air, and satellite results, *Science,* 195, 353-359, 1977.

Bray, N. A., and C. L. Greengrove, Circulation over the shelf and slope off Northern California, *J. Geophys. Res.,* 98(C10), 18,119-18,145, 1993.

Breaker, L. C., R. P. Gilliland, A satellite sequence on upwelling along the California coast, in *Coastal Upwelling, Coastal Estuarine Sci.,* vol. 1, edited by F. A. Richards, pp. 87-94, AGU, Washington, D. C., 1981.

Brink, K. H., and T. J. Cowles, The coastal transition zone program, *J. Geophys. Res.,* 96(C8), 14,637-14,647, 1991.

Brink, K. H., J. S. Allen, and R. L. Smith, A study of low-frequency fluctuations near the Peru coast, *J. Phys. Oceanogr.,* 8, 1025-1041, 1978.

Brink, K. H., D. Halpern, and R. L. Smith, Circulation in the Peruvian upwelling system near 15°S, *J. Geophys. Res.,* 85, 4036-4048, 1980.

Brink, K. H., R. C. Beardsley, P. P. Niiler, M. Abbott, A. Huyer, S. Ramp, T. Stanton, and D. Stuart Statistical properties of near-surface flow in the California coastal transition zone, *J. Geophys. Res.,* 96(C8), 14,693-14,706, 1991.

Chelton, D. B., Seasonal variability of alongshore geostrophic velocity off Central California, *J. Geophys. Res.,* 89(C3), 3473-3486, 1984.

Chelton, D. B., and D. B. Enfield, Ocean signals in the tide gauge records, *J. Geophys. Res.,* 91(B9), 9081-9098, 1986.

Chelton, D. B., A. W. Bratkovich, R. L. Bernstein, and P. M. Kosro, Poleward flow off central California during the spring and summer of 1981 and 1984, *J. Geophys. Res.,* 93, 10604-10620, 1988.

Chen, D., Dynamics of time-variable coastal upwelling, Ph.D. thesis, 83 pp, Mar. Sci. Res. Cen., Uni. of N. Y. at Stony Brook, 1989.

Crépon, M., C. Richez, and M. Chartier, Effects of coastline geometry on upwellings, *J. Phys. Oceanogr.,* 14, 1365-1382, 1984.

Dewey, R. K., J. N. Moum, C. A. Paulson, D. R. Caldwell, and S. D. Pierce, Structure and dynamics of a coastal filament, *J. Geophys. Res.,* 96(C8), 14,885-14,907, 1991.

Fanjul, E. A., B. P. Gómez, and I. R. Sánchez-Arévalo, A description of the tides in the Eastern North Atlantic, *Prog. Oceanogr.,* 40, 217-244, 1997.

Fiúza, A. F. G., The Portuguese coastal upwelling system, in *Actual Problems of Oceanography in Portugal.* pp. 45-71, Junta Nacional de Investigação Científica e Tecnológica, Lisbon, 1982.

Fiúza, A. F. G., Upwelling patterns off Portugal, in *Coastal Upwelling: Its Sediment Record,* part A, edited by E. Suess and J. Thiede, pp. 85-98, Plenum, New York, 1983.

Fiúza, A., Hidrologia e dinãmica das águas costeiras de Portugal (Hydrology and dynamics of the Portuguese coastal waters), Ph.D. thesis, 294pp., Univ. de Lisboa, Lisbon, 1984.

Fíuza, A., and D. Halpern, Hydrographic observations of the Canary Current between 21°N and 25.5°N in March/April 1974, Rapport et Proces-verbaux de Reunions, *Conseil International pour l'Exploration de la Mer*, 180, 58-54, 1982.

Fíuza, A. F. G., M. E. Macedo, and M. R. Guerreiro, Climatological space and time variation of the portuguese coastal upwelling, *Oceanol. Acta,* 5, 31-40, 1982.

Flament, P., Finestructure and subduction associated with upwelling filaments, Ph. D. Dissertation, University of California, San Diego, 1986.

Flament, P., L. Armi, and L. Washburn, The evolving structure of an upwelling filament, *J. Geophys. Res.,* 90(C6), 11,765-11,778, 1985.

Fofonoff, N. P., and R. C. Millard, Algorithms for computation of fundamental properties of sea water, *UNESCO Technical Papers in Marine Science,* 44, 53 pp., 1983.

Firing, E. and J. Ranada, Access to the CODAS High-Resolution Shipboard ADCP Data Sets. Manual version 3.1 from the Joint Institute for Marine and Atmospheric Research. School of Ocean and Earth Science and Technology, University of Hawaii, 124 pp, 1995.

Frouin, R., A. F. G. Fiúza, I. Ambar, and T. J. Boyd, Observations of a poleward surface current off the coasts of Portugal and Spain during winter, *J. Geophys. Res.,* 95(C1), 679-691, 1990.

Gill, A. E., Atmosphere-Ocean Dynamics, 662 pp., Academic, San Diego, Calif., 1982.

Haidvogel, D. B., A. Beckmann, and K. S. Hedstrõm, Dynamical simulations of filament formation and evolution in the coastal transiton zone, *J. Geophys. Res.,* 96(C8), 15,017-15,040, 1991.

Hamming, R. V., Digital Filters, Prentice Hall Inc., Englewood Cliffs, New Jersey, 257 pp., 1983.

Harms, S., and C. D. Winant, Characteristic patterns of the circulation in the Santa Barbara Channel, *J. Geophys. Res.,* 103(C2), 3041-3065, 1998.

Harvey, J., $\theta$-S relationship and water masses in the eastern North Atlantic, *Deep Sea Res.,* 29, 1021-1033, 1982.

Haynes, R., Eulerian and lagrangian observations in the Iberian coastal transition zone, Ph.D. thesis, 123 pp., Univ. of Wales, Bangor, 1993.

Haynes, R., and E. D. Barton, A poleward flow along the Atlantic coast of the Iberian Peninsula, *J. Geophys. Res.,* 95(C7), 11,425-11,442, 1990.

Haynes, R., and E. D. Barton, Lagrangian observations in the Iberian coastal transition zone, *J. Geophys. Res.,* 96(C8), 14,731-14,741, 1991.

Haynes, R., E. D. Barton and I. Pilling, Development, persistence, and variability of upwelling filaments off the Atlantic Coast of the Iberian Peninsula, *J. Geophys. Res.,* 98(C12), 22,681-22,692, 1993.

Hickey, B., The relationship between fluctuations in sea level, wind stress and sea surface temperature in the Equatorial Pacific, *J. Phys. Oceanogr.,* 5, 460-475, 1975.

Hickey, B. M., The California Current system — hypotheses and facts, *Prog. Oceanogr.,* 8, 191-279, 1979.

Hickey, B., and N. E. Pola, The seasonal alongshore pressure gradient on the west coast of the United States, *J. Geophys. Res.,* 88(C12), 7623-7633, 1983.

Hinrichsen, H.-H., M. Rein, R. H. Käse, and W. Zenk, The Mediterranean water tongue and its chlorofluoromethane signal in the Iberian basin in early summer 1989, *J. Geophys. Res.,* 98(C5), 8405-8412, 1993.

Hofmann E. E., K. S. Hedström, J. R. Moisan, D. B. Haidvogel, and D. L. Mackas, The use of simulated drifters tracks to investigate general transport patterns and residence times in the coastal transition zone, *J. Geophys. Res.,* 96(C8), 15,041-15,052, 1991.

Huthnance, J. M., Slope currents and JEBAR, *J. Phys. Oceanogr.,* 14, 795-810, 1984.

Huyer, A., Seasonal variation in temperature, salinity, and density over the continental shelf off Oregon, *Limnol. Oceanogr.,* 22(3), 442-453, 1977.

Huyer, A., R. D. Pillsbury, and R. L. Smith, Seasonal variation of the alongshore velocity field over the continental shelf of Oregon, *Limnol. Oceanogr.,* 20(1), 90-95, 1975.

Huyer, A., and P. M. Kosro, Mesoscale surveys over the shelf and slope in the upwelling region near Point Arena, California, *J. Geophys. Res.,* 92(C2), 1655-1681, 1987.

Huyer, A., P. M. Kosro, J. Fleischbein, S. Ramp, T. Stanton, L. Washburn, F. P. Chavez, T. J. Cowles, S. D. Pierce, and R. L. Smith, Currents and water masses of the coastal transition zone off northern California, June to August 1988, *J. Geophys. Res.,* 96(C8), 14,809-14,831, 1991.

Ikeda M., and W. J. Emery, Satellite observations and modeling of meanders in the California Current system off Oregon and northern California, *J. Phys. Oceanogr.,* 14, 1434-1450, 1984.

Ikeda M., L. A. Mysak, and W. J. Emery, Observations and modeling of satellite-sensed meanders and eddies of Vancouver Island, *J. Phys. Oceanogr.,* 14, 3-21, 1984.

Instituto Hidrográfico, Tabelas de Marés 1997, vol I, M.D.N./Marinha, Lisboa, 202pp., 1996.

Johnson, J. A., and I. Stevens, A fine resolution model of the circulation over the Iberian shelf. Proceedings of the Second International Conference on Air-Sea Interations and on Meteorology and Oceanography of the Coastal Zone. American Meteorological Society, Lisbon, pp 154-155, 1994.

Kadko, D. C., L. Washburn, and B. Jones, Evidence of subduction within cold filaments of the northern California coastal transition zone, *J. Geophys. Res.,* 96(C8), 14,909-14,926, 1991.

Käse, R. H., A. Beckmann, and H. H. Hinrichsen, Observational evidence of salt lens formation in the Iberian Basin, *J. Geophys. Res.,* 94(C4), 4905-4912, 1989.

Kelley, K. A., The influence of winds and topography on the sea surface temperature patterns over the northern California slope, *J. Geophys. Res.,* 90(C6), 11,783-11,795, 1985.

Kosro, P. M., and A. Huyer, CTD and velocity surveys of seaward jets off northern California, July 1981 and 1982, *J. Geophys. Res.,* 91(C6), 7680-7690, 1986.

Kosro, P. M., A. Huyer, S. R. Ramp, R. L. Smith, F. P. Chavez, T. J. Cowles, M. R. Abbott, P. T. Strub, R. T. Barber, P. Jessen, and L. F. Small, The structure of the transition zone between coastal waters and the open ocean off northern California, winter and spring 1987, *J. Geophys. Res.,* 96(C8), 14,707-14,730, 1991.

Lentz, S. J., The surface boundary layer in coastal upwelling regions, *J. Phys. Oceanogr.,* 22, 1517-1539, 1992.

Lisitzin, E., Sea Level Changes, *Elsevier Oceanographic Series* 8, 286pp., 1974.

Lisitzin, E., and J. Pattullo, The principal factors influencing the seasonal oscillation of the sea level, *J. Geophys. Res.,* 66(3), 845-852, 1961.

Lynn, R. J., and J. J. Simpson, The California Current system: the seasonal variability of its physical characteristics, *J. Geophys. Res.,* 92(C12), 12,947-12,966, 1987.

Madelain, F., Influence de la topographie du fond sur l'ecoulement méditerranéen entre le detroit de Gibraltar et le cap de S. Vicent, *Cah. Ocean.* (22-1), pp. 43-61, 1970.

McClain, E. P., W. G. Pichel, and C. C. Walton, Comparative perfomance of AVHRR-based multichannel sea surface temperatures, *J. Geophys. Res.,* 90, 11587-11601, 1985.

McCreary, J. P., Y. Fukamachi, and P. K. Kundu, A numerical investigation of jets and eddies near an eastern ocean boundary, *J. Geophys. Res.,* 96(C2), 2515-2534, 1991.

Meincke, J., G. Seidler, and W. Zenk, Some current observations near the continental slope off Portugal, *Meteor Forschungsergebnisse A,* 16, 15-22, 1975.

Miller, P., S. Groom, A. McManus, J. Selly, J. Woolfenden, and L. Osborne, Remote sensing activities in OMEX. Ocean Margins Exchange Project I Final Report, 52 pp., 1996.

Mooers, C. N. K., and A. R. Robinson, Turbulent jets and eddies in the California Current and inferred cross-shore transports, *Science,* 223, 51-53, 1984.

Moran, J.M., and M. D. Morgan, Meteorology: the atmosphere and the science of weather, 517 pp., Macmillan College Publishing Company, New York, 1994.

Moum, J. N., D. R. Caldwell, and P. J. Stabeno, Mixing and intrusions in a rotating cold-core feature off Cape Blanco, Oregon, *J. Phys. Oceanogr.,* 18, 823-833, 1988.

Narimousa, S., and T. Maxworthy, Two-layer model of shear driven coastal upwelling in the presence of bottom topography, *J. Fluid Mech.,* 159, 503-531, 1985.

Narimousa, S., and T. Maxworthy, Effects of a discontinuous surface stress on a model of coastal upwelling, *J. Phys. Oceanogr.,* 16, 2071-2083, 1986.

Narimousa, S., and T. Maxworthy, Coastal upwelling on a sloping bottom. The formation of plumes , jets and pinched-off cyclones, *J. Fluid Mech.,* 176, 169-190, 1987a.

Narimousa, S., and T. Maxworthy, On the effects of coastline perturbations on coastal currents and fronts, *J. Phys. Oceanogr.,* 17, 1296-1303, 1987b.

Narimousa, S., and T. Maxworthy, Application of a laboratory model to the interpretation of satellite and field observations of coastal upwelling, *Dyn. Atmos. Oceans.,* 13, 1-46, 1989.

Navarro-Pérez, E., Physical oceanography of the Canarias Current: short term, seasonal and interannual variability, Ph.D. thesis, School of Ocean Sciences, University of Wales, Bangor, 160 pp, 1996.

Neves, R. J., H. S. Coelho, P. C. Leitão, and A. J. Santos, Numerical modelling of North Atlantic eastern boundary current system, Ocean Margin Exchange (OMEX), Final Report, Université Libre de Bruxelles, pp 517-536, 1996.

Ochoa, J., and N. A. Bray, Water mass exchange in the Gulf of Cadiz, *Deep Sea Res.,* 38(*Suppl. 1*), 5465-5503, 1991.

Oey, L-Y., Flow around a coastal bend: a model of the Santa Barbara Channel eddy, *J. Geophys. Res.,* 101(C7), 16667-16682, 1996.

Onken, R., J. Fisher, and J. D. Woods, Thermohaline finestructure and its relation to frontogenesis dynamics, *J. Phys. Oceanogr.,* 20(9), 1379-1394, 1990.

Paduan, J. D., and Niiler, P. P., A Lagrangean description of motion in northern California coastal transition filaments, *J. Geophys. Res.,* 95(C10), 18,095-18,109, 1990.

Pattullo J., W. Munk, R. Revelle, and E. Strong, The seasonal oscillation in sea level, *J. Mar. Res.,* 14, 88-155, 1955.

Peffley, M. B., and J. J. O'Brien, A three-dimensional simulation of coastal upwelling off Oregon, *J. Phys. Oceanogr.,* 6, 164-180, 1976.

Pérez, F. F., A. F. Ríos, B. A. King, and R. T. Pollard, Decadal changes of the $\theta$-S relationship of the Eastern North Atlantic Central Water, *Deep Sea Res.,* 42, 1849-1864, 1995.

Pollard, R. T., and S. Pu, Structure and circulation of the upper Atlantic ocean northeast of the Azores, *Prog. Oceanogr.,* 14, 443-462, 1985.

Prater, M. D., and T. B. Sanford, Generation of meddies off Cape St. Vincent, Portugal (abstract), *Eos Trans. AGU,* 71, 1416, 1990.

Ramp, S. R., P. F. Jessen, K. H. Brink, P. P. Niiler, F. L. Daggett, and J. S. Best, The physical structure of cold filaments near Point Arena, California, during June 1987, *J. Geophys. Res.,* 96(C8), 14,859-14,883, 1991.

Ramp, S. R., and C. L. Abbott, The vertical structure of currents over the Continental Shelf off Point Sur, CA, during Spring 1990, *Deep Sea Res.,* 45, 1443-1470, 1998.

Reid, J. L., and A. W. Mantyla, The effect of the geostrophic flow upon elevations in the northern North Pacific ocean, *J. Geophys. Res.,* 81(18), 3100-3110, 1976.

Relvas, P. and E.D. Barton, Poseidon Cruise 201/9 Report: Physical Oceanography Data Report, 284pp., University of Algarve, Faro, 1995.

Relvas, P. and E.D. Barton, Poseidon Cruise 201/9 Report: Acoustic Doppler Current Profiler Data – Velocity Fields, 51pp., University of Algarve, Faro, 1996.

Rhein, M., and H.-H. Hinrichsen, Modification of Mediterranean water in the Gulf of Cadiz, studied with hydrographic and chlorofluoromethanes data, *Deep Sea Res.,* 40, 267-291, 1993.

Richardson, P. L., M. S. McCartney, and C. Maillard, A search for meddies in historical data, *Dyn. Atmos. Oceans.,* , 15, 241-265, 1991.

Rienecker M. M., and C. N. K. Mooers, Mesoscale eddies, jets, and fronts off Point Arena, California, July 1986, *J. Geophys. Res.,* 94(C9), 12,555-12,569, 1989.

Rienecker M. M., C. N. K. Mooers, D. E. Hagan, and A. R. Robinson, A cool anomaly off northern California: An investigation using IR imagery and in situ data, *J. Geophys. Res.,* 90(C3), 4807-4818, 1985.

Rienecker M. M., C. N. K. Mooers, and A. R. Robinson, Dynamical interpolation and forecast of the evolution of mesoscale features off northern California, *J. Phys. Oceanogr.,* 17, 1189-1213, 1987.

Ríos A. F., F. F. Pérez, and F. Fraga, Water masses in the upper and middle North Atlantic Ocean east of the Azores, *Deep Sea Res.,* 39, 645-658, 1992.

Robinson, I. S., Satellite Oceanography - An introduction for oceanographers and remote-sensing scientists, 455 pp., Ellis Howood Limited, Chichester, 1985.

Roden, G. I., On atmospheric pressure oscillations along the Pacific coast of North America, 1873-1963, *J. Atmos. Sci.,* 22, 280-295, 1965.

Saunders, P. M., Circulation in the eastern North Atlantic, *J. Mar. Res.,* 40, suppl., 641-657, 1982.

Saur, J. F. T., The variability of monthly mean sea level at six stations in the eastern North Pacific Ocean, *J. Geophys. Res.,* 67, 2781-2790, 1962.

Send, U., R. C. Beardsley, and C. D. Winant, Relaxation from upwelling in the coastal ocean dynamics experiment, *J. Geophys. Res.,* 92(C2), 1683-1698, 1987.

Simpson, J. J., and R. J. Lynn, A mesoscale eddy dipole in the offshore California Current, *J. Geophys. Res.,* 95(C8), 13,009-13,022, 1990.

Smith, R. L., Upwelling, *Oceanogr. Mar. Biol. Ann. Rev.,* 6, 11-46, 1968.

Smith, R. L., The physical processes of coastal ocean upwelling systems, in *Upwelling in the Ocean: Modern Processes and Ancient Records*, edited by C. P. Summerhayes, K.-C. Emeis, M. V. Angel, R. L. Smith, and B. Zeitzschel, John Wiley and Sons Ltd., 1995.

Sousa, F. M.,and A. Bricaud, Satellite-derived phytoplankton pigment structures in the Portuguese upwelling area, *J. Geophys. Res.,* 97, 11,343-11,356, 1992.

Spall, M. A., Frontogenesis, subdution, and cross-front exchange at upper ocean fronts, *J. Geophys. Res.,* 100(C2), 2543-2557, 1995.

Stammer, D., H. H. Hinrichsen, and R. H. Käse, Can meddies be detected by satellite altimetry?, *J. Geophys. Res.,* 96(C4), 7005-7014, 1991.

Stern, M. E., and J. A. Whitehead, Separation of a boundary jet in a rotating fluid, *J. Fluid Mech.,* 217, 41-69, 1990.

Stramma, L., and G. Siedler, Seasonal changes in the North Atlantic subtropical gyre, *J. Geophys. Res.,* 93(C7), 8111-8118, 1988.

Strub, P. T., J. S. Allen, A. Huyer, and R. L. Smith, Seasonal cycles of currents, temperature, winds, and sea level over the northeast Pacific continental shelf: 35°N to 48°N, *J. Geophys. Res.,* 92(C2), 1507-1526, 1987.

Strub, P. T., P. M. Kosro, and A. Huyer, The nature of the cold filaments in the California Current system, *J. Geophys. Res.,* 96(C8), 14,743-14,768, 1991.

Sverdrup, H. U., M. W. Johnson, and R. H. Fleming, The Oceans, 1087 pp., Prentice-Hall, New York, 1942.

Swallow, J. C., A deep sea eddy off Cape St. Vincent, *Deep Sea Res.,* 16, 285-295, 1969.

Swenson, M. S., P. P. Niiler, K. H. Brink, and M. R. Abbott, Drifter observations of a cold filament off Point Arena, California, in July 1988, *J. Geophys. Res.,* 97(C3), 3593-3610, 1992.

Thompson, R. O. R. Y., Observations of the Leeuwin Current off western Australia, *J. Phys. Oceanogr.,* 14, 623-628, 1984.

Traganza, E. D., D. A. Nestor, and A. K. McDonald, Satellite observations of a nutrient upwelling off the coast of California, *J. Geophys. Res.,* 85, 4104-4106, 1980.

UNESCO, Tenth report of the joint panel on oceanographic tables and standards, Sidney, B. C., Canada, 1-5 September 1980, sponsored by UNESCO, SCOR, IAPSO, *UNESCO Technical Papers in Marine Science,* 36, 23 pp., 1981.

UNESCO, JPOTS panel, Processing of Oceanographic Station Data, 138 pp., Paris, 1991.

Van Camp, L., J. Nykjær, E. Mittelstaedt, and P. Schlittenhardt, Upwelling and boundary circulation off northwest Africa as depicted by infrared and visible satellite observations, *Prog. Oceanogr.,* 26, 357-402, 1991.

Voropayev, S. I., Ya. D. Afanasyev, and I. A. Filippov, Horizontal jets and vortex dipoles in a stratified fluid, *J. Fluid Mech.,* 227, 543-566, 1991.

Walstad, L. J., J. S. Allen, P. M. Kosro, and A. Huyer, Dynamics of the coastal transition zone through data assimilation studies, *J. Geophys. Res.,* 96(C8), 14,959-14,977, 1991.

Wang, D-P., Model of frontogenesis – subduction and upwelling, *J. Mar. Res.,* 51, 497-513, 1993a.

Wang, D-P., The strait of Gibraltar model: internal tide, diurnal inequality and fortnightly modulation, *Deep Sea Res.,* 40, 1187-1203, 1993b.

Wang, D-P., Effects of small-scale wind on coastal upwelling with application to Point Conception, *J. Geophys. Res.,* 102(C7), 15555-15566, 1997.

Washburn, L., D. C. Kadko, B. H. Jones, T. Hayward, P. M. Kosro, T. P. Stanton, S. Ramp, and T. Cowles, Water mass subduction and the transport of phytoplankton in a coastal upwelling system, *J. Geophys. Res.,* 96(C8), 14,927-14,945, 1991.

Winant, C. D., R. C. Beardsley, and R. E. Davis, Moored wind, temperature and current observations made during Coastal Ocean Dynmics Experiment 1 and 2 over the northern California continental shelf and upper slope, *J. Geophys. Res.,* 92, 1569-1604, 1987.

Wooster, W. S., and J. L. Reid, Eastern boundary currents, in *The Sea,* vol. 2, edited by M. N. Hill, pp 253-280, Interscience, New York, 1963.

Wooster, W. S., A. Bakun, and D. R. McLain, The seasonal upwelling cycle along the eastern boundary of the North Atlantic, *J. Mar. Res.,* 34, 131-141, 1976.

Wunsch, C., and D. Stammer, Atmospheric loading and the oceanic "inverted barometer" effect, *Reviews of Geophysics,* 35(1), 79-107, 1997.

Yoshida, K., Circulation in the eastern tropical oceans with special references to upwelling and undercurrents, *Jap. J. Geophys.,* 4(2), 1-75, 1967.

Zenk, W., On the Mediterranean outflow west of Gibraltar, *Meteor Forschungsergebnisse A,* 16, 23-34, 1975.

Zenk, W., and L. Armi, The complex spreading pattern of Mediterranean Water off the Portuguese continental slope, *Deep Sea Res.,* 37(12), 1805-1823, 1990.

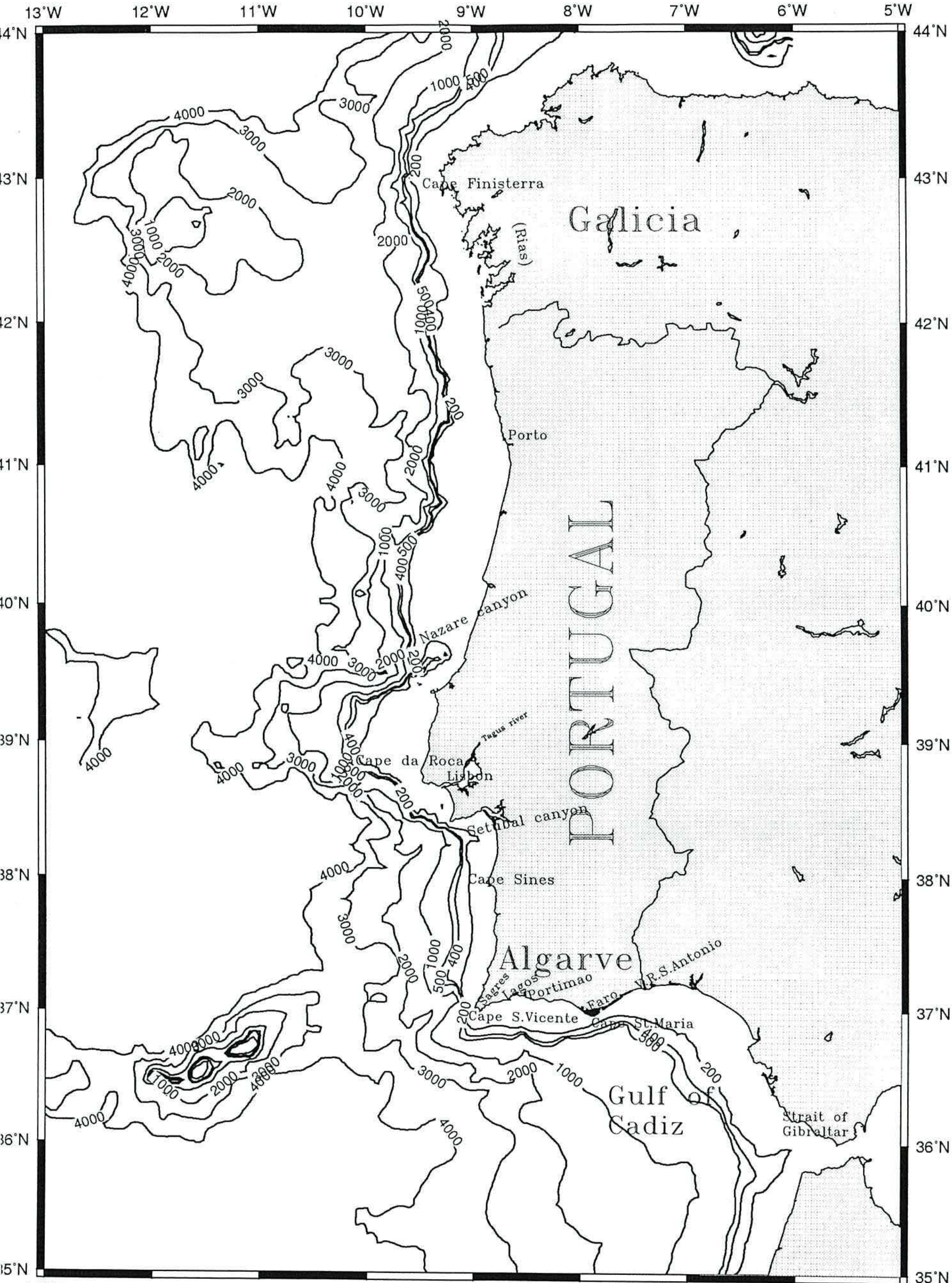
13°W
12°W
11°W
10°W
9°W
8°W
7°W
6°W
5°W
44°N
43°N
42°N
41°N
40°N
39°N
38°N
37°N
36°N
35°N
Cape Finisterra
Galicia
(Rias)
Porto
PORTUGAL
Nazare canyon
Tagus river
Cape da Roca
Lisbon
Setubal canyon
Cape Sines
Algarve
Sagres
Lagos
Portimao
Faro
V.R.S.Antonio
Cape S.Vicente
Cape St.Maria
Gulf of
Cadiz
Strait of
Gibraltar
200
400
500
1000
2000
3000
4000